STUDY S-341

DETERMINATION OF WINDS AND OTHER ATMOSPHERIC PARAMETERS BY SATELLITE TECHNIQUES

in four volumes

VOLUME IV: Physics of the Atmosphere

Alan J. Grobecker

December 1969

INSTITUTE FOR DEFENSE ANALYSES
SCIENCE AND TECHNOLOGY DIVISION
400 Army-Navy Drive, Arlington, Virginia 22202

Company Independent Research
Program

FOR OFFICIAL USE ONLY

READER'S REFERENCE

This report is Volume IV of IDA Study S-341 "Determination of Winds and Other Atmospheric Parameters by Satellite Techniques."

The volumes describing the study are the following:

Volume	I	Summary
	II	Potential Needs for Determination of Atmospheric Parameters
	III	Techniques for Determining Winds and Other Atmospheric Parameters
	IV	Physics of the Atmosphere

PREFACE

The work reported in this volume was accomplished under IDA's Independent Research Program. It is included here as part of S-341 because of its relevance as a background to the measurements of winds and densities from satellites and to the computational simulation of winds.

ACKNOWLEDGMENT

Significant contributions to this volume were made by Drs. E. Bauer and C.M. Tchen.

ABSTRACT

The physical characteristics of the terrestrial atmosphere are reviewed for the purpose of providing a physical background for a study of requirements and techniques for the determination from satellites of winds and other atmospheric parameters. The nature of the atmosphere, its physical processes, and the variability of its parameters are described. Topics treated, in turn, are solar radiation as its affects the atmosphere, the troposphere, stratosphere and mesosphere, the thermosphere and the ionosphere.

CONTENTS

FIGURES

TABLES

INTRODUCTION

Physics of the Atmosphere, Volume IV of a study of requirements and techniques for the determination of winds and other atmospheric parameters by measurements made from earth orbiting satellites, is a review of the physical characteristics of the terrestrial atmosphere which is to be observed. The nature of that atmosphere, its physical processes and the variability of the parameters by which they may be described are essential knowledge required for the understanding and evaluation of measurement data, for the design of instrumentation systems, and for the computational simulation of the atmosphere.

Much of the material contained in this description may seem either unnecessarily complicated for the needs of the pragmatic reader, or too elementarily tutorial for the knowledgeful specialist. The meteorologist, for instance, will find little new in the discussion of the troposphere. The radio communications physicist will not be particularly enlightened by the discussion of the ionosphere. However, in this volume is the background essential for a proper appreciation of the requirements and of the measurement techniques discussed in Volumes II and III. It is hoped that even the specialists will find some value in this review of the total picture.

In the following pages, the influence of the solar radiation on the terrestrial atmosphere is described first. The sun provides the driving energy of the atmosphere and causes its large variability. Most of the sun's energy arriving at the earth is absorbed by the solid earth, the oceans and by the lower atmosphere, the troposphere. A very small fraction of this energy is deposited in the upper atmosphere; however, its effect is very large.

With the energy derived from insolation as the primary cause of variability, the terrestrial atmosphere varies most strongly as a function of altitude. In trying to characterize the variation with altitude, a number of models of the atmosphere have been described as "standards" for use in detailed studies. Of these, a recent example commonly cited is the U. S. Standard Atmosphere of 1962. Shown in Fig. 1 is the variation of temperature, pressure, density, and molecular weight, with altitude, according to the U. S. Standard Atmosphere, 1962. Also, in Fig. 2 is the variation with altitude of other atmospheric parameters: number density, collision frequency, mean free path and particle speed, according to the same standard.

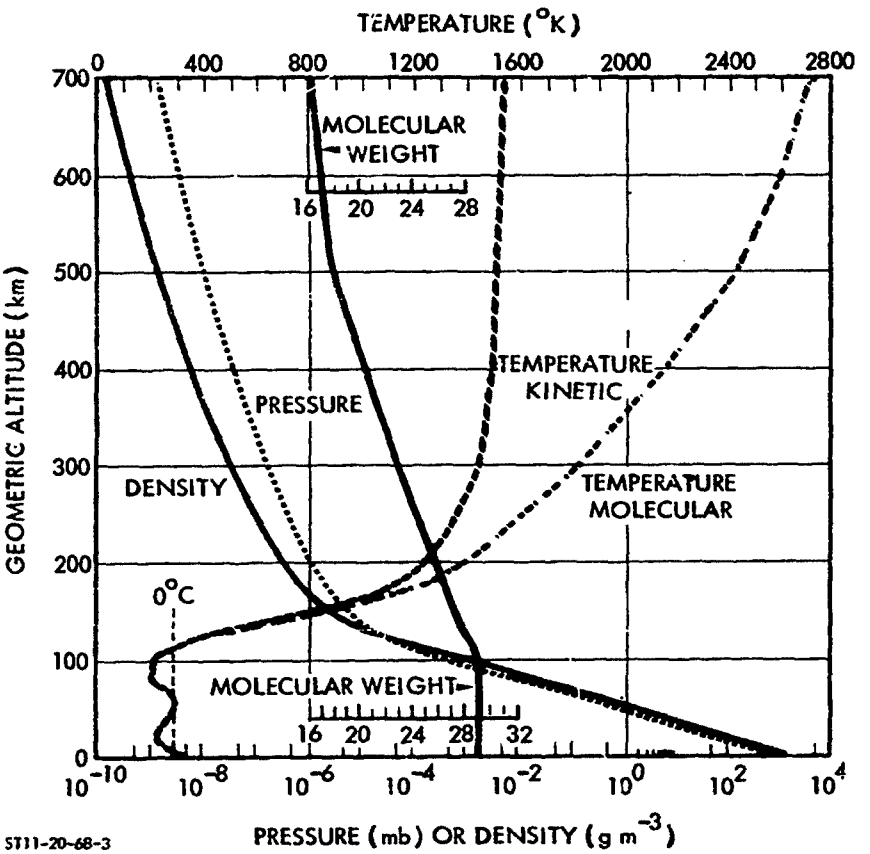

FIGURE 1. Temperature, Pressure, Density, Molecular Weight (U.S. Standard Atmosphere, 1962)(After Valley, 1965)

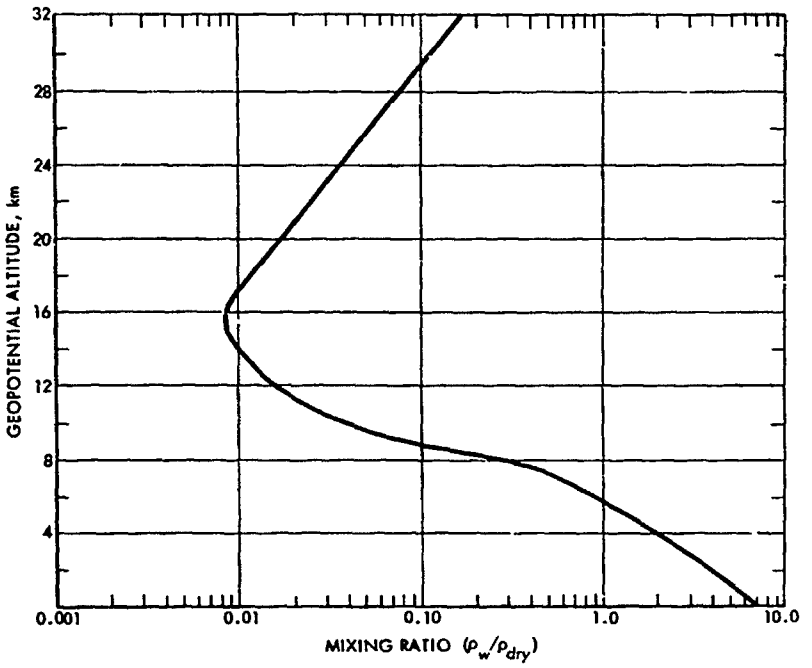

FIGURE 3. Moisture in Lower Troposphere (After Valley, 1965)

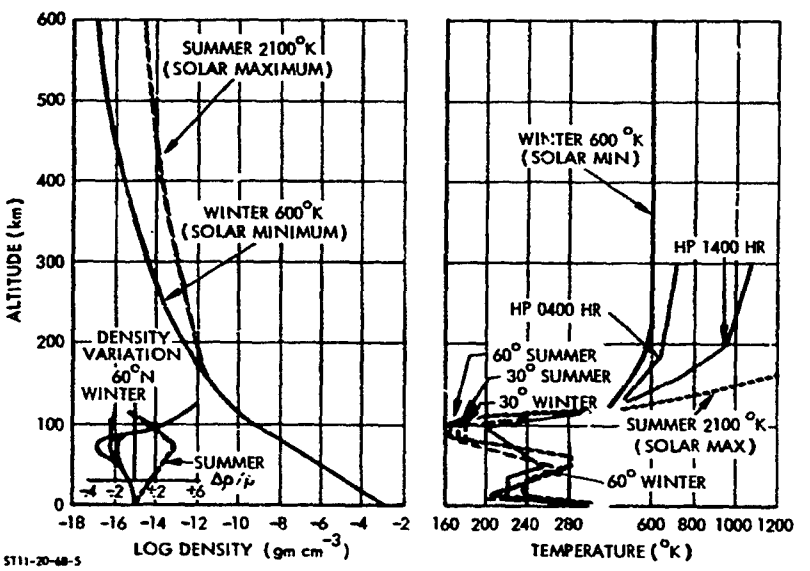

FIGURE 4. Variability of the Atmosphere (U.S. Standard Atmosphere Supp, 1966)

of excursions of two of the parameters: mass density and temperature. Mass density may vary from plus 60 to minus 40 percent of standard magnitude at altitudes below 120 km, and by a factor of 100 at altitudes of 600 km. Temperature may vary over a range of 10 to 25 percent of standard value at altitudes below 120 km, and by a factor of three at an altitude of 600 km.

The variation of the atmospheric temperature profile has been the basis for the nomenclature of the atmospheric regions, which is currently common and which will be used in this report hereafter and is given in Fig. 5. The extrema of the temperature profile are called the tropopause, the stratopause and the mesopause, and occur at altitudes of about 20, 50, and 80 km, respectively. Below the tropopause is the troposphere; between tropopause and stratopause is the stratosphere; between the stratopause and the mesopause is the mesosphere, and above the mesopause is the thermosphere. The physics of each of the regions is distinctive.

The review of the physics of the troposphere is concerned mainly with estimating the characteristic dimensions of the large-scale phenomena which are of importance to numerical weather prediction, and with a treatment of the theory and examples of the atmospheric wave motion largely a paraphrase of Eliassen and Kleinschmidt (1957), Mintz (1961), Lorenz (1965), and Starr (1968). Such wave motions, including both impulsive and quasi-continuous phenomena, have a highly complicated theory, which is however a powerful tool for understanding the dynamic processes of the atmosphere.

In the review of the physics of the stratosphere and the mesosphere, some distinctive characteristics of this stable altitude region are given. The region is quite unlike either the thermosphere above it, or the troposphere below. To a degree, it behaves as an energy trap, it inhibits the transmission of several forms of energy flux from outer space to the earth, and from the earth outward. Its importance lies in the fact that it possibly serves as an upper bound to the troposphere (and thereby affects our weather) and certainly

of excursions of two of the parameters: mass density and temperature. Mass density may vary from plus 60 to minus 40 percent of standard magnitude at altitudes below 120 km, and by a factor of 100 at altitudes of 600 km. Temperature may vary over a range of 10 to 25 percent of standard value at altitudes below 120 km, and by a factor of three at an altitude of 600 km.

The variation of the atmospheric temperature profile has been the basis for the nomenclature of the atmospheric regions, which is currently common and which will be used in this report hereafter and is given in Fig. 5. The extrema of the temperature profile are called the tropopause, the stratopause and the mesopause, and occur at altitudes of about 20, 50, and 80 km, respectively. Below the tropopause is the troposphere; between tropopause and stratopause is the stratosphere; between the stratopause and the mesopause is the mesosphere, and above the mesopause is the thermosphere. The physics of each of the regions is distinctive.

The review of the physics of the troposphere is concerned mainly with estimating the characteristic dimensions of the large-scale phenomena which are of importance to numerical weather prediction, and with a treatment of the theory and examples of the atmospheric wave motion largely a paraphrase of Eliassen and Kleinschmidt (1957), Mintz (1961), Lorenz (1965), and Starr (1968). Such wave motions, including both impulsive and quasi-continuous phenomena, have a highly complicated theory, which is however a powerful tool for understanding the dynamic processes of the atmosphere.

In the review of the physics of the stratosphere and the mesosphere, some distinctive characteristics of this stable altitude region are given. The region is quite unlike either the thermosphere above it, or the troposphere below. To a degree, it behaves as an energy trap, it inhibits the transmission of several forms of energy flux from outer space to the earth, and from the earth outward. Its importance lies in the fact that it possibly serves as an upper bound to the troposphere (and thereby affects our weather) and certainly

is involved in the full exploitation of radio communications and in the military problem of targeting of weapons from higher regions in the atmosphere and outer space.

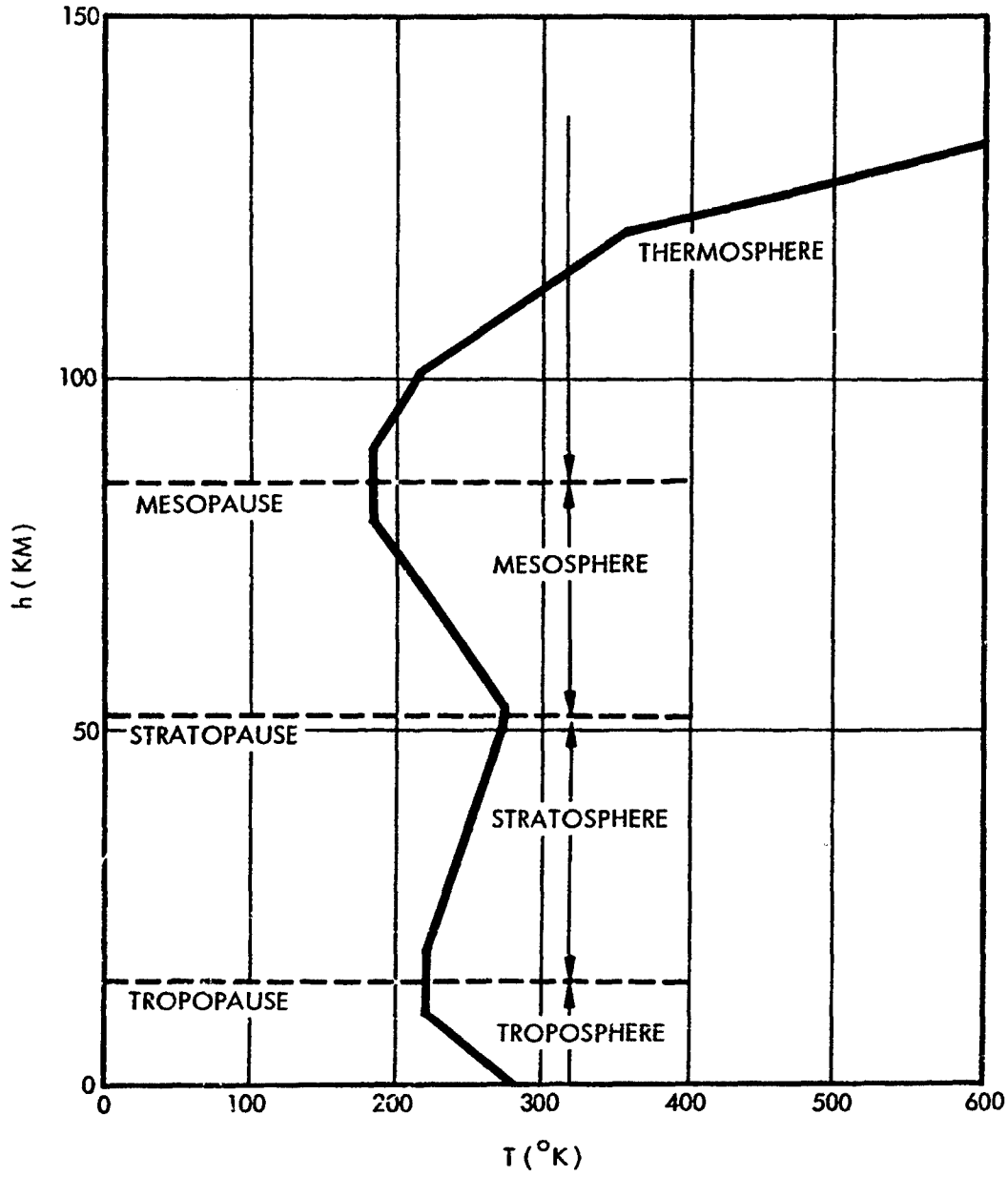

FIGURE 5. Atmospheric Temperature Profile and Different Regions

In the review of the physics of the thermosphere and ionosphere are given some features of a quite distinctively different region which affects radio communications, targeting of ballistic weapons and the predictability of low orbits of earth satellites.

I. INFLUENCE OF SOLAR RADIATION IN THE ATMOSPHERE

The driving source in producing the variability of the terrestrial atmosphere is the sun which is, itself, a very complex system. The regions of the visible sun have been named in a manner illustrated in Fig. 6.

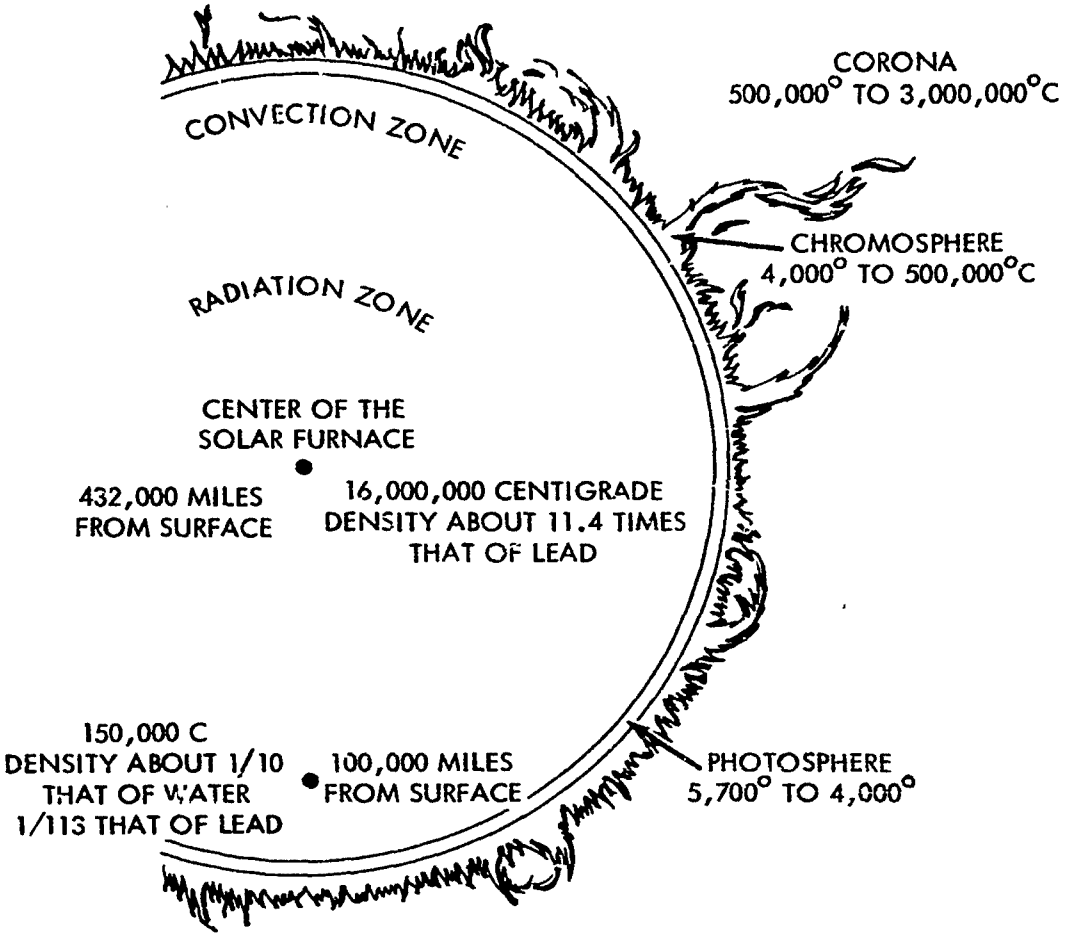

FIGURE 6. Regions of the Sun (After Friedman, 1965)

The interior of the sun consists mainly of hydrogen which by exothermic nuclear transformation produces heavier elements. The heat of the exothermic process is transferred from the outer shell by a combination of convection and radiation processes and from the inner core by radiation alone. Only a small fraction of the exothermal energy escapes. It is thought that the sun has been in essentially its present form for about seven billion years, and will remain essentially in its present form for another three billion years; then it will become a "red giant." As a "red giant," it will expand to a diameter which will extend to the present orbit of Mars. It will consume the interior planets (including the earth).

Be that as it may, the present sun is for the time of recorded observation in an essentially stationary, although complex, state. The most obvious visual feature of the sun is the photosphere, which we may see with the naked eye. It subtends about a half-degree. Its minimum surface temperature is about 5700 to 4000^{o}C. The sun suffers small temporal variations of apparent size and temperature that are due principally to the variations of orbital geometry and to the absorption in so called sunspots by cooler gases of a small fraction of its total radiation. The chromosphere and corona, on the other hand, are at much higher temperatures and are much more variable.

The chromosphere extends from the surface of the photosphere out about 10,000 km and is extremely variable in thickness. It is made up of cool spicules which penetrate into the corona and of hotter inter-spicules. Its temperature and density, illustrated in Fig. 7, range from about 4400 ^{o}K and $(10)^{15}$ cm^{-3} near the photosphere to about 40,000 ^{o}K and $(10)^{9}$ cm^{-3} at a distance 10,000 km from the photosphere.

Shown in Fig. 8 is a model of chromospheric and coronal temperature and density. One may see that at about 10,000 km from the photosphere, there is a sudden transition to the much higher temperatures of the near corona (millions of degrees Kelvin). The density distribution and the temperature are strongly variable according to magnetic fields in the sun.

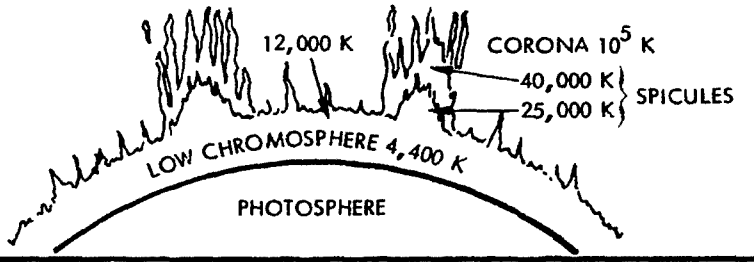

H ABOVE PHOTOSPHERE	COOL ELEM			HOT		SPICULE		INTERSPIC		TEMP OF EXC		
	T_{el}	LOG N	LOG Ne	T_{el}	LOG Ne	T_{el}	LOG Ne	T_{el}	LOG Ne	T_{exN_2}	T_{ion_H}	$T_{ion_{Fe}}$
0	4,400	15.6	-	4,400						6,000	5,600	4,900
2,000	5,500	12.8	10.8	12,000	11.3					6,300	5,700	4,900
4,000	-	11.9	10.0	-	10.6					6,250	5,400	
6,000						25,000	10.9	$> 10^5$	9.4	5,500		
8,000												
10,000						40,000	8.8	$>10^5$	8.8			

ST11-20-68-7

FIGURE 7. Density and Temperature in Chromosphere

H. W. Babcock (1961) has given the most plausible explanation of the principal mechanism that produces the variability of the visible sun. His ideas are illustrated in Fig. 9. The magnetic field of the sun, thought to have an exterior expression like that of a in Stage 1 of Fig. 9 is dragged at different speeds in the interior by the solar plasma. The solar plasma, located within the photosphere, is known to rotate more rapidly at the solar equator than at the solar poles. The distribution of the angular velocity (w) is as shown in b in Stage 1 of Fig. 9. Moreover, the magnetic field lines do not penetrate to a great depth within the sun, but rather as illustrated by H in b. As a consequence of the shallow penetration, and of the dragging, the magnetic field lines are wound around the solar sphere, as illustrated in Stage 2 of Fig. 9. With more and more lines pressed ever more tightly together with successive rotations of the solar equator with respect to the solar interior, the consequent lateral

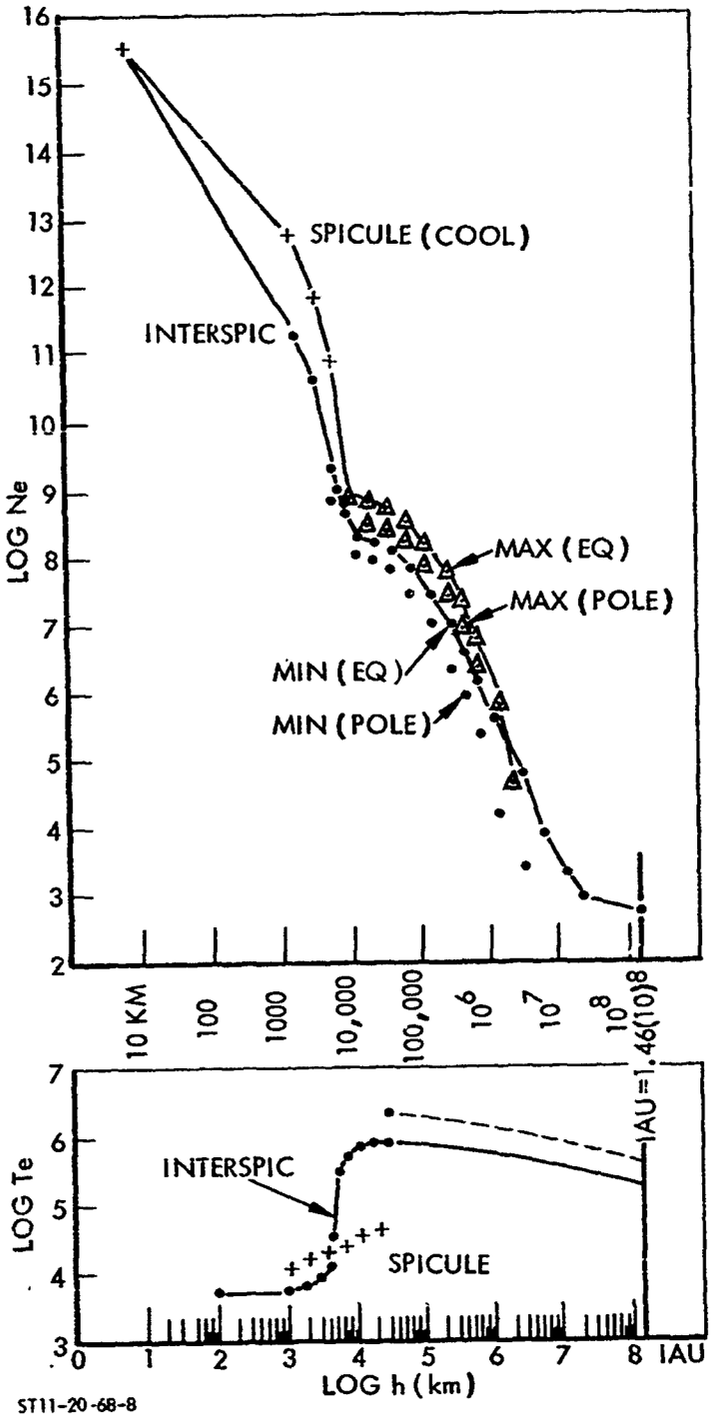

FIGURE 8. Model of Chromospheric and Coronal Temperature and Density

pressure may cause one of the lines to be extruded as a small loop, as illustrated in Stage 3 of Fig. 9. The small loop of magnetic field is the site of the sunspot as cooler gases from below are entrained in the magnetic field to flow along the loop into a higher region of hot gas. The sunspot itself is the region of the sun in which radiation normally visible from the hot gas is self-absorbed by the cooler entrained gas. Seen from the side, the hot gases in the magnetic loops are the "solar prominences" which project out in the corona where the temperature is the maximum.

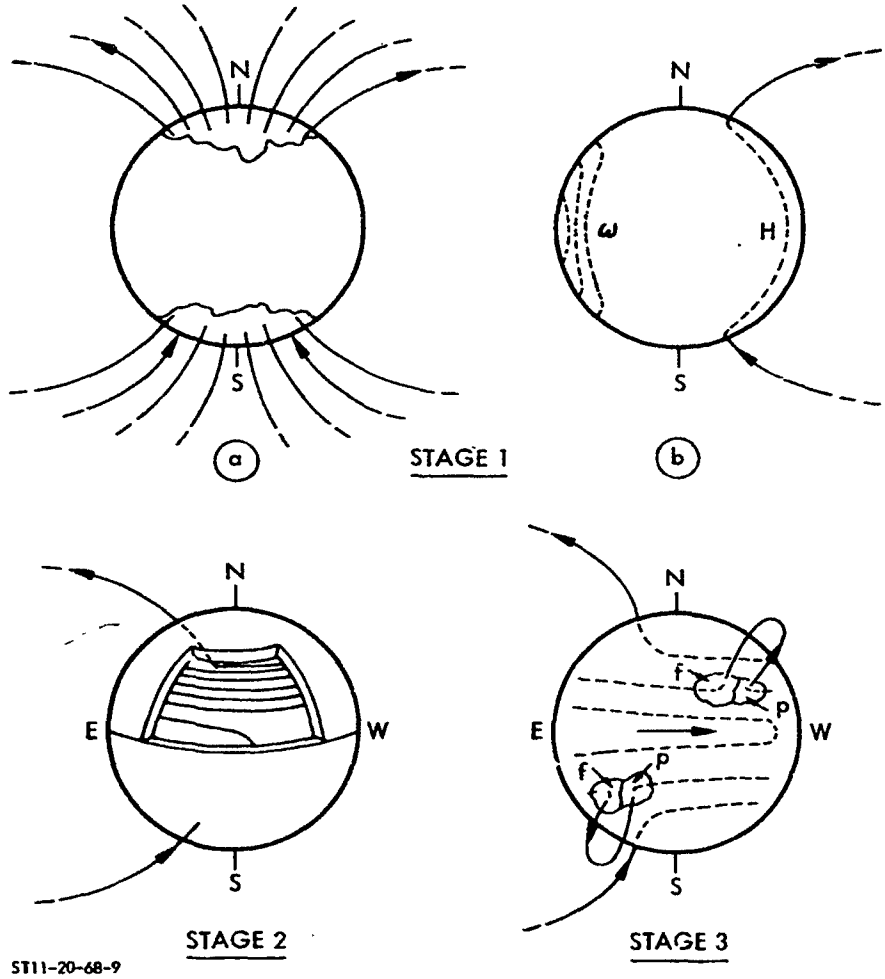

FIGURE 9. Development of Bipolar Field (After H.W. Babcock, 1961)

We now begin to have a basis for understanding some reasons for the variability in character of the solar sources of radiation that affect the terrestrial atmosphere. Some of the ideas are outlined in Fig. 10.

BOUND-BOUND $$E_{nn'} = NiNe \frac{KZ^4}{Te^{3/2}} b_n \frac{g}{n'^3} \frac{2hRZ^2}{n^3} e^{X_n}$$

LYMAN-ALPHA: NEAR PHOTOSPHERE
XRAY: NEAR CORONA

BOUND-FREE $$E_{kn} = NiNe \frac{KZ^4}{Te^{3/2}} \frac{hg_{II}}{n^3} e \frac{-h(\upsilon-\upsilon_n)}{KTe}$$

SCHUMANN-RUNGE CONTINUUM CHROMOSPHERE
XRAY: NEAR CORONA

FREE-FREE $$E_{\upsilon} = 3.8(10)^{-38} \frac{NiNe}{Te^{3/2}} Ti \ln\left(\frac{420\ Te}{ZNi^{1/3}}\right)$$

RADIO: FAR CORONA
PARTICLES: NEAR, FAR CORONA

ST11-20-68-10

FIGURE 10. Source Location of Solar Emission

The atomic processes that give rise to the radiation may be classified as transitions from bound to bound states, from bound to free (and vice versa) states, and from free to free states. The energy relations characteristic of the three types of transition are listed in Fig. 10 as functions of density, temperature, and frequency according to Aller's classification (1963). By using the energy relations, and the temperature and density distributions of Fig. 8, one perceives that the visible spectrum originates within the cool photosphere, that the Hydrogen Lyman-alpha line originates within an area of about a 1000 km above the photosphere, that the Schumann-Range continuum originates in the mid-chromosphere about 6000 km above the

photosphere, and that the X-radiation of wavelength greater than a few Angstroms originates in the near (hot) corona. In general, the radio frequency radiation must originate in the far corona where the smaller densities make possible the radiation to earth without self-absorption. Although the mechanism is not clearly understood, particles radiated to the earth from "solar sources" do not originate within the sun, but also come from a location in the far corona. Apparently they, like the X-radiation, arise from the interaction of jets of magnetically confined cooler gases from the sun into the hot solar corona. Travelling at slower speeds than the electromagnetic radiation, the particles travel from the source to the earth by a different route, and once within the magnetosphere are further constrained to travel along the lines of the earth's magnetic field.

The spectrum of the solar electromagnetic radiation in the visible range may be roughly characterized as a group of lines and continua in an envelope like the black-body characteristic of 6000 ^{o}K. For shorter wavelengths (less than 2000 A) the radiative spectrum is as shown in Fig. 11. For wavelengths 1000 to 2000 A, the radiation appears in general to emanate from a black-body of temperature 4500 to 5000 ^{o}K. Notably differing from this generalization are lines of helium and hydrogen. Since these gases, however, are the principal constituents of interplanetary space, the lines represent an accumulation, in degraded form, of energy originating in much more energetic form, but not reduced to the lowest energy levels (HLyA, He I, He II) characteristic of the two species.

In contrast to the radiation at wavelengths greater than 1000 A, there is the radiation at wavelengths less than 200 A. This appears (as we have already shown to be plausible) to originate from different sources; a black-body of highly variable area (peak energy varying by factor ten between minimum and maximum of eleven-year solar sunspot cycle) and of temperature about 500,000 ^{o}K seems to be a source of radiation greater than 20 A, and a different black-body of even more variable area (the shaded zones in Fig. 11 which vary according to solar flare activity) and of temperature of about two billion ^{o}K. The

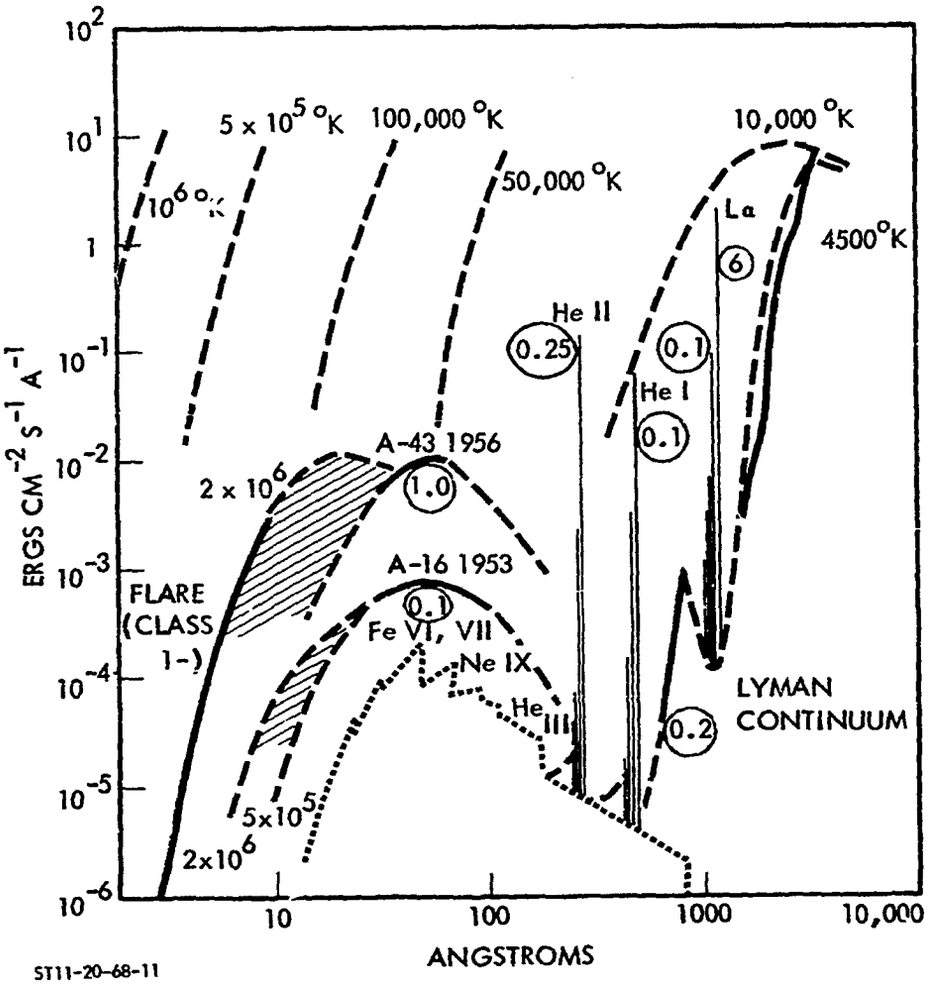

FIGURE 11. Solar Spectral Energy Below 2000 A
(After Friedman, 1962)

dotted lines of Fig. 11 show an energy flux curve expected of an area like that of the photosphere at various black-body temperatures. One may see by comparing the actual flux curves with the hypothetical black-body curves (dashed lines), that the solar radiation at wavelengths greater than 1000 °K seems to emanate from a source area approximately that of the photosphere, but that solar radiation at wavelengths less than 200 A emanates from a source area that is orders of

magnitude smaller than the photosphere. Photographs of the sun, made with X-radiation, confirm that the solar sources are indeed spots on the sun in locations roughly coinciding with solar sunspot activity and of area of the order of one millionth of the photosphere area. Seen in profile, the activity which causes the X-radiation is at the extremes of the solar prominences where the chromosphere penetrates the corona.

The measured variability of the solar X-ray flux is shown in Fig. 12 in which is compiled measurements by a number of observers. Radiation in the band 44-60 A varies over a factor of about ten between solar minimum and the maximum. Radiation in the band 2-8 A, on the other hand, is seen to vary over five orders of magnitude between solar minimum quiet conditions and solar maximum (2 + flare) conditions.

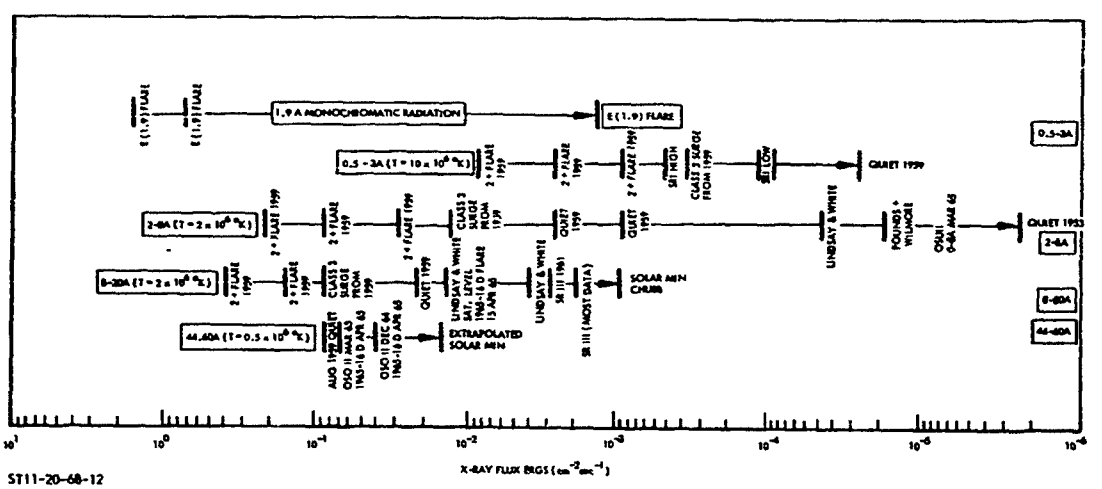

FIGURE 12. X-Ray Solar Flux Measurements (After Kreplin, 1963)

The occurrence of radio bursts and flares has been described by H. W. Dodson (1959), as shown in Fig. 13. Also shown in the figure are the minimum distances from the photosphere of the sources of the radiation perceived at the earth, as indicated by the limiting plasma frequency

$$\omega_p = \sqrt{\frac{4\pi e^2}{m} n_o} = 5.6(10)^4 \sqrt{n_o} \qquad 1.1$$

where n_o is the electron number density (it is assumed to be equivalent to the number density of the model of Fig. 8). Of particular note in Fig. 13 is the 3000 MHz radiation which roughly correlates in time with solar ultraviolet radiation and is indicated as possibly originating similarly in the chromosphere about 2000 km from the photosphere. Radiation at 3000 MHz is taken as an index of solar activity as a parameter differentiating between CIRA 1965 (COSPAR International Reference Atmosphere of 1965) models of the thermosphere. Such an index, while a feeble measure by which to characterize variability of the thermosphere, is better than none at all.

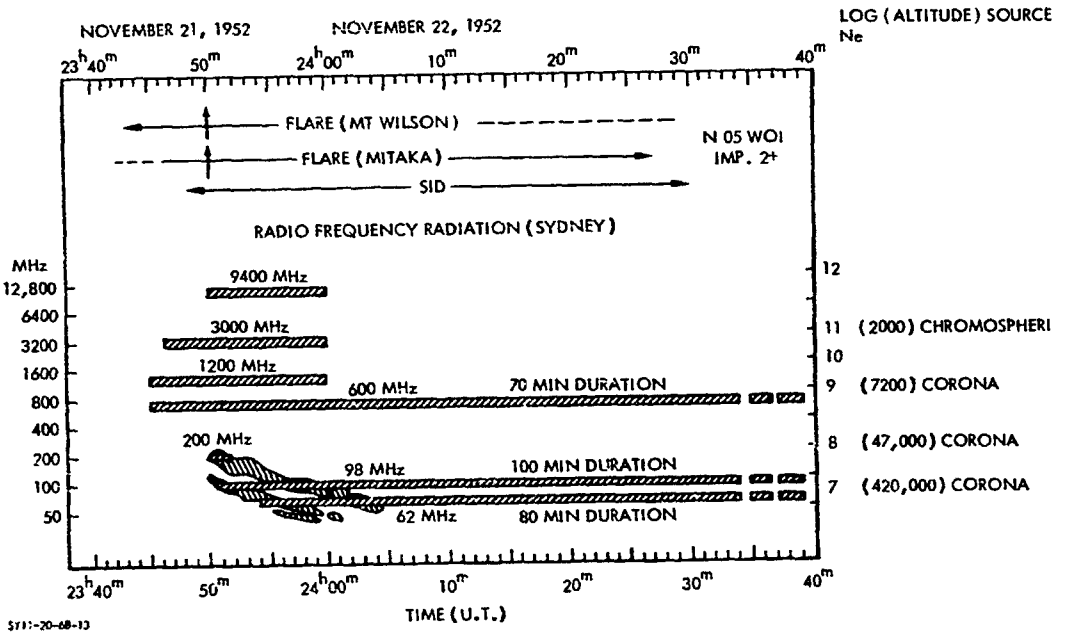

FIGURE 13. Radio Bursts and Flares
(Adapted from H. W. Dodson, 1959)

The delayed arrival of particulate radiation on earth is due to transit time. An example is the cosmic ray burst of February 23, 1956, pictured in Fig. 14. The originating flare observed in H_α apparently started at 03 hr 31 min ± 1 min UT. The first cosmic ray particles arrived at earth's nightside at 03 hr 45 min ± 1 min. The time distribution of relative increases as observed at Stockholm, Chicago and Berkeley are shown in the figure. The earth's magnetic field acts as a spectrograph separating particles of different energies according to geomagnetic latitude. The energy may be parameterized as rigidity, Z, defined to be

$$Z = \frac{p\,c}{q\,e} \qquad 1.2$$

wherein qe is the electric charge of the particle, p is momentum, and c is velocity of light in a vacuum. Z is usually measured in units of $(10)^9$ eV (i.e., GeV). The vertical cutoff rigidity at the equator is 14.9 GeV; only particles with energies greater than 60 GeV can approach the earth from any direction. Stormer's theory has shown that the cutoff rigidity for vertical incidence is

$$Z_c = 14.9 \cos^4\theta \qquad 1.3$$

where θ is the geomagnetic latitude. Particles with a rigidity of somewhat less than Z_c can reach the earth at latitude θ at large zenith angles and at certain azimuths. For positively charged particles in the northern hemisphere, the minimum rigidity is realized for particles arriving from the western horizon.

The path traveled by a particle from the sun to the earth is not radial. One hypothesis, proposed by Parker (1958), holds that the ejected particles, having been ionized, travel along magnetic field lines that are anchored to the emissive region on the sun. Since the sun is rotating counterclockwise (see Fig. 15), its rotation produces a curvature of the field lines which intercepts the earth's orbit along which the earth moves counterclockwise (see Fig. 15). The angle between the magnetic field path of particles and the radial path of the electromagnetic radiation can be computed in the following manner

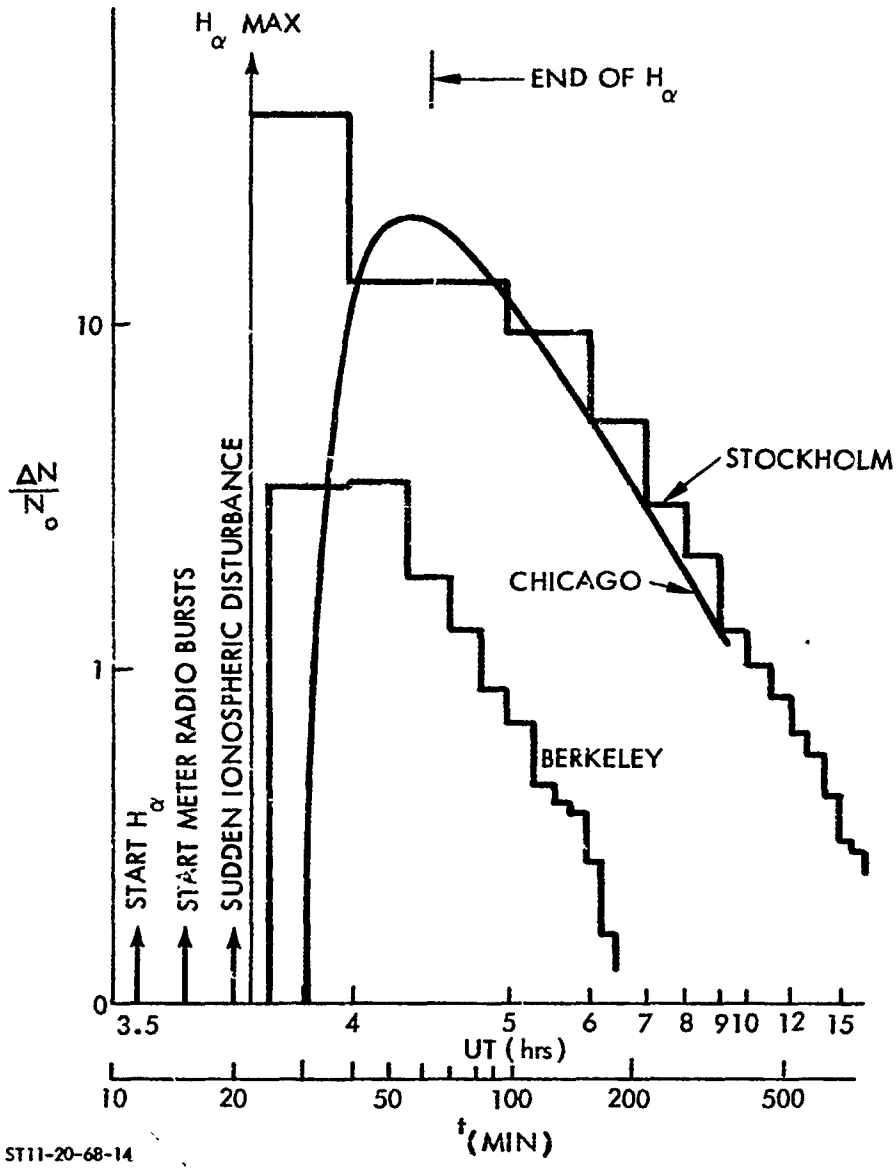

FIGURE 14. Onset of Cosmic-Ray Burst (After Ehmert and Pfetzer, 1956)

$$\theta = \tan^{-1}\left(\frac{\omega r}{v}\right) \qquad 1.4$$

wherein ω is the angular rotation velocity of the sun, r is distance from the sun, and v is the velocity of the particle.

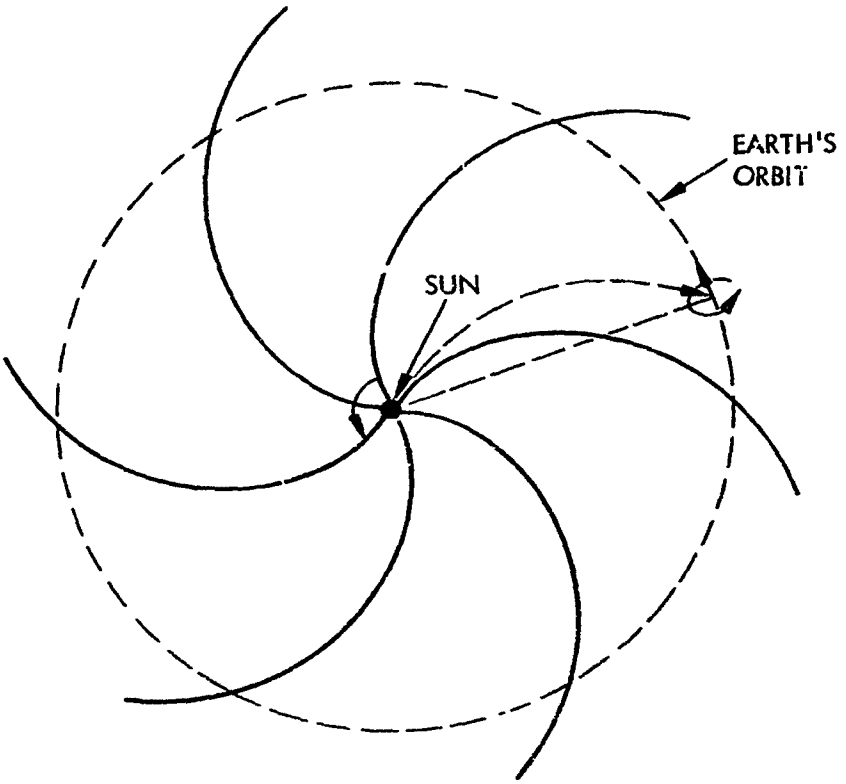

FIGURE 15. Solar Magnetic Field Lines as Viewed from Sun's North Pole (After Parker, 1958)

A spectrum of solar particles energies is shown in Fig. 16 which also indicates the integrated intensity of particles and cosmic rays of galactic (non-solar) origin.

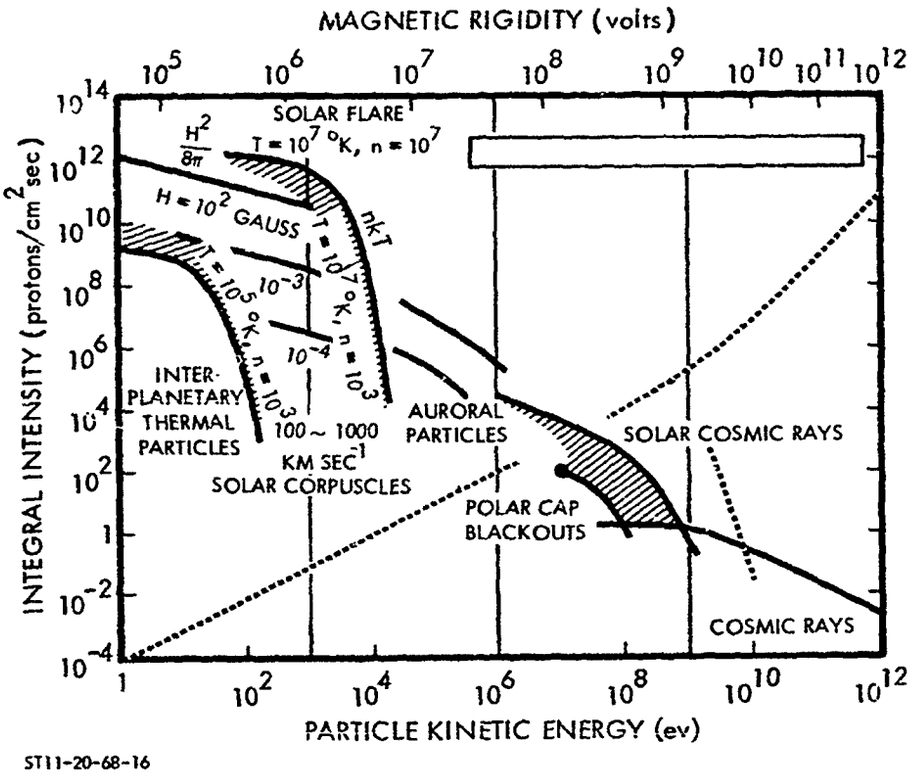

FIGURE 16. Integrated Energy Spectrum of Solar Particles Associated with Solar Flares (After Obayashi and Hakura, 1960)

ATMOSPHERIC ENERGY SOURCES

The sources of atmospheric energy are the difference between the solar-originated energy absorbed by the atmosphere and the energy emitted by the atmosphere.

At the distance earth is from the sun the solar flux is given by the so-called "solar constant" (1.99 cal cm^{-2} min^{-1}, or 1.388 $(10)^6$ erg cm^{-2} sec^{-1})(Allen, 1963). Of this energy a fraction of about 0.99 is absorbed at the surface and by carbon dioxide and water vapor in

the troposphere, primarily in the visible range of the spectrum. The distribution of absorbing water vapor and of reflecting water particles in the troposphere is strongly variable in time, latitude, longitude, and altitude.

Above the troposphere, the distribution of absorbers is not so strongly variable. A measure of the absorption capabilities is the absorption cross section σ; the fraction of incident flux that is absorbed in unit distance (dx) of a radiation path in which the number density is n is given by

$$\frac{dE}{E} = \sigma n \, dx \qquad 1.5$$

The principal constituents of the atmosphere below 200 km are atomic oxygen (O), molecular oxygen (O_2), and molecular nitrogen (N_2). These constituents have the absorption cross sections shown in Fig. 17.

As we have shown in Fig. 6, the hydrogen Lyman-alpha line is a very intense one. It penetrates to the mesosphere because it coincides with a minimum in the wavelength versus absorption cross section plot of the principal absorber molecular oxygen. This minimum appears in the illustration of the absorption cross section for O_2, shown in Fig. 18.

A principal absorber in the stratosphere is ozone O_3. (Its absorption cross section is shown in Fig. 19.) It may be noted that the absorption cross section of O_3 at the wavelength of hydrogen Lyman-alpha (1215.7 A) is larger than that of O_2. However, in the region where Ly-A is absorbed (70 - 90 km), the number density of O_3 is not large enough to match the absorption by O_2 in spite of the larger absorption cross section.

In summary, then, the solar heat sources in the atmosphere above the troposphere are as indicated in Table 1 which shows the magnitude of the solar flux absorbed in the altitude regime, and the spectral band of the solar radiation from which the heat is derived.

In Fig. 20 is shown the rate of energy absorption of X-rays -- 220 to 900 A and 1300 to 1800 A wavelength bands.

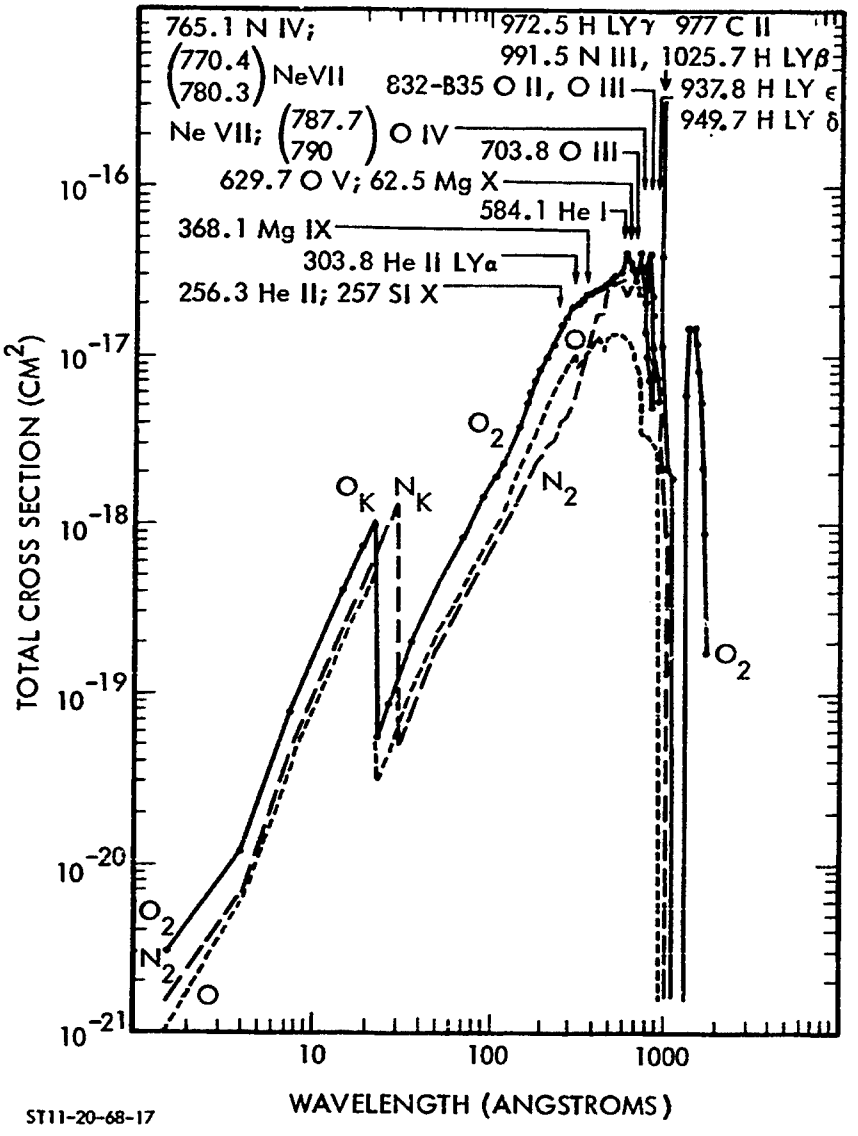

FIGURE 17. Absorption Cross Section of O, O_2, and N_2 (After Hinteregger et al., 1964)

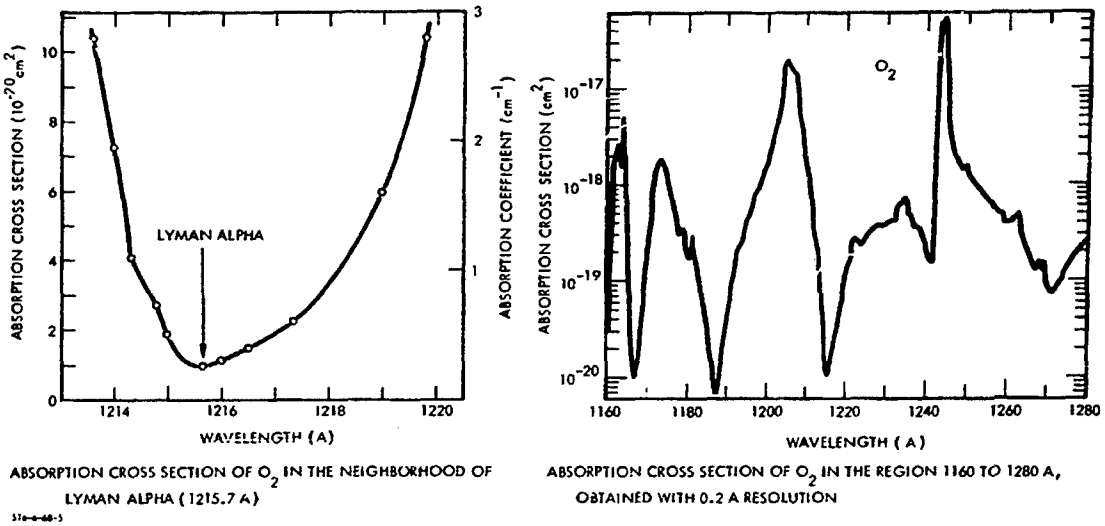

FIGURE 18. Absorption Cross Section of O_2 (After Watanabe, 1958)

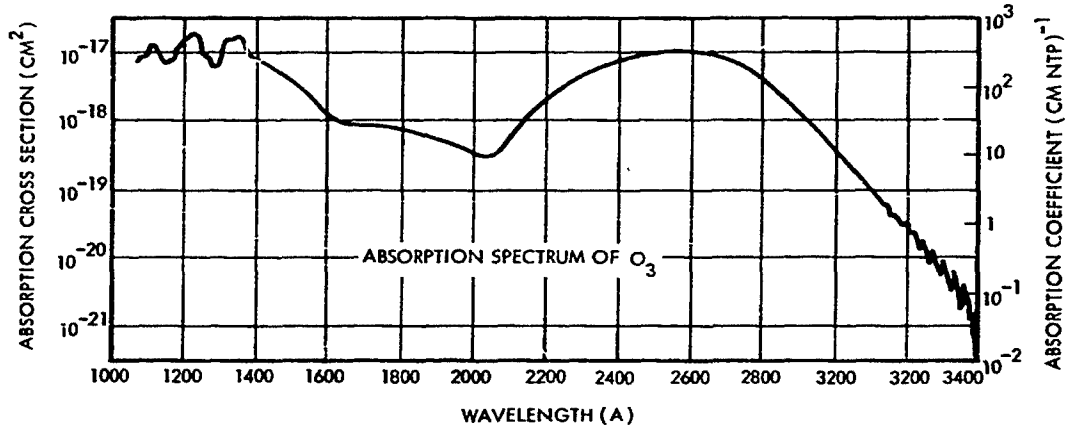

FIGURE 19. Ozone Absorption Cross Section in the UV (From Craig, 1965)

TABLE 1. SOLAR HEAT SOURCES IN THE ATMOSPHERE
(After Craig, 1965)

REGION	ION REG	ALTITUDE (KM)	SOLAR HEAT SOURCE	FLUX (ergs $cm^{-2}sec^{-1}$)
Thermosphere				
Upper	F	150 - 300	Conduction From Corona	0.25
Lower	E	80 - 150	Schumann-Runge Cont. 1300-1750A EUV (λ<1000A) From Chromosphere	30.0
Mesosphere	D	50 - 80	Schumann Runge Bands 1750-1950A From Chromosphere	100.0
Stratosphere		30 - 50	Hartley Continuum 2000-3000A From Lower Chromosphere	$1.8(10)^4$
Troposphere		0 - 30	Absorption From Photosphere And Re-Emission From CO_2, H_2O, Surface	$1.37(10)^6$

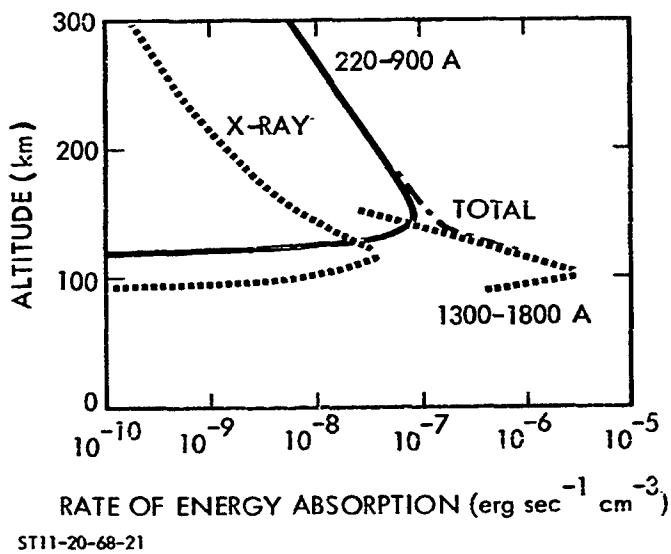

FIGURE 20. Rate of Energy Absorption
(After Johnson, 1958)

In addition to the sources of heat in the atmosphere, it is necessary to consider the sinks of energy. Chief among these is the radiative emission of energy out of the atmosphere. In Fig. 21 is shown a composite plot of vertical radiance, as measured by a number of observers from balloons, aircraft, rockets and satellites in a variety of observation zenith angles. The daylight radiance appears to emanate from a source like a black-body at about 6000° K, and the nighttime radiance as from a black-body of about 300° K. An exception to the latter generalization is the nighttime Ly-A, for which there may be several explanations.

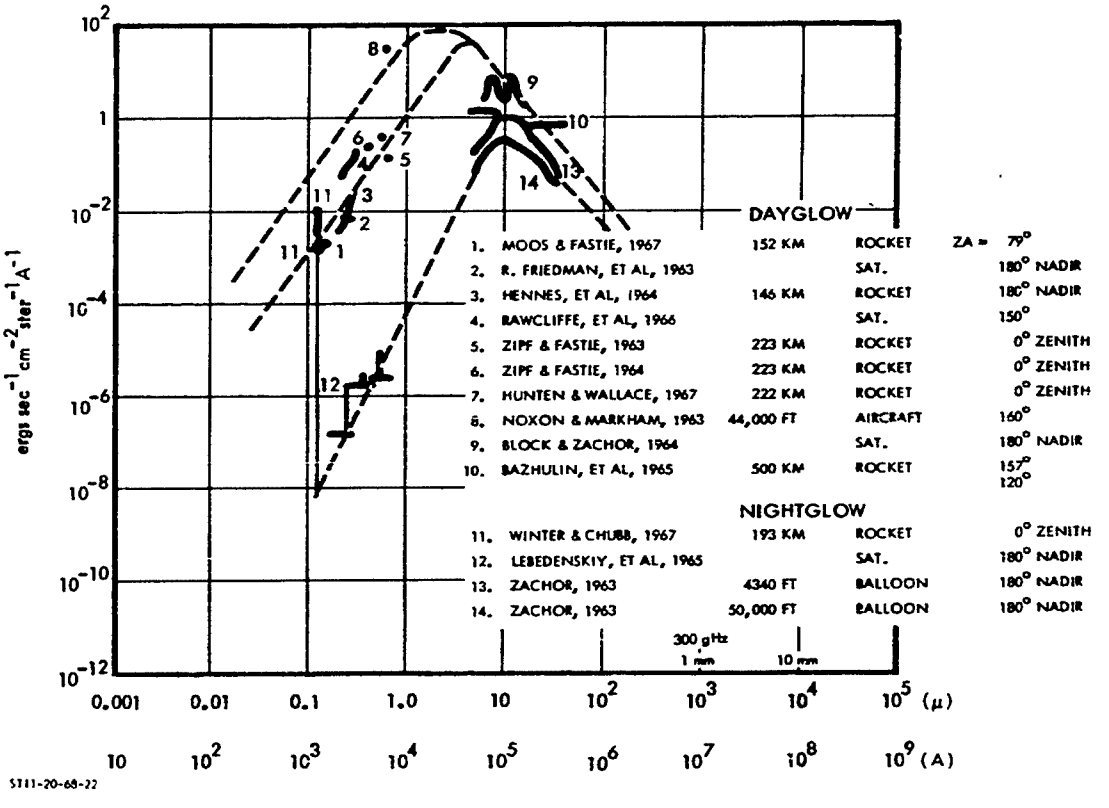

FIGURE 21. Vertical Radiance (Dayglow, Nightglow)

In Fig. 22 is shown a schematic representation of the infrared spectrum of air. The curve shows black-body emittance at 300° K in relative units. The hatched areas represent the spectral regions of appreciable absorption and emission due to CO_2, H_2O, and O_3. In Fig. 23 are given the cooling rates due to the 15 micron CO_2 band and to the 9.6 ozone band, according to calculations by Plass (1956).

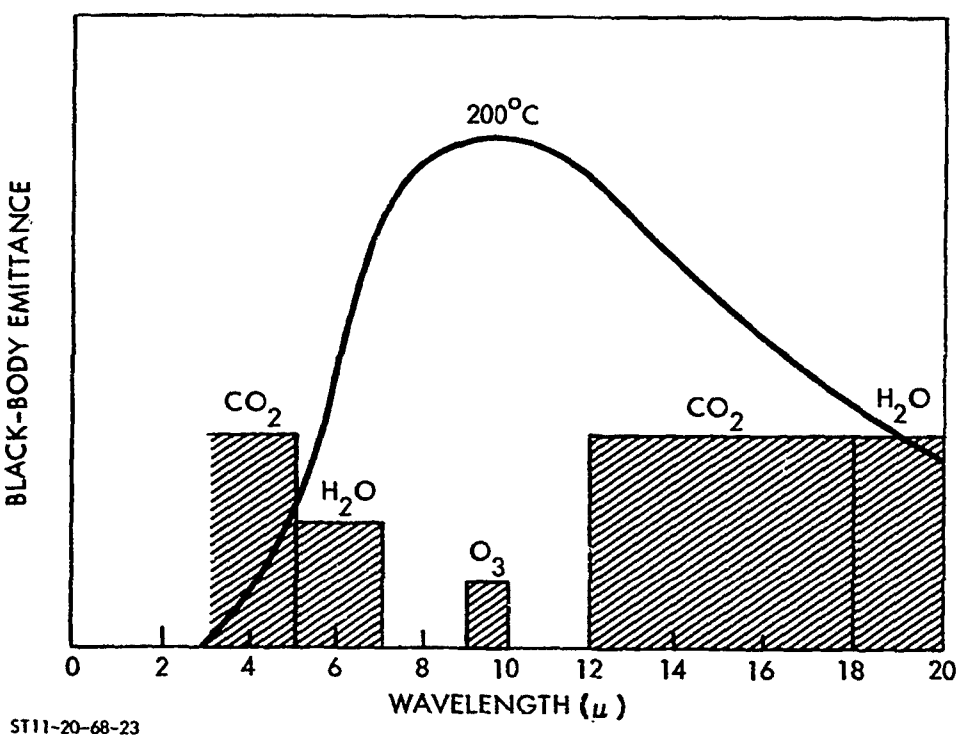

FIGURE 22. Infrared Spectrum of Air and Spectral Regions of Appreciable Absorption Due to CO_2, H_2O, and O_3 (After Craig, 1965)

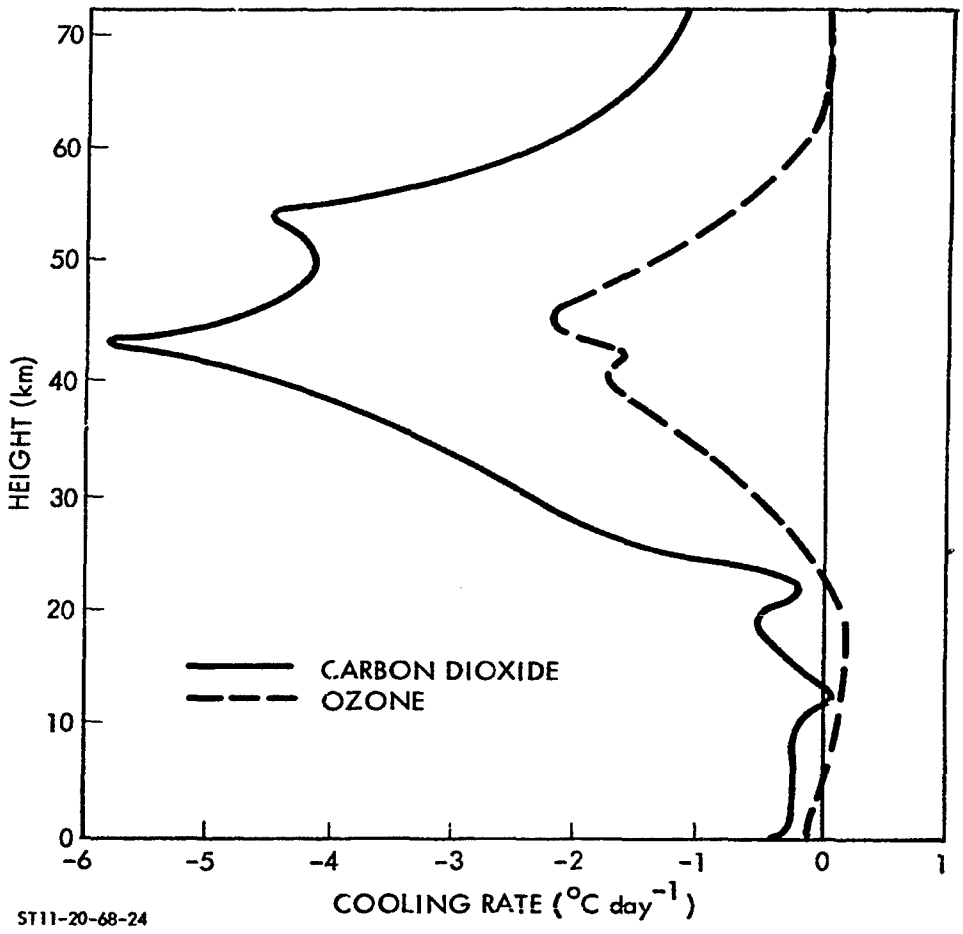

FIGURE 23. Cooling Rates Due to 15-μ CO_2 Band and 9.6-μ O_3 Band (After Plass, 1956)

II. PHYSICS OF THE TROPOSPHERE

The following review of the physics of the troposphere is an attempt to summarize, from a very large body of literature, the features of the troposphere which are pertinent to observations made from satellites. A particular need is to relate the features by some sort of generalization which makes possible an appreciation of the techniques for determination of tropospheric parameters. Treated first is an effort to appraise in general the magnitude and range of variation ("scale") of important atmospheric parameters in terms of spectral distribution in frequency, lifetime and dimension and in particular, the scale of those parameters treated in numerical weather prediction. By "numerical weather prediction" is meant the forecasting of weather for more than 24 hours ahead. This, as well as the analysis of the current weather situation, is accomplished by the use of high-speed electronic computing machines.

Following this general description of particular features of the troposphere is a review of some important features of the hydrodynamic theory of wave motion in the troposphere. Finally, some of the gross features of the general circulation of the atmosphere, involving both friction and heat sources and sinks, are described.

GENERAL DESCRIPTION OF PARTICULAR FEATURES OF THE TROPOSPHERE

The climate that we experience is affected by a variety of influences. Of these influences on climate (some of which have been listed by Landsberg [1945], and are shown in Fig. 24), a dominant one is insolation which has effects listed in Tables 2 to 4. At the surface of the earth some of these parameters of the weather have had extreme values (see Table 5). The scales of various phenomena

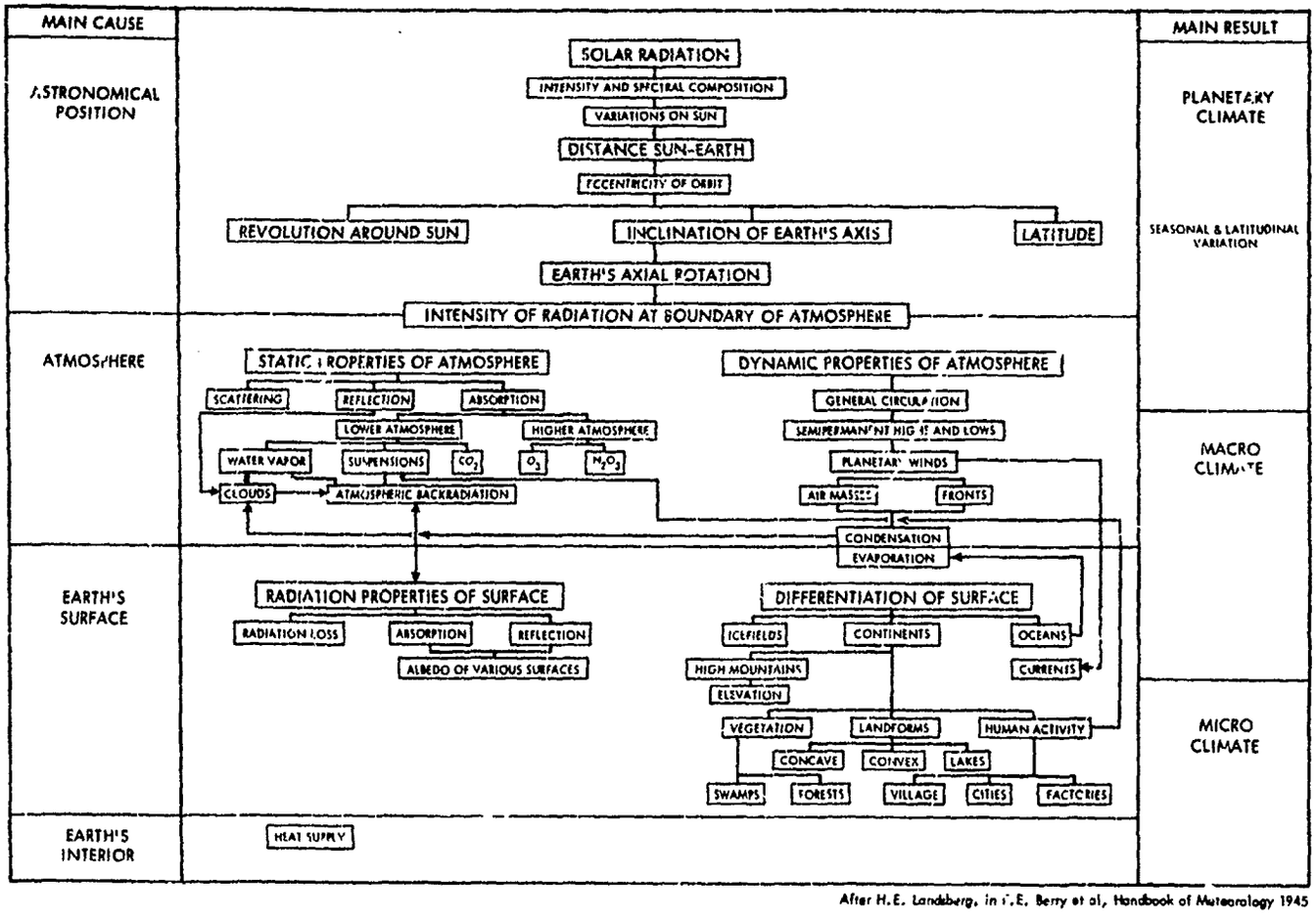

After H.E. Landsberg, in J.E. Berry et al, Handbook of Meteorology 1945

FIGURE 24. Influences on Climate

TABLE 2. ALBEDO OF SOLID AND SMOOTH SEA SURFACES

SOLID SURFACES				
TYPE OF SURFACE	CULTIVATED SOIL AND VEGETATION	SAND AREAS	FRESH SNOW	OLD SNOW AND SEA ICE
PERCENT REFLECTION	7-9	13-18	80-90	50-60

SMOOTH SEA SURFACE						
SOLAR ELEVATION, DEGREE	5	10	20	30	40	50-90
PERCENT REFLECTION	40	25	12	6	4	3

TABLE 3. MEAN DAILY HEAT SUM RECEIVED ON CLEAR DAYS IN VARIOUS LATITUDES OF THE NORTHERN HEMISPHERE

LATITUDE, DEGREE	0	15	30	45	60	75
HEAT SUM, CAL/CM^2/DAY	510	510	470	380	300	220

TABLE 4. HEAT BUDGET OF THE EARTH AS A WHOLE FOR AVERAGE DAY OF THE YEAR

HEAT RECEIVED BY	CAL/CM^2/DAY	HEAT LOST BY	CAL/CM^2/DAY
DIRECT SOLAR RADIATION	170	OUTGOING RADIATION	790
DIFFUSE RADIATION	140	EVAPORATION	120
BACK RADIATION FROM ATMOSPHERE	600		
TOTAL	910	TOTAL	910

AFTER H. E. LANDSBERG, IN F. E. BERRY ET AL, HANDBOOK OF METEOROLOGY 1945

TABLE 5. EXTREMES OF SOME CLIMATIC ELEMENTS OBSERVED ON EARTH*

ELEMENT	VALUE	LOCATION	IN THE UNITED STATES	
			VALUE	LOCATION
ABSOLUTE MAXIMUM TEMPERATURE	136°F	AZIZIYA, TRIPOLITANIA	134°F	GREENLAND RANCH, DEATH VALLEY, CALIF.
ABSOLUTE MINIMUM TEMPERATURE	-108°F	OIMEKON, SIBERIA, USSR	-66°F	RIVERSIDE, YELLOWSTONE PARK, WYO.
ABSOLUTE MAXIMUM PRESSURE	1,078 MB	WESTERN SIBERIA	1,060 MB	LANDER, WYO.
ABSOLUTE MINIMUM PRESSURE	887 MB	PACIFIC OCEAN, OFF PHILIPPINES	892 MB	LOWER MATECUMBE KEY, FLA.
ABSOLUTE MAXIMUM RAINFALL IN 24HR	46 IN	BAGUIO, PHILIPPINES	25.83 IN	CAMP LEROY, CALIF.
ABSOLUTE MAXIMUM RAINFALL IN 1 MONTH	241 IN	CHERRAPUNJI, INDIA		
HIGHEST MEAN ANNUAL RAINFALL	476 IN	MT. WAIALEALE, T.H.**	150 IN	WYNOOCHEE OXBOW, WASH.
ABSOLUTE MAXIMUM RAINFALL MEASURED IN 1 MIN.			1.02 IN	OPID'S CAMP, CALIF.
ABSOLUTE MAXIMUM WIND SPEED, ACCURATELY MEASURED			225 MPH	MOUNT WASHINGTON, N.H.
MAXIMUM MEAN WIND SPEED, ACCURATELY MEASURED FOR 5 MIN.	***	***	188 MPH	MOUNT WASHINGTON, N.H.
MAXIMUM MEAN WIND SPEED, ACCURATELY MEASURED FOR 1 HR			173 MPH	MOUNT WASHINGTON, N.H.
MAXIMUM MEAN WIND SPEED, ACCURATELY MEASURED FOR 24 HR			129 MPH	MOUNT WASHINGTON, N.H.

* THE VALUES GIVEN DO NOT INCLUDE MEASUREMENTS IN THE FREE ATMOSPHERE.

** VALUE BASED ON 7 YEARS OF INTERRUPTED RECORD. A COMPUTATION BY USING THE NORMAL VALUE AT A BASE STATION WITH LONG RECORD (FORMULA ON P. 958) YIELDS 462 IN. BOTH VALUES ARE DEFINITELY ABOVE THE LONG RECORD VALUE OF 428 IN. AT CHERRAPUNJI, INDIA.

*** FOR WINDS THE VALUES GIVEN FOR MOUNT WASHINGTON IN THE COLUMN FOR THE U.S. EXTREMES ARE THE HIGHEST THAT ARE ACCURATELY MEASURED AT STATIONS ON THE EARTH'S SURFACE. THEY ARE KNOWN TO HAVE BEEN EXCEEDED IN THE FREE ATMOSPHERE.

AFTER H. E. LANDSBERG, IN F. E. BERRY ET AL, HANDBOOK OF METEOROLOGY 1945

characteristics of the troposphere are essential features to be borne in mind in any analysis. These are the scales of the weather as we know it, to be sure, but the dimensions of the phenomena are not always clearly understood.

FREQUENCY SCALES OF TROPOSPHERIC MOTIONS

The characteristic spectrum of atmospheric motions is not well known. Its range of frequency may be comparable to its range of characteristic lengths, which ranges from the equator-to-pole distance (about 10^7 m) to atomic dimensions (about 10^{-10} m), a total range of 17 orders of magnitude. Some idea of wind speed spectra, made by measurement of wind speeds at Brookhaven, Long Island, and Caribou, Maine, from towers about 100 and 10 m high, respectively, and covering many orders of magnitude of frequency, has been described by van der Hoven (1957) and Oort and Taylor (1969), as shown in Fig. 25. The peak of power at periods of about four days corresponds perhaps to planetary wave propagation represented, for example, by the propagation of cyclones and anti-cyclones. The lesser peaks near the 12 and 24 hour periods correspond to the semidiurnal and diurnal tides. The peak near one minute seems to correspond to the motion associated with small-scale turbulence, familiar as gusts and lulls of wind. Oort and Taylor (1969) have also shown effects of aliasing from periods of one minute (the basic averaging period of the wind speed of the wind reports) and the two hour Nyquist frequency of their own study, with the assumption that the true spectrum at high frequency is the dotted curve which has been drawn to correspond with Van der Hoven (1957) data. The difference between the true data (the dotted curve) and the apparent but erroneous spectrum (solid line) is a dramatic demonstration of possible error of using one minute averaged observational data as inputs at two or three hour intervals for purposes of numerical weather analysis and prediction.

TIME SCALES FOR ATMOSPHERIC MOTIONS

In numerical weather analysis and prediction it is important to distinguish between large and small length-scales of weather phenomena.

In the past, the effort has been chiefly concerned with weather phenomena of large dimension on the supposition that the small-scale activity is embedded within the large-scale effects and is carried along with it.

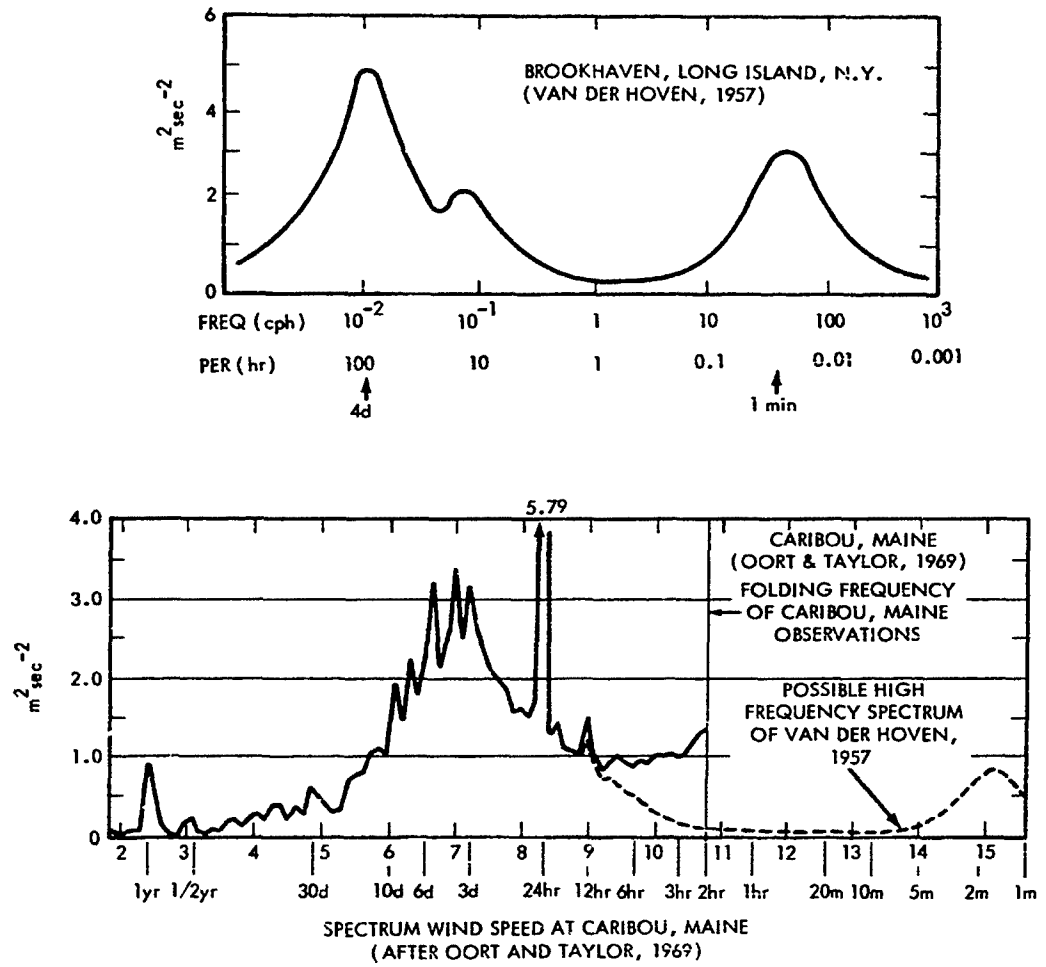

FIGURE 25. Horizontal Wind Speed Spectra

G. D. Robinson (1967) has suggested one basis for identifying specific time scales with specific space scales. He notes that the Navier-Stokes equation, the basic equation of hydrogynamics, is in the form

$$\frac{du}{dt}\left[\equiv \frac{\partial u}{\partial t} + u\,\frac{\partial u}{\partial x}\ \text{etc}\right] = \text{forces} + \nu\nabla^2 u, \text{ etc.} \qquad (2.1)$$

where ν is a coefficient of viscosity and u is a velocity component. It is concerned with the equation of motion of a fluid.

The lifetime of the "forms" of the fluid variations may be estimated to be of order

$$L^2 D \simeq L^2/\nu \qquad (2.2)$$

if L is a characteristic dimension and D is the coefficient of diffusion. Then, if the bulk velocity is U, the time for a form to travel distance L is L/U. A form cannot travel more than this distance as a recognizable entity if

$$L/U > L^2 D \qquad \text{(prediction impracticable)}$$

or if

$$LU\,D \simeq LU/\nu < 1 \qquad (2.3)$$

In turbulent conditions, the analog of Eq. 2.3 is

$$L/U > L^2/K \qquad \text{(prediction impracticable)}$$

or

$$LU/K < 1 \qquad (2.4)$$

wherein K is a lateral eddy diffusion coefficient for momentum appropriate to the length scale.

The scales L, K and ν are not independent of time; however, as an example by which the predictability time may be estimated, Robinson considers the following model: a region of diameter L with parabolic velocity distribution, zero at the boundary, maximum U. He has also taken:

$$\bar{u} = \frac{2}{3}U, \quad \overline{\left| u \frac{\partial u}{\partial x} \right|} = \frac{U^2}{L}, \quad \frac{\partial^2 u}{\partial y^2} = \frac{8U}{L^2} \tag{2.5}$$

Taking a particle to be accelerated to its maximum velocity by external forces and thereafter retarded by lateral diffusion of momentum, he equates average inertial and dissipative terms

$$\overline{\left| u \frac{\partial u}{\partial x} \right|} \simeq K \frac{\partial^2 u}{\partial y^2} \tag{2.6}$$

and finds that

$$K \simeq \frac{LU}{8} \tag{2.7}$$

The rate of dissipation of the energy of the large scale motion is

$$\epsilon = \bar{u} K \frac{\partial^2 u}{\partial y^2} = \frac{16}{3} K \frac{U^2}{L^2} = \frac{2}{3} \frac{U^3}{L} \tag{2.8}$$

By deriving U from (2.8) in terms of ϵ, and by substituting into (2.7), we find

$$K = \frac{1}{8}\left(\frac{3}{2}\right)^{1/3} \epsilon^{1/3} L^{4/3} \tag{2.9}$$

This is the Richardson's law (1926), which predicts that the diffusion of a pair of particles separated by a distance L has a diffusivity K proportional to $L^{4/3}$. The numerical coefficient $\frac{1}{8}\left(\frac{3}{2}\right)^{1/3} = 0.14$ obtained here is, however, at variance with that proposed by Richardson.

The limiting values of the frictional dissipation of kinetic energy tabulated by Robinson are $1 < \epsilon < 10$ cm^2 sec^{-3}, established from the observed radiation field without regard to atmospheric motion. Actually other observers have reported values of $\epsilon \sim 10^3$ cm^2 sec^{-3},

using Eq. 2.9, Robinson found, with his assumptions, the limits of K are

$$0.15L^{4/3} < K < 0.3L^{4/3} \qquad (2.10)$$

Robinson's values of the eddy diffusion coefficient K, bulk velocity U and predictability time $T = L/U = L^2/8\,K$ for the various scales of atmospheric motion are given in Table 6. For values of dissipation rate greater than those assumed by Robinson, predictability times are even shorter than those of Table 6.

Robinson's suggested relationship assumes that predictability time (or time interval over which a state is predictable) is the same as the lifetime (or the time over which a state may be expected to exist). That they are the same is controversial. Also, neither is likely to be the same as the scale time, which for phenomena of interest (length scale of 1000 km), is more than 10^5 sec, say about four days, as described in later paragraphs.

SCALE OF ATMOSPHERIC PARAMETERS FOR NUMERICAL WEATHER PREDICTION

The need for exact knowledge of atmospheric parameters for the purpose of numerical prediction of weather for more than 24 hours in advance has been reviewed by Phillips (1960). In his review, Phillips notes that J. G. Charney (1948) made useful estimates of space and time scales of the meteorologically important motions of the troposphere which may be numerically simulated with electronic computer computations.

Charney (1948) and Phillips (1960) have been guided by the experience of synoptic meteorologists who have found that the weather producing motions of the free atmosphere can be characterized as quasi-hydrostatic, quasi-adiabatic, quasi-horizontal and quasi-geostrophic. The theory is based on a kind of dimensional analysis similar to that used in the boundary layer theory of aerodynamics, in which the motion is characterized by a length parameter and a velocity parameter, in terms of which the orders of magnitude of the individual terms of the equations of motion are evaluated. In the

TABLE 6. VELOCITY, DIFFUSIVITY COEFFICIENT AND PREDICTABILITY TIME APPROPRIATE TO VARIOUS SCALES OF MOTION AND DISSIPATION RATES (After Robinson, 1967)

SCALE LENGTH L		DISSIPATION RATE	DIFFUSIVITY K	VELOCITY U	PREDICTABILITY TIME T	
KM	CM	CM^2SEC^{-3}	CM^2SEC^{-1}	$CM\ SEC^{-1}$	SEC	DAYS-HOURS MINUTES
5000	5×10^8	10	1.2×10^{11}	1.9×10^3	2.6×10^5	3.0_d
		1	5.8×10^{10}	9.4×10^2	5.4×10^5	6.3_d
500	5×10^7	10	5.8×10^9	9.4×10^2	5.4×10^4	15.0_{hr}
		1	2.7×10^9	4.2×10^2	1.2×10^5	1.4_d
50	5×10^6	10	2.7×10^8	4.2×10^2	1.2×10^4	3.3_{hr}
		1	1.2×10^8	2.0×10^2	2.5×10^4	6.9_{hr}
5	5×10^5	10	1.2×10^7	2.0×10^2	2.5×10^3	0.7_{hr}
		1	5.8×10^6	9.2×10^1	5.4×10^1	1.5_{hr}

Charney treatment, the parameters characterize the horizontal and vertical scales of motion, the speed of propagation of the streamline pattern, the horizontal particle speed, and the internal static stability.

Since the governing equations are non-linear and the small scale motions are not superposable on the large scale motions, it is not strictly proper to regard the two scales of motions as independent. However, in the atmosphere, since the bulk of the energy is associated with the large-scale systems, the small-scale motions may be regarded as turbulent fluctuations giving rise to small Reynolds' stresses and heat transports which, in the first approximation, may be ignored.

Charney's analysis begins by assigning the following orders of magnitude for the large-scale motions, which are assumed to be wave-like in shape:

S = horizontal scales mean horizontal distance between velocity extremes ($\sim 10^6$ m)

H = vertical distance scale, mean vertical distance between velocity extremes ($\sim 10^4$ m)

V = mean horizontal velocity (~ 10 m sec^{-1})

C = mean speed of propagation along horizontal streamlines (~ 10 m sec^{-1})

K = non-dimensional parameter characterizing the static stability of the atmosphere

$K = \frac{H}{T}\left(\gamma_d - \gamma\right)$ where γ_d = dry adiabatic lapse rate $\frac{g}{c_p}$ and γ is the actual lapse rate in the atmosphere ($\sim 10^{-1}$)

g = acceleration due to gravity (~ 10 m sec^{-2})

f = the z-component of the earth's vorticity, $f = 2\pi\Omega\sin\Phi$, where Ω is the angular speed of the earth's rotation about its axis and Φ is the latitude ($\sim 10^{-4}$ sec^{-1})

j = the y-component of the earth's vorticity, $j = 2\pi\Omega\cos\Phi$, ($\sim 10^{-4}$ sec^{-1}).

The first four of these are determined by observation of weather maps; values of K are given for normally observed lapse rates in the troposphere; values of f, j hold for latitudes between 0.5^{o} and 75^{o}.

The basic equations for the motions in the atmosphere are given by the equation of motion,

$$\frac{d\underset{\sim}{v}}{dt} = \frac{\partial \underset{\sim}{v}}{\partial t} + \underset{\sim}{v} \cdot \nabla \underset{\sim}{v} = -2\Omega \times \underset{\sim}{v} - \frac{\nabla \tau}{\rho} - g\hat{k} + \underset{\sim}{F} \qquad (2.11)$$

for which the components are written if we neglect external forces $\underset{\sim}{F}$, and viscous forces $\nabla\tau$

$$\frac{\partial u}{\partial t} + \left(\frac{u\partial u}{\partial x} + \frac{v\partial u}{\partial y} + \frac{w\partial u}{\partial z} \right) - fv + jw = \frac{-1}{\rho} \frac{\partial p}{\partial x}$$

$$\frac{\partial v}{\partial t} + \left(\frac{u\partial v}{\partial x} + \frac{v\partial v}{\partial y} + \frac{w\partial v}{\partial z} \right) + fu = \frac{-1}{\rho} \frac{\partial p}{\partial y}$$

$$\frac{\partial w}{\partial t} + \left(\frac{u\partial w}{\partial x} + \frac{v\partial w}{\partial y} + \frac{w\partial w}{\partial z} \right) + ju + g = \frac{-1}{\rho} \frac{\partial p}{\partial z} \qquad (2.12)$$

The equation of continuity of density ρ

$$\frac{\partial \rho}{\partial t} = -\underset{\sim}{v} \cdot \nabla \rho \qquad (2.13)$$

and the equation for the conservation of entropy s

$$\frac{\partial s}{\partial t} + \underset{\sim}{v} \cdot \nabla s = \frac{q}{T} \qquad (2.14)$$

In Eq. 2.14, the atmosphere is considered as a perfect gas,

$$s = c_v \ell n\, p - c_p \ell n\, \rho = c_p \ell n\, T - R \ell n\, p \qquad (2.15)$$

and the equation of state is

$$T = \frac{p}{R\rho} \qquad (2.16)$$

In these equations, $\underset{\sim}{v}$ is the velocity (three dimensional in u, v, w) relative to the rotating earth, $\hat{k}$ is the vertical unit vector, f is the z-component of earth's vorticity $2\pi \sin\Phi$, j is the corresponding South versus North (y axis) component ($2\Omega\cos\varphi$), Ω is the angular

speed of earth rotation, φ is the latitude, $\underset{\sim}{F}$ is the frictional force per unit mass, ρ is the density, p is the pressure, s is the specific entropy, q is the rate of heating per unit mass, T is the temperature, c_p and c_v are the specific heats at constant pressure and volume, and $R = c_p - c_v = 287\ m^2\ sec^{-2}\ deg^{-1}$ is the universal gas constant. Additional equations are required to describe the flux of water vapor and the condensation process.

A convenient measure of the entropy of dry air is the potential temperature which may be defined by $s = c_p \ell n\theta$ + constant, from which

$$\theta = \left(\frac{p_o}{p}\right)^{R/c_p} T \tag{2.17}$$

If the right side of the Eqs. 2.11 to 2.14 is expanded, operators like $\frac{\partial}{\partial x}$, $\frac{\partial}{\partial y}$, $\frac{\partial}{\partial z}$ appear in addition to the $\frac{\partial}{\partial t}$ operator. These may be assigned the order of magnitude

$$\frac{\partial}{\partial x} \sim \frac{\partial}{\partial y} \sim \frac{1}{S} = 10^{-6}\ m^{-1} \tag{2.18}$$

$$\frac{\partial}{\partial z} \sim \frac{1}{H} = 10^{-4}\ m^{-1} \tag{2.19}$$

$$\frac{\partial}{\partial t} \sim C\frac{\partial}{\partial x} = 10^{-5}\ sec^{-1} \tag{2.20}$$

Given these orders of magnitude, the following statements may be made:

1. The continuity Eq. 2.13 sets an upper limit on the value of the vertical velocity, which may also by the geostrophic approximation to have the value

$$W \lesssim \left(\frac{HV}{s} = 10^{-1} m\ sec^{-1}\right) \simeq 10^{-2}\ m\ sec^{-1} \tag{2.21}$$

2. Introduction of the inequality relation of Eq. 2.21 into the vertical component of the equation of motion (Eq. 2.11) shows that all terms are smaller by a factor of 10^{-4} than gravity

(g) and the vertical pressure force. This justifies the use of the hydrostatic equation

$$\frac{\partial p}{\partial z} = -\rho g \tag{2.22}$$

in place of the vertical component of Eq. 2.11 in which the second and third term of the left hand side effectively cancel each other.

3. Introduction of Charney's original scales and the inequality of Eq. 2.20 into the horizontal components of Eq. 2.11 shows that the horizontal components of the Coriolis acceleration ($\sim fV$) and the pressure forces are about ten times as large as the horizontal acceleration terms ($\sim V^2/S$). In this way, the geostrophic relations are justified:

$$u = -\frac{1}{\rho f}\frac{\partial p}{\partial y}, \quad v = \frac{1}{\rho f}\frac{\partial p}{\partial x} \tag{2.23}$$

Here the differentiation of p is carried out on a surface of constant z, which yields the same result if the differentiation of p takes place on a constant pressure surface whenever the hydrostatic relation Eq. 2.21 is valid. Phillips notes that the geostrophic approximation is not as good as the hydrostatic approximation and becomes worse at higher velocities (when V/S increases) and at low latitudes (when f decreases).

4. Introduction of the hydrostatic Eq. 2.21 and the geostrophic approximations 2.12 into the first law of thermodynamics Eq. 2.14 and disregarding q/T, as though the process were adiabatic, leads to a refined estimate of W, given by the equality of Eq. 2.21. The small value of W so implied means that the vertical advection terms $\frac{w\partial u}{\partial z}$ and $\frac{w\partial v}{\partial z}$ on the left side of the component Eq. 2.11 are even less important than the horizontal advection terms $\frac{u\partial u}{\partial x}$ by factor $\frac{1}{10}$ and should be neglected in any theory based on Eqs. 2.22 and 2.23. The

acceleration of the horizontal wind may be computed as if the motion were purely horizontal. A further conclusion stemming from the inequality (W/H) < (V/S) is that the horizontal divergence

$$\nabla_p \cdot (\hat{i}u + \hat{j}v) \sim \frac{W}{H} \tag{2.24}$$

is smaller than the vorticity of the horizontal wind

$$\zeta = \hat{k} \cdot \zeta \nabla_p \times (\hat{i}u + \hat{j}v) \sim \frac{V}{S} \tag{2.25}$$

By a slightly different analysis, Burger (1958) has shown that the inequality (W/H) < (V/S) becomes an equality when S is as large as 10^7m, comparable to the radius of the earth. This invalidates the geostrophic theory for predicting motions of such great horizontal extent.

5. The horizontal increments of the pressure and density fields are of the same magnitude as their mean values, and vary in the same horizontal scale S as do the velocity increments. Similarly the vertical increments of pressure and density vary in the same vertical scale H as do the velocity increments, and are of the same order as the pressure and density itself. Accordingly, Charney notes by using Eqs. 2.22 and 2.23

$$\frac{\partial \ell n p}{\partial x} \sim \frac{\partial}{\partial y} \ell n p \sim \frac{fV}{gH} = 10^{-8} \; ; \quad \frac{\partial \ell n \rho}{\partial x} \sim \frac{\partial \ell n \rho}{\partial y} \sim \frac{fV}{gH} = 10^{-8} \tag{2.26}$$

and

$$\frac{\partial}{\partial z} \ell n p \sim \frac{1}{H} = 10^{-4}; \quad \frac{\partial}{\partial z} \ell n p \sim \frac{1}{H} = 10^{-4} \tag{2.27}$$

Differentiating Eq. 2.17 with respect to x or y, and substituting Eqs. 2.26 and 2.27 yields

$$\frac{\partial}{\partial x} (\ell n \theta) \sim \frac{fV}{gH} = 10^{-8}; \quad \frac{\partial}{\partial y} (\ell n \theta) \sim \frac{fV}{gH} = 10^{-8} \tag{2.28}$$

Then using Eq. 2.20 yields

$$\frac{\partial}{\partial t}(\ell n\theta) \sim \frac{fCV}{gH} = 10^{-7} \tag{2.29}$$

Applying the geostrophic and hydrostatic Eqs. 2.22 and 2.23 and the equality 10 giving W into the equation

$$\frac{d\bar{v}_n}{dt} = \frac{d_n\bar{v}_n}{dt} + w\frac{\partial\bar{v}_n}{\partial z} \tag{2.30}$$

Charney obtains

$$\frac{du}{dt} \sim \frac{dv}{dt} \sim \frac{cv}{s} \div \frac{fcv^2}{gHK} \sim 10^{-4}\left(1 + \frac{10^{-2}}{K}\right) \tag{2.31}$$

So it may be seen that the term in $d\bar{v}_h/dt$ involving w is one order of magnitud: smaller than the other. Similarly, Eqs. 2.22, 2.23, and the equality of 10, taken with Eq. 2.26 yields

$$\frac{d}{dt}(\ell np) = \frac{d_h(\ell np)}{dt} - w\frac{\partial}{\partial z}(\ell np) \sim$$

$$\left[\frac{fCV}{gH}\left(1 + \frac{1}{K}\right) = 10^{-7} + 10^{-6}\right] \sim \frac{w\partial\ell np}{\partial z} \tag{2.32}$$

The implication of Eq. 2.32 is that the individual change in pressure is due almost entirely to the vertical motion, and hence,

$$\frac{d\bar{v}_h}{dt} \approx \frac{d_h\bar{v}_h}{dt} \tag{2.33}$$

By similar reasoning, Charney shows

$$\frac{d(\ell n\rho)}{dt} \sim \frac{w\partial\ell n\rho}{\partial z} \tag{2.34}$$

Using Eqs. 2.18, 2.20, 2.21, and 2.34 in the equation of continuity (Eq. 2.13 written out component by component) yields

$$\frac{\partial u}{\partial x} + \frac{\partial v}{\partial y} \sim \frac{fCV}{gHK} \sim 10^{-6} \text{ sec}^{-1} \tag{2.35}$$

Contrasting this result with $\frac{\partial u}{\partial x} \sim \frac{\partial v}{\partial y} \sim \frac{v}{s} = 10^{-5} \text{ sec}^{-1}$ shows that the terms $\frac{\partial u}{\partial x}$ and $\frac{\partial v}{\partial y}$ comprising the horizontal divergence tend to compensate each other, explaining perhaps the ever present difficulties of computing mutually consistent values of horizontal divergence. In short, because of the compensation, it may be impractical to compute divergence at all.

Charney's analysis leads from the hydrostatic Eq. 2.22 and the approximation 2.21 to the form of the Eulerian equations most often used in meteorology

$$\frac{d_h \underset{\sim}{v}_h}{dt} + f\hat{k} \times \underset{\sim}{v}_h = -\frac{1}{\rho} \nabla_h p \tag{2.36}$$

$$g = -\frac{1}{\rho} \frac{\partial p}{\partial z} \tag{2.37}$$

These scales, developed by Charney, are summarized in Table 7.

HYDRODYNAMIC THEORY OF WAVE MOTION IN THE TROPOSPHERE

A most powerful tool aiding the understanding of the dynamics of the atmosphere below the ionosphere is the hydrodynamic theory of wave motion. In addition to obviously periodic phenomena, even one-time only, short-time event may be described and understood in terms of wave motion theory. Since that theory is rewarding to the student of atmospheric physics, it will be discussed at some length in the following pages, reviewing the basic hydrodynamic equations, linearization of the equations with some other approximations useful in the study of the troposphere, some special forms of the equations of limited, but useful applicability, and analyses of typical problems which may be closely identified with meteorological phenomena. This section follows the development of the review by Eliassen and Kleinschmidt (1957).

TABLE 7. SCALES OF WEATHER PREDICTION

PARAMETER		SCALE	NOTE
HORIZONTAL DISTANCE	S	10^6 m	
VERTICAL DISTANCE	H	10^4 m	
HORIZONTAL VELOCITY	V	10 m sec^{-1}	
HORIZ. VEL. GRADIENT	V/S	10^{-5} sec^{-1}	$\left(\frac{\partial u}{\partial x}+\frac{\partial v}{\partial g}\right)\sim 10^{-6}$ sec^{-1}
HORIZ. ACCELERATION	CV/S	10^{-4} m sec^{-2}	$\frac{1}{10}$ HORIZONTAL CORIOLIS FORCE
VERTICAL VELOCITY	W	10^{-2} m sec^{-1}	
VERT. VEL. GRADIENT	W/S	10^{-5} sec^{-1}	
VERT. ACCELERATION	CW/S	10^{-8} m sec^{-2}	10^{-7} ACCELERATION OF GRAVITY
VELOCITY OF METEOR. PROP.	C	10 m sec^{-1}	
VEL. PROP. OF GRAV. WAVES		10^2 m sec^{-1}	
VEL. PROP. OF TIDAL WAVES		10^2 m sec^{-1}	
LOG POT. TEMPERATURE ($\theta = RT_p^{\gamma-1}$)	K	10^{-1}	STATIC STABILITY $K = H\frac{\partial \ell n\theta}{\partial z} \cong 10^{-1}$, $\gamma = \frac{c_p}{c_v}$
TIME RATE OF LOG POT. TEMP.	fCV/gH	10^{-7} sec^{-1}	$R = c_p - c_v$
ACCELERATION OF GRAVITY	g	10 m sec^{-2}	NEGLIGIBLE FOR $\Delta z < 63$ km
HORIZ. CORIOLIS FORCE	fV	10^{-3} m sec^{-2}	
HORIZ. EARTH VORTICITY $f=2\pi\Omega\sin\varphi$		10^{-4} sec^{-1}	
VERTICAL CORIOLIS FORCE	jW	10^{-6} m sec^{-2}	10^{-4} ACCELERATION OF GRAVITY
VERTICAL EARTH VORTICITY $j=2\pi\Omega\cos\varphi$		10^{-4} sec^{-1}	
LATITUDE	φ	$\left(0-\frac{\pi}{2}\right)$ rad	
LOG PRESSURE	ℓn p	1	
HORIZ. GRAD. OF LOG PRESS	fV/gH	10^{-8} m^{-1}	
TIME RATE OF LOG PRESS	$\frac{fV}{gH}\left(1+\frac{1}{K}\right)$	10^{-6} sec^{-1}	
LOG DENSITY	ℓn p	1	
HORIZ. GRAD. OF LOG DENSITY	fV/gH	10^{-8} m^{-1}	
TIME RATE OF LOG DENSITY	$\frac{fCV}{gH}\left(1+\frac{1}{K}\right)$	10^{-6} sec^{-1}	
TIME	S/C	10^5 sec	

Basic Hydrodynamic Equations

In Cartesian coordinates, the complete set of equations governing the atmosphere are the following.

The equations of motion -

$$\frac{\partial u}{\partial t} + u\frac{\partial u}{\partial x} + v\frac{\partial u}{\partial y} + w\frac{\partial u}{\partial z} = 2\Omega\,(v\sin\Phi - w\cos\Phi) - \frac{1}{\rho}\frac{\partial p}{\partial x} + \frac{1}{m}F_x \quad (2.38)$$

$$\frac{\partial v}{\partial t} + u\frac{\partial v}{\partial x} + v\frac{\partial v}{\partial y} + w\frac{\partial v}{\partial z} = -2\Omega u\sin\Phi - \frac{1}{\rho}\frac{\partial p}{\partial y} + \frac{1}{m}F_y \quad (2.39)$$

$$\frac{\partial w}{\partial t} + u\frac{\partial w}{\partial x} + v\frac{\partial w}{\partial y} + w\frac{\partial w}{\partial z} = 2\Omega u\cos\Phi - \frac{1}{\rho}\frac{\partial p}{\partial z} + \frac{1}{m}F_z - g \quad (2.40)$$

and the equation of continuity -

$$\frac{\partial \rho}{\partial t} + u\frac{\partial \rho}{\partial x} + v\frac{\partial \rho}{\partial y} + w\frac{\partial \rho}{\partial z} = -\rho\left(\frac{\partial u}{\partial x} + \frac{\partial v}{\partial y} + \frac{\partial w}{\partial z}\right) \quad (2.41)$$

These are the four equations in five dependent variables, u, v, w, ρ, and p. A fifth relationship, an "equation of state," is usually derived from some physical restriction on the system based on the first law of thermodynamics, for example:

$$Tds = de + p\,d\left(\frac{1}{\rho}\right) = dh - \frac{1}{\rho}dp$$

$$= C_p dT - \frac{1}{\rho}dp = C_v dT + p\frac{d\left(\frac{1}{\rho}\right)}{dt} \quad (2.42)$$

The thermodynamic, or internal energy, of dry air may be described by the equation

$$\frac{De}{Dt} = -p\frac{D\left(\frac{1}{\rho}\right)}{Dt} + \delta + \frac{Dq}{Dt} \quad (2.43)$$

wherein $\delta = \frac{1}{\rho}F\cdot\nabla v$, Stokes viscous dissipation function and D represents the Eulerian derivative

$\frac{Dq}{Dt}$ = heat received per unit mass and unit time

$e = C_v T$ + constant = internal energy per unit mass of dry air

δ = entropy per unit mass of dry air.

The thermodynamic equation indicates that internal energy may be increased by compression, dissipation and heat supply.

As long as the effects of water vapor are ignored, the thermodynamic-hydrodynamic state of the atmosphere is characterized by the velocity field $\underset{\sim}{v}$ and the two scalar fields p and ρ. The change with time of these fields is described by the above equations of motior, continuity, and thermodynamic energy.

The effect of water vapor may be taken into account by introducing the specific humidity as another dependent variable, for which must be introduced the continuity equation for the water component, and a suitable energy equation.

Denoting the partial pressure and density of water vapor by p' and ρ', its equation of state may be written

$$\rho' = \sigma \frac{p'}{RT} \tag{2.44}$$

wherein R is the gas constant of dry air, and $\sigma = 0.622$ is the relative density of water vapor with respect to dry air. The enthalpy of water vapor is

$$h' = c_p' T + \text{constant}$$

and of liquid water is

$$h'' = c'' T + \text{constant}$$

wherein c_p' is the specific heat of water vapor at constant pressure, c'' is the specific heat of liquid water, and the latent heat of evaporation is given by

$$L = h' - h'' \tag{2.45}$$

The enthalpy of water vapor may also be written

$$h' = c''T + L + \text{constant} \tag{2.46}$$

The mixing ratio is defined as

$$\mu' = \frac{\rho'}{\rho d} = \sigma \frac{p'}{p - p'} \tag{2.47}$$

It is a small quantity, of the order 1% in the lower troposphere and still smaller at greater heights. In unsaturated air it changes only as a result of diffusion and turbulent mixing, a slow process. In many cases the mixing ratio may be considered a constant. In this case, the enthalpy per unit mass of moist unsaturated air

$$h = \frac{c_p + \mu' c''}{1 + \mu'} T + \frac{\mu'}{1 + \mu'} L + \text{constant} \tag{2.48}$$

may be approximated by

$$h \approx c_p T + \mu' L + \text{constant} \tag{2.49}$$

and the energy equation for unsaturated moist air is

$$TDs = Dh - \frac{1}{\rho} Dp \tag{2.50}$$

as in the case of the dry air energy equation. Thus, nonsaturated air behaves in this approximation in the same way as dry air. In particular, the isentropic change of state will be very nearly unaffected by the humidity.

The case of saturated air is, however, different. If a mass of moist air contains liquid water, so that one mass unit of dry air is associated with μ' mass units of water vapor and μ'' mass units of liquid water, the vapor may be assumed to be in equilibrium with the liquid phase so that

$$p' = P(T) \tag{2.51}$$

wherein P(T) denotes the saturation pressure of water vapor with respect to liquid water with a plane interface. In this case, the mixing ratio is

$$\mu' = \sigma \frac{P(T)}{p - P(T)} \approx \sigma \frac{P(T)}{p} \tag{2.52}$$

that is, the mixing ratio in saturated air is no longer a small constant, but is a function of both p and T. The quantity will change as a result of condensation and evaporation.

The total mass of the water component per unit mass of dry air is

$$\mu = \mu' + \mu''$$

In the absence of diffusion, turbulent mixing and precipitation, one has an equation of continuity,

$$\frac{D\mu}{Dt} = 0 \tag{2.53}$$

The enthalpy per unit mass of the two-phase system is

$$h = \frac{c_p + \mu c''}{1 + \mu} T + \frac{\mu'}{1 + \mu} L + \text{constant} \tag{2.54}$$

and the energy equation is

$$TDs = Dh - \frac{1}{\rho} Dp \approx \left(c_p + \frac{\sigma L}{p} \frac{dP}{dt}\right) DT - \left(\frac{1}{\rho} + \sigma \frac{LP}{p^2}\right) Dp \tag{2.55}$$

The difference between the saturated case and the nonsaturated case is apparent from consideration of the entropy equations.

From the above considerations, one may see that the thermodynamic properties of atmospheric air are such that nonsaturated or clear air behaves nearly like dry air, regardless of humidity, and saturated or cloudy air has properties differing from those of nonsaturated air and which are nearly independent of the content of the liquid water or ice. The total content of the water constituent is primarily important as a means of determining when saturation will begin and

end, and as means of distinguishing between the two alternate forms of the energy equation.

Complete Linearized Equations

Since the complete non-linear equations of thermodynamics and hydrodynamics are difficult to solve, many efforts have been made to linearize the equations by considering only small departures from a state of static equilibrium.

The complete linearized equations of motion, derived by the methods of perturbation theory which result in omission of the advection term $\bar{u}\cdot\nabla$, are given in a convenient form by Eckart (1960) in the form:

$$\frac{\partial \underset{\sim}{u}}{\partial t} + Co(v + \Gamma\hat{\zeta})\, P - N^2 Q + \underset{\sim}{\Omega} \times \underset{\sim}{U} = \underset{\sim}{F} \qquad (2.56)$$

The equation of continuity of pressure is

$$\frac{\partial P}{\partial t} + Co\ v.\underset{\sim}{U} = G \qquad (2.57)$$

The equation for conservation of entropy is

$$\frac{\partial Q}{\partial t} = \hat{\zeta}.\underset{\sim}{U} = H \qquad (2.58)$$

Expressed in spherical coordinates (r, θ, λ), where r is the distance from earth center, λ is longitude measured from west to east, and θ is latitude measured from equator north, the equations become

$$\frac{\partial Ur}{\partial t} + Co\,\frac{\partial P}{\partial r} + Co\,\Gamma P - N^2 Q - \Omega\cos\theta U_\lambda = F_r \qquad (2.59)$$

$$\frac{\partial U_\lambda}{\partial t} + \frac{Co}{r\cos\theta}\frac{\partial P}{\partial \lambda} - \Omega\sin\theta U_\theta + \Omega\cos\theta U_r = F_\lambda \qquad (2.60)$$

$$\frac{\partial U\theta}{\partial t} + \frac{Co}{r}\frac{\partial P}{\partial \theta} + \Omega\sin\theta U_\lambda = F_\theta \qquad (2.61)$$

$$\frac{\partial P}{\partial t} + Co\,\frac{\partial Ur}{\partial r} + \frac{Co}{r\cos\theta}\frac{\partial U\lambda}{\partial \lambda} + \frac{Co}{r} = G \qquad (2.62)$$

$$\frac{\partial Q}{\partial t} + Ur = H \qquad (2.63)$$

wherein boundary conditions are

$$Ur = 0 \qquad \text{at} \qquad r = r_s \tag{2.64}$$

$$Ur = 0 \qquad \text{at} \qquad r = \infty \tag{2.65}$$

and the variables of the field equations are

$$\underset{\sim}{U} = (\rho_o C_o)^{\frac{1}{2}} \underset{\sim}{v}_1 \qquad \Gamma = \frac{1}{2}\frac{d}{dz}(\log \rho_o C_o) + \frac{g}{C_o^2}$$

$$P = (\rho_o C_o)^{-\frac{1}{2}} p_1 \qquad G = \frac{\rho_o(\gamma - 1)}{(\rho_o C_o)^{\frac{1}{2}}} q_1$$

$$Q = \left[\frac{ds_o}{dz}\rho_o C_o\right]^{-\frac{1}{2}} \rho_1 \qquad H = \frac{(\rho_o C_o)^{\frac{1}{2}}}{T_o\left(\frac{ds_o}{dz}\right)} \cdot q_1$$

$$\underset{\sim}{F} = (\rho_o C_o)^{\frac{1}{2}} \underset{\sim}{f}_1 \qquad N = \left[\frac{(\gamma - 1)}{C_o^2} T_o \frac{ds_o}{dz}\right]^{\frac{1}{2}} \tag{2.66}$$

The chief error introduced by the linearization is the elimination of $(\bar{v} \cdot \text{grad } \bar{v})$ of the complete equations. In the perturbation theory approximation, in which $\bar{v}_c = 0$, the term falls out. However, for many tropospheric phenomena involving large scale motions, the perturbation theory approximation is not applicable, and the non-linearity must be taken into account.

The subscripts o and 1 imply steady state and first order perturbations, respectively, of the variables, which may be written as functions of (r, θ, λ, t)

Velocity	Velocity Change	
$\underset{\sim}{v}_o = 0$	$\underset{\sim}{v}_1 = \underset{\sim}{v}_1$	(2.67)
Pressure	**Pressure Change**	
$p_o = p_o(z)$	$p_1 = p_1$	(2.68)

Density

$$\rho_o = -\frac{1}{g}\frac{dp_o}{dz} = \frac{g}{RT_o}p_o$$

Force

$$\underset{\sim}{f}_o = 0$$

Density Change

$$\rho_1 = \rho_1 \qquad (2.69)$$

Force Change

$$\underset{\sim}{f}_1 = \rho_o \nabla . G_m - F.\nabla p_o$$

where F = Frictional stress tensor

G_m = Tidal force potential of moon less that of the earth

$$= \frac{3}{2} Kg\ M \frac{r^3}{D^3}\left(\frac{1}{3} - \cos^2\theta\right)$$

M = Moon mass

Kg = Gravitational constant

θ_m = Moon-zenith distance

r = Distance from earth center

D_m = Moon distance from earth center (2.70)

Entropy

$$S_o = \rho_o(c_p \ell n T_o - R \ell n p_o + \text{constant}) = \rho_o(c_v \ell n p_o - c_p \ell n \rho_o + \text{constant})$$

Entropy Change

$$S_1 = \rho_o\left[\int \frac{\sigma L}{p}\frac{dP}{dT}\frac{DT}{T} - \int \frac{\sigma LP}{p^2 T} Dp\right] + \rho_o \int \frac{\Delta t (q_1 + \delta)dt}{T_o} \qquad (2.71)$$

q_1 = Energy density flux

δ = Frictional dissipation = $\frac{F}{\rho}\nabla.\bar{v} \cong 0$

Latent heat of sublimation entropy change indicated within square brackets

L = Latent heat of sublimation

σ = Relative density of water vapor with respect to dry air

$$\sigma = 0.622 \qquad (2.72)$$

P = Saturation pressure of water vapor

$$P = P(T) \qquad (2.73)$$

Total heat accession

$$q_o = 0$$

Heat accession change

$$q_1 = q_c + q_v + q_{conv} + q_{corp} + q_{rad} - q_R \qquad (2.74)$$

Heat by conduction

$$q_c(z) = \rho_o \nabla.(K\nabla T_o) \qquad (2.75)$$

K = Thermal conductivity

Heat by viscous dissipation

$$q_v(z) = \mu\rho \frac{w^2}{L^2}$$

μ = Coefficient of viscosity

w = Vertical velocity dz/dt

L = Characteristic length (2.76)

Heat by convection

$$q_{conv}(z) = -\rho c_p w \frac{\partial T}{\partial z} \qquad (2.77)$$

Heat by absorption of radiation

$$q_{rad}(z) = \rho_o \sum_{\lambda} \sum_{i} \epsilon_{i_\lambda} n_i(z,t) F(\lambda) \sigma e^{-T_{i_\lambda}}$$

τ_{i_λ} = Optical thickness = $\int_z^\infty \sigma_{i_\lambda} \frac{n_i(z,t)}{\cos\Xi}\, dz$

F_λ = Flux at top of atmosphere

σ'_{i_λ} = Photoionization cross section

σ_{i_λ} = Total absorption cross section

Ξ = Solar zenith angle

ϵ_{i_λ} = Efficiency factor for conversion to heat (ergs photon^{-1}) (2.78)

Heat by absorption of corpuscular radiation

$q_{corp}(z)$ as in $q_{rad}(\dot{z})$ where ϵ_{i_λ}

ergs per particle (2.79)

Heat loss by radiative emission

$$q_R(z) = \rho_o \left[\int K_\nu B_\nu(T) d\nu + \frac{1.68(10)^{-18} e^{\frac{-228}{T_o}}}{1 + 0.6e^{\frac{-228}{T_o}} + 0.2e^{\frac{-325.3}{T}}} \right]$$

K_ν Mass absorption coefficient

B_ν Planck blackbody function (2.80)

Other Approximations and Special Forms

A number of approximations to the complete equations, other than linearization, are commonly used. The other approximations usually take $(\underset{\sim}{v}.\nabla)\underset{\sim}{v}$ into account, but simplify equations to eliminate modes of motion usually associated with gravity waves.

None of these are applicable at all altitudes and latitudes except as rules of thumb for which the crudest ones - the geostrophic equation for wind and the hydrostatic equation serve at mid-latitudes and low altitudes with about 20% uncertainty.

1. Quasi-static Approximation

The quasi-static approximation is one in which

a. Vertical acceleration is ignored in Eq. 2.40

$$\frac{dUr}{dt} = 0$$

b. Horizontal component of Coriolis force is ignored in Eqs. 2.38 and 2.39

Horizontal $f = 2\Omega\cos\theta = 0$
Vertical $\lambda = 2\Omega\sin\theta$

c. $\left(\frac{DU}{Dt}\right)_h$ becomes $\frac{DU_h}{Dt}$

d. $\mathrm{div}_h(\rho U)$ becomes $\mathrm{div}_h(\rho U_h)$ (2.81)

If the approximation $\frac{dUr}{dt} = 0$ is applied consistently, it is found that the eigenfrequencies (linear response to small perturbations) are not all real. Such an approximation completely changes the character of the solution. The application of setting Ω COS $\theta = 0$ is also in many cases done carelessly. If done at all, Ω COS θ must be set to zero in all equations, not only in Eq. 2.59, where it makes the most difficulty for easy solutions. If Ω COS θ U_r is omitted from Eq. 2.59, but the term Ω COS θ U_λ

retained in Eq. 2.58, the equations cease to be self-adjoint, that is eigenfrequencies become complex, and the nature of solutions is completely altered.

Although in many circumstances it is possible to justify the two approximations $\frac{dUr}{dt} = 0$ and $\Omega \cos\theta = 0$, the former seems likely to be untrue at high altitudes, and the latter is certainly untrue in the tropics.

2. Geostrophic Approximations

The geostrophic approximation includes the quasi-static approximation discussed above, and, as well, that the Coriolis parameter is constant

$$\Omega \cos\theta = 0$$

$$f = 2\Omega \sin\theta = \text{constant},$$

that the earth's curvature is neglected, that there is no friction $F = 0$ in Eqs. 2.58, 2.59 and 2.60 and that all processes are adiabatic

$$Q = G = H = 0 \tag{2.82}$$

in Eqs. 2.58, 2.61 and 2.62. The Eqs. 2.58 to 2.62, therefore, reduce to

$$\frac{\partial p}{\partial x} = \frac{1}{r}\frac{\partial p}{\partial \theta} = 0 \tag{2.83}$$

$$\frac{\partial p}{\partial y} = \frac{1}{r\cos\theta}\frac{\partial p}{\partial \lambda} = -2\Omega \sin\theta\ \rho\ U_\lambda\ (\rho_o c_o)^{-\frac{1}{2}}$$

$$= -2\Omega \sin\theta\ \rho\ U \tag{2.84}$$

$$\frac{\partial p}{\partial z} = \frac{\partial p}{\partial r} = -g\ \rho \tag{2.85}$$

This approximation yields handy, easily remembered rules of thumb; the hydrostatic equation

$$\rho = -\frac{1}{g}\frac{\partial p}{\partial z} \tag{2.86}$$

and the geostrophic equation

$$\underset{\sim}{v}_g = \hat{k} \times \frac{1}{\rho(2\,\Omega \sin\theta)} \nabla_h p = \hat{k} \times \frac{R}{\rho(2\,\Omega \sin\theta)} \nabla_h T \tag{2.87}$$

with solutions true within 10 to 20% error in mid-latitudes, and in high latitudes.

It will not be valid at high altitudes and in the tropics.

The geostrophic wind blows in a direction normal to the horizontal pressure gradient with lower pressure to the left in the northern hemisphere (to the right in the southern hemisphere). The geostrophic wind vector is directed along the isobars in a horizontal surface, or what is equivalent along the contour lines of an isobaric surface.

A measure of the error of the geostrophic wind equation is given by the geostrophic departure

$$\underset{\sim}{v}_h - \underset{\sim}{v}_g = \hat{k} \times \frac{1}{f}\left(\frac{D\underset{\sim}{v}_h}{Dt}\right)_n \tag{2.88}$$

In the absence of friction, the geostrophic departure $\underset{\sim}{v}_h - \underset{\sim}{v}_g$ is an expression for the horizontal acceleration. The geostrophic departures are generally of the order 1 to 10 m sec^{-1} -- hence, on the average are 10 to 20% of the wind.

Differentiation of the geostrophic wind equation with respect to altitude z yields the Thermal Wind Equation

$$\frac{\partial \underset{\sim}{v}_g}{\partial z} = -\frac{1}{f}\left(\hat{k} \times \frac{\partial}{\partial z}\left(\frac{1}{\rho}\text{grad}_n p\right)\right) = -\frac{g}{f}\left[\hat{k} \times \frac{\partial}{\partial z}\left(\rho\ \text{grad}_p\left(\frac{1}{\rho}\right)\right)\right]$$

$$= -\frac{g}{f}\left(\hat{k} \times \frac{\partial}{\partial z}\left(\frac{\text{grad}_p T}{T}\right)\right) \tag{2.89}$$

3. Quasi-geostrophic Approximation

The quasi-geostrophic approximation includes the geostrophic approximation

$$\frac{dUr}{dt} = 0 \qquad \text{in Eq. 2.58}$$

$$\Omega\cos\theta = 0 \qquad \text{in Eqs. 2.58 and 2.59}$$

$$\Omega\sin\theta = 0 \qquad \text{in Eqs. 2.59 and 2.60}$$

$$\mathcal{E} = 0 \qquad \text{in Eqs. 2.58, 2.59 and 2.60}$$

$$Q = 0 \qquad \text{in Eqs. 2.58 and 2.62}$$

$$G = H = 0 \qquad \text{in Eqs. 2.61 and 2.62} \qquad (2.90)$$

In addition to the geostrophic approximations, since the horizontal divergence is much smaller than relative vorticity, the quasi-geostrophic approximation assumes that the motion is rotational, not solenoidal, and hence, that the horizontal pressure gradient is quasi-balanced by the geostrophic wind field. The equations also neglect certain terms required by conservation of vorticity.

The quasi-geostrophic equations are useful in high and mid-latitudes. The solution of the equations requires both upper and lower boundaries as well as lateral boundaries.

The approximation is not applicable to high altitudes and the tropics.

4. Quasi-solenoidal Approximation

The quasi-solenoidal approximation uses all the quasi-static approximations

$$\frac{dUr}{dt} = 0$$

$$\Omega\cos\theta = 0$$

$$F = 0$$

$$Q = 0$$

$$G = H = 0 \qquad (2.91)$$

However, it partitions

$$\underset{\sim}{v}_h = \underset{\sim}{v}_\psi + \underset{\sim}{v}_\epsilon$$

so that v_ψ is the solenoidal part; for which

$$\nabla_p \cdot \underset{\sim}{v}_\psi = 0$$

and v_ϵ is the nonrotational part; for which

$$\nabla_p \times \underset{\sim}{v}_\epsilon = 0 \qquad (2.92)$$

Since $\nabla_p \cdot \underset{\sim}{v}_h \ll (\zeta = \hat{k} \cdot \nabla \times \underset{\sim}{v})$ for large motion systems we use

$$\underset{\sim}{v}_\psi = \underset{\sim}{v}_h \qquad (2.93)$$

and with the divergence equation (by taking divergence operation on Eqs. 2.59 and 2.60) so that divergence is not produced, to reach a double-Poisson equation equating the fields of the potentials of velocity and vorticity.

5. Barotropic Approximation

The barotropic approximation is a two-dimensional model represented by horizontal (isobaric) maps. It may be applied to one or more layers, each of which is a boundary condition for the other.

The barotropic equation treats large scale motion as horizontal and non-divergent so that

$$\left(\frac{\partial}{\partial t} + \underset{\sim}{V}_n \cdot \nabla\right)\left(\lambda + \zeta\right) = 0 \qquad (2.94)$$

$$\nabla_n \cdot \underset{\sim}{V} = 0 \qquad (2.95)$$

This approximation includes all approximations of the others described above

$$\frac{dUr}{dt} = 0$$

$$\Omega\cos\theta = 0$$

$$\overline{F} = 0$$

$$Q \approx 0$$

$$G = H = 0$$

as well as

$$Ur = 0$$

$$\frac{\partial P}{\partial t} = 0 \qquad (2.96)$$

6. Treatment for Computational Simulati

If $T(z)$, $\rho(z)$, $q(z)$, T_s, ρ_s, q_s, $U_r(z)$ are the most likely inputs to be derived experimentally, computational simulation should be designed so that the values of these measurable variables receive most emphasis. The variables so used in the simulation computation should all be sampled at frequency $f > 1\ min^{-1}$ and $K > 1\ km^{-1}$, and subsequently filtered so that the data contain no frequencies or wave numbers larger than 2π times the inverse of half the time step, or of

half the grid spacing. The sampling at high frequency and small grid spacing must be done before filtering in order to avoid deleterious "aliasing." In short, the measurements should be instrumented to sample with frequency greater than one per minute and by spacings closer than one per kilometer, before reducing the bandwidth of the data contained to one sample per period of computer updating and one sample per 100 to 300 km.

As Eliasson and Kleinschmidt (1957) have pointed out, the general solution of the nonlinear hydrodynamic equations is handicapped by the following considerations:

1. The processes are nonlinear in their "mature" stage
2. The solutions of nonlinear equations cannot be expressed as a superposition of eigensolution, hence they cannot be discussed analytically, but only by numerical or geophysical methods.
3. The solutions, called "numerical forecasting" or "physical forecasting," was first attempted by L. F. Richardson (1922), are susceptible to oversensitivity of the equation of motion. Margules pointed out that the pressure continuity equation (Eq. 2.62) would require an accuracy of 10^{-7} sec^{-1} in determination of div $\underset{\sim}{v}$, which is not attainable from wind observations (i.e., 10 m sec^{-1} per kilometer implies frequency 10^{-2} sec^{-1})
4. Internal and external gravitational sound, inertial waves, and oscillations do not correspond to long period waves seen on weather maps, and introduce "meteorological noise" (a term by Charney (1948)). The "meteorological noise" is evidence of "aliasing" or folding back of higher frequencies to appear as spurious lower frequencies.

Four procedures may be considered as alternatives in seeking solutions to the fundamental Eqs. 2.59 to 2.63.

1. Calculate the motion with fictitious noise waves included, and smooth the solution. This method is laborious, as

pointed out by Eliasson and Kleinschmidt (1957), but also will yield results which are fallacious because of aliasing.

2. Change the form of prognostic Eqs. 2.59 to 2.63 so that they are no longer satisfied by the noise waves. This procedure is the one followed by each of the major efforts at physical forecasting. The approximations are called "filtering approximations," since their effect is to filter noise from the solution. Each requires a compromise with accuracy or generality.
3. Before time integration of Eqs. 2.59 to 2.62, the initial values of pressure and wind may be adjusted to each other so that no noise waves of appreciable magnitude will occur in the solutions. This is tantamount to filtering values of $\underset{\sim}{U}$ and P so that they retain no frequencies or wave numbers to produce noise in the solution. This step is a desirable one, but in itself may be inadequate.
4. Compute the motions, by Laplace or Fourier transformation, in the (ω, K) domain wherein the band limits of the data and the computed variables may be rigorously controlled. In order that the results of such a laborious process may be appropriately realized, it will be worthwhile to design the (ω, K) characteristics of the input data to avoid the errors of aliasing and to exclude the unwanted frequencies and wave numbers. Accordingly, it may be necessary to extend the effort to the design of instruments for meteorological observation.

The fourth procedure listed above has received small attention. In the advent of more capacious and faster computers, and of efficient algorithms for Fourier transformations (Cooley and Tukey, 1965), this procedure should be given appropriate consideration.

Solving the Complete Equations

MacDonald (1962) has described the form of the eigen solution equations for wave solutions of Eqs. 2.59 to 2.63. These eigen

solutions to the perturbation relations may perhaps be numerically calculable. MacDonald assumed solutions of the form

$$\begin{aligned} U &= U(r,\ \theta)\ e^{2(k\lambda-\omega t)} \\ P &= P(r,\ \theta)\ e^{2(k\lambda-\omega t)} \\ Q &= Q(r,\ \theta)\ e^{2(k\lambda-\omega t)} \end{aligned} \tag{2.97}$$

where k is the angular wave number associated with longitude, and it is recognized that r and θ coordinates are not separable.

To obtain a partial differential equation in the spatial coordinates (r, θ, λ) of form

$$A\frac{\partial^2 P}{\partial r^2} + 2B\frac{\partial^2 P}{\partial r \partial \theta} + C\frac{\partial^2 P}{\partial \theta^2} + \text{lower order terms} = 0 \tag{2.98}$$

The character of the equation is given by the sign of $AC-B^2$, which is given by the sign of:

$$[\omega^2(\omega^2-N^2-\Omega^2) + N^2\Omega^2\sin^2\theta] = \omega^4-\omega^2(N^2+\Omega^2) + N^2\Omega^2\sin^2\theta \tag{2.99}$$

For frequencies larger than Ω (one per 12 hr = 2.3 $(10)^{-5}$ sec^{-1})

$$\begin{aligned} &\omega > N;\ AC - B^2 > 0 \text{ Elliptic (i.e., 2-D potential equation)} \\ &\omega < N;\ AC - B^2 < 0 \text{ Hyperbolic (i.e., equation of vibrating string)} \\ &\omega = N;\ AC = B^2 \text{ Parabolic (i.e., equation for linear heat conduction)} \end{aligned} \tag{2.100}$$

For frequencies less than Ω

$$\begin{aligned} &\text{Elliptic, if } \omega^2(N^2 + \Omega^2) < \omega^4 + N^2\Omega^2\sin^2\theta \\ &\qquad \text{or if } N > \Omega \text{ and } \omega < \Omega\sin\theta \end{aligned} \tag{2.101}$$

In short, for case

$N < \omega$	Differential equation is Elliptic	
$\Omega\sin\theta < \omega < N$	Differential equation is Hyperbolic	(2.102)
$0 < \omega < \Omega\sin\theta$	Differential equation is Elliptic	

For the case of solutions involving characteristic lengths L > 100 km, and characteristic periods greater than 10 min, the equation is elliptic for $\omega < \Omega\sin\theta$ and hyperbolic for $\omega > \Omega\sin\theta$ (as seen in Fig. 26).

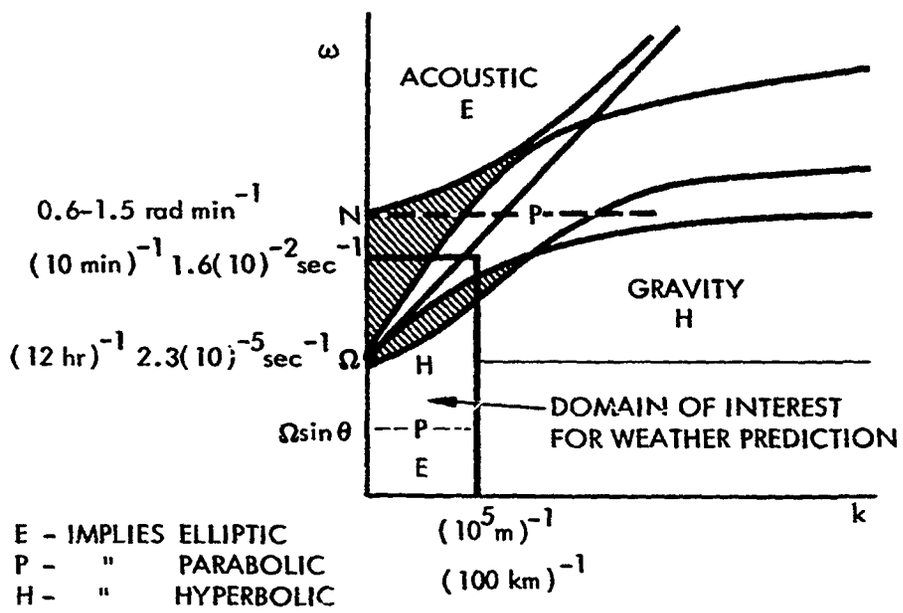

FIGURE 26. Form of Differential Equations for Atmospheric Simulation

The solutions of the hyperbolic differential equation are analogous to those of the equation of the vibrating string; those of the elliptic differential equation are analogous to those of the two-dimensional potential equation, and those of the parabolic form to those of the linear heat conduction equation.

In solving the complete equations in the case of global circulation, one may take advantage of the notion that the frequencies of interest are in every case smaller than the Vaisala frequency, N

$$N^2 = \frac{g}{T_0}\left(\frac{dT}{dz} + 10 \text{ deg/km}\right) \qquad (2.103)$$

which varies between $0.6 < N < 1.4$ for $0 < z < 140$ km, as discussed subsequently in this report.

On this basis, the equation may be solved as a hyperbolic equation for cases in which $\omega > \Omega\sin\theta$, and as a parabolic equation for $\omega = \sin\theta$, and as an elliptic equation for $\omega < \Omega\sin\theta$.

The hyperbolic equation may be solved by integration; the elliptic differential equation may be solved differently as a boundary value problem in two dimensions and the parabolic differential equations as a boundary value problem in one dimension.

Typical Wave Motions

As indicated by the equations for the hydrodynamics and thermodynamics of the atmosphere, heat sources and sinks are necessary in order to maintain motions in the atmosphere against frictional dissipation. However, heat sources and friction are comparatively slow effects which do not directly lead to the very rapid changes seen on weather maps in disturbed regions. Hence, although heat sources and friction are of vital importance in creating the supply of potential energy, they are usually negligible in effect during a limited time interval of conversion from potential to kinetic energy. In the limited time interval, the motion may be treated as

if adiabatic and frictionless. Most of the work in dynamic meteorology has been done on the basis of the theory of small-scale linear, frictionless and adiabatic oscillations.

Perturbation theory, applied in the form of the linearized equations described above, may be used to study the small scale oscillation, and, in particular, the stability properties of the atmosphere. The existence of any one discrete eigenfrequency which is imaginary or complex so that the corresponding eigensolution will grow exponentially with time suffices to prove that the state is unstable.

In any kind of oscillation or wave motion, the energy will fluctuate between kinetic energy and some other energy form. It is natural to classify the various types of oscillations and waves according to the energy forms involved. In this respect there are three fundamental types of hydrodynamic oscillations and waves:

a) Gravity waves: In pure gravitational oscillations, the energy is stored as gravity potential when it is not in kinetic form.

b) Acoustic waves: In pure compressibility or acoustic oscillations, the energy is stored as internal energy when it is not in kinetic form.

c) Inertial oscillations: In the case of perturbations of steady currents, the kinetic energy of the current represents a supply of energy from which the kinetic energy of the perturbation may be fed. There exist, therefore, pure inertial oscillations in which only kinetic energy is involved.

Besides these three fundamental types there are mixed types, where apart from the kinetic perturbation energy, two or three forms of energy are involved. Actually nearly all wave motions in the atmosphere are of such mixed character; however, when one energy storage form predominates the wave is described as being predominantly gravitational, acoustic or intertial in character.

The following discussion of atmospheric waves is along the lines developed by Eliassen and Kleinschmidt in 1957.

Wave motion under the influence of gravity on a resting earth

Two topics may be described without reference to the rotation of the earth: static stability, and combined gravitational-compressibility oscillations.

Static stability. As shown by Fjortoft (1946), the criterion of static stability can be derived rigorously from the energy equation. The second time derivative of the energy store cannot be negative if grad φ and grad s_o have everywhere the same direction. That is

$$\frac{\rho}{c_p} \frac{ds_o}{d\varphi} > 0 \tag{2.104}$$

at all levels implies static stability.

In a simpler, but less exact, concept consider an air mass in equilibrium, and let a small air particle at the level z_o where the pressure is p_o, the density ρ_o and the entropy s_o be displaced to a level z_1 where the equilibrium state is characterized by p_1, ρ_1, and s_1. It is assumed that the displacement of the particle does not disturb the equilibrium pressure field so that the particle arrives at the level z_1 in a state characterized by p_1, ρ', and s_o. As a result the particle is then exposed to a vertical buoyancy force per unit mass

$$F = -g \frac{\rho' - \rho_1}{\rho'} \tag{2.105}$$

Since the density may be considered as a function of pressure and entropy,

$$d\rho = \gamma \, dp - \mu \, ds \tag{2.106}$$

wherein

$$\gamma = \frac{1}{\frac{c_p}{c_v} RT}, \text{ and } \mu = \frac{\rho}{c_p} \tag{2.107}$$

The particle and the environment have the same pressure, but different entropy this

$$\rho' - \rho_1 = -\mu(s_o - s_1) = \mu \frac{ds}{dz}(z_1 - z_o) \tag{2.108}$$

and hence

$$F = -\frac{g\mu}{\rho} \frac{ds}{dz}(z_1 - z_o) \tag{2.109}$$

Since F is reckoned positive upward, the buoyancy force will accelerate the particle towards the equilibrium position if $\mu \frac{ds}{dz} > 0$, and from this position if this configuration is not met, thus indicating stability in the first case, and instability in the second.

As a measure of the static stability, we consider the restoring buoyancy force per unit length of vertical displacement. This quantity has the dimension of (frequency) squared. Its square root is termed the Brunt-Vaisala frequency N

$$N^2 = -\frac{F}{z_1 - z_o} = \frac{g\mu}{\rho} \frac{ds}{dz} = \frac{g}{c_p} \frac{ds}{dz} \tag{2.110}$$

Also by the gas equation,

$$N^2 = \frac{g^2\rho}{T}\left(\frac{DT}{Dp} - \frac{\partial T/\partial z}{\partial p/\partial z}\right) \tag{2.111}$$

For dry or nonsaturated air,

$$N^2 = \frac{g}{\theta}\frac{\partial \theta}{\partial z} = \frac{g}{T}\left(\frac{\partial T}{\partial z} + \frac{g}{c_p}\right) \tag{2.112}$$

and for saturated air,

$$N^2 = \frac{g}{T}\left(\frac{\partial T}{\partial z} + \delta_m\right) \tag{2.113}$$

Dry or nonsaturated air is statically stable when the potential temperature increases with height, or when the lapse rate of temperatures does not exceed $g/c_p = 0.01\ ^oC\ m^{-1}$. On the other hand, if

the air is saturated, then the lapse rate for moist air δ_m must be used. The moist-adiabatic lapse rate is a function of p and T. At low temperatures,

$$\delta_m \approx \frac{g}{c_p} \qquad \text{(at low temperatures)}$$

$$\delta_m = 0.0065\ ^{o}C\ m^{-1} \qquad \text{(at 0 } ^{o}C\text{, 1000 mb)}$$

$$\delta_m = 0.0044\ ^{o}C\ m^{-1} \qquad \text{(at 20}^{o}\text{ C, 1000 mb)} \qquad (2.114)$$

The static stability of cloudy air is seen to be considerably less than that of clear air with the same lapse rate. If the air mass is statically stable as long as it is nonsaturated, the mass will be unstable if saturation occurs. Such cases are usually referred to as "conditional instability."

The principal difficulty in dealing with systems where condensation occurs lies in the circumstance that the location of the regions of saturated air will depend upon the motion itself. Condensation will normally take place within the ascending currents, whereas clear air prevails in regions of subsidence. Combined gravitational-compressibility oscillations.

Waves which combine the effects of gravity and compressibility are important in the troposphere in that they account in general for the short periodic fluctuations of winds--the gusts and other wind phenomena that seem to have phase coherence as opposed to turbulence that lacks it. Eckart, 1960, has given a careful discussion of the forms of these waves. The following description of the fundamental solutions of the wave equations for an isothermal atmosphere, taken after Eliassen and Kleinschmidt (1957), greatly oversimplify the problem, but illustrate the general nature of the waves.

For an isothermal atmosphere, the coefficients N^2, Γ and c_o^2 are taken as constant:

$$N \cong \left[\frac{g}{T}\left(\frac{\partial T}{\partial z} + \frac{g}{c_p}\right)\right]^{\frac{1}{2}} \qquad \text{(Brunt-Vaisala frequency)}$$

$$\Gamma = \left(\frac{1}{c_o^2} - \frac{1}{2}\frac{d\rho_o}{dp_o}\right) g \qquad \text{(Large scale stability parameter)}$$

$$C_o = \sqrt{\frac{c_p}{c_v} RT} \qquad \text{(Speed of sound)} \qquad (2.115)$$

In the atmosphere, the above coefficients (Eq. 2.115) are not constant, but have values similar to those illustrated in Fig. 27. The perturbation equations of motion are satisfied by solutions of the form, wherein ξ and ζ are displacements in the x, and z directions.

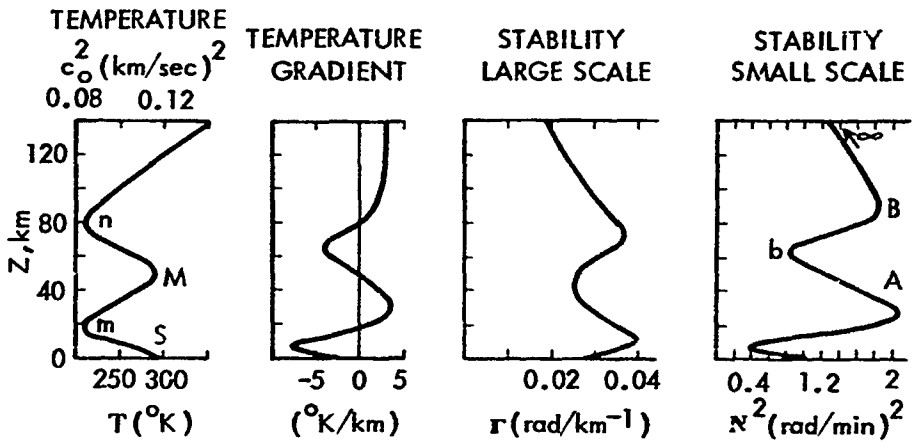

FIGURE 27. Dynamic Characteristics of Field Equation Variables (After Eckart, 1960)

$$\xi = -A \frac{1}{\rho_o^{\frac{1}{2}}} \frac{ik}{\nu^2} \frac{N^2 - \nu^2}{\Gamma + im} e^{i(kx + mz + \nu t)} \qquad (2.116)$$

$$\zeta = -A \frac{1}{\rho_o^{\frac{1}{2}}} e^{i(kx + mz + \nu t)} \qquad (2.117)$$

$$p = -A \frac{1}{\rho_o^{\frac{1}{2}}} \frac{N^2 - \nu^2}{\Gamma + im} e^{i(kx + mz + \nu t)} \qquad (2.118)$$

and where A is an arbitrary amplification factor, and k, m and ν are three constants satisfying the dispersion relation

$$\left(\Gamma^2 + m^2\right)\nu^2 = \left(k^2 - c_o^2\nu^2\right)\left(N^2 - \nu^2\right) \qquad (2.119)$$

The constants k and m are the horizontal and vertical wave numbers, respectively and ν is the frequency.

The different types of fundamental solutions may be conveniently represented in the frequency-wave number (ν, k) diagram for the isothermal planar atmosphere of Fig. 28.

The horizontal line $\nu = N$ represents purely vertical oscillations in an undisturbed pressure field. The line $k^2 = c_o^2\nu^2$ represents Lamb waves whose horizontal phase velocity ($\frac{\nu}{k}$) equals the speed of sound c_o. For given values of k^2 and ν^2, the dispersion relation (Eq. 2.119) gives a corresponding value of m^2 (square of the vertical wave number). The curves m^2 = constant are a family of hyperbolas. The hyperbola $m^2 = 0$ separates the domain of external waves ($m^2 < 0$) which have finite amplitudes at the boundaries (such as near the earth's surface) from the domain of internal waves ($m^2 > 0$), for which the amplitudes at the boundaries are zero. The internal waves may, therefore, be subdivided into low frequency internal waves (lower region) which are dominated by the influence of gravity and hence are called "internal gravity waves," and high frequency internal waves (upper region) which are dominated by compressibility terms, hence called "internal acoustic waves."

Any of the eight combinations $\pm k$, $\pm m$, $\pm\nu$ will satisfy the dispersion relation (Eq. 2.119). Linear combinations of the eight solutions give the various types of possible real solutions. These include the following:

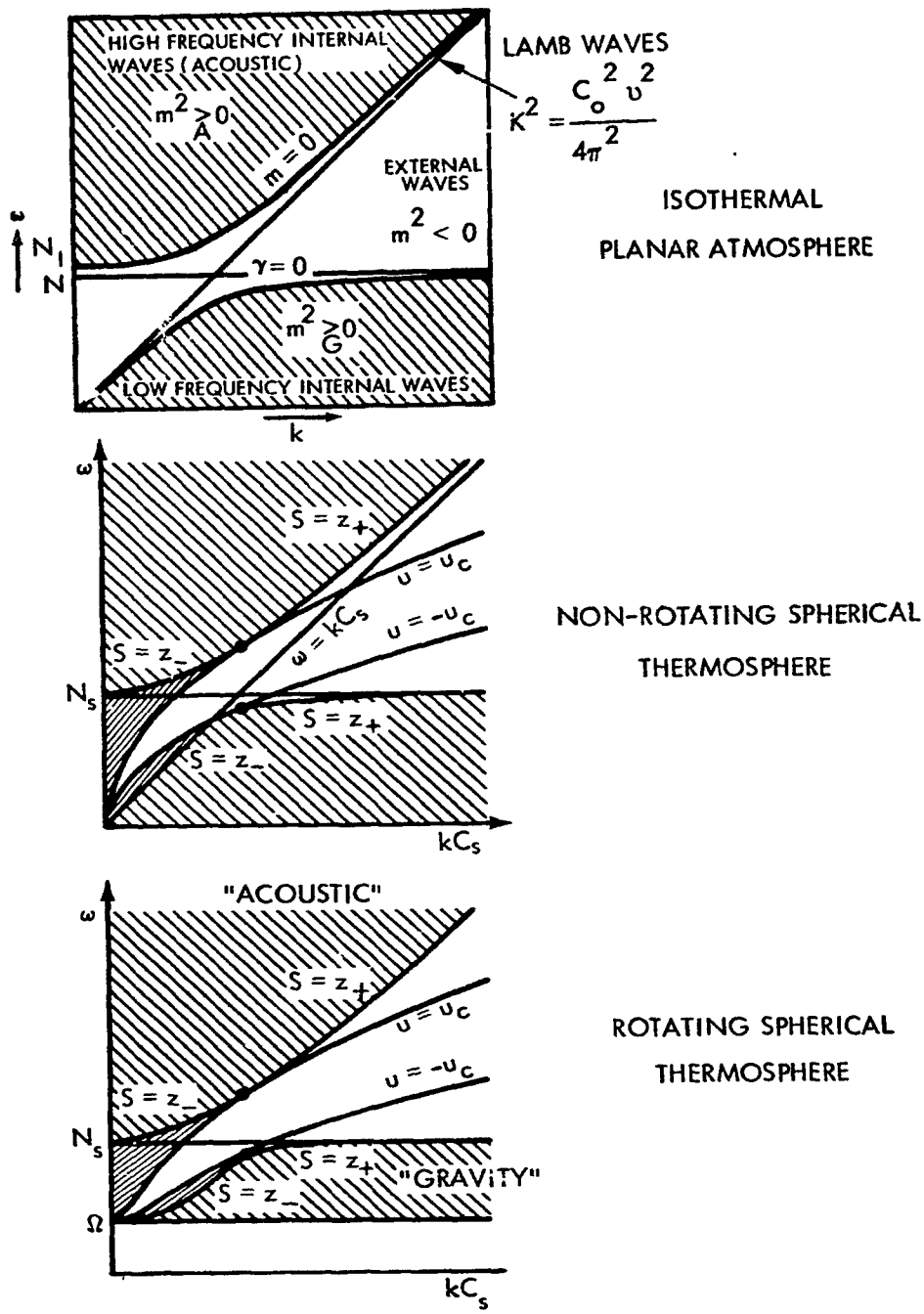

FIGURE 28. Diagnostic Diagrams (ω, k)

A. External waves for which $-m^2 = m_1^2 > 0$

1. Standing oscillations may be represented by

$$\rho_o^{\frac{1}{2}}\zeta = A \sin kx \, e^{\pm m_1 z} \sin \nu t \qquad (2.120)$$

2. Waves with horizontal propagation may be represented by

$$\rho_o\zeta = A \, e^{\pm m_1 z} \sin (kx + \nu t) \qquad (2.121)$$

By inspection of the term $e^{\pm m_1 z}$, it may be inferred that external waves cannot occur in a layer of air confined between two rigid horizontal planes, nor as free waves over a level ground in an infinite atmosphere of uniform stability. External waves may exist as forced waves, produced by motions of the boundaries, as in the phenomenon of mountain waves, or as free waves in an atmospheric layer which is bounded by other layers with different properties. Propagation of external wave energy is transported horizontally in the direction of propagation, but this energy cannot be transported in a vertical direction.

B. Internal waves, for which $m^2 > 0$

3. Standing oscillations, represented by

$$\rho_o^{\frac{1}{2}}\zeta = A \sin kx \sin m z \sin \nu t \qquad (2.122)$$

The wave energy flux for this form vanished when averaged over one period. The low frequency type, called gravity waves and modified by compressibility, represents a circulatory motion. The high frequency type, called compressibility or acoustic oscillations and modified by gravity, represents a more complicated streamline pattern of different kinematics.

4. Waves with horizontal propagation may be represented by

$$\rho_o^{\frac{1}{2}}\zeta = A \sin m z \sin (kx + \nu t) \qquad (2.123)$$

The wave energy has a mean value, averaged with respect to z and x (or t), which is

$$\overline{Q} = \frac{A^2}{4} \frac{N^2k^2 - c_o^2\nu^4}{k^2 - c_o^2\nu^2} \tag{2.124}$$

The mean wave energy flux is

$$\overline{F}_x = -\frac{A^2}{4} \frac{k}{\nu} \frac{(N^2 - \nu^2)^2}{\ell^2 + m^2}, \quad \overline{F}_z = 0 \tag{2.125}$$

That is, the wave transports energy in the direction of propagation

5. Waves with vertical propagation may be represented by

$$\rho_o^{\frac{1}{2}}\zeta = A \sin kx \sin (mz + \nu t) \tag{2.126}$$

The mean wave energy (averaged with respect to x and z, or t) equals that of horizontally propagated waves (Eq. 2.124). The mean wave energy flux is:

$$\overline{F}_x = 0, \quad \overline{F}_z = \frac{A^2}{4} \frac{m}{\nu} \frac{\nu^2(N^2 - \nu^2)}{\ell^2 + m^2} \tag{2.127}$$

Comparison of the sign of the vertical energy flux with that of the vertical phase velocity ($-\nu/m$) indicates that the signs are equal for high frequency internal waves ($\nu^2 > N^2$) and opposite for low frequency internal waves ($\nu^2 < N^2$). Thus, low frequency internal waves (so called "gravity" waves) with vertical propagation possess the unusual property that they transport energy in a direction opposite to the direction of propagation.

6. Waves with tilting phase-lines, represented by

$$\rho_o^{\frac{1}{2}}\zeta = A \sin (kx + mz + \nu t) \tag{2.128}$$

These waves have a horizontal as well as a vertical propagation. The mean wave energy is twice the value given by Eq. 2.124. The mean horizontal wave energy flux is twice the value given by Eq. 2.125. The mean vertical energy flux is twice the value given by Eq. 2.127. The vertical energy propagation, opposite to the vertical velocity, occurs again when $\nu^2 < N^2$.

Axially symmetric wave motions in a circular vortex

In the vortex motions of the atmosphere, inertial stability considerations must be taken into account in addition to the static stability considerations described in the previous section.

Pure inertial stability. A revolving mass of fluid possesses a particular kind of stability, usually referred to as inertial stability, first found by Rayleigh (1916), then treated by V. Bjerknes and Solberg (1929).

The circulation c of a circle R = constant, z = constant of a homogeneous and incompressible fluid rotating around an axis with no external force is

$$c = 2\pi R^2 w \tag{2.129}$$

where R is the distance from the axis and z is the distance from a plane normal to the axis. The kinetic energy of the vortex bounded by a rigid surface of revolution symmetric with respect to the axis and enclosing a volume τ is

$$K_v = \int_\tau Q_v \rho c^2 d\tau = \int_\tau \frac{\rho c^2}{8\pi^2 R^2} d\tau \tag{2.130}$$

Suppose that, in addition to the vortex motion, there is also an axially symmetric meridional motion, characterized by a meridional velocity field $\underset{\sim}{v}_m$. The total kinetic energy of the fluid is

$$K_m + K_v = \text{constant}$$

wherein

$$K_m = \int_\tau \frac{\underset{\sim}{V}^2 m \rho d\tau}{2} \tag{2.131}$$

The field corresponding to an extremum of K_v may be obtained by requiring the variation K_v to vanish for a virtual meridional displacement, so that

$$\rho c_o^2 \text{ grad } \varphi_v + \text{grad } p_o = 0 \tag{2.132}$$

The above equation shows that the pressure increases with R and is independent of z. So also does c_o depend only on R, being independent of z. The balanced vortex is stable with respect to axially symmetric motions when K_v is a minimum; that is, when c_o^2 increases monotonically with R. The criterion of inertial stability may, therefore, be written

$$d\, c_o^2/d\, R > 0 \quad \text{for all values of R} \tag{2.133}$$

The stability criterion can also be derived, in a less rigorous manner, by means of the particle method. The particle is chosen as a symmetric circle which is assumed to expand, or contract, without change in circulation, through an undisturbed environment. If c_o^2 increases with R, then a symmetric circle which has been brought to expand will arrive in z environment which rotates faster than the circle itself. The pressure gradient which balances the centrifugal force of the environment will exceed the centrifugal force of the displaced circle and thus give a net restoring force, which may be termed a "dynamic buoyancy." The vortex is thus inertially stable, and the restoring force per unit mass and per unit length displacement normal to the axis is found to be

$$\nu_i^2 = \text{grad } c_o^2 \cdot (-\text{ grad } \varphi_v) = \frac{c_o}{2\pi^2 R^3} \frac{dc_o}{dR} \tag{2.134}$$

This quantity has the dimension of a frequency squared and may be taken as a measure of the inertial stability. If c_o^2 decreases with R, the dynamic buoyancy, acting on an expanding or contracting circle, will be directed away from its equilibrium position, thus indicating inertial instability.

In an inertially stable vortex an axially symmetric disturbance of the balanced state will result in inertial oscillations. In these motions, the meridional displacements satisfy differential equations analogous to the perturbation equations for two-dimensional gravitational waves, with v_t^2 instead of v_s^2. For inertial oscillations, the displacements normal to the axis are the ones which give rise to restoring forces, while the displacements parallel to the axis are inactive and must be driven by the pressure force alone.

Combined effect of static and inertial stability

The stability with respect to axially symmetric motions of a compressible baroclinic vortex in a gravity field is an example of the combined effects of static and inertial stability.

The energy equation of the system is

$$K_m + K_v - \Phi - E = \text{constant} \qquad (2.135)$$

wherein K_m is the kinetic energy due to the meridional motions, K_v is that due to the vortex motion, Φ is the gravity potential energy of mass, and E is the internal energy (all of these are energy per unit).

The motion is such that a fluid line which at one time forms a symmetric circle around the axis will always remain a symmetric circle. Its circulation c as well as its specific entropy s will remain unchanged. Consequently, the change of the quantity $J = K_v + \Phi - E$ will depend only upon the meridional displacements $\delta\underset{\sim}{r}_m$. J may be considered an "effective potential energy" or energy store for the meridional motion. Differentiation of J with respect to time, and the continuity of potential φ, implies that J will be an extremum when

$$\text{grad } \varphi + c_o^2 \text{ grad } \varphi_v + \frac{1}{\rho} \text{grad } p_o = 0 \qquad (2.136)$$

The second variation of J is given by

$$\delta^2 J = \frac{1}{2} \int \left[\delta \underset{\sim}{r}_m \cdot M \cdot \delta \underset{\sim}{r}_m + \frac{c_v}{c_p RT} \left(\text{div } \delta \underset{\sim}{r}_m + \frac{c_p RT}{c_v} \delta \underset{\sim}{r}_m \cdot \frac{\text{grad } p_o}{\rho} \right)^2 \right] \rho_o d\tau \qquad (2.137)$$

where M is a tensor defined by

$$M = \frac{1}{c_p} \text{grad } s_o \, (-\alpha_o \text{ grad } p_o) + \text{grad } c_o^2 \, (-\text{grad } \varphi_v) \qquad (2.138)$$

If the quadratic form $\delta \underset{\sim}{r}_m \cdot M \cdot \delta \underset{\sim}{r}_m$ is positive definite, then $\delta^2 J$ is positive for all virtual axially symmetric meridional displacements, J is a minimum, K_m is bounded, and the vortex is stable with respect to axially symmetric disturbances.

The criterion for a stable vortex is then

$$\text{Det}(M) = \frac{1}{c_p} \text{grad } s_o \times \text{grad } c_o^2 \cdot \text{grad } \varphi \times (-\text{grad } \varphi_v) > 0 \qquad (2.139)$$

and

$$\text{Trace}(M) = \frac{1}{c_p} \text{grad } s_o \cdot \left(- \frac{\text{grad } p_o}{\rho_o} \right) + \text{grad } c_o^2 \cdot (-\text{grad } \varphi_v) > 0 \qquad (2.140)$$

Stability criteria for the baroclinic vortex applied to the atmosphere.

In an absolute frame of reference, the motion of the atmosphere is nearly a circular vortex motion around the earth's axis. Consider the earth as a sphere with radius a. In a point with latitude Φ and

height z above the earth's surface, the distance from the axis is

$$R = (a\ \varphi\ z)\ \cos\Phi \tag{2.141}$$

and the absolute circulation of a symmetric circle is

$$c_a = 2\pi\ (\Omega R^2 + Ru) \tag{2.142}$$

where Ω denotes the angular speed of rotation of the earth, and u the relative zonal wind speed, assumed independent of longitude.

Under these circumstances, the criteria for stability may be written

$$\left(\frac{\delta c_a}{\partial \varphi}\right)_s < 0 \quad \text{(Stable)} \tag{2.143}$$

where the index s means differentiation at constant s, i.e. in an isentropic surface. Also, it may be written, if z is neglected with respect to a, as

$$\left(2\Omega + \frac{u}{R}\right)\left[\left(1 + \frac{z}{a}\right)\sin\Phi - \frac{1}{a}\left(\frac{\partial z}{\partial \Phi}\right)_s \cos\Phi - \frac{1}{a}\left(\frac{\partial u}{\partial \Phi}\right)_s\right] > 0 \tag{2.144}$$

(Stable)

Since the slope of the isentropic surface is very small, the term in $\cos\Phi$ may also be neglected, so that the criterion becomes

$$\lambda + \frac{u}{a}\tan\Phi - \left(\frac{\partial u}{\partial y}\right)_s > 0 \quad \text{(Stable)} \tag{2.145}$$

If use is not too great, the second term may be neglected so that

$$\lambda - \left(\frac{\partial u}{\partial y}\right)_s > 0 \qquad \text{Stable} \tag{2.146}$$

In this form, the criterion applies strictly to a straight, parallel current of arbitrary direction on a flat earth, rotating with angular velocity $\Omega \sin\Phi$.

It is noteworthy that the direction of least stability is nearly along the isentropic slope. The result is commonly superimposed meridianal circulations in flat cells oriented along the isentropic slope.

Application of the above criterion to atmospheric currents has indicated two kinds of flow patterns where the stability with respect to meridianal or transverse circulations is normally small and where the current may be unstable in pronounced cases. The first type is the frontal zone in the lower troposphere, in which the unstable direction coincides with the frontal slope. The significance of the instability is that the air makes little resistance against an upgliding motion in the direction of the frontal slope. The other type of flow, where the stability is small, is found in the upper troposphere to the south of strong jets. Here the isentropic surfaces are almost horizontal, so that there is little resistance just south of a jet stream maximum against meridianal or transverse circulations in flat horizontal cells superimposed upon the current. In all other parts of the atmosphere a pronounced stability with respect to meridianal motions seems to prevail.

Two dimensional wave disturbances of linear currents

If a mean current $\underset{\sim}{u}$ is defined by averaging with respect to x, then

$$u = \underset{\sim}{u} + u' \qquad w = w' \qquad \underset{\sim}{w} = 0 \tag{2.147}$$

the transport of momentum through a line z = constant is, apart from a density factor,

$$\underset{\sim}{w}_m = \overline{u'w'} \tag{2.148}$$

the change in mean velocity is

$$\frac{\partial \underset{\sim}{u}}{\partial t} = -\frac{\partial}{\partial z}\overline{u'w'} \tag{2.149}$$

and the rate of change of kinetic energy of the mean flow is

$$\frac{\partial}{\partial t}\left(\tfrac{1}{2}\underset{\sim}{u}^2\right) = -\underset{\sim}{u}\frac{\partial}{\partial z}\overline{u'w'} \tag{2.150}$$

so that integration through the layer gives the total kinetic energy of the mean motion

$$\frac{dK_m}{dt} = -\int_{z_1}^{z_2} \underset{\sim}{u}\frac{\partial \overline{u'w'}}{\partial z}\,dz$$

$$= \int_{z_1}^{z_2} \overline{u'w'}\frac{\partial \underset{\sim}{u}}{\partial z}\,dz > 0 \quad \text{(Stability)} \tag{2.151}$$

For amplifying perturbations, $d K_m/d t$ must be negative, that is, the momentum transport must be directed from layers with large $\underset{\sim}{u}$ values to layers with small $\underset{\sim}{u}$ values.

Stability of zonal currents in the case of horizontal non-divergent motion

Fjortoft, R. (1950) has generalized the theory of stability of linear currents so that it applies to two-dimensional non-divergent motion on a sphere. This case is of interest in meteorology, since at a level near 500 mb, the large scale motions may be approximated as horizontal and non-divergent.

Consider the earth as a sphere with radius a, and latitude Φ. The area of a ring between Φ and $\Phi + d\Phi$ is

$$dF = 2\pi a^2 \cos\Phi d\Phi = 2\pi a R d\Phi \tag{2.152}$$

The absolute circulation along a latitude circle is

$$c_a(\Phi) = 2\pi R \underset{\sim}{u}_a \tag{2.153}$$

where a bar designates mean values over a latitude circle. The two-dimensional velocity field defines a scalar vorticity, i.e. the absolute vorticity component ζ_a normal to the sphere, which is individually conserved.

From theorems of Stokes and Kelvin for the conservation of circulation

$$\int_{F_1}^{F_2} \zeta_a dF = \text{constant} \tag{2.154}$$

From the principle of conservation of total absolute angular momentum

$$\int_{F_1}^{F_2} F\zeta_a dF = \text{constant} \tag{2.155}$$

From Eqs. 2.154 and 2.155, a zonal current is stable if ζ_a varies monotonically with latitude. If c_a for such a current is plotted as a function of F, the curvature of the profile curve will be of one sign in all latitudes.

If the mean absolute angular speed of rotation along a latitude circle is

$$\Omega_a = \frac{c_a}{2\pi R^2} \tag{2.156}$$

then, as shown by Fjortoft (1950), a zonal current is stable if the values of Ω_a in all latitudes where $\delta\zeta_a/\partial\Phi < 0$ are larger than any value of Ω_a in latitudes where $\frac{\delta\zeta_a}{\partial\Phi} > 0$. These stability criteria are sufficient, but not necessary.

Introducing the relative circulation

$$c = 2\pi R u \tag{2.157}$$

then

$$c_a = 2\pi R^2 \Omega + c$$

$$\zeta_a = - \frac{\partial c_a}{\partial F}$$

$$\frac{\partial \zeta_a}{\partial F} = \frac{\Omega}{\pi c^2} - \frac{\partial^2 c}{\partial F^2}$$

$$\Omega_a = \Omega + \frac{c}{2\pi R^2} \qquad (2.158)$$

The time rate of change of kinetic energy of the mean flow is

$$\frac{dK_m}{dt} = \frac{d}{dt} \int_{F_1}^{F_2} \tfrac{1}{2} u_a^2 dF$$

$$= \int_{F_1}^{F_2} \frac{\Omega_a}{2\pi} \frac{\partial c_a}{\partial t} dF > 0 \quad \text{(Stable)} \qquad (2.159)$$

Then if

$$\frac{\partial c_a}{\partial t} = -2\pi \frac{\partial W_m}{\partial R} \qquad (2.160)$$

wherein W_m is the northward eddy flux of angular momentum

$$W_m = 2\pi R^2 \overline{u'v'} \qquad (2.161)$$

then

$$\frac{\partial K_m}{\partial t} = -\int_{F_1}^{F_2} \underset{\sim}{\Omega}_a \frac{\partial W_m}{\partial F}\, dF$$

$$= \int_{F_1}^{F_2} W_m \frac{\partial \Omega_a}{\partial F}\, dF > 0 \quad \text{(Stable)} \tag{2.162}$$

Measurements of the mean meridianal eddy flux of angular momentum indicate a pronounced northward flux south of the latitude of maximum westerlies, in agreement with the fact that a northeast-southwest tilt of troughs and ridges, corresponding to a positive correlation between u' and v' is predominant in these latitudes. North of the maximum westerlies, on the other hand, only small values of W_m are observed which are partly directed southward. On the average, therefore, $d K_m/d t$ is positive in the atmosphere, indicating that kinetic energy of the perturbations is continually being converted into kinetic energy of the mean current. Perturbations in general must take their energy from sources other than the kinetic energy of the mean current. This does not exclude the possibility, however, that some growing disturbances (perhaps the fastest growing ones) develop their instability as one of this type, taking part of their energy from the kinetic energy of the mean zonal current.

Rossby waves. The application of the theory of horizontal, non-divergent motion to large scale currents in the atmosphere is due to Rossby and colleagues (1939).

Noting the conservation of the vertical component of the absolute vorticity $\zeta_a = (\lambda + \zeta) = 0$, with the notation

$$\beta = \frac{1}{a}\frac{\partial \lambda}{\partial \varphi} = \frac{2\Omega \cos\Phi}{a} \tag{2.163}$$

the conservation may be described by

$$\frac{\partial \zeta}{\partial t} = -\underset{\sim}{v} \cdot \nabla\zeta - \beta v \tag{2.164}$$

Rossby derived a wave of form

$$V = \underset{\sim}{\beta} \cdot \sin K(x - ct) \tag{2.165}$$

in a non-divergent flow, and constant β, to have a velocity of propagation

$$C = C_R = U_o - \frac{\beta}{k^2} \tag{2.166}$$

Rossby's formula says that the waves propagate westward relative to the air at a speed proportional to the square of its wavelength. The waves of wave number k_s

$$k_s = \sqrt{\frac{\beta}{M_o}} \tag{2.167}$$

are stationary. Waves with wavelengths greater than the stationary wavelength $L_s = 2\pi/k_s$ move westward and shorter waves eastward.

Shearing instability

A linear current of a homogeneous and incompressible fluid is possibly unstable if the shear of the velocity profile has a maximum somewhere within the layer. Instability of this kind is particularly pronounced if the shear of the current is concentrated in a shear line, which represents a discontinuity in the velocity field. Hoiland (1942) has derived the shearing instability by adapting the vorticity equation. Introducing a unit vector $\hat{t}$ tangential to the line of the shear discontinuity s, and letting the sliding vorticity ζ in a point on s be defined by

$$\zeta = (\underset{\sim}{v}_1 - \underset{\sim}{v}_2) \cdot \hat{t} \tag{2.168}$$

so that

$$\frac{\delta \zeta}{\delta t} = -(\underset{\sim}{v}_1 - \underset{\sim}{v}_2) \cdot \text{grad } \underset{\sim}{v} \cdot t \qquad (2.169)$$

This may be generalized to the case when the two fluid layers, of velocity $\underset{\sim}{v}_1 = U_1$, $\underset{\sim}{v}_2 = U_2$ have different densities ρ_1, ρ_2, and there is a uniform gravity field directed normal to the undisturbed surface. If the lower fluid is the heavier one, the effect will act to stabilize the system, waves longer than a certain critical wavelength will be stable, and shorter waves unstable. Perturbation theory gives, in this case, a formula for the velocity of propagation.

$$c = \frac{\rho_1 U_1 + \rho_2 U_2}{\rho_1 + \rho_2} \pm \sqrt{\frac{g}{h} \frac{\rho_1 - \rho_2}{\rho_1 + \rho_2} - \frac{\rho_1 \rho_2}{(\rho_1 + \rho_2)^2} (U_1 - U_2)^2} \qquad (2.170)$$

The system described by the above equation is unrealistic because strict velocity discontinuities do not exist in nature. If the velocity discontinuity is replaced by a transition layer of continuous velocity variation, this will not have noticeable effect upon waves of wavelength considerably longer than the depth of the transition layer, but waves of comparable or shorter dimension will not be stable. In this case, the amplifying waves are confined to an intermediate band of wavelengths, whose width depends upon the differences in velocity and density in the upper and lower layer and the depth of the transition layer.

Billow clouds, which are formed in a layer of high static stability and strong vertical wind shear, are generally assumed to result from instability of this kind.

Wave motions in zonal currents

Considering a steady, linear, barotropic current, Eliassen and Kleinschmidt (1957) describe an equation in third degree in c, the velocity of propagation of wave motion in which the particles move horizontally under a horizontal pressure force which is independent of height.

$$\left[gH - (u_o - C)^2\right]\left(u_o - C - \frac{\beta}{k^2}\right) = \frac{\lambda^2 C}{k^2} \qquad (2.171)$$

wherein $H = RT/g$, $\lambda = 2\Omega\sin\Phi$. The equation has two large roots, approximately given by

$$C \approx u_o \pm \sqrt{gH} \qquad (2.172)$$

which are predominantly sound waves, slightly modified by gravity. The third root of 2.171, which is much smaller is found by neglecting $(u_o - c)^2$ versus gH, yielding

$$C \approx \frac{u_o - \frac{\beta}{k^2}}{1 + \frac{\lambda^2}{gHk^2}} \qquad (2.173)$$

This root agrees with the observed speed of waves in the westerlies in order of magnitude, and is an improved, but still approximate form descriptive of the Rossby waves. The difference is slight for wavelengths less than 6000 km.

Fjortoft (1951) obtained a generalization of the Rossby formula to the case of the baroclinic current. This simple but crude theory introduced the advective assumption that entropy changes result from horizontal advection only. Using the hydrostatic and geostrophic equations, Fjortoft derived the formula for velocity of propagation as

$$C = \underset{\sim}{u}_o - \tfrac{1}{2}\frac{\beta}{k^2} \pm \sqrt{\frac{\beta^2}{4k^4} - (\underset{\sim}{u}^2 - \underset{\sim}{u}_o^2)} \qquad (2.174)$$

The radicand vanishes for waves whose wavelength is

$$L_1 = 2\pi\sqrt{\frac{2}{\beta}}\left(\underset{\sim}{u}^2 - \underset{\sim}{u}_o^2\right)^{\frac{1}{4}} \qquad (2.175)$$

This quantity may be calculated if u_o is known at all levels. Clearly, L_1 increases with increasing wind shear. For wind profiles observed in the westerlies, L_1 is the order of several thousand kilometers, even for moderate wind shear.

A more complicated solution, for the two layer baroclinic atmosphere middle, has been worked out by P. D. Thompson (1961).

According to Charney (1947) amplification will take place provided the wavelength is shorter than the critical value L_1. According to Eady and Fjortoft sufficiently short waves are again stable, so that amplification is confined to an intermediate band of wavelengths. The growth rate for a given wind shear has a maximum for a certain wavelength L_{max} of the order of 3000 km, which depends upon both latitude and static stability,

$$L_{max} = \frac{\nu_s}{2\Omega \sin\Phi} \tag{2.176}$$

When the polar front had been discovered by the Norwegian school about 1920, V. Bjerknes and his collaborators put forward the hypothesis that the extratropical cyclones are amplifying wave motions which develop spontaneously on the frontal surface as a result of some kind of instability connected with it. H. Solberg (1928) investigated theoretically the possible wave types in a system consisting of two statically stable, barotropic layers of different density moving zonally at different speeds and separated by a sloping interface. Solberg found that two types of amplifying waves are possible in this system. The first type is of very short wavelength, up to a few kilometers, and has clearly nothing to do with cyclones. The second type is found in a band of wavelengths of the order 1000 to 2000 km which is in agreement with the dimensions of cyclones. Since the latter type have certain kinematical features in common with growing cyclones, it represents one possible explanation for the growth of cyclones. One explanation for the two wave

types is the following. The growth of very short unstable waves is due to the shearing instability connected with the wind discontinuity at the frontal surface. At sufficiently short wavelengths, the shearing instability dominates over the static stability, so that the disturbances amplify. However, as the wavelength increases, the static stability becomes relatively more important, and for wavelengths greater than a few kilometers, the waves are stable. For all the shorter wavelengths, the earth's rotation has no noticeable effect; the fluid particles move in orbits in planes nearly vertical. As the wavelength is further increased, however, the earth's rotation has the effect of turning the orbital planes towards the horizontal, so that the static stability becomes less effective. From a certain wavelength on, the role of the static stability has been thus reduced so that the shearing instability again dominates, and the waves become instable. These longer instable wavelengths are the cyclone-like long waves, with quasi-horizontal particle orbits. For still longer wavelengths, the inertial stability due to the earth's rotation comes to dominate, and the waves are again stable.

Solberg's long unstable waves take their energy from the kinetic energy of the mean zonal motion, whereas the potential energy of the system is increased during their growth. Since it is known that the perturbations in the westerlies on the average lose energy to the kinetic energy of the mean zonal flow, it does not seem possible that Solberg's type of instability is responsible for the growth of all kinds of disturbances in the westerlies. Certain types of frontal waves of relatively short wavelengths may develop in accordance with Solberg's theory.

GENERAL CIRCULATION

The conception, "general circulation", comprises the largest wind systems in the spectrum of atmospheric motions down to systems of the magnitude of the cyclones and anticyclones. Averaging over sufficiently long periods of time does away with the smaller among these systems. The remaining ones are large streams encircling the entire globe which remain nearly unchanged when annual averages are taken. These are in the first instance implied by the term general circulation. Certain irregularities are caused by land and sea distribution and by mountains. The following treatment is largely taken from reviews by Lorenz (1967), Starr (1968), and Mintz (1961).

The motion in these currents, which have a crude symmetry with respect to the earth's axis, is predominantly zonally directed, but has also a meridional component that transports energy poleward from the equator.

The principal problem pertaining to these streams is the question of their maintenance. Friction opposes their continuation, presumably seeking to reduce all velocities to that of a solid rotation with the earth, that is to produce a general calm. To maintain the general circulation against friction, heat sources and sinks are necessary. The theory of the general circulation thus differs from much of the other theoretical work that has been performed in that both friction and heat sources and sinks are drawn into consideration. Friction and heating energetics lead to flow, which is taken as an assumed parameter by most mathematical treatments.

The eddy motions evolving from the predominantly zonal currents comprise the convective cells for the conversion of essentially heat energy into kinetic energy in a rotating atmosphere. There are two modes of response of a convective model: symmetric and cellular. The symmetric mode, which occurs when the rate of rotation is small, is meridionally similar to the field of motion induced in a non-rotating stratum of gas by a constant and symmetric distribution of heating at low and cooling at high latitudes. Such non-rotational motion is devoid of zonal components and takes place in meridianal

planes, being identical for all longitudes. The symmetric mode is that field of motion induced in a curved stratum of gas having a relatively slow rate of basic rotation about the polar axis and heated by a constant and symmetric distribution of heating at low latitudes and cooling at high latitudes. It is characterized in the meridianal plane as a single cell with air rising near the equator and sinking near the pole. As compared with the non-rotating case, relative westerlies appear at higher and relative easterlies at lower latitudes with a sloping surface of separation between the two. The flow is still the same at all longitudes, thus being symmetric about the polar axis.

The cellular mode, called also a high-rotation regime or Rossby regime, is developed by passing from the low-rotation regime by keeping other quantities the same but increasing the rotation a moderate amount. Such motions are turbulent, forming in the meridianal plane three cells. Of these, the cell in middle latitudes has a mean circulation, in the meridianal plane, which is contrary to the local thermal forcing, involving a descent of relatively warm gas and an ascent of colder gas. This forced effect is a result of the turbulent character of the motions. The relative mean flow of the cellular mode also shows westerlies at higher latitudes and easterlies at lower latitudes.

The convection in the turbulent regime is difficult to picture simply because of the random components of motion associated with it. However, convection requires a net systematic statistical effect, in the sense of cold gas sinking and warm gas rising.

The radiative cooling at high latitudes and heating at low latitudes creates a pool of dense and a pool of light gas, creating a zonally distributed store of available internal and potential energy for conversion into kinetic. The effect of the turbulence is to break off smaller masses of cold gas at individual longitudes here and there, which then migrate to middle and lower latitudes and do their sinking sporadically in these places. Also, the warm gas is first moved in individual poleward-moving streamers toward middle and higher latitudes over narrow longitude sectors, to be then displaced upward by the sinking and horizontally spreading cold gas blobs. In the turbulent

process are four steps of the energy cycle of the earth's atmosphere: (1) the generation of zonal available potential plus internal energy by differential heating through radiation; (2) the transformation of the zonal available into the eddy available form of this energy; (3) the transformation of eddy available potential plus internal energy into eddy kinetic energy, evidenced by a pattern along a single zone of warm air in general rising and cold air sinking; and (4) a transport of momentum either in the direction of or contrary to the gradient of mean flow. Required for the latter transport, called an effect of negative viscosity, is a supply of eddy kinetic energy, drawn from the eddies by conversion of other forms of energy (potential, internal, etc.) within the eddies or transferred from another scale of eddies, including smaller ones in which case the smaller ones must receive a supply from other sources. In the case of a system in which the eddies are thermally driven, the heat dissipated by braking of the mean flow by friction or the heat produced by hydromagnetic action, by the second law of thermodynamics, cannot again be used to drive the eddies.

Following the notation of Starr (1968), u, v, and w are the zonal, meridional, and vertical components of wind velocity, R, Φ, and θ are the radius, latitude, and longitude coordinates of the earth, and p and ρ are the pressure and density of the atmosphere. Also, a bar ($-$) denotes the time average of any quantity, a prime ($'$) the departure of a quantity from its time average, brackets ([]) the average of any quantity with respect to longitude, and a star ($*$) the departure of a quantity from its longitudinal average. The operators $-$, $'$, [], and $*$ are commutative.

The wind field vector components may be resolved with such notation according to the formulae for u

$$u = \bar{u} + u' \tag{2.177}$$

$$u = [u] + u^* \tag{2.178}$$

and thus, in greater detail,

$$u = [\bar{u}] + \bar{u}^* + [u]' + u^{*\prime} \tag{2.179}$$

Resolutions of the fields of temperature T, specific humidity q, and other quantities may be similarly performed. Since his data consist mainly of observations at standard pressure levels, Starr lets $\overline{U}$ represent the time average for fixed λ, φ, p (not the same as for fixed λ, φ, z). Similarly, [U] is the average with respect to longitude along a latitude circle on an instantaneous isobaric surface.

To a considerable extent the features appearing respectively in the fields of $[\overline{U}]$, $\overline{U}^*$, $[U]'$ and $U^{*\prime}$ are those appearing in the field of $[\overline{U}]$, in $\overline{U}$ but not $[\overline{U}]$, in [U] but not $[\overline{U}]$, and in U but neither $\overline{U}'$ nor [U]. Similar remarks apply to the features of T and q. However, some meteorological features, such as the jet stream, do not clearly fall into any one category.

The fields of $\overline{U}$ and U' in (2.177) are called the long-term or time-averaged or standing motion and the transient motion. The components [U] and [V] are called the zonal circulation and the meridional circulation, and the components of U^* and V^* are called eddies. The field of [W] demanded by continuity is also included as part of the meridional circulation. Thus the terms in (2.179) are respectively the time-averaged or standing zonal and meridional circulations, the time-averaged or standing eddies, the transient zonal and meridional circulations, and the transient eddies.

To avoid ambiquity in use of the terms "zonal" and "meridional" in this report, a "zone" means a latitude circule or a region extending along a latitude circle, "zonal motion" means motion <u>parallel</u> to the zones, and is synonymous with U, "meridional motion" means motions parallel to the meridians or meridional planes. A "zonal average" means an average <u>within</u> zones, or with respect to longitude, and "zonal symmetry" denotes invariability within zones.

Figure 29 shows the cellular meridional flow suggested by Rossby (1945). Although some features of his model are no longer acceptable, Rossby's picture relates the meridional cells to the wavy bounds of the polar front zone and the horse latitudes, which separate the polar easterlies and the mid-latitude westerlies, in one case, and the mid-latitude westerlies and the equatorial easterlies in the other.

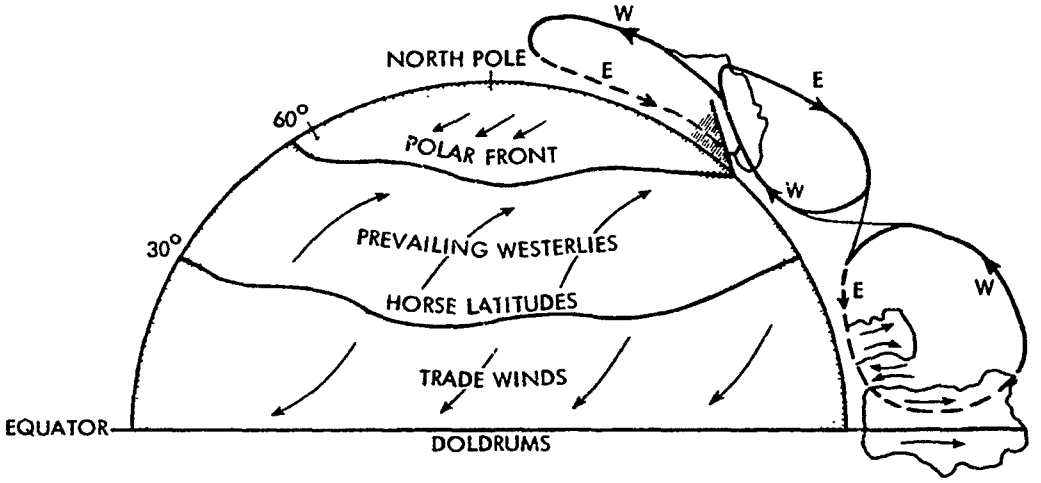

FIGURE 29. Cellular Meridional Circulation on a Rotating Earth (After G.C. Rossby, 1945)

The vertical distribution of annual mean zonal velocities in the atmosphere, averaged for all longitudes $[\bar{u}]$, adapted from observational material compiled by Buch (1954) for the Northern Hemisphere and by Obasi (1965) for the Southern Hemisphere is shown in Fig. 30. More recent compilations, such as that by Starr (1969) given in Figs. 31 and 32, suggest that Buch's maximum westerlies are slightly too low.

The vertical distribution of annual mean meridional velocities in the atmosphere averaged for all longitudes $[\bar{v}]$ is shown in Fig. 33. These data given by Starr (1968) were adapted from Lorenz (1967) who in turn utilized observational material from Buch (1954) for the Northern Hemisphere and by Obasi (1963) for the Southern Hemisphere. The horizontal arrows in Fig. 33 were obtained by calculation from measurements of momentum transports and other observed data. The vertical arrows are only schematic and are not to scale. A more recent compilation of Northern Hemisphere data is given in Figs. 31 and 32.

The vertical distribution of the mean annual eddy transport of angular momentum $2\pi R^2 \cos^2 \Phi \{[\overline{u'v'}] + [\bar{u}^*\bar{v}^*]\}$ in the actual atmosphere is given in Fig. 34. The data of Fig. 34 were adapted by Starr (1968) after Lorenz (1967), who used data compilations of Buch (1954) for the

Northern and of Obasi (1963) for the Southern Hemisphere. Both the effect of transient eddies and of the standing eddies are included.

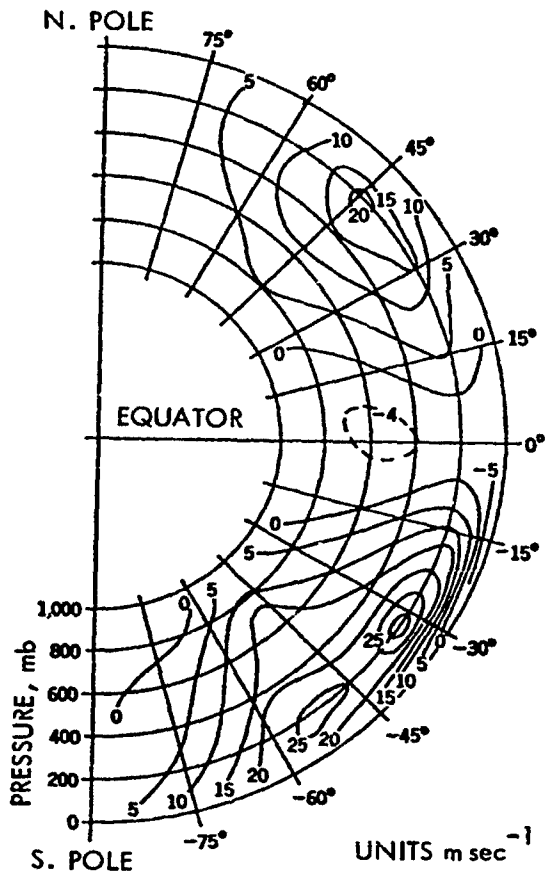

FIGURE 30. Zonal Velocities (After Starr, 1968)

The annual average curves derived from observations in the actual atmosphere giving the relative mean angular velocity about the polar axis $[\bar{u}]/R\cos\Phi$ (dotted line), the northward angular momentum transport by turbulent eddies $2\pi R^2 \cos^2\Phi \int \rho[\overline{u'v'}]dz$ (smooth line) and the angular momentum transport by mean meridianal circulations $2\pi R^2 \cos^2\Phi \int \rho[\bar{u}][\bar{v}]dz$ (dashed line) are shown in Fig. 35. The two transports are integrated vertically through almost the entire mass of the atmosphere (up to 20 km). The angular velocity represents a vertical average through the

$\overline{[U]}$ 60 mo

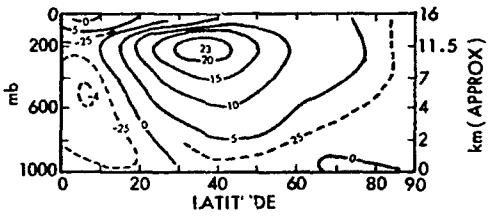

a. TIME AND ZONALLY AVERAGED ZONAL WIND
UNITS: m sec^{-1}

$\overline{[V]}$ 60 mo

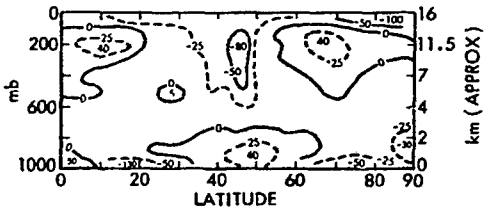

b. TIME AND ZONALLY AVERAGED MERIDIONAL WIND
UNITS: m sec^{-1}

$\overline{\Psi}$ 60 mo

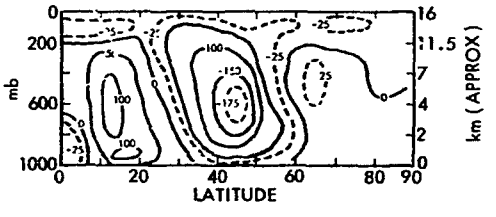

c. TIME AND ZONALLY AVERAGED MASS FLOW DENOTED BY CONTOURS OF STREAM FUNCTION Ψ
UNITS: $2(10)^{11}$ g sec^{-1}
AVERAGED OVER ALTITUDES TO 20 KM

MOMENTUM PARAMETERS

ⓓ $[\overline{U^*V^*}]\cos^2\phi$;

ⓔ $[\overline{U}]/\cos\phi$;

ⓕ $[\overline{U^*V^*}]\cos^2\phi$

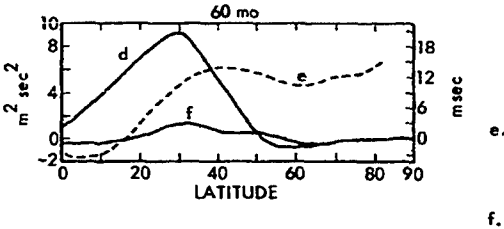

d. NORTHWARD ANGULAR MOMENTUM TRANSPORT BY TRANSIENT EDDIES
(TIMES FACTOR $\frac{1}{2\pi R^2 \rho}$)
UNITS: (m sec^{-1})^2

e. RELATIVE ANGULAR VELOCITY (TIMES FACTOR R)
UNITS: (m sec^{-1})

f. NORTHWARD ANGULAR MOMENTUM TRANSPORT BY STANDING EDDIES
(TIMES FACTOR $\frac{1}{2\pi R^2 \rho}$)
UNITS: (m sec^{-1})^2

FIGURE 31. Long-Term Averages of Wind Velocities, Mass Flow and Momentum Parameters (After V.P. Starr et al., to be Published, 1969)

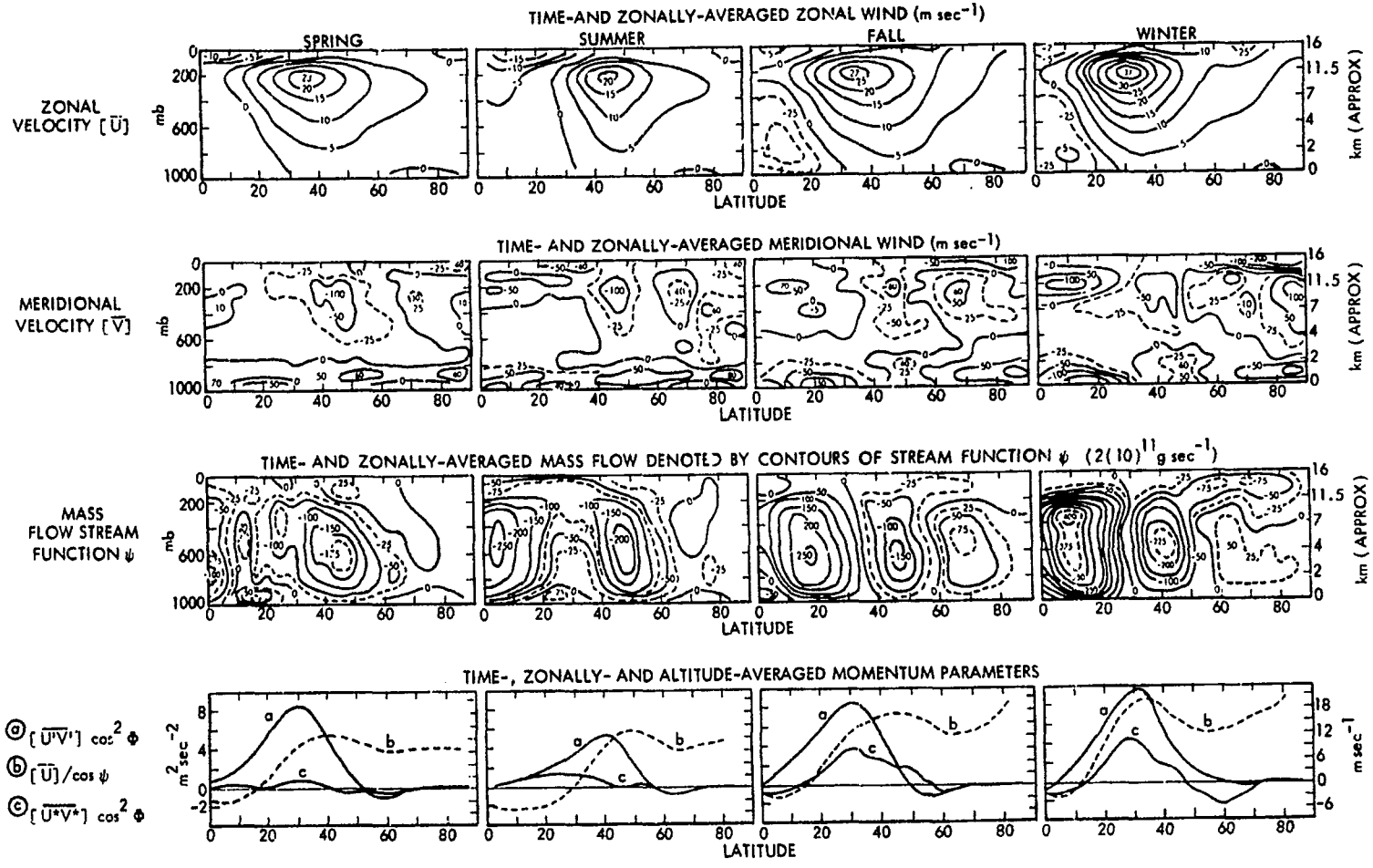

FIGURE 32. Seasonal Averages of Wind Velocities, Mass Flow and Momentun. Parameters (After V.P. Starr et al., to be Published, 1969)

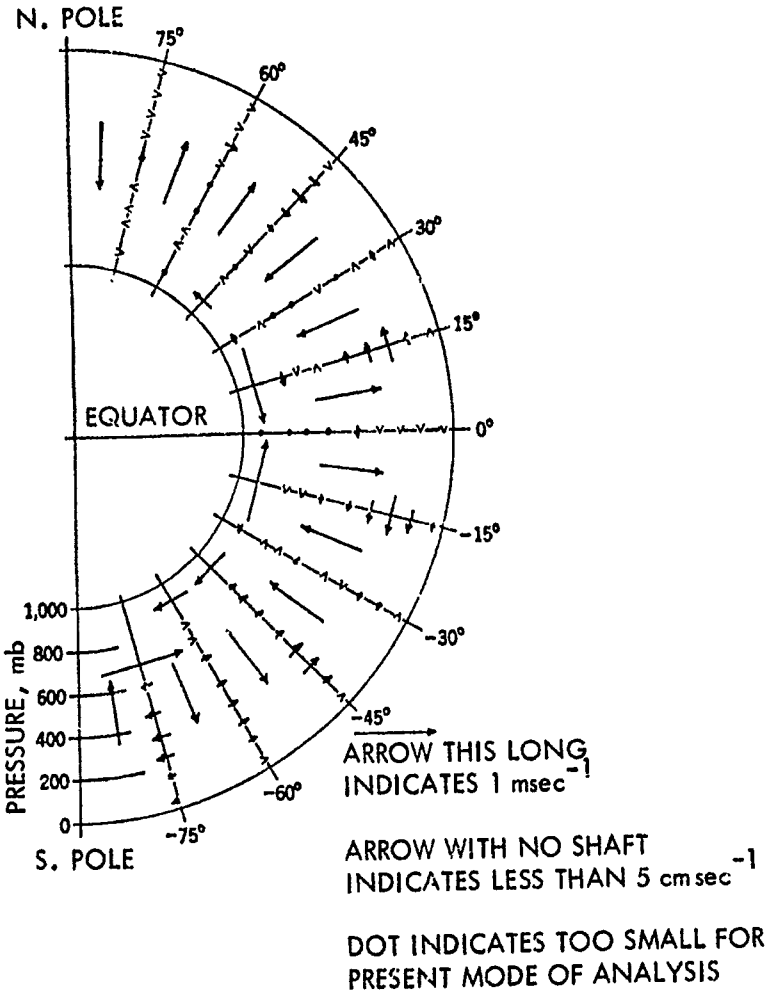

FIGURE 33. Meridional Velocities (After Starr, 1968, Adapted from Lorenz, 1967)

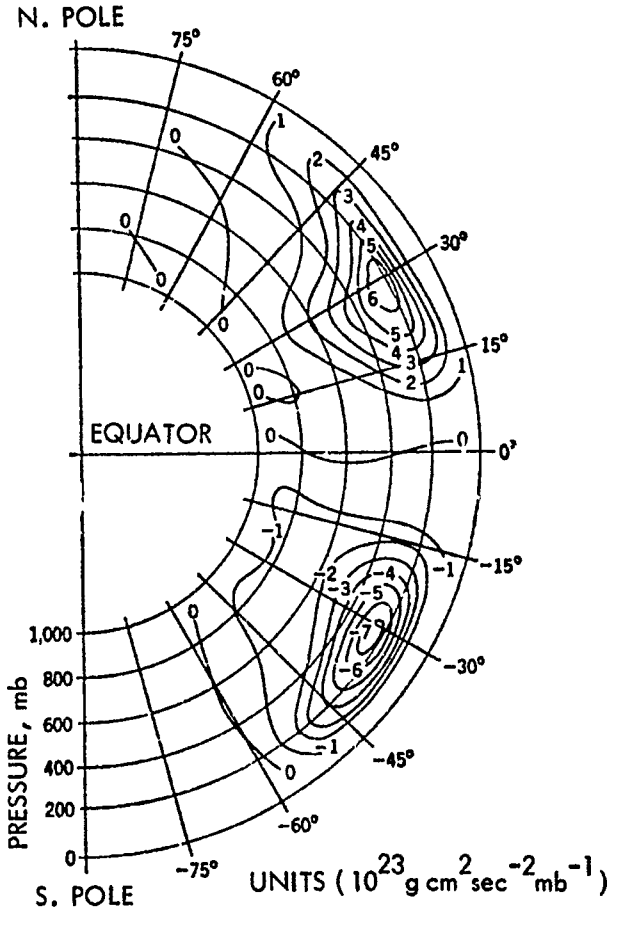

FIGURE 34. Angular Momentum Transport by Eddies (After Starr, 1968, Adapted from Lorenz, 1967)

same mass. All curves are by Starr (1968) who adapted them from the review by Lorenz (1967) who in turn used data analyses by Buch (1954) for the calendar year 1950 for the Northern Hemisphere and by Obasi (1965) for the calendar year 1958 for the Southern Hemisphere. More recent data by others, including the data by Starr (1969) given in Figs. 31 and 32, corroborate in a general way these data. The difference between the hemispheres, shown in Fig. 35, is real. Also, a negative eddy viscosity effect is illustrated by the data that have largest numerical values of eddy transport located in the zones of greatest shear in angular velocity.

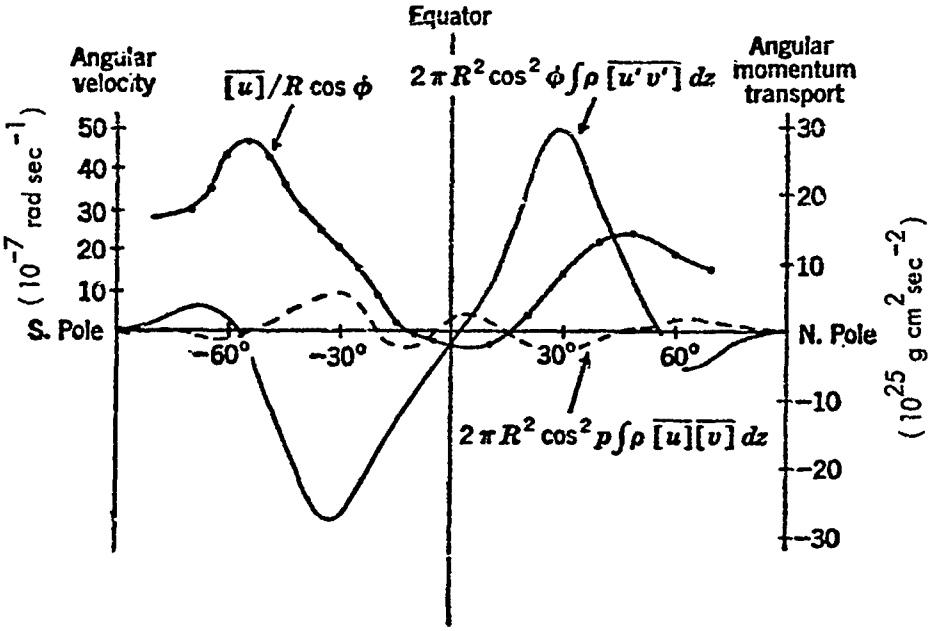

FIGURE 35. Angular Velocity Averaged over Vertical and Angular Momentum Transports Integrated over Vertical (After Starr, 1968)

Figure 31 shows data, recently compiled by Starr (1969) from reports of about 800 stations over the five-year period starting May 1, 1958, which describe the long-term (60-month) time- and zonally-averages in the Northern Hemisphere of zonal wind $[\bar{u}]$, meridional wind $[\bar{v}]$ and stream function ψ. The stream function ψ measures mass flow. Between adjacent lines of the stream function, mass transport is constant. The mass flow is dependent on $\cos\Phi$, since

$$q \frac{\partial \psi}{\partial p} = 2\pi R \cos\Phi \, [\bar{v}]$$

$$q \frac{\partial \psi}{\partial \Phi} = -2\pi R^2 \cos\Phi \, [\bar{w}]$$

In Fig. 32 are shown the seasonal averages of the same data used for Fig. 31.

Also shown in Figs. 31 and 32 are the momentum parameters: $[\overline{u'v'}] \cos^2\Phi$ which is proportional to the northward angular momentum transport by transient eddies, $[\bar{u}]/\cos\Phi$ which is proportional to the relative angular velocity and $[\bar{u}^*\bar{v}^*]\cos^2\Phi$ which is proportional to the northward angular momentum transport by standing eddies.

Figure 36 displays vertical meridional cross sections through the atmosphere showing (a) the distribution of the mean temperature $[\bar{T}]$, (b) the distribution of northward heat transport by transient eddies to be obtained from the values of $[\overline{v'T'}]\cos\Phi$ by multiplying the values by $2\pi C_p R$, and (c) the distribution of northward heat transport by standing eddies to be obtained from the values of $[\bar{v}^*\bar{T}^*]\cos\Phi$ by multiplying the values by $2\pi C_p R$. These data were obtained by Starr (1968) by automatic computing from five years of daily data at ten levels for about 700 stations in the Northern Hemisphere.

Figure 37 shows the transport of water vapor across latitude circles by the motions of the atmosphere on a mean annual basis for the calendar year 1958, adapted by Starr (1968) from transport calculations, by Peixoto and Crisi (1965) over the Northern Hemisphere, and by Starr, Peixoto, and McKean (1968) over the Southern Hemisphere.

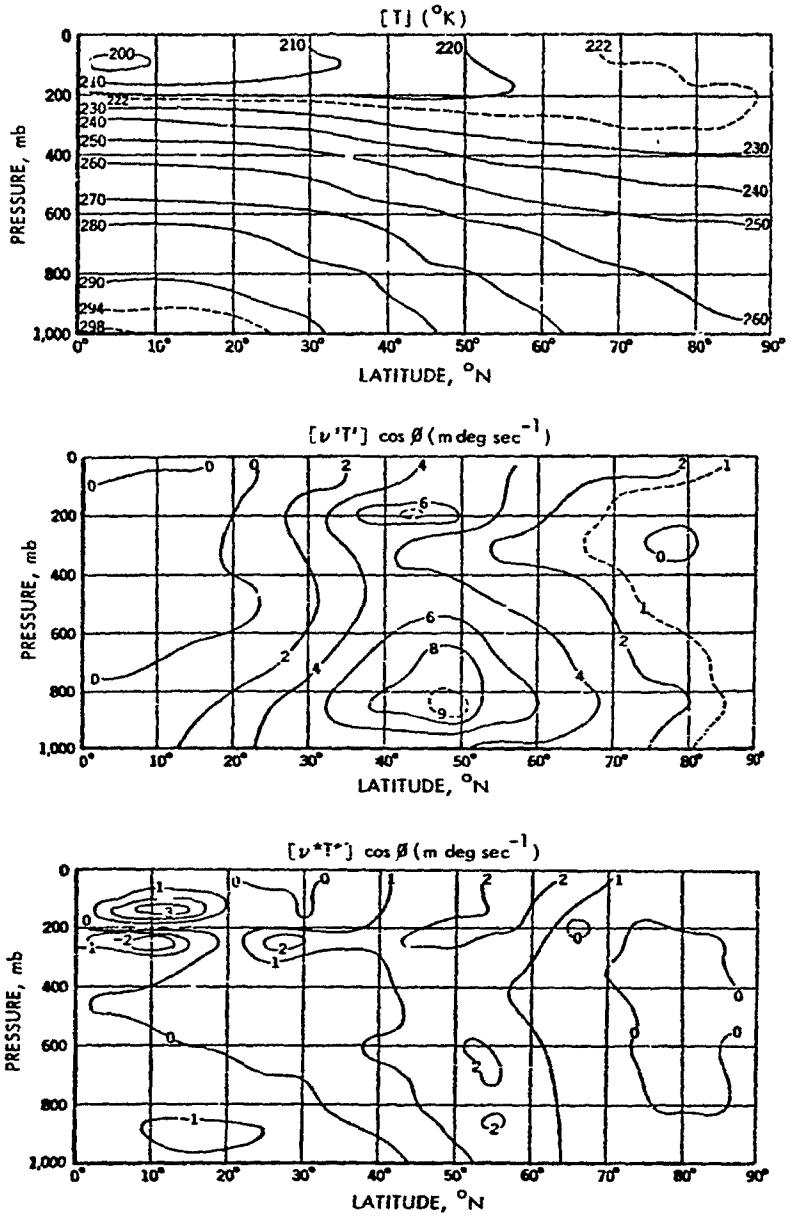

FIGURE 36. Temperature and Transpor' of Heat (After Starr, 1968)

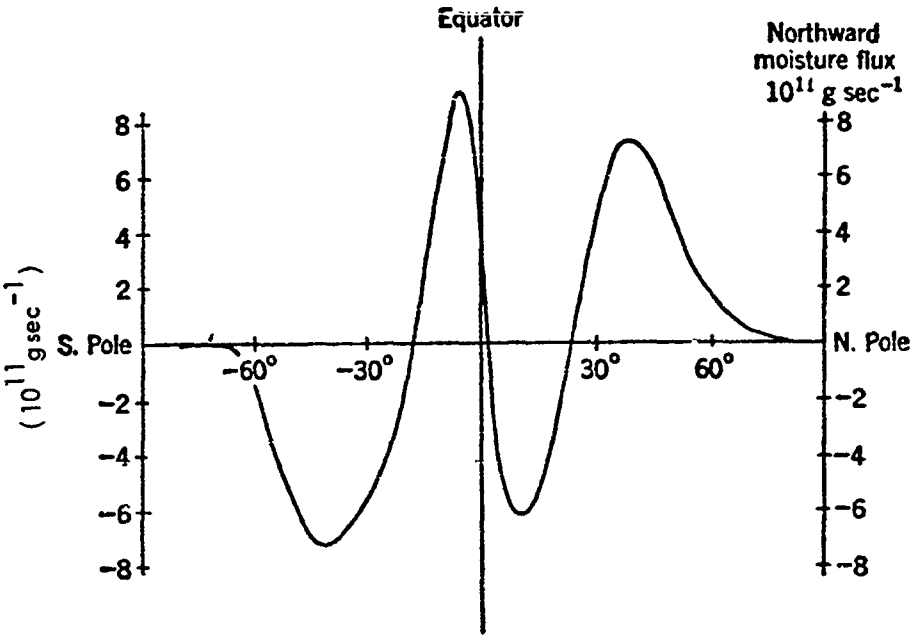

FIGURE 37. Transport of Water Vapor (After Starr, 1968)

Just as there exists a transfer of kinetic energy from the eddies to the 0 harmonic (i.e., the mean zonal kinetic energy), a redistribution of kinetic energy takes place among the wave numbers from 1 to 15 and probably beyond. Figure 38 shows the results of a spectral study based upon daily hemispheric wind data for a period of nine years at the 5 km level (near 500 mb). The main loss to other wave numbers is from the central band, from wave numbers 5 to 11 inclusive, corresponding to wavelengths at 45 deg latitude of about 2000 to about 5000 km. This energy is given up to both lower and higher wave numbers, with the loss being made good again by a transformation of potential and heat energy into kinetic in this central band. At the right in the diagram is shown the loss of kinetic energy from each wave number to the zonal flow. All 15 wave numbers feed energy to the zonal flow. The especially large loss from the box for wave number 2 probably reflects a monsoonal action.

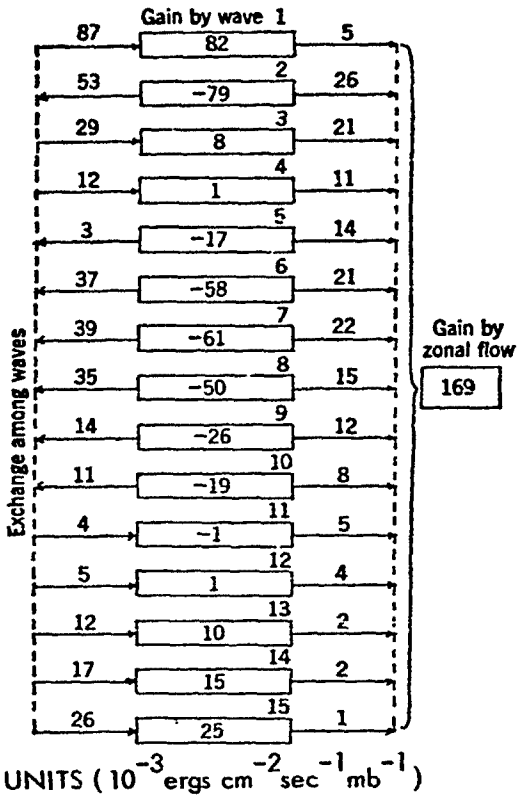

FIGURE 38. Spectrum of Kinetic Energy Exchange at 5-km Altitude (After Starr, 1968, Adapted from Saltzman and Teweles, 1964)

Figure 39 is after Oort (1964) and Starr (1968) and is a schematic diagram illustrating the balance of four types of energy for the annual average condition of the entire atmosphere. The parentheses enclose Starr's estimates.

The arrow C indicates a flow of energy from the eddies to the mean flow. The heating of the atmosphere indicated at the top of the diagram is due to such sources as heating by condensation of water vapor and by radiation.

Table 8 shows five-year and seasonal averages for the transformations of energy in the atmosphere, derived by Starr (1968). His estimates are derived from available data for the Northern Hemisphere atmosphere for the period May 1, 1958, to April 30, 1963. Because of nonlinear effects, the figures for the total five-year period are not equal to the means for the four individual seasons.

Wave Regime of Thermal Circulation

Mintz (1961) has noted that there are two regimes of large-scale thermal circulation that can develop in a thin layer of fluid which is gravitationally held to a rotating sphere and is heated at the equator of rotation and cooled at the poles. In each of these general circulation regimes the fluid performs two basic functions which can hold for a rotating sphere: it maintains thermal equilibrium by transporting

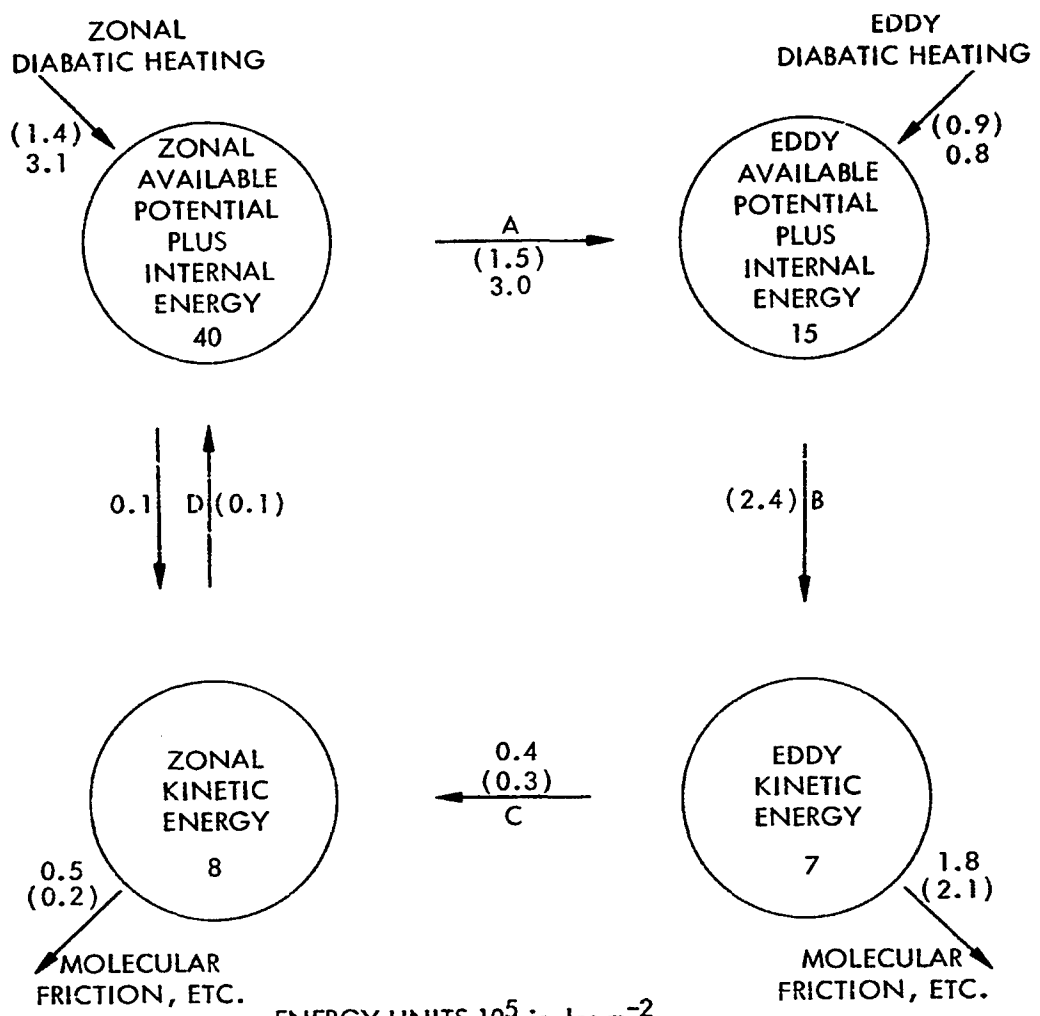

FIGURE 39. Energy Balance and Transport (After Oort, 1964, and Starr, 1968)

TABLE 8. TRANSFORMATIONS OF ENERCY IN THE ATMOSPHERE, UNITS OF 10^{20} ergs sec^{-1} (After Starr, 1968)

KE signifies kinetic energy and P+I is potential plus internal energy.

Period	5 years (60 months)	Spring (15 months)	Summer (15 months)	Fall (15 months)	Winter (15 months)
Generation of zonal KE by transient eddies	+ 6.5	+ 5.3	+ 4.3	+ 6.7	+ 6.1
Generation of zonal KE by standing eddies	+ 0.5	+ 0.5	+ 0.8	+ 1.8	+ 1.0
Generation of zonal KE by meridional circulations	- 6.0	-11.1	- 9.3	+ 1.1	- 1.8
Generation of eddy P+I by transient eddies	+20.3	+14.2	+ 7.6	+28.5	+33.0
Generation of eddy P+I by standing eddies	+ 2.6	- 2.1	- 0.8	+ 9.7	+18.2

heat from the equatorial heat source to the polar cold source, and it produces the kinetic energy necessary to maintain the circulation against frictional dissipation. The earth's atmosphere is characterized by the wave region. Discussion of the symmetric region is given to illustrate why the earth is in the wave regime.

In the symmetric regime of general circulation, the fluid in all longitudes, ascends near the equator of the rotating sphere, flows poleward in the upper levels, descends near the pole and flows equatorward, increasing in intensity with height in the direction of rotation of the sphere. In this regime the meridional and zonal components of the motion are the same in all longitudes. The circulation is symmetric about the pole, as shown in Fig. 40.

In the other form of general circulation, called the "wave regime," the flow is characterized by large amplitude horizontal waves (baroclinic Rossby waves described earlier by Eq. 2.174) in the middle and upper levels, and by large horizontal eddies (cyclones and anti-cyclones) in the lower levels of the fluid, as shown schematically in Fig. 41. In each hemisphere, the centers of the cyclones, in the mean, lie closer to the pole than the centers of the anticyclones and, as a result, the relative zonal flow at low levels, when averaged over all longitudes, is easterly near the equator and easterly near the pole, but westerly in middle latitudes. In addition, in the wave regime the zonally averaged meridional circulation is reversed in middle latitudes, as shown in the figure.

In the wave regime of circulation, there are the tongues of warm fluid moving poleward in some longitudes, while at the same elevation tongues of colder fluid move equatorward in other longitudes, which produce the poleward heat transport that balances the differential latitudinal heating. Unlike the wave regime, in the symmetric regime a net poleward heat transport occurs only when the vertical lapse rate of temperature is less than the adiabatic rate, so that the northward moving fluid of Fig. 41. has a higher potential temperature than the southward moving fluid.

Critical poleward temperature gradient

Mintz (1961) has described the critical poleward temperature gradient for dynamic stability of each wave number in the symmetric regime. Change in poleward temperature gradient may affect the dynamic stability. For temperature gradient smaller than the critical temperature gradient, the symmetric regime is stable; for larger

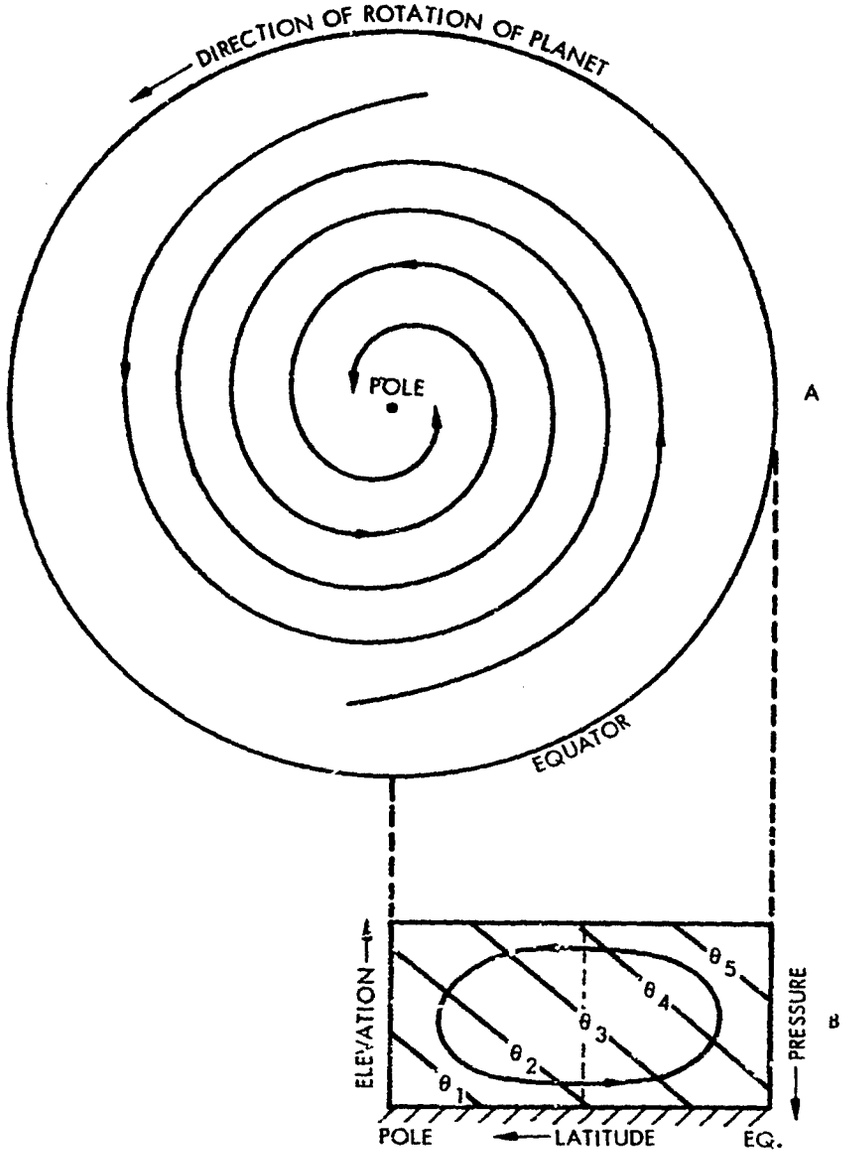

A. STREAMLINES OF THE FLOW AT THE UPPER LEVELS.
B. CROSS SECTION SHOWING THE MERIDIONAL PROJECTION OF THE CIRCULATION AND ISOTHERMS OF POTENTIAL TEMPERATURE θ.

FIGURE 40. Symmetric Regime of General Circulation
(After Mintz, 1961)

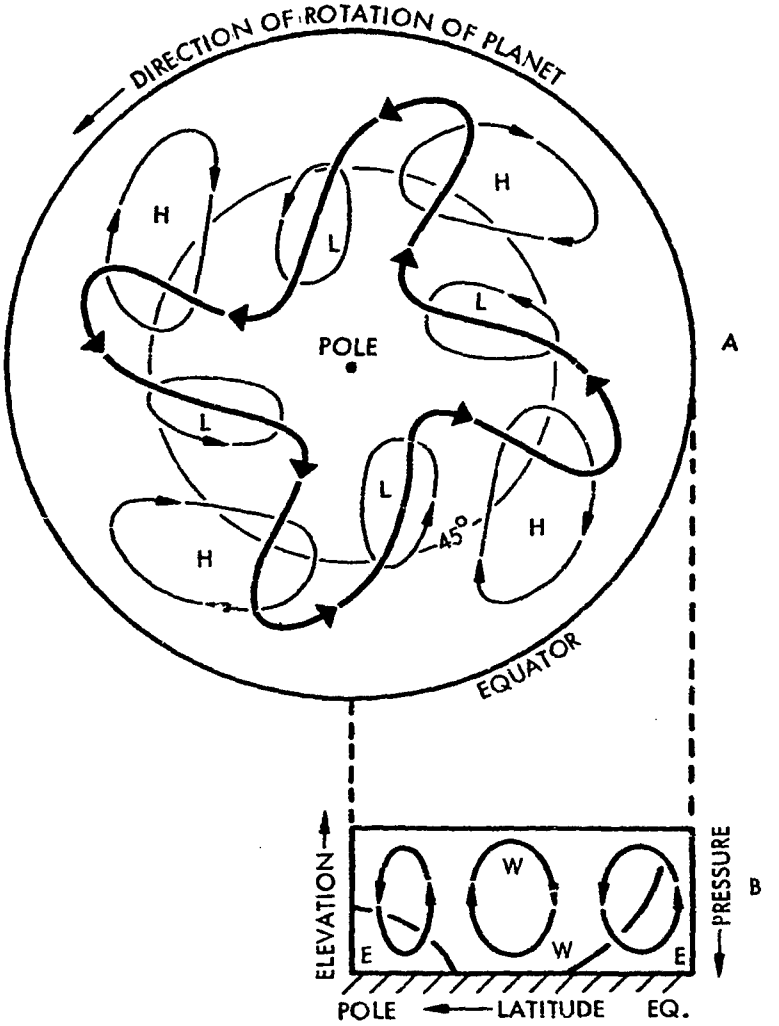

A) STREAMLINES OF THE FLOW AT THE MIDDLE AND UPPER LEVELS (HEAVY LINE) AND NEAR THE GROUND (THIN LINE). L = LOW PRESSURE, H = HIGH PRESSURE.

B) CROSS SECTION SHOWING THE ZONALLY-AVERAGED MERIDIONAL CIRCULATION; AND THE ZONALLY-AVERAGED ZONAL WIND, WHERE W = WESTERLY WIND, E = EASTERLY WIND.

FIGURE 41. A Wave Regime of General Circulation (After Mintz, 1961)

gradients, the symmetric regime is unstable and waves develop. In his development Mintz uses the two-level baroclinic model, applying the quasi-geostrophic vorticity equation

$$\frac{\partial \delta_g}{\partial t} = -\underset{\sim}{v}_g \cdot \nabla(\zeta_g + f) - f\nabla \cdot \underset{\sim}{v} + \hat{k} \cdot \underset{\sim}{v} \times F \qquad (2.180)$$

to levels 1 and 3, taken as the 250 and 750 mb levels, and the thermodynamic equation

$$\frac{\partial \theta}{\partial t} = -\underset{\sim}{v} \cdot \nabla\theta - w\frac{\partial \theta}{\partial p} + \frac{\theta}{c_p T}\dot{q} \qquad (2.181)$$

to level 2, taken at the 500 mb level. Where $\zeta_g = \hat{k} \cdot \nabla \times \underset{\sim}{v}_g$ is the vertical component of the curl of the geostrophic wind, $w = \partial p/dt$ is the vertical velocity in x, y, p-space, θ is the potential temperature and $\dot{q}$ is the rate of non-adiabatic heating per unit mass. Mintz makes further use of the geostrophic wind equation

$$\underset{\sim}{v}_g = \frac{g}{f}\hat{k} \times \nabla z_1 \qquad (2.182)$$

the equation of continuity of mass

$$\nabla \cdot \underset{\sim}{v} = -\partial w/\partial p \qquad (2.183)$$

Poisson's equation for potential temperature

$$\theta = T\left(\frac{p_s}{p}\right)^{\frac{R}{c_p}} \qquad (2.184)$$

the equation of state

$$T = p\frac{m}{\rho R} \qquad (2.185)$$

and the hydrostatic equation

$$\rho g = \frac{-\partial p}{\partial z_1} \qquad (2.186)$$

In the above expressions, $f = 2\Omega \sin \Phi$ is the Coriolis force, Ω is the rate of rotation of the planet, Φ is the latitude, $\underset{\sim}{F}$ is the horizontal friction force, ∇ is the horizontal del operator on the isobaric surface, $\hat{k}$ is the unit vertical vector, t is the time, z is the height of the isobaric surface, $\underset{\sim}{v}$ is the horizontal velocity, g is the acceleration of gravity, μ is the vertical eddy viscosity, δ is the density, $s = (1 - \frac{\gamma}{\gamma_d})$ is the static stability, $\gamma = \partial T/\partial z$ is the vertical temperature gradient, $\gamma_d = -\frac{g}{c_p}$ is the adiabatic vertical temperature gradient, R is the universal gas constant, m is the mean molecular weight, c_p is the coefficient of specific heat at constant pressure, a is the radius of the earth, ΔQ is the net heating of the atmosphere on the equatorward side of the central latitude.

Using the relations developed by P. D. Thompson (1961) for the two level baroclinic atmosphere, and linearizing by neglecting the heating and friction terms and by requiring that the zonal component of the geostrophic wind be horizontally uniform and independent of time, Mintz describes the behavior of any sinusoidal perturbation of zonal flow as being determined by the parameter

$$\delta = \left(\frac{-\partial \tilde{T}_2}{\partial \dot{\varphi}}\right) - \frac{a^2\Omega^2 m\lambda^2}{Rn^2(\lambda^4 - n^4)^{\frac{1}{2}}} \qquad (2.187)$$

where

$$\lambda = \frac{a\Omega m}{R}\left(\frac{2c_p}{T_2 s}\right)^{\frac{1}{2}} \qquad (2.188)$$

and n is the planetary wave number, i.e., the number of waves around the hemisphere. When $\delta < 0$, the perturbation at both levels oscillates about its initial amplitude. When $\delta > 0$, the perturbation grows in amplitude without limit--that is, the waves amplify and the wave perturbation acts to reduce the poleward temperature gradient.

Critical temperature gradient and dominant wave number

A plot of the neutral curve $\delta = 0$ as a function of poleward temperature gradient ($-\partial T_2/\partial \Phi$) and planetary wave number n is shown in Fig. 42. As may be seen in the figure there is a critical value of the poleward temperature gradient.

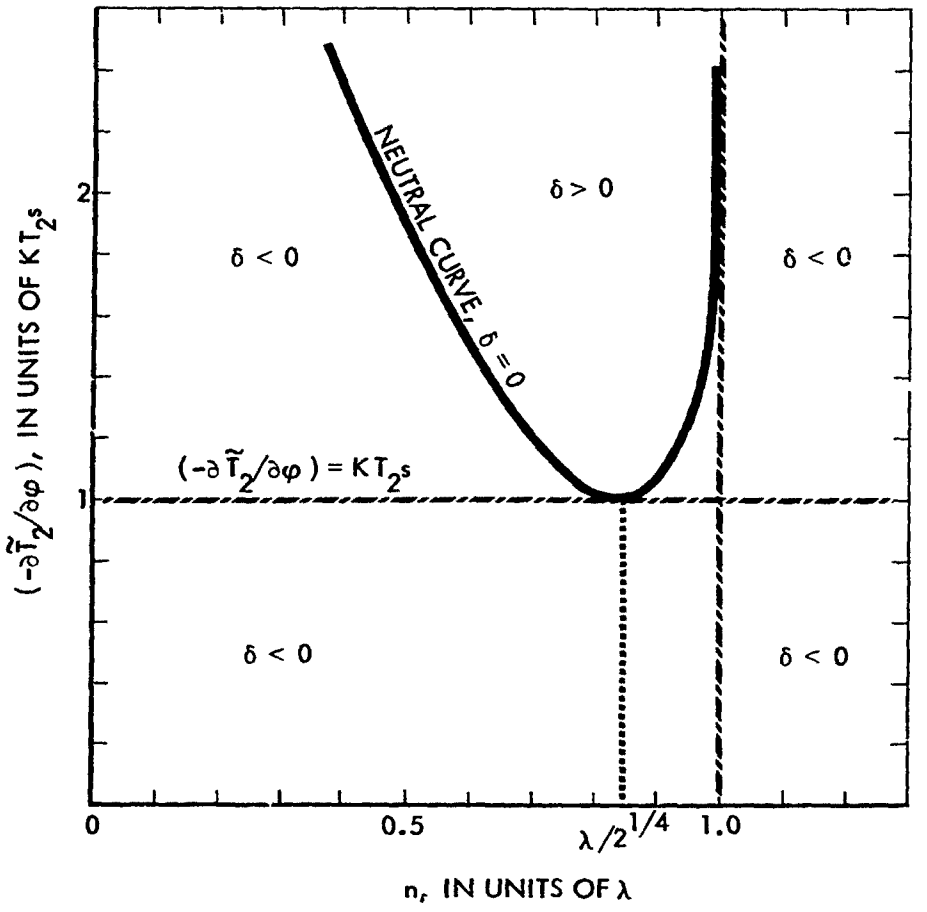

FIGURE 42. Stability of the Symmetric Circulation (After Mintz, 1961)

$$\left(\frac{\partial \tilde{T}_2}{\partial \phi}\right)_{crit} = \frac{R}{c_p} T_2 s \qquad (2.189)$$

below which $\delta < 0$ for perturbations of all wavelengths. When $(-\partial T_2/\partial\phi)$ barely exceeds $(R/c_p)T_2 s$, perturbations of planetary wave number $n = \lambda/2^{\frac{1}{4}}$ have $\delta > 0$ while longer and shorter waves still have $\delta < 0$. This particular value of wave number is a critical one, and is termed the "dominant wave number":

$$n_d = \frac{\lambda}{2^{\frac{1}{4}}} \qquad (2.190)$$

Should the poleward temperature gradient be larger than the critical value $(R/c_s)T_2 s$, then δ is positive over a broader range of wavelengths. However, it is never positive for wave numbers larger than λ.

Velocity of wave propagation

The dominant wave number n_d is important because the critical value of $(\partial \tilde{T}_2/\partial\phi)$ never can be very much exceeded except when $\lambda \leq 1$. We may imagine a differential heating ΔQ which exceeds the heat transport characteristic of the symmetric regime and thereby makes the poleward temperature gradient $(\partial \tilde{T}_2/\partial\phi)$ gradually increase to approach its critical value from below. Because of irregularities of the surface of the atmosphere, small amplitude perturbations in all wavelengths will always be present. As $(\partial T_2/\partial\phi)$ passes its critical value, perturbations whose wavelengths lie near the dominant wavelength will start amplifying, and transport heat polewards. Thermal equilibrium will first be reached when the waves have grown large enough in phase lag and amplitude for the poleward transport to balance the heating. As the waves continue to grow, the heat transport becomes larger than the ΔQ heat input, $(\partial \tilde{T}_2/\partial\phi)$ in time is reduced to less than its critical value, giving rise to an oscillation in which thermal equilibrium is maintained by the waves only in the long term average.

The criterion for the establishment and maintenance of the wave regime, is whether $(-\partial T_2/\partial\phi)_{H_s=\Delta Q}$ is larger or smaller than $(-\partial T_2/\partial\phi)_{crit}$ wherein $(-\partial T_2/\partial\phi)_{H_s=\Delta Q}$ is the poleward temperature gradient sufficient to transport the net heating of the atmosphere on the equatorward side of the central latitude under steady state symmetric circulation

$$\left(\frac{-\partial\tilde{T}_2}{\partial\phi}\right)_{H_s=\Delta Q} = \left(\frac{\sqrt{2}\,\Omega^2 m}{\pi g R s \mu_2}\right)\Delta Q \tag{2.191}$$

and the critical value of net heating is

$$\Delta Q_{crit} = \frac{\pi g R^2 \tilde{T}_2 \mu_2 s^2}{\sqrt{2}\, m c_p \Omega^2} \tag{2.192}$$

That is, when

$$\left(\frac{-\partial T_2}{\partial\phi}\right)_{H_s=\Delta Q} > \left(\frac{-\partial T_2}{\partial\phi}\right)_{crit} \tag{2.193}$$

and

$$\Delta Q > \Delta Q_{crit}$$

the wave regime of general circulation will form.

In the long time average, the heat transport equals the net heating equatorward of the central latitude. The total poleward heat transport across the central latitude by the waves when the surface winds are weak compared to the upper levels is compared to the upper levels is

$$\bar{H}_w = \frac{\pi a^2 c_p \Omega P_s \overline{V_2^2 \sin\alpha}}{Rgn} \tag{2.194}$$

where α is the phase lag between the waves at levels 1 and 3. $\bar{H}_w$ depends not only on the magnitudes of V_2 and α but also on the correlation between them. An order of magnitude estimate of the

wind speed average of levels 1 and 3 required for wave regime transport of net heating ΔQ is

$$\overline{V_2^2} \simeq \left(\frac{Rg\lambda}{2^{\frac{1}{4}}\pi a^2 c_p \Omega p_s (\sin 30^\circ)} \right) \Delta Q \qquad (2.195)$$

Wave dynamic parameters of the earth

The theoretical determination of the regime of general circulation of the earth's atmosphere is obtained by comparing ΔQ with ΔQ_{crit}. To a first approximation, Q for the earth is independent of the temperature distribution. The net heating per unit horizontal area, as a function of latitude is $(S(1 - A) - W)$, where S is the incident solar radiation derived from astronomical relations, A is the planetary albedo, taken as a constant $A = 0.34$, and W is the long-wave radiation emitted by the planet. This yields the mean annual distribution of $S(1 - A)$ shown in Fig. 43.

Because the earth has extensive oceans that are heated by the sun, there is widespread and persistent upward diffusion of water vapor from the ocean source, and the air in all latitudes is in a state of near saturation. Mintz assumes for his model of the earth that the relative humidity is uniformly high in all latitudes and that there is sufficient water vapor in the atmosphere so that all the outward radiation may come from the water vapor in the air. Under these conditions, where the temperature is high, as it is near the equator, the water vapor which emits the outgoing radiation will be at relatively high levels in the atmosphere; where the temperature is low, as it is in the troposphere of the poles, the emitting water vapor will be at lower levels. But the intensity of the outgoing radiation, which depends essentially only on the temperature of the water vapor and not on its elevation, will be of the same magnitude everywhere. Hence, in Mintz' model, the outgoing radiation W is taken as constant with latitude. For thermal equilibrium, the magnitude of W must equal the latitude mean of $S(1 - A)$ which is known. Hence, there results a net heating between the equator and latitude 37°,

and the pole of 10.6 $(10)^{19}$ cal day^{-1}

$$\Delta Q \approx 10.6(10)^{19} \text{ cal day}^{-1} \tag{2.196}$$

Further, Mintz takes the following values of the earth parameters:

$$\begin{aligned}
a &= 6.37(10)^{6} \text{m} \\
g &= 9.81 \text{ m sec}^{-2} \\
\Omega &= 7.29\ (10)^{-5} \text{ sec}^{-1} \\
T_2 &= 260^{\circ}\text{C} \\
c_p &= 1004 \text{ KJ ton}^{-1} \text{ deg}^{-1} \\
R/m &= 287 \text{ KJ ton}^{-1} \text{ deg}^{-1} \\
\mu &= 2.2(10)^{-2} \text{ton m}^{-1} \text{ sec}^{-1} \\
\gamma_d &= -g/c_p = -10^{\circ}\text{C/Km} \\
\gamma &= \gamma d/2 \\
S &= \left(1 - \frac{\gamma}{\gamma_d}\right) = 0.5
\end{aligned} \tag{2.197}$$

to derive the computer parameters

$$\begin{aligned}
\Delta Q &= 5.1(10)^{12} \text{ KJ sec}^{-1} \\
\Delta Q_{crit} &= 0.6(10)^{12} \text{ KJ sec}^{-1} \\
\left(\frac{-\partial T_2}{\partial \phi}\right)_{H_s=\Delta Q} &= 310^{\circ}\text{C/rad} \\
\left(\frac{-\partial T_2}{\partial \phi}\right)_{crit} &= 38^{\circ}\text{C/rad} \\
\gamma &= 6.36 \\
n_d &= 5.4 \\
L_d &= 5300 \text{ Km} \\
\left(\overline{V_2^2}\right)^{\frac{1}{2}}_{H_w=\Delta Q} &= 13 \text{ m sec}^{-1}
\end{aligned}$$

$$\text{RMS } (V_2)_{H_w=\infty} = 9 \text{ m sec}^{-1} \tag{2.198}$$

and the pole of 10.6 $(10)^{19}$ cal day^{-1}

$$\Delta Q \approx 10.6(10)^{19} \text{ cal day}^{-1} \tag{2.196}$$

Further, Mintz takes the following values of the earth parameters:

$$\begin{aligned}
\alpha &= 6.37(10)^{6} \text{m} \\
g &= 9.81 \text{ m sec}^{-2} \\
\Omega &= 7.29\ (10)^{-5} \text{ sec}^{-1} \\
T_2 &= 260^{\circ}\text{C} \\
c_p &= 1004 \text{ KJ ton}^{-1} \text{ deg}^{-1} \\
R/m &= 287 \text{ KJ ton}^{-1} \text{ deg}^{-1} \\
\mu &= 2.2(10)^{-2} \text{ton m}^{-1} \text{ sec}^{-1} \\
\gamma_d &= -g/c_p = -10^{\circ}\text{C/Km} \\
\gamma &= \gamma d/2 \\
S &= \left(1 - \frac{\gamma}{\gamma_d}\right) = 0.5
\end{aligned} \tag{2.197}$$

to derive the computer parameters

$$\begin{aligned}
\Delta Q &= 5.1(10)^{12} \text{ KJ sec}^{-1} \\
\Delta Q_{crit} &= 0.6(10)^{12} \text{ KJ sec}^{-1} \\
\left(\frac{-\partial T_2}{\partial \phi}\right)_{H_s=\Delta Q} &= 310^{\circ}\text{C/rad} \\
\left(\frac{-\partial T_2}{\partial \phi}\right)_{crit} &= 38^{\circ}\text{C/rad} \\
\gamma &= 6.36 \\
n_d &= 5.4 \\
L_d &= 5300 \text{ Km} \\
\left(\overline{V_2^2}\right)^{\frac{1}{2}}_{H_w=\Delta Q} &= 13 \text{ m sec}^{-1} \\
\text{RMS } (V_2)_{H_w=\infty} &= 9 \text{ m sec}^{-1}
\end{aligned} \tag{2.198}$$

For the Mintz model of the earth's atmosphere the differential heating ΔQ is many times larger than ΔQ_{crit}, the maximum for a dynamically stable symmetric circulation. Since with only symmetric circulation the poleward temperature gradient required to transport the heat from the equator to the poles would require a gradient of 310^{o}C per radian, but the critical dynamical limit of the poleward temperature gradient is only 38^{o}C per radian, planetary waves must develop in the atmosphere whose greater efficiency can transport the net heating. The number of waves around the earth will be the nearest whole number to the dominant wave number $n_d = 5.4$, corresponding to the dominant wavelength at latitude 45 deg of 5300 km. The root means spare meridional wind is 9 m sec^{-1}.

The computations described above are for an atmosphere in which there is no release of latent heat of condensation. If condensation is taken into account then the saturated adiabatic process rate γ_s must replace the unsaturated adiabatic process rate γ_d over about one-half of the wave domain, so that

$$s^* = \frac{1}{2}\left[\left(1 - \frac{\gamma}{\gamma_d}\right) + \left(1 - \frac{\gamma}{\gamma_s}\right)\right] \simeq 0.3 \qquad (2.199)$$

The effect of replacing s in the computations by s*, after the waves have developed to the extent of producing condensation, has two important consequences: it reduces the critical poleward temperature gradient with only a small change in the dominant wave number, and it produces a condition of hypercritical instability leading to a rapid rate of wave amplification in the one dimensional case and a rapid rate of cyclogenesis in the two dimensional system.

As illustrated by Fig. 44, this hypercritical instability ensues when the vertical motion of the amplifying perturbations brings about condensation in the ascending branches of the waves, causing the stability criterion to change abruptly from $\frac{RT_2 s}{c_p}$ to $\frac{RT_2 s^*}{c_p}$.

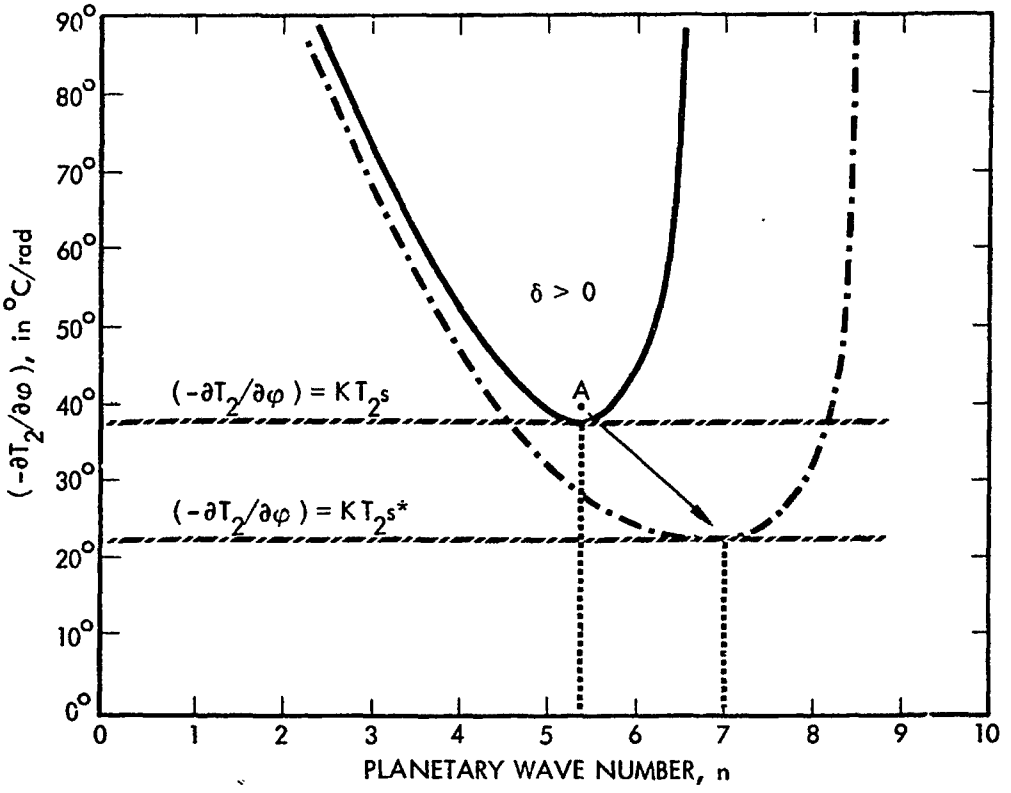

FIGURE 44. Illustration of Hypercritical Instability of Atmospheric Waves Resulting from Wave-Produced Condensation (After Mintz, 1961)

Because s^*/s - 0.6, about two-thirds of all the potential energy that was slowly stored in the buildup of the temperature gradient to its magnitude $\frac{R}{c_p} T_2 s$ now is available for rapid conversion to kinetic energy. Therefore, in this model atmosphere, waves which would grow only slowly and to moderate amplitudes (rms V_2 = 13 m sec^{-1}) when the temperature gradient is brought past its critical value from below and no condensation is permitted, will with the condensation grow rapidly and for a shorter time to larger amplitudes. With the larger amplitudes, $H_w \gg \Delta Q$ and the poleward temperature gradient falls rapidly to the saturation-critical value $\frac{R}{c_p} T_2 s^*$. Only after $(\frac{-\partial T_2}{\partial \phi})$ falls below $\frac{R}{c_p} T_2 s^*$ do the waves die out, so that the cycle may begin again with $\frac{R}{c_p} T_2 s$ again as the determining value for the next releave of hypercritical instability.

The following Table 9 shows Mintz' theoretically predicted values of the critical (and hence the limiting) poleward temperature gradients, the dominant wave numbers, and the root mean square meridional wind for his model of the earth's atmosphere, compared with the observed values for the real earth atmosphere. Both sets are yearly averages.

TABLE 9. THEORETICAL AND OBSERVED VALUES OF CRITICAL POLEWARD TEMPERATURE GRADIENT DOMINANT WAVE NUMBER AND MERIDIONAL WIND (After Mintz, 1961)

PREDICTED	OBSERVED
$\left(\frac{-\partial \tilde{T}_2}{\partial \varphi}\right)_{crit,\ S=0.5} = 38C^{\circ}/rad$ $\left(\frac{-\partial \tilde{T}_2}{\partial \varphi}\right)_{crit,\ S^*=0.3} = 23C^{\circ}/rad$	$\left(\frac{-\partial \tilde{T}_2}{\partial \varphi}\right)_{observed} = 29C^{\circ}/rad$
$n_{d(s=0.5)} = (5.4) \sim 5$ $n_{d(s^*=0.3)} = 7$	$n_{d,\ observed} = 6$ or 7
$rms(V_2)_{H_W=\Delta Q} \sim 9\ m\ s^{-1}$	$rms(V_2)_{observed} = 10.6\ m\ s^{-1}$

The agreement between the theoretically derived quantities for the Mintz model atmosphere and the observed quantities for the real atmosphere of the earth is good. The observed poleward temperature gradient falls almost halfway between the two limiting values, the observed dominant wave number is in close agreement with the theoretical numbers, and the observed rms meridianal wind is approximately the same as the theoretical estimate.

With respect to seasonal changes of the general circulation, Mintz notes first that the intensity of the atmospheric waves depends directly upon ΔQ. Neither the critical poleward temperature gradient $\left(\frac{-\partial \tilde{T}_2}{\partial \phi}\right)_{crit}$, and hence the actual poleward temperature gradient, nor the dominant wave number n_d depend directly upon ΔQ.

Using the measured poleward transport of sensible heat at the central latitude, which is about four times greater in summer than in winter, to arrive at a rough estimate of the seasonal values of the differential heating of the atmosphere, Mintz obtains

$$\Delta Q_{summer} \sim 2(10)^{12} \text{ KJ sec}^{-1}$$
$$\Delta Q_{winter} \sim 8(10)^{12} \text{ KJ sec}^{-1} \qquad (2.200)$$

From this, Mintz concludes that the rms meridianal wind must be twice as large in winter as in summer; this is approximately what is observed.

On the other hand, the static stabilities, s and s*, change relatively little with season in the earth's atmosphere, since the greater winter upward heat transport is compensated by the greater heat of condensation produced by the waves and released in the lower half of the atmosphere. Observations show that at the central latitude,

$$\left(\frac{-\partial \tilde{T}_2}{\partial \phi}\right)_{summer} = 22^{\circ}\text{C/rad}$$

$$\left(\frac{-\partial \tilde{T}_2}{\partial \phi}\right)_{winter} = 36^{\circ}\text{C/rad} \qquad (2.201)$$

This seasonal change of poleward temperature gradient is relatively small compared to the fourfold increase in ΔQ. The dominant wave number depends inversely on the square root of the static stability. Therefore, in spite of the large seasonal change in ΔQ, the wave number can decrease only slightly from summer to winter (from 7 or 8 to 5 or 6), as is observed.

Effects of the oceans and continents

There are several important ways in which the oceans influence the general circulation of the atmosphere of the earth. One of these is that evaporation from the oceans keeps the atmosphere in a state of near saturation. With its characteristic temperatures, the order of magnitude of which is given by the effective insolation $S(1 - A)$, near saturation means sufficient water vapor in the earth's atmosphere to make the infrared emission to space almost constant with altitude. As a result, the differential heating ΔQ exceeds the critical value for a stable symmetric circulation and the wave regime results.

A second important effect of water in the earth's atmosphere is that once the static stability s is reduced to its new value s^* by condensation in the waves, the heat of condensation thereafter keeps s^* constant. In the wave regime there is a positive correlation between the ascending motion and the temperature to produce a net upward transport of heat which, by itself, would make the space-averaged vertical gradient of temperature more stable. The heat of condensation, however, is almost entirely released in the lower half of the atmosphere, in contrast with the principal cooling term, the divergence of the net vertical infrared radiative flux, which is relatively constant with elevation. Being released in the lower half of the atmosphere, the heat of condensation therefore opposes the reduction of the space averaged vertical temperature gradient by the upward heat transport of the waves. In this way, s^* remains relatively constant in value.

In addition to the effect of evaporation from the ocean producing the water vapor of the atmosphere, the oceans also importantly influence the atmosphere through the seasonal storage of insolation. Since little insolation is absorbed by the earth's atmosphere directly, by far the larger part of the effective insolation $S(1 - A)$ is absorbed by the underlying surface. Because land has small thermal conductivity, especially when dry, little heat is stored in the land as the season changes. In contrast, the upper layer of the oceans has a high thermal eddy-conductivity and produces a large seasonal

storage of insolation. Since the temperature of the ocean surface changes little with the season, the heat transfer from ocean to overlying atmosphere has relatively seasonal variation. If a planet were completely ocean covered, the ΔQ would have only a small seasonal variation. On earth there is sufficient ocean area, even the northern hemisphere, for ΔQ to maintain a preponderance over ΔQ_{crit} throughout the year, and thereby maintain the normal wave regime year around.

As a consequence of the storage process and the limited longitudinal extent of the oceans, there is the important effect of the seasonal storage of insolation by the oceans in producing large zonal variations in the heating of the atmosphere. In the winter of the northern hemisphere, for example, in middle and high latitudes there is strong relative cooling of the air over the continents and heating over the oceans as the air of the troposphere flows from west to east. Over the continents the air cools because $S(1 - A)$ is smaller than W, while the temperature of the ground adjusts itself to the temperature of the air because the thermal conductivity of the ground is small. When the air that has been cooled over a continent moves over the ocean again, it is heated because it is colder than the warm ocean surface, while the temperature of the ocean surface remains almost unchanged because the thermal eddy-conductivity of the oceans is large. There are two important consequences of this zonally varying heating of the atmosphere. One is that low-level convergence is produced in the longitudes where there is heating of the air and low-level divergence when there is cooling. As a result, in the winter season there will be general low level horizontal convergence over the oceans and divergence over the continents, and therefore, lower mean surface pressure over the oceans than over the continents. In the summer season, the reverse pattern of heating and cooling and reverse distribution of high and low surface pressures over oceans and continents will occur. At the same time, the heating established in the upper levels an ultra-long-wave pattern of opposite phase to the surface pressure distribution.

The second important consequence of the zonally varying heating due to the ocean-land contrast is that it affects the horizontal temperature gradients, and hence the baroclinic stability at the coast lines. Especially near the eastern coastlines of the two northern hemisphere continents in the winter season, the contrast between cold continental air and warm maritime air produces a zone of large horizontal temperature gradient and hence a zone of maximum baroclinic instability. Thus, the eastern coastlines become preferred regions of baroclinic wave development. As a baroclinic disturbance moves eastward from its source region of maximum horizontal temperature gradient and moves through the region of maximum heating, and consequent surface convergence, of the ultra-long atmospheric wave, the low-level cyclonic part of the moving disturbance is amplified. In this way the baroclinic wave-cyclones, instead of being uniformly distributed around the globe, are concentrated in the oceanic longitudes, especially in the winter season.

Still another important influence of the ocean lies in its own ability to transport heat. The mean latitudinal heat transport by the ocean is indirectly estimated to be about $1(10)^{19}$ cal day^{-1} at the central latitude of the northern hemisphere, and hence has no controlling on the form of the atmospheric general circulation, since a reduction by that amount from the $10.6(10)^{19}$ cal day^{-1} required poleward heat transport would not change the circulation from wave to symmetric regime. However, important aspects of the atmospheric circulation, within the wave regime, can be influenced by the oceanic transport of heat. As a hypothetical example, an anomalous excess of insolation, resulting from a period of non-cloudiness, could be stored in the ocean in a region of down-welling current. This anomalous heat, when brought to the surface and transferred to the air, could affect the phase of the ultra-long atmospheric waves. Because of the interaction between the ultra-long waves and the baroclinic disturbances, this could result in a shift of the tracks of the rain producing baroclinic disturbances, east or west, resulting in long-period weather

anomalies over extensive regions of the globe. The atmosphere's small heat capacity and large velocity gives the atmosphere a short memory for anomalies of insolation, but the ocean with its large heat capacity and small velocities, has a long memory for anomalies of insolation.

III. PHYSICS OF THE STRATOSPHERE AND MESOSPHERE

Extending in altitude between the two temperature minima of the temperature-altitude profile illustrated in Fig. 4, the stratosphere and mesosphere form a region from perhaps 15 to 80 km altitude, characterized by a temperature maximum in the 40 to 60 km range, which acts somewhat as a barrier to the flow of energy, in forms other than radiative and conductive, between the two regions of the atmosphere which bound it. Energy within the region is derived mainly by absorption of solar ultraviolet radiation by ozone. Wave motion in the stratosphere and mesosphere is strongly suppressed.

TEMPERATURE STRATIFICATION

The temperature maximum is due to the absorption of solar UV in the 2000-3000 A region, largely by the Hartley system of ozone for which the absorption cross section peaks near 2600 A (See Fig. 19). The transition corresponding to the photodissociation of ozone is

$$O_3 + h\nu \text{ (Hartley)} \rightarrow O_2 \rightarrow O^*;$$

$$\kappa_1 \sim 1 \times 10^{-2} \text{ sec}^{-1} \text{ above 40 km.} \qquad (3.1)$$

At the altitude near 50 km the atmosphere is optically thick for this wavelength region, that is

$$\xi(h) \approx 1 \text{ for } h \cong 50 \text{ km}$$

wherein $$\xi(h) = \sigma_{(\text{Hartley})} \int_h^\infty n(O_3;h')\, dh' \qquad (3.2)$$

$n(O_3; h)$ is the particle number density of ozone at altitude h, as given by Nagata et al. (1957) and plotted in Fig. 45.

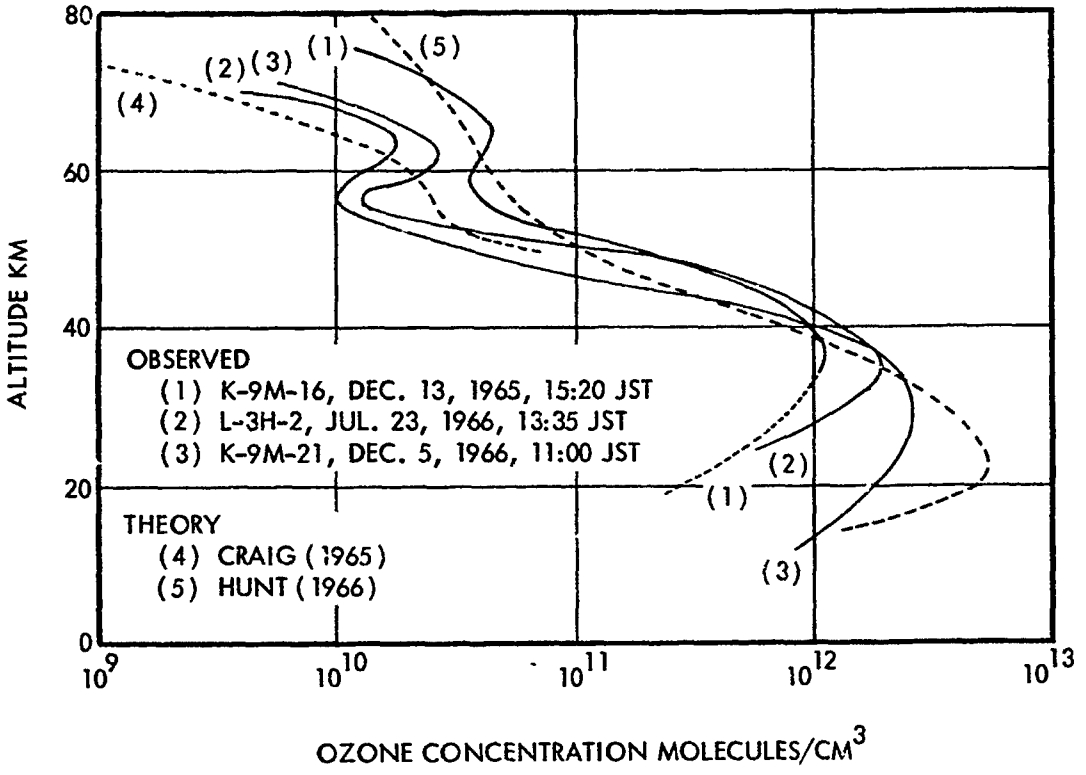

FIGURE 45. Ozone Concentration as a Function of Height (After T. Nagata et al., 1967)

Although $n(O_3; h)$ peaks at h = 20 km, since $\xi(h) = 1$ already at 50 km, the peak heating occurs at the relatively higher altitude. Evidently, above the tropopause, the ozone concentration may be explained by "photochemical equilibrium", that is, the ozone concentration is determined by the balance between the Hartley absorption reaction (3.1) and the processes

$$O + O + M \rightleftarrows O_2 + M; \; k_4;$$

$$\left[\text{Above the upper mesosphere, } k_4 \simeq 3 \times 10^{-33} \text{cm}^6\text{sec}^{-1}\right] \quad (3.3)$$

$$O + O_2 + M \rightleftarrows O_3 + M;\ k_5;$$

$$\left[k_5 \cong 5.6 \times 10^{-11} \exp\left(\frac{-2850}{T}\right) \text{cm}^6\text{sec}^{-1}\right] \quad (3.4)$$

$$O + O_3 \rightleftarrows 2\ O_2^*;\ k_6;$$

$$\left[\text{Below the lower mesosphere; } k_6 \cong 8.2(10)^{-35} \exp\left(\frac{445}{T}\right) \text{cm}^6\text{sec}^{-1}\right] \quad (3.5)$$

$$O_2 + M \rightleftarrows O_2^* + M \quad (3.6)$$

Under steady-state conditions for which

$$(d/dt)\ n(O) = (d/dt)\ n(O_2) = (d/dt)\ n(O_3) = 0 \quad (3.7)$$

At altitudes of 50 km and above the concentration of ozone is drastically reduced because of the higher intensity of solar UV which leads not only to the ozone photodissociation (3.1), but also to the O_2 dissociation reactions:

$$O_2 + h\nu \text{ (Schumann-Runge)} \rightarrow O(^3P) + O(^1D);\ \sigma_9;$$

$$\left[\sigma_9 \leqslant 10^{-17} \text{ cm}^2\right] \quad (3.8)$$

$$O_2 + h\nu \text{ (Herzberg)} \rightarrow 2\ O(^3P);\ \sigma_{10};\left[\sigma_{10} \leqslant 10^{-23} \text{ cm}^2\right] \quad (3.9)$$

The details of the photochemistry of atomic oxygen and ozone in the stratosphere are complicated by reactions involving water [Hunt, 1966 and Leavy, 1969].

At altitudes below 20 km, i.e., in the troposphere, the ozone concentration is higher than can be explained in the terms which

describe it for the stratosphere and mesosphere. Evidently this high concentration arises from low-level photochemistry of a different nature, such as that generating smog, etc.

To summarize, at altitudes above 50 km $\xi(h) < 1$ because there is too little ozone to make the atmosphere optically thick; at altitudes below 50 km, since most of the solar radiation incident on the atmosphere has already been absorbed at higher altitudes ($\xi > 1$), there is inadequate solar radiation in the Hartley band to heat up the atmosphere.

Having explained the temperature maximum at the stratopause, the lower bound of the stratosphere and the upper bound of the mesosphere will next be described.

The lower bound of the stratosphere is given by the tropopause, which corresponds to the temperature minimum between the tropopause, or that portion of the atmosphere which is in direct "contact" with the surface of the earth, and the thermopause.

If the temperature gradient (with increasing height) within the troposphere is negative, so that the adiabatic lapse rate

$$-dT/dh < g/c_p \tag{3.10}$$

(where g = acceleration due to gravity and c_p = specific heat at constant pressure), there is possibility of a fluid mechanical static instability by which a parcel of air of slightly different temperature can move a significant vertical distance, leading to overturning of the atmosphere. Such an overturning in the troposphere is particularly visible in the case of cumulus clouds.

The vertical motion arising from static instability is of vital importance in keeping water droplets or ice crystals in suspension in the troposphere. Since the terminal velocity of a spherical water droplet of 1μ radius predicted by the Stokes' formula is about 10^{-2} cm/sec, modest mean vertical motions may keep such droplets in suspension.

The clouds made up of ice and water particles fulfill an essential role in maintaining the thermal balance of the troposphere by absorbing, re-radiating and scattering solar and terrestrial radiation, as well as by the large thermal inertial provided by their heat capacity.

There are rare occurrences of other types of clouds at higher altitudes-"nacreous clouds", which occur rarely between 20 and 30 km under certain geographic and climatic conditions associated with strong winds, and "noctilucent clouds" which occur occasionally between 75 and 90 km, also associated with winds.

Under meteorological conditions the criterion for the maintenance of turbulence is commonly expressed in terms of the dimensionless Richardson's Number Ri, which is the ratio of the restoring buoyancy force per unit length of vertical displacement to the square of the wind shear

$$Ri = \frac{(g/T)(\partial T/\partial z + g/c_p)}{(\partial u/\partial z)^2} \tag{3.11}$$

where u is the horizontal wind velocity. Turbulence persists if

$$Ri < Ri_c \tag{3.12}$$

where various values of Ri_c have been quoted, ranging from 2 down to 0.4 (Schlichting, 1960).

Typical values of Richardson number, as computed for various altitudes, are plotted in Fig. 46. Also indicated are the values of temperature and of wind velocity used in the computations. In Fig. 46(a), Kochanski's wind data (Kochanski, 1964, 1966) are taken with temperature profiles of the U.S. Standard Atmosphere to be a basis for estimates of Reynolds and Richardson numbers. In Fig. 46(b) are Zimmermann's computations of Richardson number based on Sechrist et al. (1969) data of simultaneous measurements of wind and temperature. Zimmermann's data show that turbulence may occur low in the mesosphere under some conditions.

(a) COMPUTATION USING KOCHANSKI (1964, 1966) WIND DATA AND U.S. STANDARD ATMOSPHERE, 1962, TEMPERATURES FOR JANUARY, LATITUDE 60°N

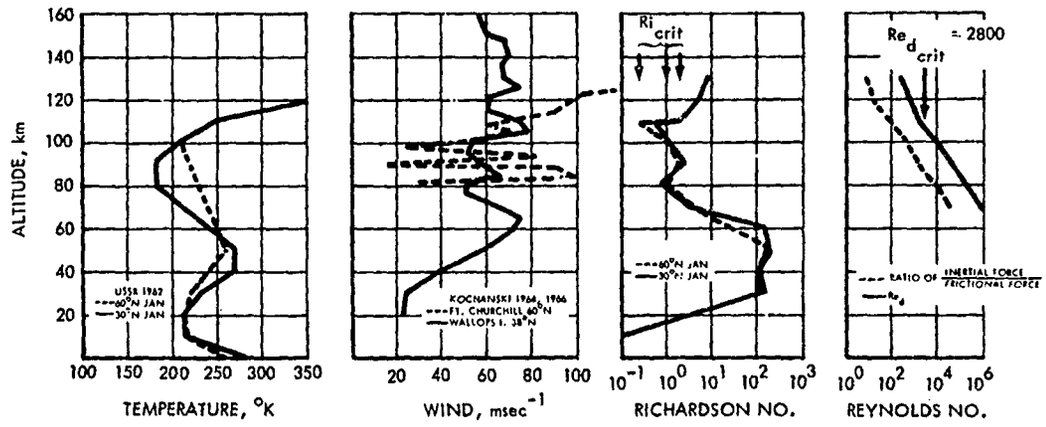

(b) COMPUTATION USING DATA BY SIMULTANEOUS MEASUREMENTS OF TEMPERATURE AND WINDS AT WALLOPS ISLAND, VA. (AFTER ZIMMERMAN, 1969)

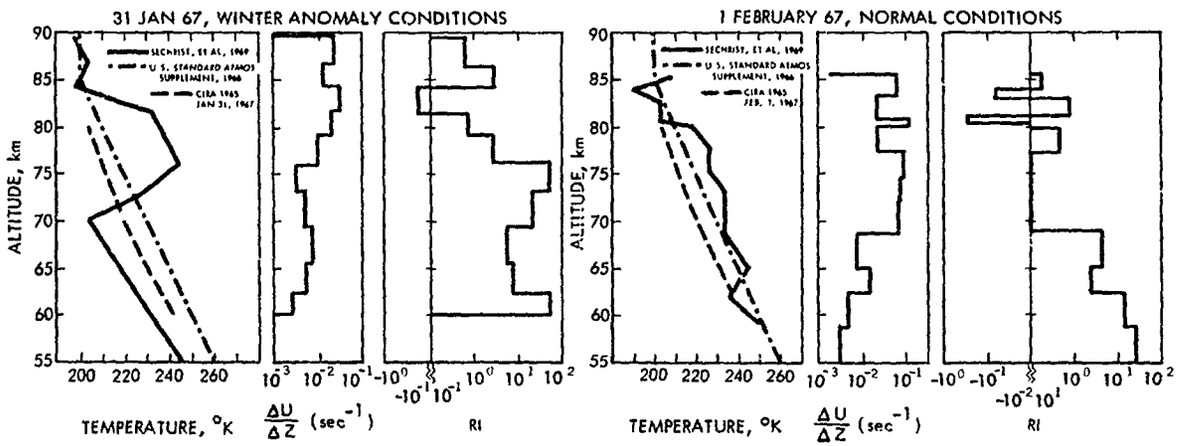

FIGURE 46. Temperature, Wind Speed, Richardson and Reynolds Numbers as a Function of Height

Conclusions to be drawn from the data on Richardson Number arrayed in Fig. 46 is that turbulence in the troposphere is unambiguously present, that the existence of turbulence in the stratosphere and mesosphere is unlikely, and that turbulence in the lower thermosphere is near the critical limit for suppression by the temperature gradient.

That the tropopause is sometimes abrupt is evidenced by the distinctive flat anvil-top of thunderclouds delineating an altitude above which condensed water cannot exist stably, and where the instabilities discussed above no longer occur. Above the tropopause there may be strong, steady, prevailing winds driven by the rotation of the earth as well as by the day/night and equator/pole heating and cooling.

The upper limit of the mesosphere is set by the mesopause, the minimum in temperature below the thermosphere which is heated largely by the Schumann-Runge continuum leading to the photodissociation of O_2, and above the stratopause arising from the heating ascribed to the Hartley continuum of ozone. The inversion due to the Schumann-Runge heating represents a smaller heat source than that of the stratopause, so that the conductive heat flow in the mesosphere is from below upwards along a negative temperature gradient.

ENERGY BALANCE AND FLOW

As in the D-region of the lower thermosphere, the chemistry of the stratosphere and mesosphere is complex, involving not only the minor species ozone and its decomposition products as indicated in Eqs. 3.1, 3.3, 3.4, 3.5, 3.6, 3.8, and 3.9, but also hydrogen compounds resulting from the dissociation of water vapor.

Horizontal transport of energy may be effected by means of strong prevailing horizontal winds, of speeds 50-100 m/sec (CIRA, 1965, p. 41 ff).

Figure 47 shows schematically the vertical energy transfer from the sun and within the various upper atmospheric regions. Other than for radiation directly from the sun, from region to region, the

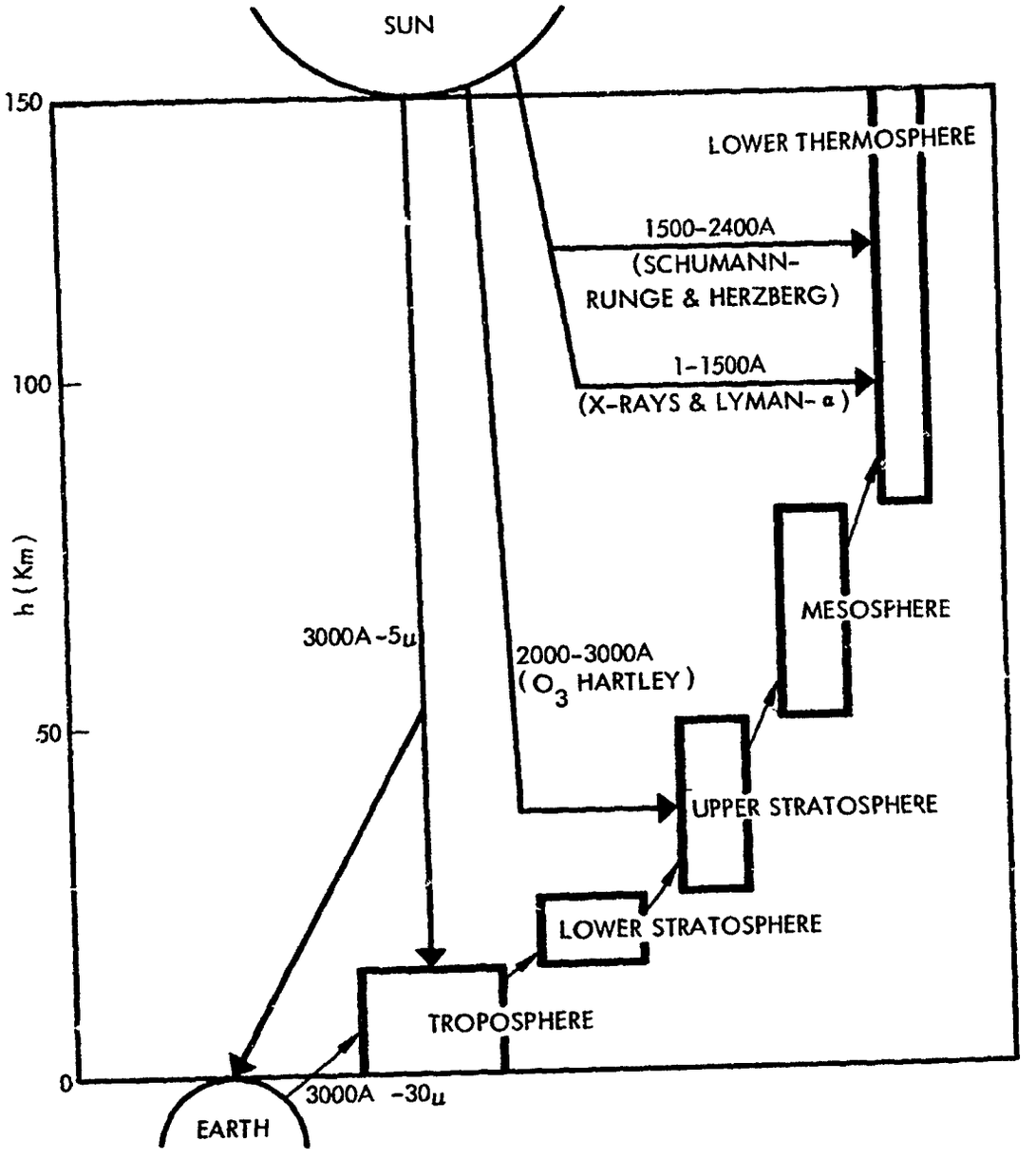

FIGURE 47. Possible Energy Flow Chart for the Upper Atmosphere (Modified from Newell, 1968)

transport is generally vertically upward, not downward. Since density decreases with height energy transport from a higher region is little able to affect a lower region. The higher region, due to its lower density, always has smaller heat capacity than the lower region, the higher region cools by radiative emission rather than conductively heats the lower region.

The following mechanisms for vertical energy transport have been considered -

(a) radiative transport; given the prevailing temperatures 200 - 300° K, the vibration-rotation levels in the infrared (2 - 30 u) are most important to this process
(b) molecular diffusivity
(c) turbulent diffusivity
(d) transport by organized macroscopic flows such as vertical winds or gravity waves
(e) chemical transport (e.g., atomic and molecular oxygen are transported from one altitude to another where they recombine, releasing the bond-energy).

Of these mechanisms, chemical transport (e) can clearly be considered negligible because of the low degree of dissociation. Molecular diffusivity (b) can be calculated by the standard techniques (Chapman & Cowling, 1939; Hirschfelder, Curtiss & Bird, 1954). Radiative transport (a) is possibly the most important single mechanism. By the theory of chemical reactions, quenching and the difficult conversion of vibrational into translational energy, perhaps half of the solar excitation absorbed remains in the form of vibrational energy. The transfer of vibration energy to form infrared-active species, which then re-radiate, tends to be rapid compared to vibration-translation deactivation. By these simplifying considerations, the radiative transport may be calculated by the generally recognized techniques of Kondrat'ev. (1965) and Goody (1964)

after the appropriate partition of energy from solar input into infrared active vibrational and rotational energy has been made.

The large-scale mechanical transport of energy, either by ordered motions, such as vertical winds or various other types of waves, or by random motion (molecular diffusion or turbulence). Because of static stability considerations (high Richardson's Number) random, or non-phase coherent motions, appear not to be important for vertical transport of energy in the stratosphere, in sharp contrast to the situation in the troposphere. Some phase coherent (ordered) motions of importance in the stratosphere and mesosphere are the driven motions of the tides (with periods of fractions of a solar day) and of the plentary waves, with longer periods. These are discussed in greater length in the following section.

MECHANICAL TRANSPORT BY WAVE MOTION

One may consider the large-scale mechanical transport of energy to be accomplished by wave action, which is phase coherent, and by turbulence, which is not phase coherent. Eckart (1960) nas given an excellent description of the several modes of wave action indicating that frequencies greater than the Brunt-Vaisala frequency $\left(N = \frac{g}{T_o}\left(\frac{\partial T}{\partial Z} + \frac{g}{c_o}\right)\right)$ the waves propagate like sound waves (hence are termed "acoustic waves"), frequencies smaller than the Brunt-Vaisala frequency but larger than the Coriolis frequency ($\Omega = 2$ day^{-1}) are characterized by the effect of gravity on buoyancy dominanting over the spring-like compressibility effect (hence are called "gravity waves"). Some of the gravity waves are propagated in modes with zero amplitude at the boundaries (hence they are termed "internal gravity waves").

Waves of another type are those called by Laplace "oscillations of the second kind" and include the tidal oscillations and the planetary waves. The tidal oscillations have periods corresponding to $1/\lambda$ of the solar or lunar day ($\lambda = 1, 2, 3$) for frequencies in the order of the Coriolis frequency; planetary waves, which have also

been described in one form by Rossby, have smaller frequencies than the Coriolis frequency.

The major period of the atmospheric tidal oscillations is half a solar day, rather than half a lunar day, as would be expected from the application of Newton's theory of gravitation. Siebert (1961) has shown that solar heating plausibly gives rise to the semi-diurnal tidal oscillation, with the diurnal solar heating tide suppressed by anti-resonance effects. Adding to Siebert's calculations for the effect of water vapor absorption, S. T. Butler and K. A. Small (1963) have shown that the water vapor and ozone absorption together can adequately account for the observed ground level atmospheric semi-diurnal and terdiurnal tides.

Theory and observation described by Charney and Drazin (1961) both indicate that only components of planetary waves (time scale long compared to a day), which are of global extent can propagate upward out of the troposphere into the stratosphere and mesosphere. R. E. Dickinson (1968) has described the following characteristics of the terrestrial planetary waves:

1. Planetary scale disturbances interact with the vorticity of the earth's rotation and propagate through the atmosphere as planetary waves.
2. Planetary waves are everywhere evanescent in the presence of an easterly zonal wind.
3. Strong westerly winds trap the vertical propagation of planetary scale waves.
4. Trapping of vertical propagation of planetary waves is absent locally near the equator.
5. Planetary waves are guided by horizontal shears. Examples are illustrated in Fig. 48 which is a schematic of the winter-summer zonal winds and the trajectories of planetary wave rays in the presence of the winds. The maximum westerly jet in middle latitudes at the stratopause acts as a reflecting

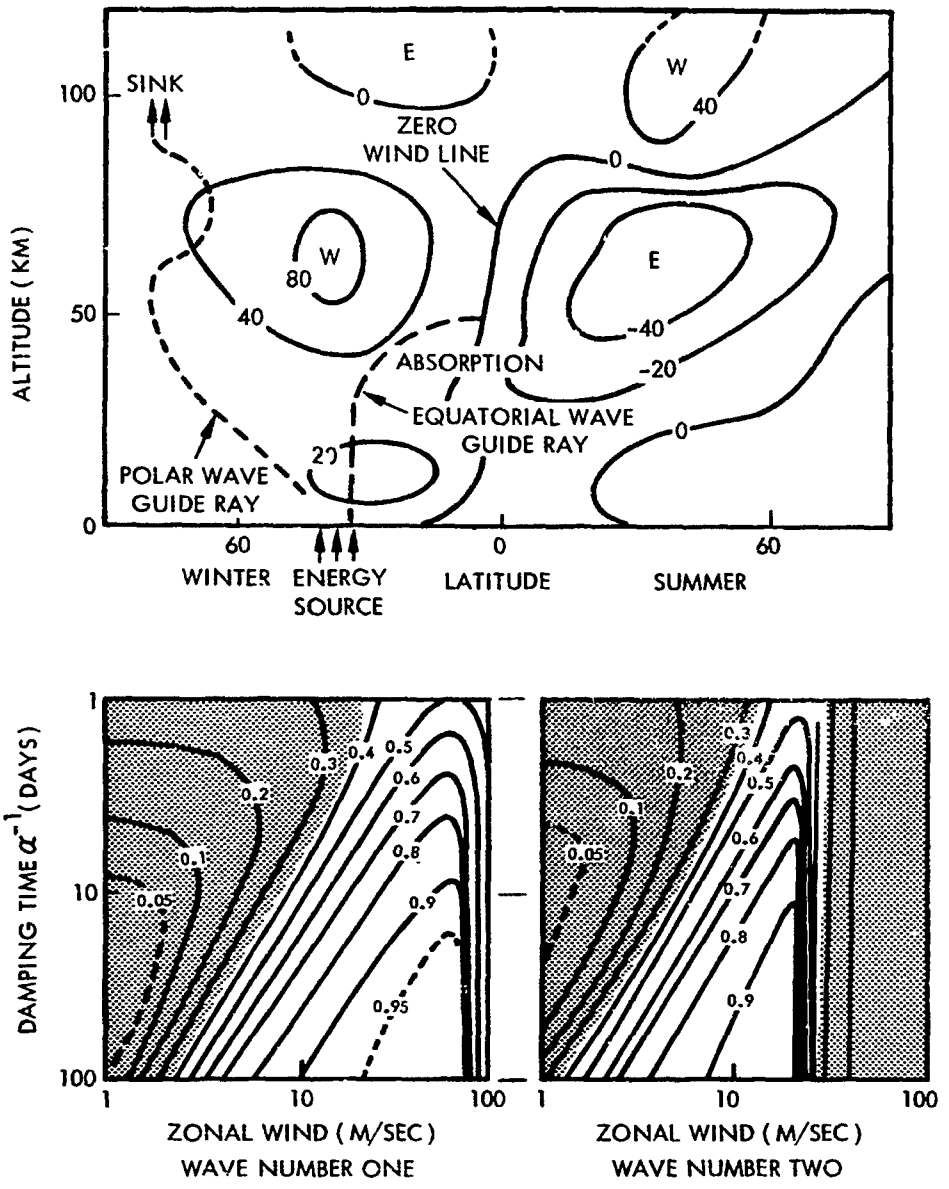

FIGURE 48. Schematic of Winter-Summer Zonal Winds and Trajectories of Planetary Wave Guides (After R.E. Dickinson, 1968)

barrier. The latitudinal variation of winds suggests the formation of polar and equatorial wave guides where the winds are weaker. Rays in the polar wave guide undergo multiple reflections between the pole and the westerly jet, setting up a standing wave normal mode in latitude. Also, in the equatorial wave guide, the rays are deflected onto the zero wind line where they are absorbed, giving rise to rapid attenuation with height.

6. Planetary waves in weak zonal winds are strongly damped by radiative processes. In Fig. 48 (after R. E. Dickinson, 1968) is shown the damping time for wave numbers one and two versus zonal wind for a number of values of the parameter representing fractional damping in one density scale height. The shaded region of parameter space indicates where the damping is severe enough to cause wave amplitudes to decrease with height.

7. Zonal motions may be coupled to both solar radiation heating and planetary waves.

Of the several types of wave motions listed above, the planetary waves seem to dominate the circulation of the troposphere; the planetary waves and tides dominate the stratosphere and mesosphere. In the lower thermosphere, in contrast, the gravity waves are important.

Gravity waves are observed within the troposphere, stratosphere, mesosphere, and the lower thermosphere. They give rise to the wind fluctuations which are seen at low levels as gusts. Observed at higher altitudes as deflections of smoke trails, they have impressive magnitude in the lower thermosphere, where Kochanski's (1966) analysis shows them to be comparable in amplitude to the tides.

In the first order, in the lower thermosphere and below, by neglecting the effects of viscosity and assuming the conservation of energy as the wave motion is propagated upward, one may note that since the density decays upward as exp (-z/H), the wave velocity must increase upward as exp (z/2H). The tides and the gravity waves

accordingly may be expected to have velocity values three orders of magnitude greater at 100 km than at the earth's surface. At 50-km altitude, on the other hand, gravity wave and tidal velocities may be but little more than an order of magnitude greater than at the surface.

Mahoney (1968) has described results of tracking falling ROBIN spheres by two different radars simultaneously, to show as in Fig. 49 that the wave motion common to the two tracks of the same sphere (tracks 1 and 3 in the figure) is of finite, but small amplitude in the stratosphere, and correlates well with the motion of a second ROBIN sphere falling at the same time about 48 km distant.

Kochanski's (1964) data shown in Fig. 50 show values of winds at Fort Churchill (60° N) and Wallops Island (30° N) and elsewhere. The large amplitudes of wind in the stratosphere and mesosphere are thought to be mainly due to tidal and planetary wave effects.

STRUCTURE OF ATMOSPHERIC TURBULENCE

The study of irregular motions in the atmosphere, by means of rocket releases of chemicals and by means of meteor trails, has established a region between 85 and 110 km called turbosphere. In this region irregular motions of both turbulent and non-turbulent nature have been observed, as described in Fig. 51. The curve in Fig. 51 represents the diffusion coefficient calculated using the altitude variation of the atmospheric density, temperature, and molecular weight given by the 1965 COSPAR international reference atmosphere for a 10.7 solar flux index 85, 0400 h, while the two lines with bars indicate the theoretical extremes of variation with season and solar cycle (Golomb and MacLeod, 1966).

Their investigations by experimental means have led to different interpretations (Zimmerman, S. P., 1966; Justus, C. G., 1966) and cast doubt to the existence of natural turbulence (Bedinger and Layzer, 1969).

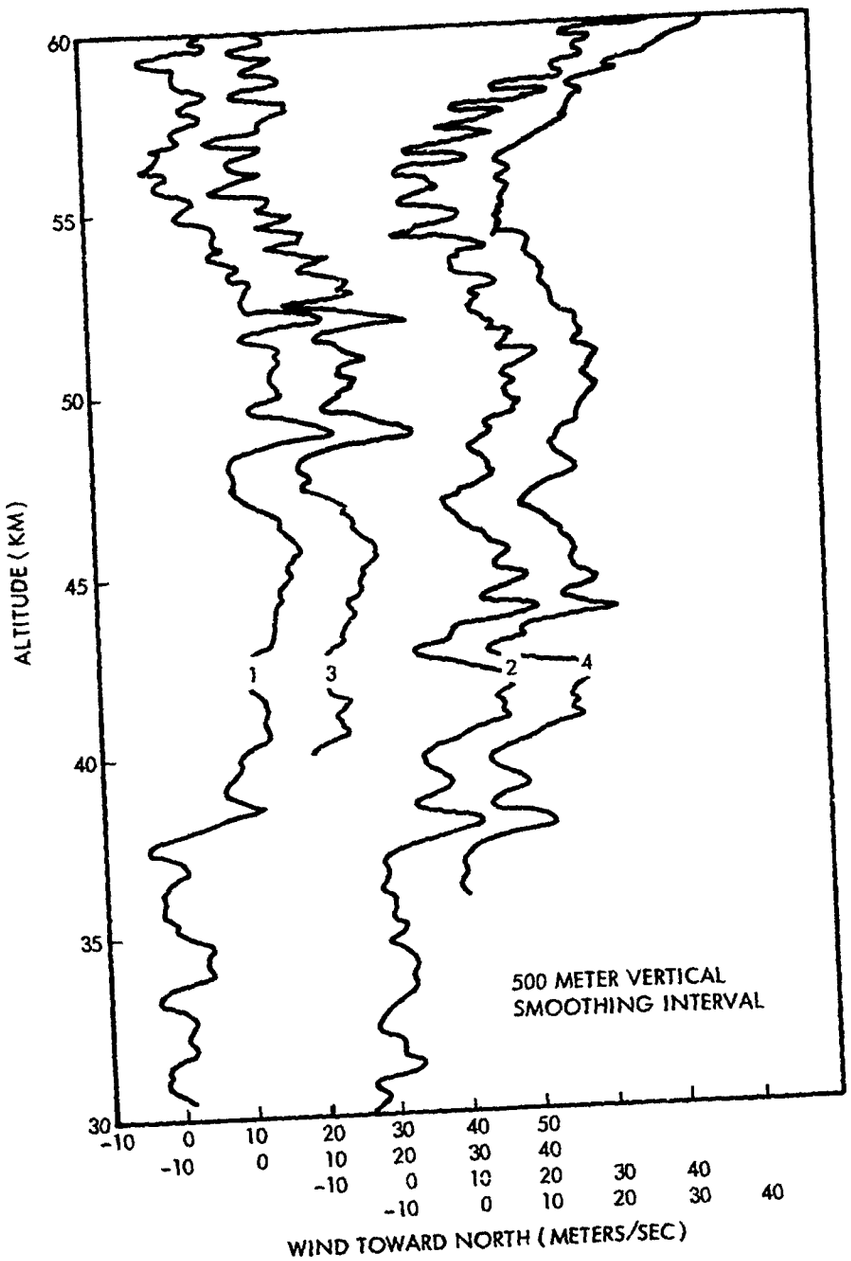

FIGURE 49. Horizontal Velocity Profiles in Stratosphere and Mesosphere by Radar Tracking of ROBIN Balloons (After J.R. Mahoney, 1968)

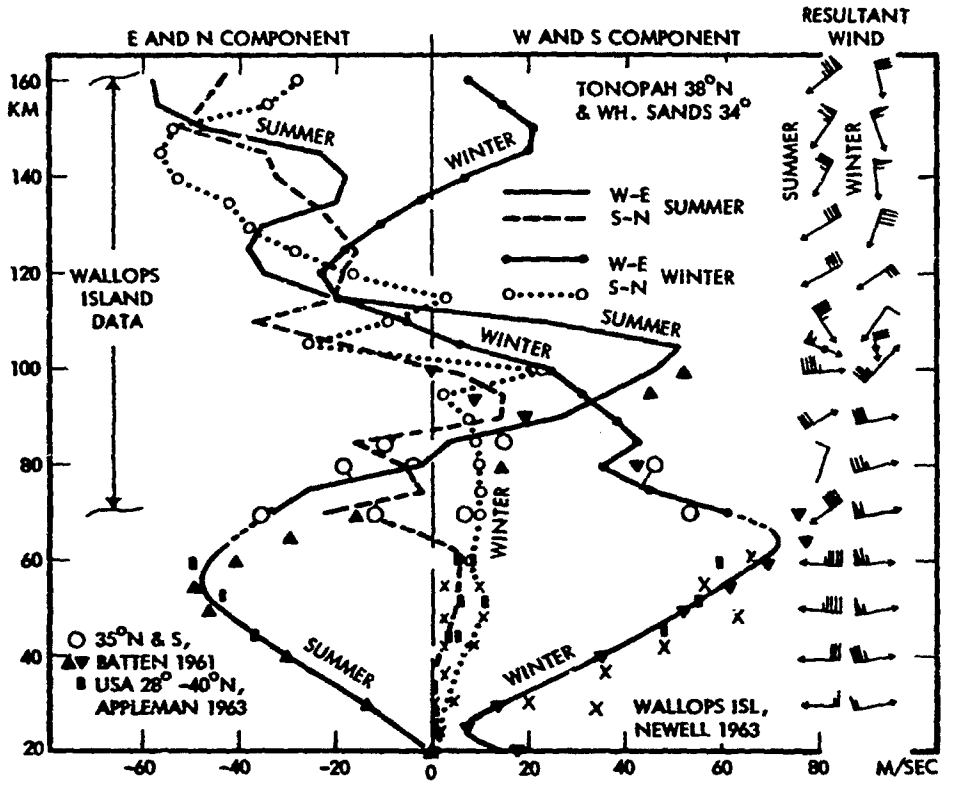

FIGURE 50. Wind Near 38° N (After Kochanski, 1964)

Measurements at 104 km indicate an energy dissipation rate of $\epsilon = 5 \times 10^3$ cgs and a molecular viscosity of $\nu = 10^6$, yielding an internal scale of turbulence (see Fig. 51).

$$k_\nu^{-1} = (\nu^3/\epsilon)^{1/4}$$

$$\sim 3 \times 10^3 \text{ cm}$$

The maximum horizontal scale of turbulent inhomogeneities may be estimated of the order 3000 km, and the vertical scale of the order of the scale height H. This indicates that the spectrum of atmospheric

turbulence is very broad, compared to spectra in laboratory turbulence, suggesting that one ought to find some portions of the spectrum obeying the Kolmogoroff law (Kolmogoroff, 1941a, 1941b):

$$F \sim \epsilon^{2/3} k^{-5/3} \tag{3.13}$$

Lower altitude flights over Australia confirm such a 5/3 - law, see Fig. 52 (Reiter, E. R. and Burns, A., 1966). However, at high altitudes (85 to 100 km), the presence of wind shear and buoyancy, or gravity waves, should complicate the structure of turbulence. It has been contemplated that the turbulence may be generated by internal gravity waves (Hodges, 1967).

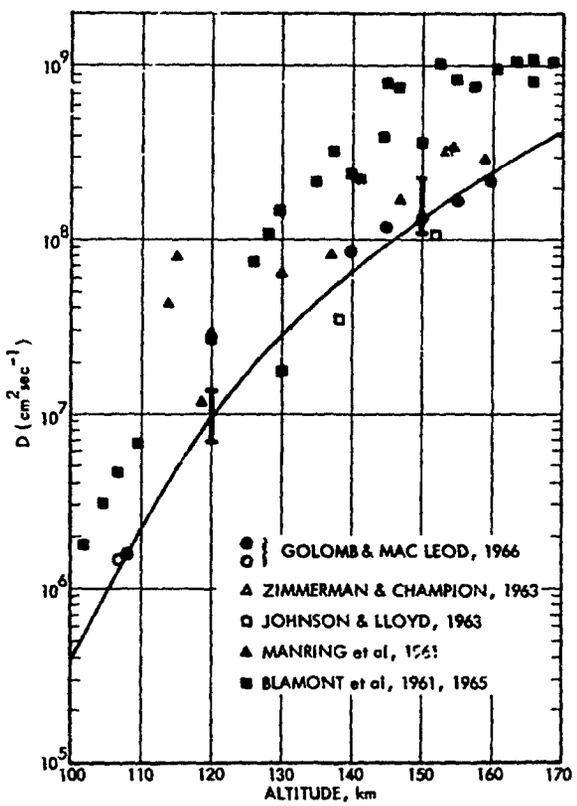

FIGURE 51. Diffusion Coefficient (After Golomb and MacLeod, 1966)

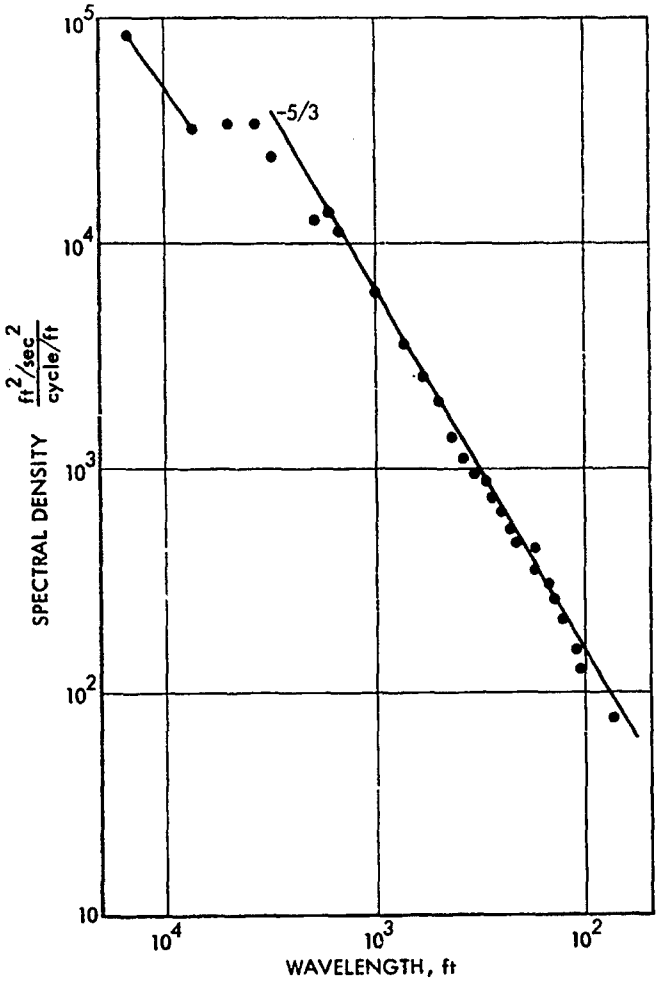

FIGURE 52. Spectra of Longitudinal (U) Component of Turbulence Measured by Project TOPCAT Over Australia (After Reiter and Burns, 1966)

The characteristic frequency N, given by

$$N^2 = \frac{g}{T}\left(\frac{g}{R}\frac{\gamma-1}{\gamma} + \frac{dT}{dz}\right)$$

determines the mode of the gravity wave, and is called the Brunt-Väisälä frequency. It serves also to derive the buoyancy subrange of the turbulent spectrum, which is found on a dimensional argument to be

$$F \sim N^2 k^{-3} \qquad (3.14)$$

Here T is the temperature, R the gas constant, and γ the ratio of specific heat. Measurements in the troposphere have found a portion of spectrum obeying the k^{-3} law (Tchen, 1969a), see Fig. 53. Spectra in the altitude of 85 to 160 km have also been compiled by Rosenberg (1967), after normalization to their scale heights, see Fig. 54. The data includes coverage of both upper and lower layers; that for upper layers may include the effects of gravity waves. According to the reduction by Tchen (1969a), these spectra follow also the k^{-3} law. See also Zimmerman (1969), Figs. 55 and 56.

It is evident that the wind shear should be strong enough at those altitudes to destroy the isotropy and to supply energy from the permanent wind shear to the turbulent motion. One may, therefore, ask whether the turbulent spectrum under such a wind shear would alter the Kolmogoroff law (Eq. 3.13) or the buoyancy law (Eq. 3.14). In this respect, Tchen (1953, 1954) has found a spectrum

$$F \sim (\epsilon/\omega_s)\, k^{-1} \tag{3.15}$$

in the shear production subrange, with support from experiments in wind tunnel turbulence, see Fig. 57 and Table 10. This result has been used by Zimmerman (1966) to derive the characteristic parameters of turbulence. Recently, by means of a cascade model of shear turbulence, Tchen (1969b) stipulates that the spectrum (Eq. 3.15) is valid in a wave number region smaller than a critical value k_s

$$k < k_s$$

where

$$k_s = (\omega_s^3/\epsilon)^{1/2}, \quad \omega_s = |dU/dz| = \text{wind shear frequency}$$

and that k should be sufficiently small that the vorticity function

$$2\int_0^k dh'k'^2F$$

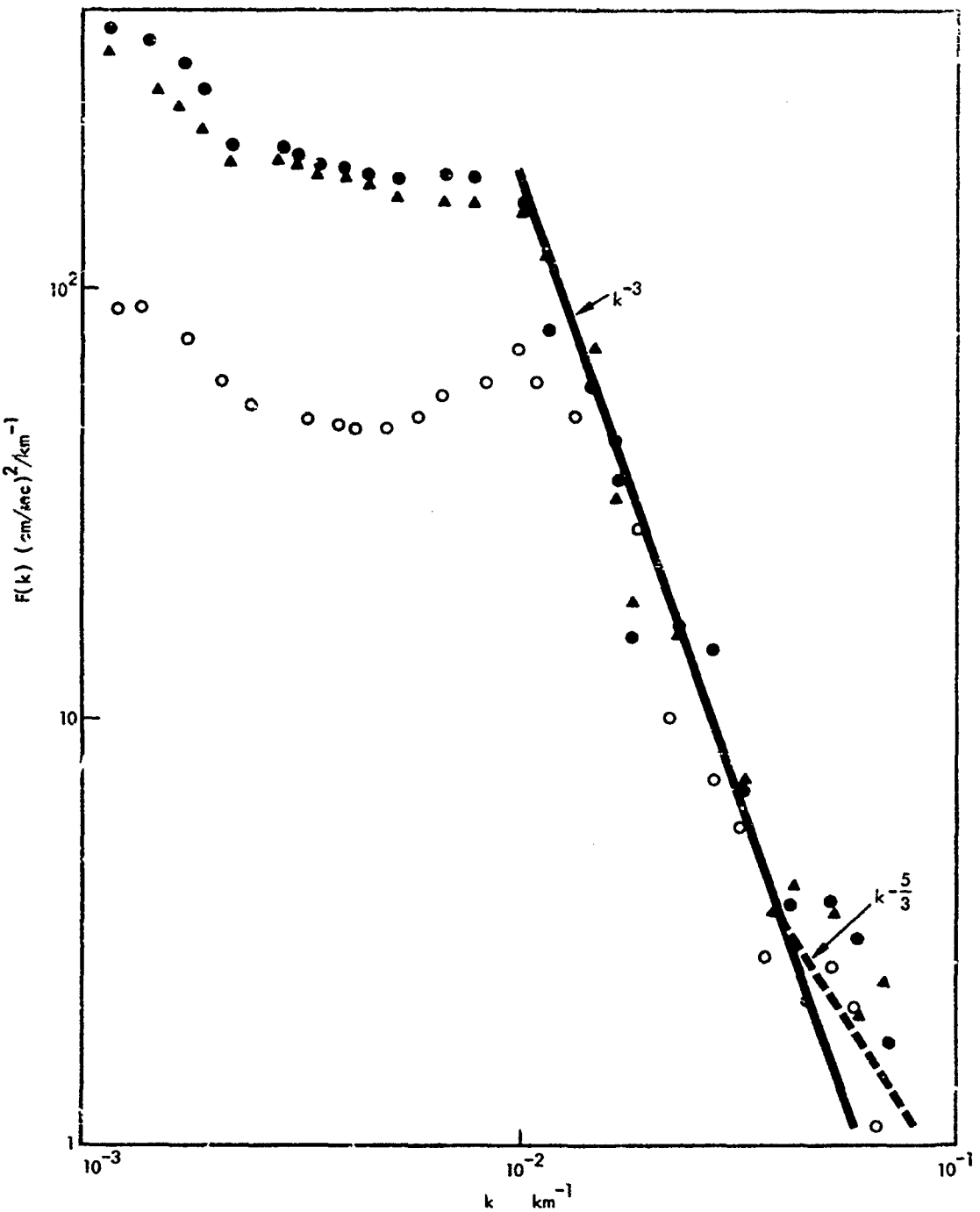

FIGURE 53. Spectrum of Turbulence Generated by Gravity Waves (Tchen, 1969a)

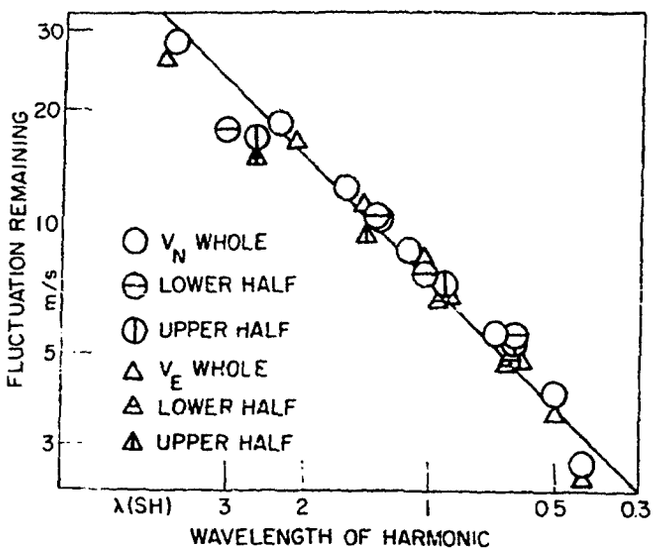

FIGURE 54. Spectrum of Residual Fluctuation Amplitude Versus Wavelength of Harmonic Removed (After Rosenberg, 1967)

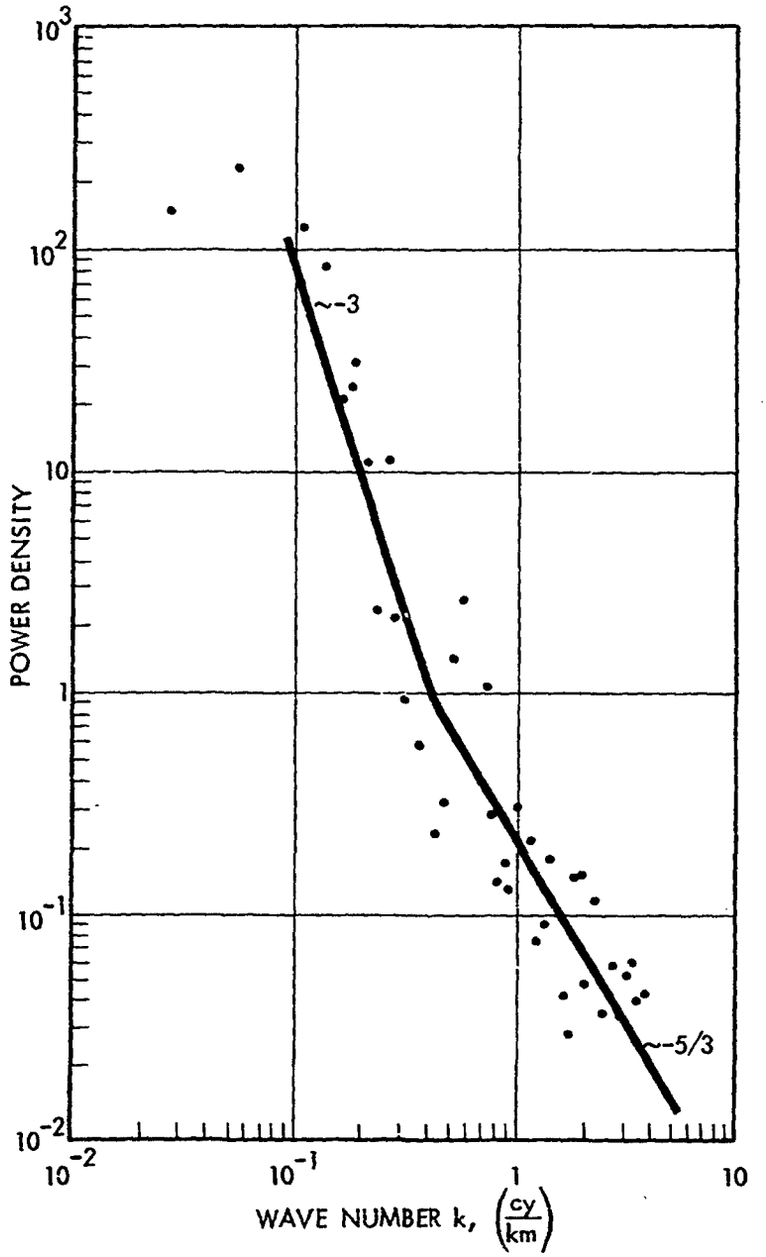

FIGURE 55. Longitudinal Component of Power Spectrum at h = 50 km (Zimmerman et al., 1969)

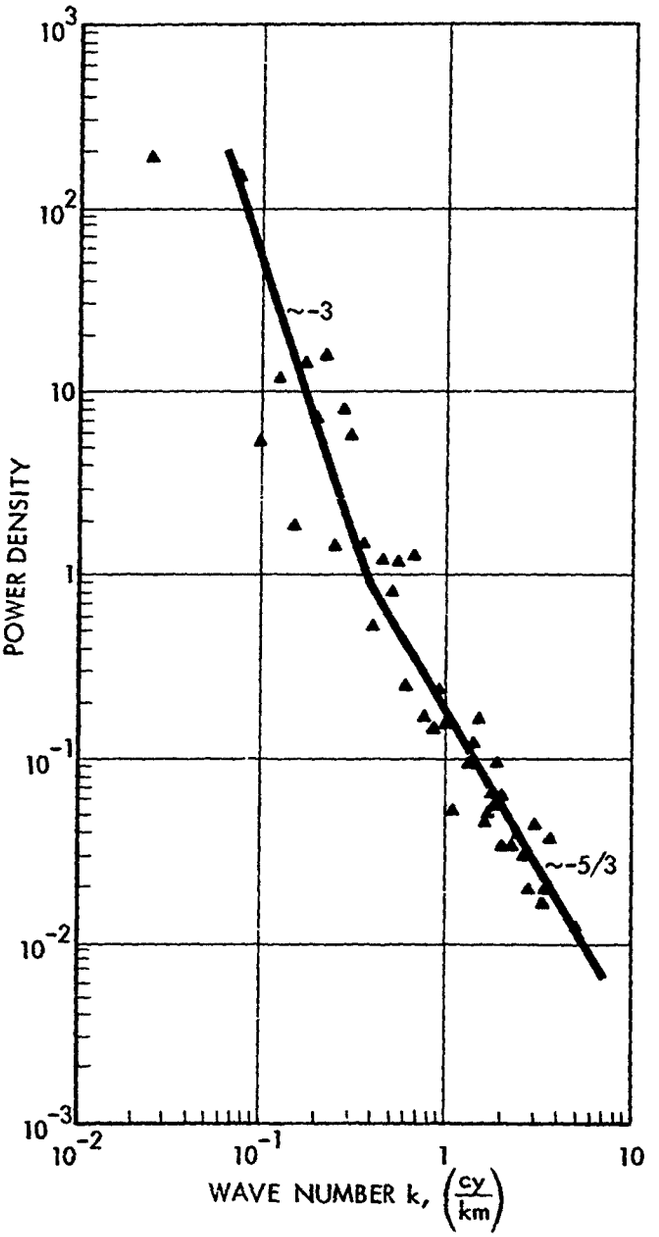

FIGURE 56. Transversal Component of Power Spectrum h = 50 km (Zimmerman et al., 1969)

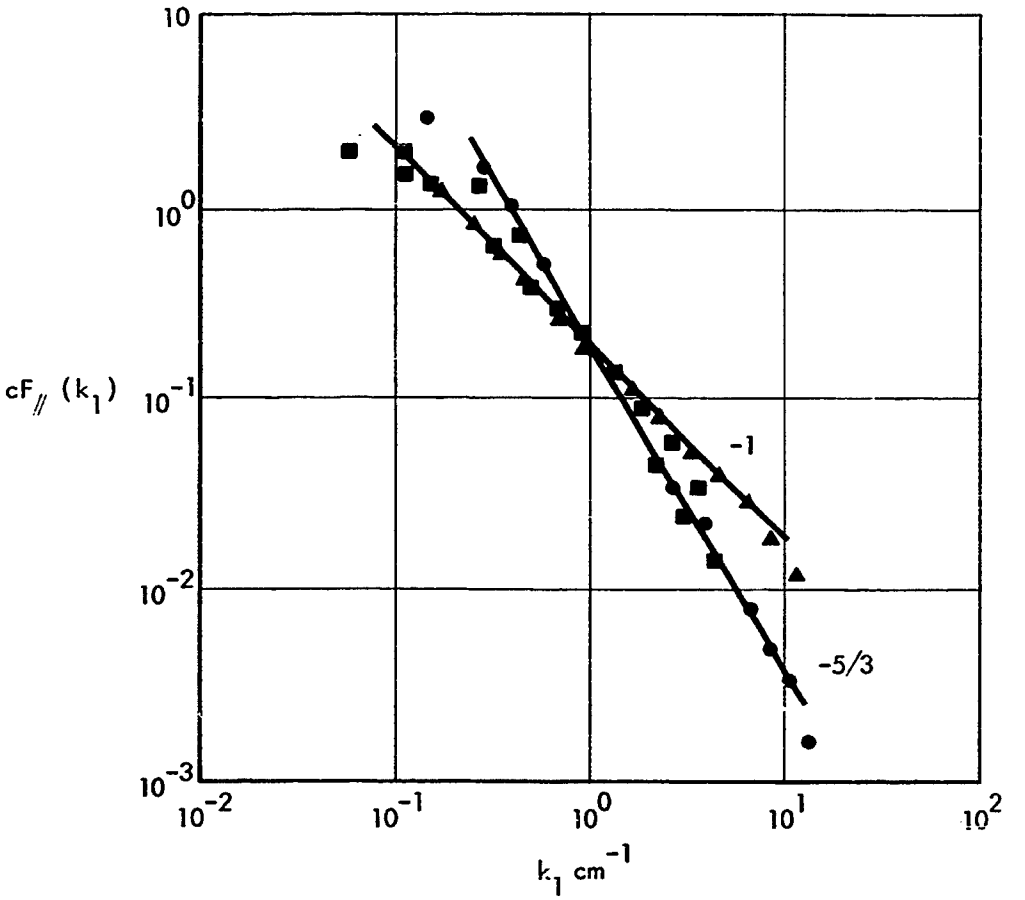

FIGURE 57. Longitudinal Energy Spectrum in a Boundary Layer and in a Pipe (Tchen, 1954)

TABLE 10. DATA FOR THE ENERGY SPECTRUM IN A BOUNDARY LAYER AND IN A PIPE (Tchen, 1954)

Experimental points	Type of flow	δ; cm	Um; cm/sec	Distance from wall; δ/x_2	Local mean velocity gradient	u' cm/sec	c
+	Boundary layer	7.6	1524	0.05	Large	119	1
▲	Pipe	12.3	3048	0.008	Large	256	3.87
x	Boundary layer	7.6	1524	0.8	Small	32	1
●	Pipe	12.3	3048	0.69	Small	113	2.51

and consequently the inertial transfer should not intervene. By increasing k, still within the above region $k < k_s$, the inertial transfer begins to intervene. From that point on, the spectral law (Eq. 3.15) is to be followed by a new spectral law

$$F \sim \omega_s^2 k^{-3} \tag{3.16}$$

in the shear turbulence.

We note now the difficulty for the same k^{-3} law in Eq. 3.14 and Eq. 3.16 to represent two different phenomena: one due to a buoyancy force and the other due to a wind shear. A discrimination between the two would be possible by a careful normalization of the experimental data to N or ω_s, respectively.

We conclude that it is extremely hard to discriminate and characterize a turbulent motion. We believe that it should possess the following features: an irregular nonlinear motion having a spectrum with a production, a mode transfer, and a dissipation. The mode transfer is a nonlinear mechanism responsible for the transfer of energy across the spectrum and must be present in general.

IV. PHYSICS OF THE THERMOSPHERE AND IONOSPHERE

The region above the mesopause, called the thermosphere, particularly affects radio communications and decay of low orbits of earth satellites.

GENERAL CHARACTERIZATION

As shown in Fig. 5, a profile of the temperature in the upper atmosphere as a function of altitude has a minima at 15 and 85 km. The region above the 85 km temperature minimum is called the thermosphere. Its upper limit, commonly placed at about 500 km altitude, depends significantly on latitude.

The thermosphere is characterized as follows:

(a) Temperature T increases with height h, going from perhaps 180^{o} K at h = 80 km to perhaps 1500^{o} K (±50%) above 400 km.

(b) The number density decreases from 10^{-6} times its sea-level value at 80 km down to 10^{-12} times its sea-level value at 500 km; or from 4×10^{14} cm^{-3} at 80 km to 5×10^{7} cm^{-3} at 50 km.

(c) There is a uniformly mixed region from sea level up to perhaps 100 km. Above 100 km, the composition changes markedly with altitude.

(d) For more than 200 km above about 90 km there is a relatively uniform density of free electrons, $n_e \sim 10^5 - 10^6$ cm^{-3}. Because of the drastic fall-off of neutral density, the plasma effects are important at the higher altitudes.

These characteristics (a) - (d) may be grossly explained as follows.

For particles of mass M and temperature T in a gravitational field, the density falls off with height according to:

$$\rho(h) = \rho(h_o)\, e^{-(h - h_o)/H} \quad ; \; H = kT/Mg \sim 10 \text{ km "scale height."} \qquad (4.1)$$

As a result of photochemistry and flow, this simple relation (4.1) does not, in fact, give the whole story. It is, however, a first approximation.

The precise/specific reasons why the atmosphere is uniformly mixed up to perhaps 100 km and not above are subjects of present scientific controversy. The rotation of the earth combined with differential day/night and equator/pole heating gives rise to large scale atmospheric winds. These move in a horizontal direction because of gravity but there are a number of large convection cells which overall serve to produce a large scale low frequency stirring and which also give rise to various high frequency disturbances including "internal gravity waves" and "turbulence" (Hines et al, 1965).

The fluid mechanical motions which lead to these irregular motions are large enough to keep the atmosphere uniformly mixed up to perhaps 100 km, where the gas kinetic mean free path is 16 cm.

The principal reason for the temperature increase above 80 km and for the composition change is that solar ultraviolet and X-radiation is absorbed in these upper fringes of the atmosphere and leading to dissociation and ionization, and consequently heating. At the 80-150 km level the biggest absorption mechanism by far is the Schumann-Runge continuum of O_2

$$O_2(X^3\Sigma_g^-) + h\nu_{Sch\text{-}R} \rightarrow O(^3P) + O(^1D) + K.E. \qquad (4.2)$$

As produced by solar radiation, the approximate energy balance of this process is as follows

wavelength of maximum absorption is 1500 A, i.e., $h\nu$	= 8.26 ev	(4.3a)
energy to dissociation $O_2(X^3\Sigma_g^+)$ into 2 $O(^3P)$	= 5.12 ev	(4.3b)
energy to excite $O(^3P)$ to $O(^1D)$	= 1.96 ev	(4.3c)
balance of energy, which appears as kinetic energy	= 1.18 ev	(4.3d)

The energy of electronic excitation eventually appears a kinetic energy as a result of quenching processes:

$$O(^1D) + N_2 \rightarrow O(^3P) + N_2(vib) + K.E. \qquad (4.4)$$

Since one electron volt (kT = 1 ev) corresponds to a temperature T = 11,600° K, and since about 1% of the atomic oxygen recombines over night to be re-dissociated in the morning, the process is the single most substantial source of heating of the thermosphere. It is moreover supplemented by kinetic energy of macroscopic mechanical motion which is transported upwards in the atmosphere by "internal gravity waves" (Hines et al, 1965) or by "internal gravity shocks" (Layzer, 1967).

At altitudes above 150 km the photo-ionization of O and N_2 contributes significantly to the photochemistry, and presumably also the heating, but there is much less flux of solar energy at the higher energies corresponding to wavelengths less than 11,200 A. Also there are fewer available absorbing atoms and molecules, since above 150 km there only remains 10^{-8} of the earth's atmosphere, or 10^{17} cm^{-2} column. Thus the rise in temperature above 150 km is slow.

The scale height H of Eq. 4.1 depends on molecular weight as well as on temperature. In the region above h = 100 km where the air is no longer uniformly mixed there will be a diffusive separation of the different species, with the lighter species (He, O) at the higher altitudes. This effect supplements the photochemistry to cause a

reduction of net molecular weight with increase in altitude from a value 29 at 80 km to a value 18 at 500 km.

Above about 200 km, the fraction of free electrons becomes appreciable (Delcroix, 1965)

$$\frac{\text{number density of free electrons}}{\text{total number density}} = \frac{n_e}{n_{tot}} \geq 10^{-4}; \; h > 200 \text{ km} \qquad (4.5)$$

under these conditions the motion of the atmosphere is determined largely by the motion of the ionized, rather than the neutral, constituents. In other words, the geomagnetic field tends to become a more important factor than the prevailing winds. In the high altitude region (h > 200 km), plasma effects dominate over the effects of continuum fluid dynamics.

At altitudes above 80 km, where there is a significant degree of dissociation, the partition of the energy of the atmosphere in different degrees of freedom differs drastically both from that of equilibrium air at room temperature, and that of equilibrium air at the more representative temperature of 1500° K. As a result of solar radiation, more energy is available as energy of dissociation of the O_2 molecules. There is also more ionization and more bound-state electronic excitation than is characteristic of local thermodynamic equilibrium (LTE).

In Fig. 58 are shown the fractions of principal neutral species. The data of Fig. 58 derived from CIRA-1965, show the change of relative proportions due to diffusion without other mixing above about 100 km. In Fig. 59 is shown the variability in electron density encountered in a number of measurements.

The breakdown of energy in different degrees of freedom, based on the standard temperature and the composition data of Figs. 59 and 60, is shown in Fig. 60.

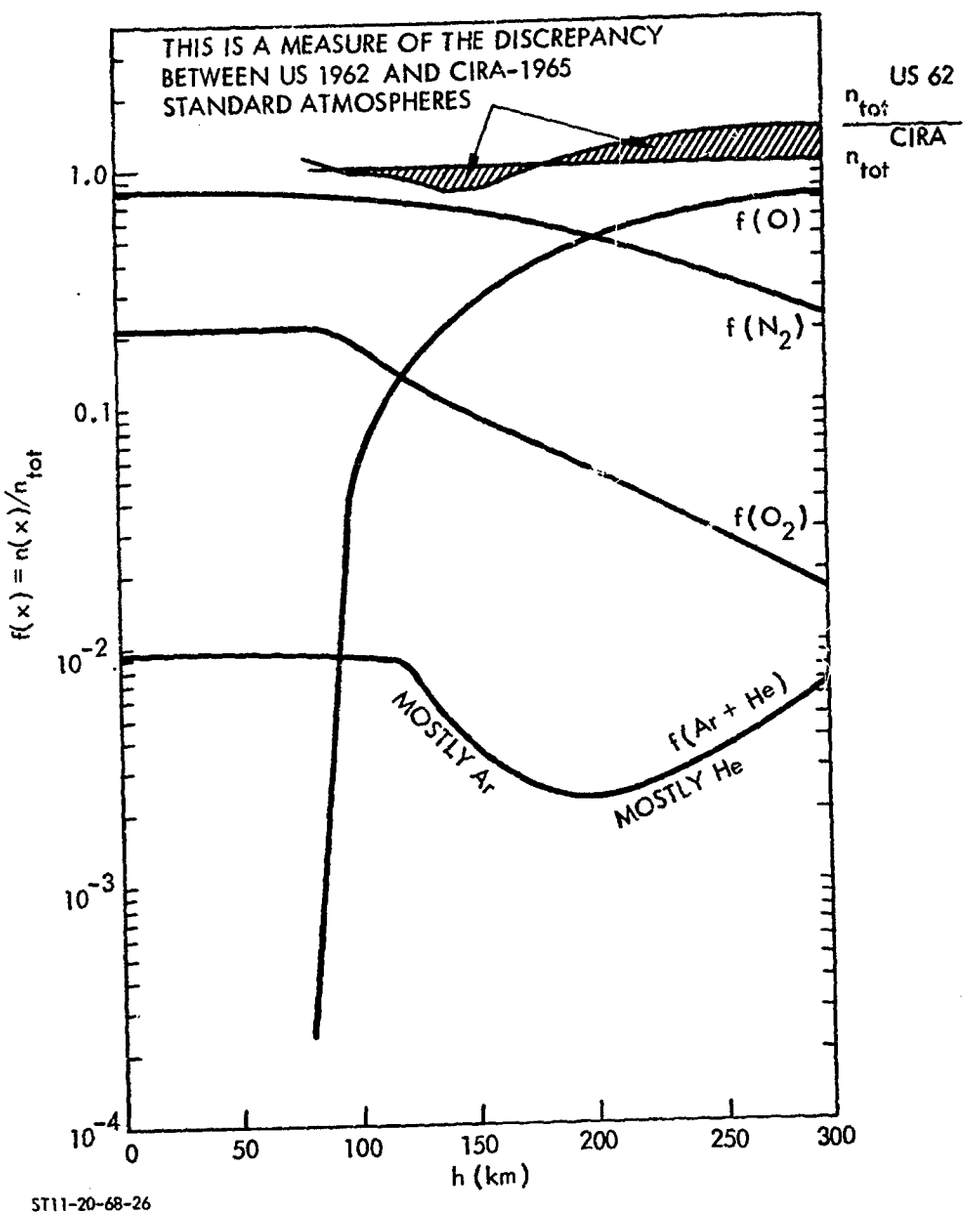

FIGURE 58. Upper Atmosphere Chemistry: Principal Neutral Species (Bauer, to be published)

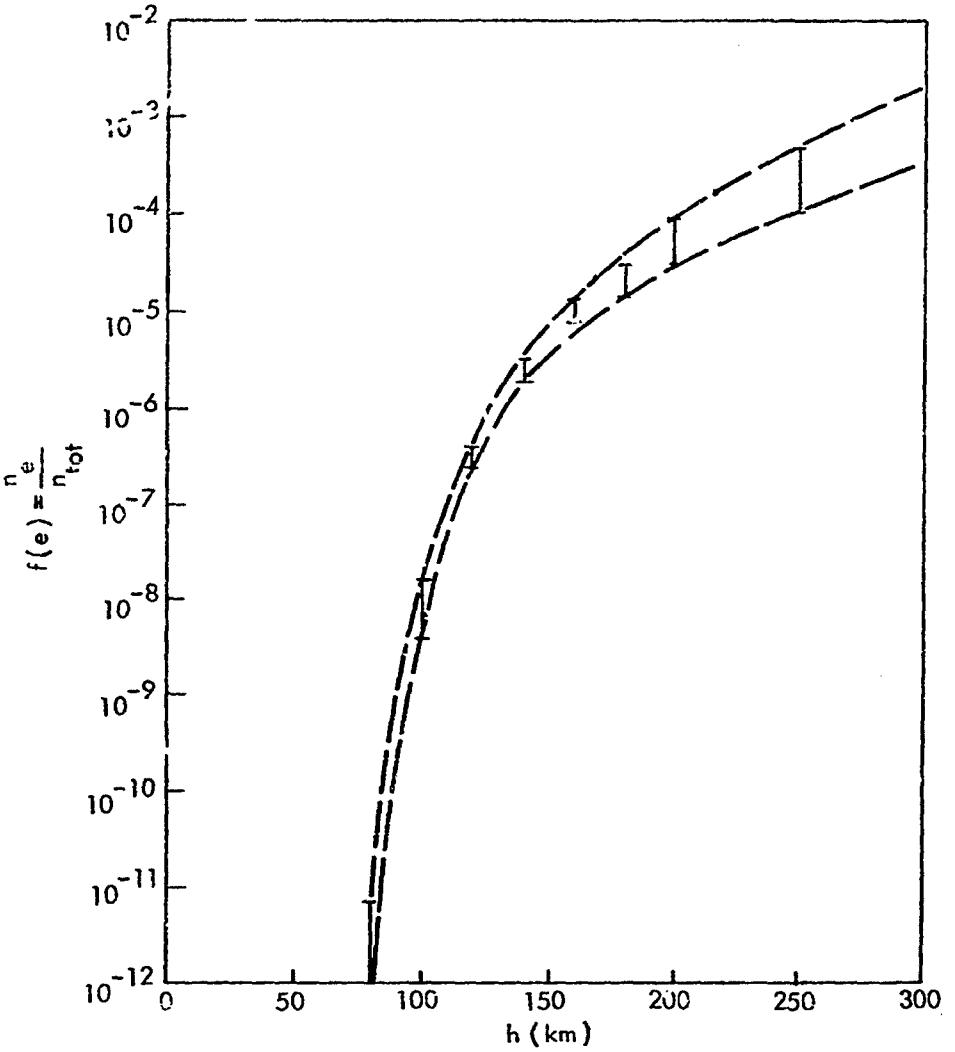

FIGURE 59. Upper Atmosphere Chemistry: Representative Range of Ionization (After Bauer, 1969)

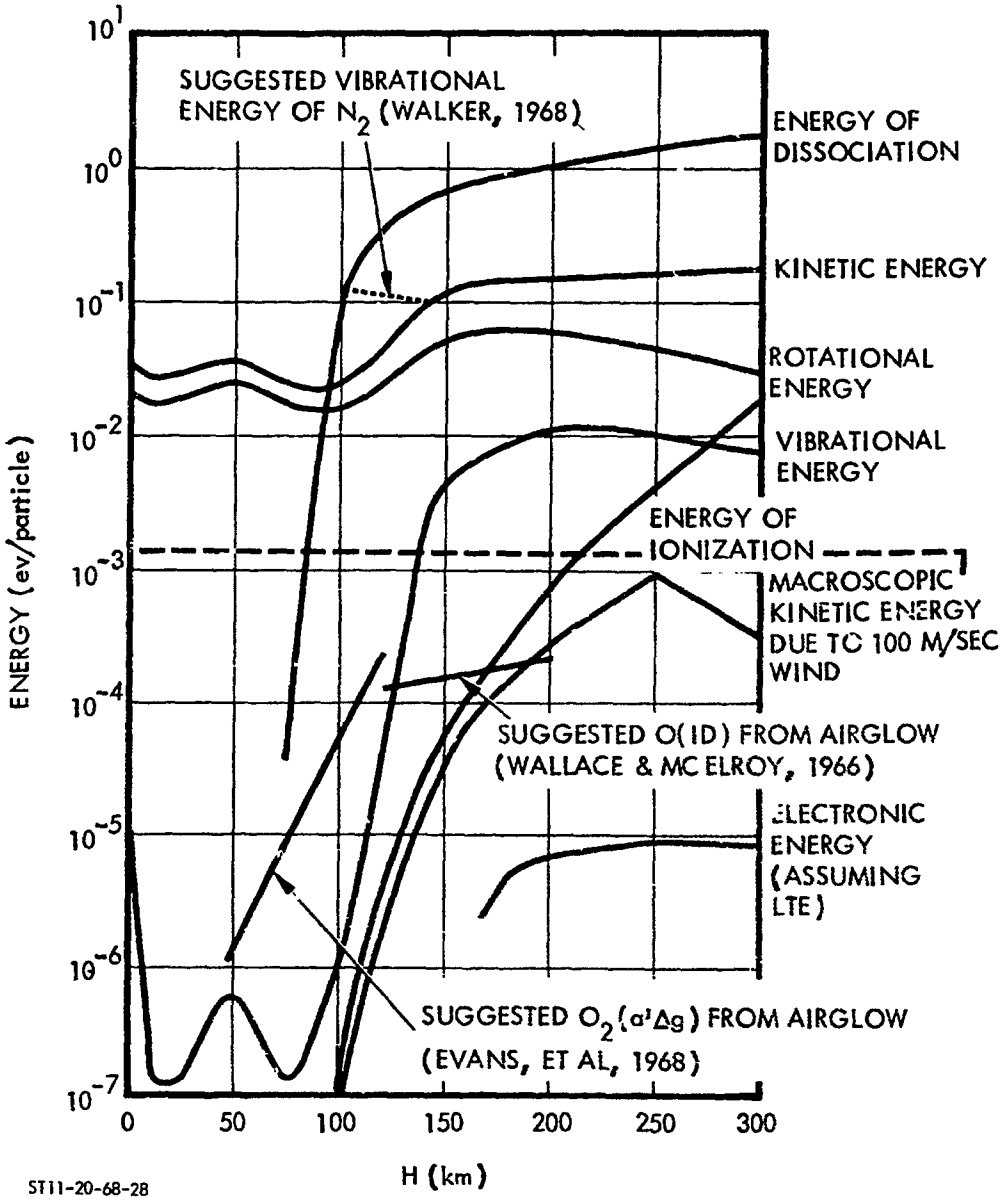

FIGURE 60. Breakdown of Energy in Different Degrees of Freedom (After Bauer, 1969)

For the electronic energy there are three curves in Fig. 60: a theoretical curve representing LTE and constituting a plausible lower bound, and two other curves deduced from experimental airglow results. Specifically, there are only three electronically excited states that have to be considered, the states ($a^1\Delta_g$) and possibly ($b^1\Sigma_g^+$) of O_2 which are respectively 0.98 and 1.60 ev above the ground state ($X^3\Sigma_g^-$), and the state $O(^1D)$ which is 1.96 ev above the ground state $O(^3P)$. Since all other electronic states of O, O_2, N_2, NO, etc. are more than 4 ev above the respective ground states, their overall occupation is extremely low because of the unfavorable Boltzmann factor exp (- E/kT). However, they may be important for specific processes.

Thus of the three curves for electronic energy in Fig. 59, the experimental data refer to airglow on $O_2(a^1\Delta_g)$ and $O(^1D)$, while the theoretical LTE curve is mainly due to $O_2(a^1\Delta_g)$. The experimental data should not be extended in altitude range.

Walker (1968) alleges that the free electrons have a temperature larger than the neutral species by a factor of two at h = 100 - 140 km. Walker accounts for the higher temperature to be a result of the Schumann-Runge absorption, described by Eq. 4.2 by which a large amount of $O(^1D)$ is produced in this altitude range. The $O(^1D)$ transfers energy efficiently into the vibration of N_2 by the quenching reaction:

$$- O(^1D) + N_2 \rightarrow O(^3P) + N_2(v) + K.E. \qquad (4.6)$$

Despite the spin change, Zipf (1968) has given evidence that the rate constant of process (4.6) is perhaps 10^{-11} cm^3/sec, and that possibly half of the energy of process (4.6), or 1 ev transfers into the vibration of N_2. Since the interchange between kinetic energy of free electrons and vibrational energy of N_2 is rapid (Schulz, 1962); Walker (1968) interprets the observed enhanced kinetic energy of the electrons in terms of a vibrational temperature of N_2 of 3000^o K.

Walker's result is included in Fig. 60, but should not be regarded as generally accepted.

Also shown in Fig. 60, the kinetic energy of a 100 m sec^{-1} wind, typical of these altitudes, is a minor contributor to the overall kinetic energy.

Until recently, the terrestrial atmosphere was thought to be mixed to a uniform composition to a uniform height of approximately 100 km. In the altitude region 80-100 km the uniform mixing was thought to be affected by atmospheric turbulence which terminated abruptly at a "turbopause" at approximately 100 km. Above the turbopause the various chemical species were supposed to diffuse separately, each with its own scale height

$$H_j = kT/M_j g;\ j = O,\ O_2,\ NO,\ N_2,\ Ar,\ He,.... \qquad (4.7)$$

Experimental work cited in Table 11 gives evidence that critical levels in the upper atmosphere such as the "turbopause," referring to "cessation of turbulence," or "homopause," referring to "cessation of uniformity," may vary by as much as 20 km in altitude depending on latitude, season and possibly even time of day. Evidence from a number of sources indicates the existence of stratification below the turbopause; e.g., sporadic-E, wind shears and different ion structure on a vertical scale of order 1-3 km (Kochanski, 1964). Evidence for compositional changes with altitude near the homopause has been reviewed by K. S. W. Champion (1967, 1968, 1969).

The evidence concerning the state of motion of the lower thermosphere may be summarized as follows:

Below 80 km, the atmosphere is uniformly mixed at all times, while above 120 km it is diffusively separated, as evidenced by measurements of the Ar-N_2 concentration ratio (Kasprzak et al., 1968).

TABLE 11. OBSERVATIONS OF THE TRANSITION FROM THE TURBULENT TO THE DIFFUSION REGIME

(THESE DATA INDICATE THAT THE HEIGHT AT WHICH MOLECULAR DIFFUSION BECOMES DOMINANT VARIES FROM 95 TO 119 KM)

HEIGHT	OBSERVER	TIME (LOCAL)	DATE	LOCATION	REFERENCE
~105 KM	MEADOWS AND TOWNSEND	2320	20 NOV '56	FT. CHURCHILL (59°N)	1
112 KM	MEADOWS AND TOWNSEND	2000	21 FEB '58	FT. CHURCHILL (59°N)	5
119 KM	MEADOWS AND TOWNSEND	1207	22 MAR '58	FT. CHURCHILL (59°N)	5
103 KM	BLAMONT	EVENING	10 MAR '59	ALGERIA (32°N)	3
112 KM	BLAMONT	MORNING	12 MAR '59	ALGERIA (32°N)	3
106 KM	BLAMONT	EVENING	2 MAR '60	ALGERIA (32°N)	3
105 KM	BLAMONT	MORNING	5 MAR '60	ALGERIA (32°N)	3
96 KM	BLAMONT	EVENING	13 JUN '60	ALGERIA (32°N)	3
<95 KM	BLAMONT	EVENING	16 JUN '60	ALGERIA (32°N)	3
105 KM	FIREFLY (OLIVE)	MORNING	18 AUG '60	EGLIN AFB (30°N)	2
110 KM	POKHUNKOV	MORNING	SUMMER '59	USSR (MIDLATITUDE)	4
111 KM	MEADOWS AND TOWNSEND	1140	15 NOV '60	WALLOPS ISLAND (37°N)	5

1. E. B. MEADOWS AND J. W. TOWNSEND, JR., DIFFUSIVE SPORATION IN THE WINTER NIGHT TIME ARCTIC UPPER ATMOSPHERE, 112 TO 105 KM, ANNALES DE GEOPHYSIQUE, VOL. 14, pp. 80-93, 1958.

2. CHEMICAL RELEASES IN THE UPPER ATMOSPHERE (PROJECT FIREFLY), A SUMMARY REPORT, JOURNAL OF GEOPHYSICAL RESEARCH, VOL. 68, pp. 3057-3063, 1963.

3. J. E. BLAMONT AND J. M. BAGUETTE, MESURES DEDUITES DES DEFORMATIONS DE SIX NUAGES DE METAUX ALCALINS FORMES PAR FUSEES DAN LA HAUTE ATMOSPHERE, ANNALES DE GEOPHYSIQUE, VOL. 17, pp. 319-337, 1961.

4. A. A. POKHUNKOV, A STUDY OF THE NEUTRAL COMPOSITION OF THE UPPER ATMOSPHERE AT ALTITUDES ABOVE 100 KM., IZV. AKAD. NAUK SSSR GEOPHYSICAL SERIES, NO. 11 NOVEMBER 1960, pp. 1649-1657, AGU TRANSLATION BY R. MUDGE, pp. 1099-1105.

5. J. E. BLAMONT, ET AL, ATMOSPHERIC MOTIONS STUDIED BY SODIUM VAPOR TRAILS RELEASED BY ROCKETS, COSPAR INFORMATION BULLETIN 13, p. 10, JANUARY 1963.

Over all altitudes up to perhaps 200 km there is evidence for horizontal winds. In the region 60-160 km the magnitude is typically up to 90 m/sec, while the direction varies, according to Kochanski (1964), whose data are given in Fig. 50 in the discussion on the stratosphere and mesosphere, and Bedinger and Constantinides (1969).

Bedinger and Constantinides (1969) have statistically analyzed wind data derived from 57 chemical release trails over Wallops Island, Virginia, released in evening twilight (23), morning twilight (19), and otherwise during the night (15). The height interval covered by the trails ranged from 63 km to 220 km, of which range data from the heights 80 to 190 km was statistically analyzed. Sample size in the interval 90 to 150 km exceeds 30; in the interval 90 to 130 km sample size exceeds 50. The seasonal distribution of the data is the following: Spring, 10 trails on 7 occasions; Summer, 20 trails on 6 occasions; Fall, 11 trails on 7 occasions; and Winter, 16 trails on 5 occasions.

Figure 61 shows the average wind speed in the range of altitude 90 to 150 km, ranging in value from less than 50 to above 90 m sec^{-1}. Figure 62 shows the North and East components of the average wind and their standard deviations. The ratio of standard deviation to mean varies from 1 to 2. Figure 63 shows the average value of the vertical wind shear and its North and East components.

There is evidence of "internal gravity waves" of a nature described in the section on the stratosphere and mesosphere. In the thermosphere, the gravity wave amplitude increases from 60 km up to about 180 km, and then falls off, as described by Kochanski (1966), whose results are shown in Fig. 64.

From rocket-borne mass spectrometer results (Narcisi and Bailey, 1965) and ionosonde measurements of sporadic-E, there is clear evidence of horizontal structure in the 80-100 km region, typically with vertical scale of 1 to 3 km, lifetime on the order of one hour and horizontal extent of about 100 km.

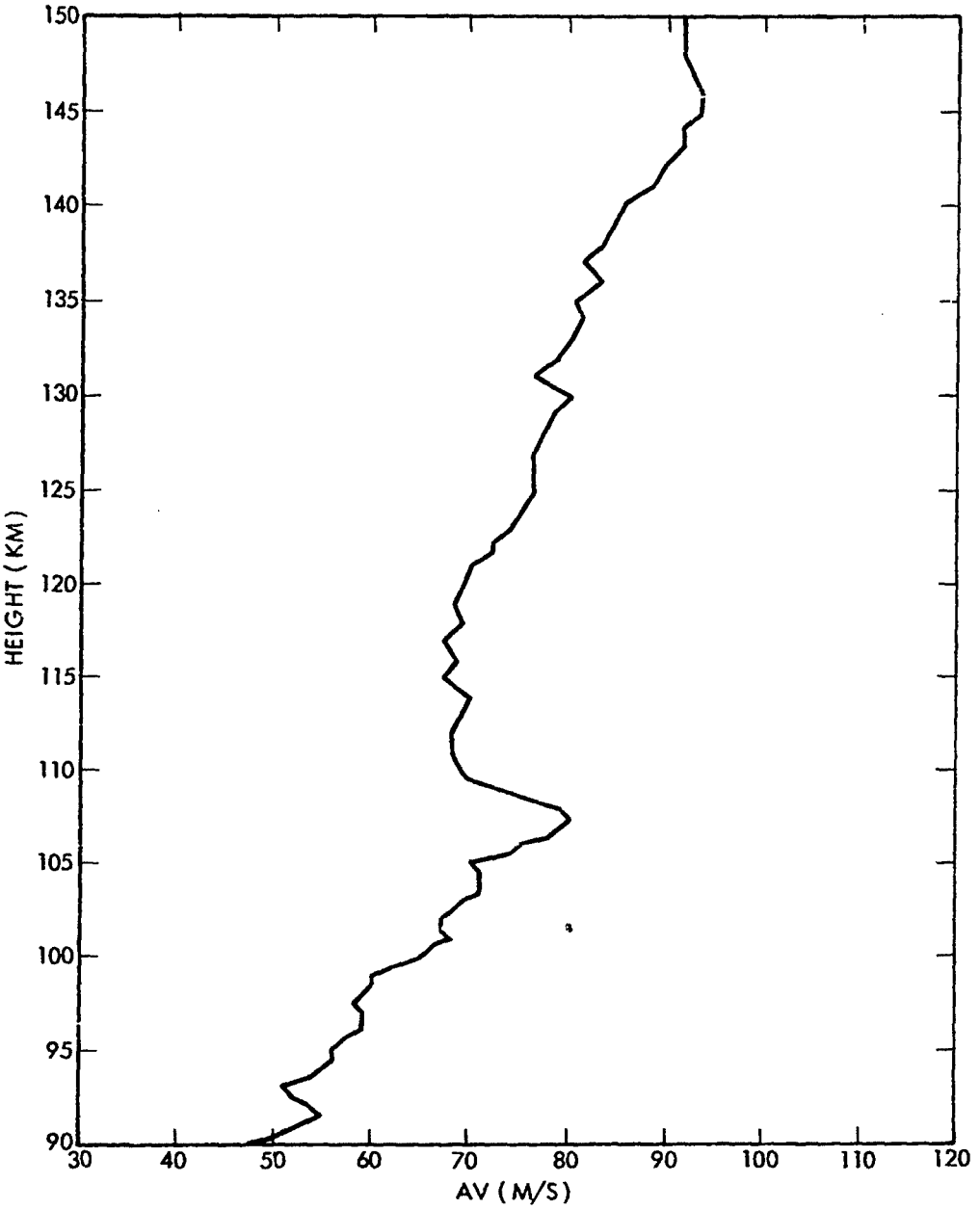

FIGURE 61. Average Value of the Speed (After Bedinger & Constantinides, 1969)

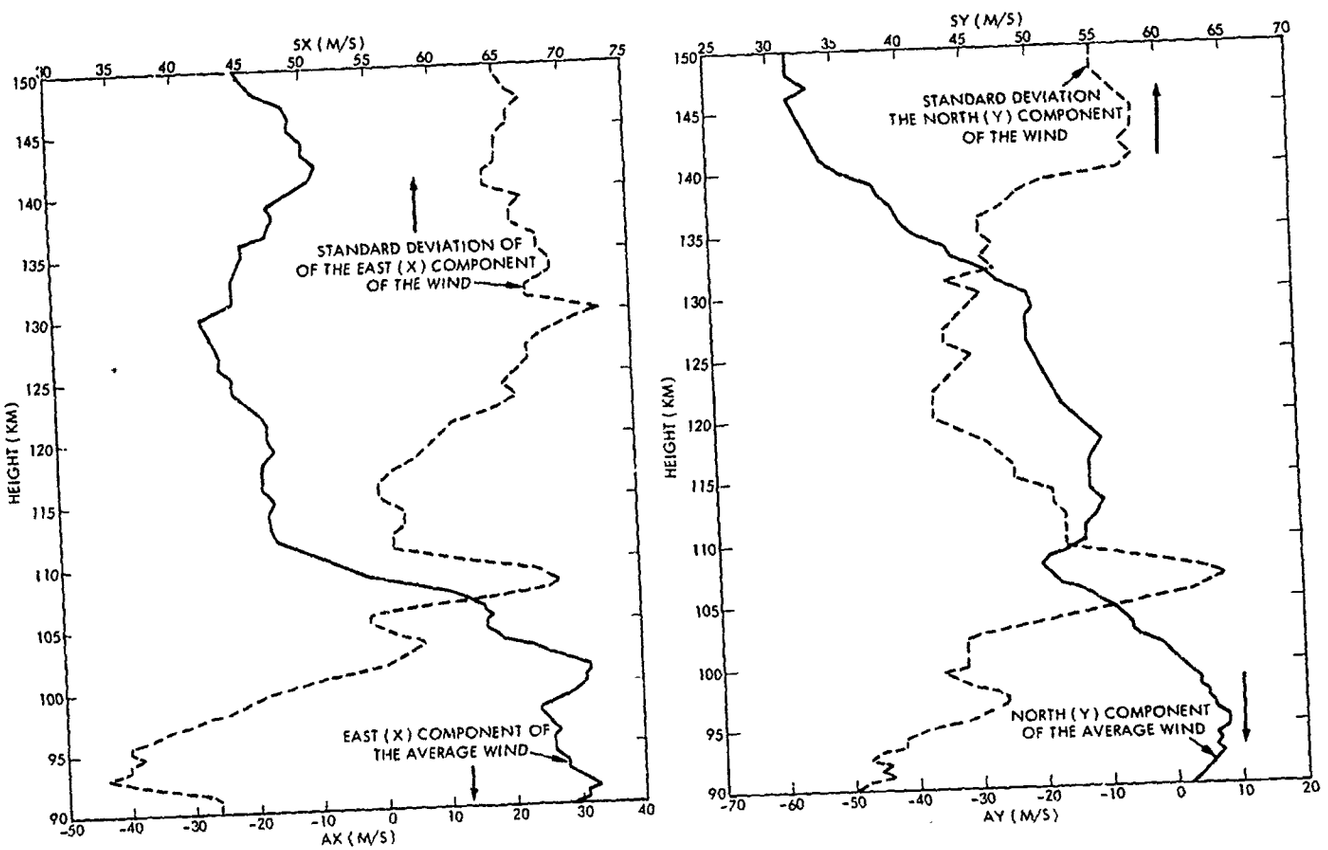

FIGURE 62. Components of Wind Velocity (After Bedinger & Constantinides, 1969)

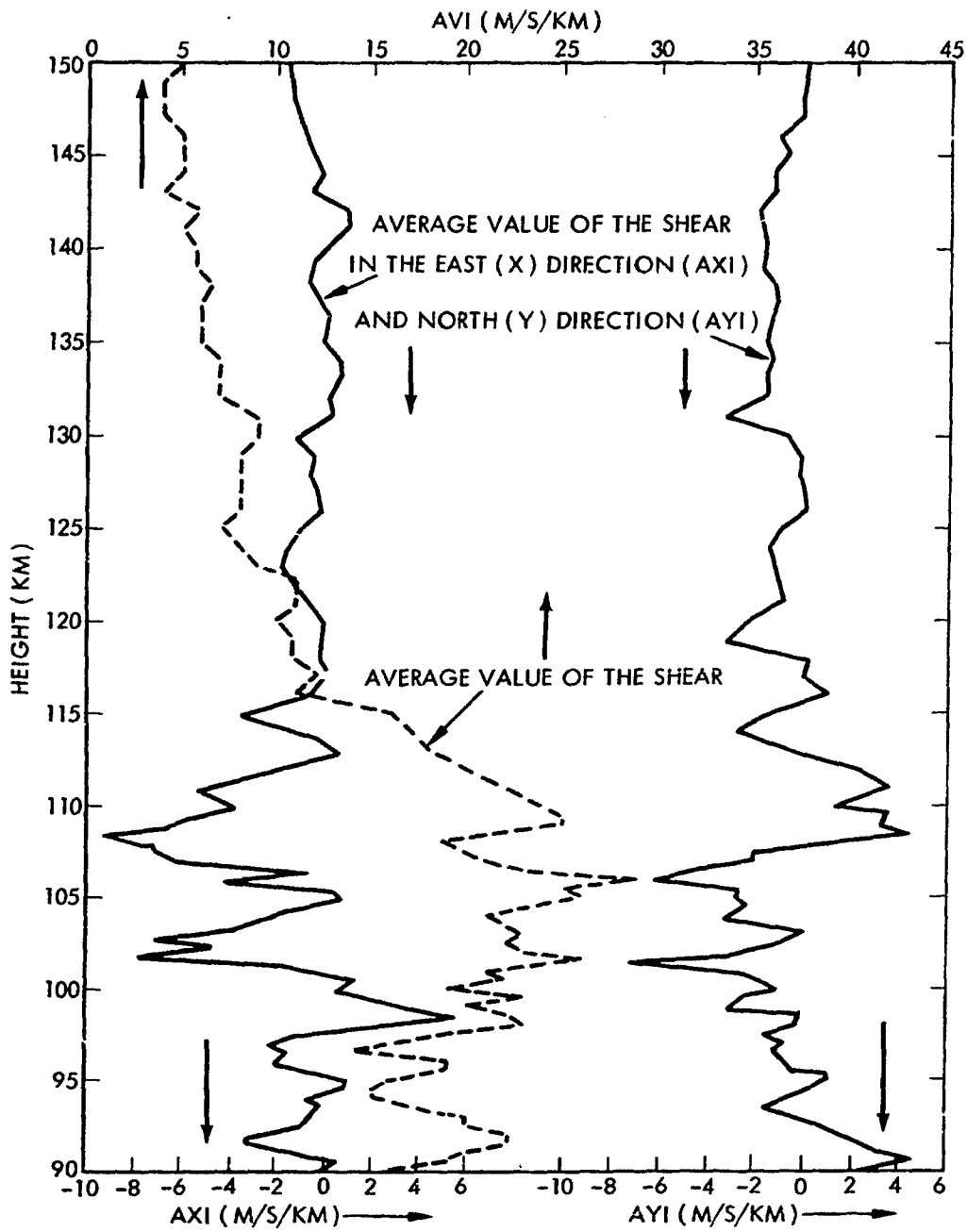

FIGURE 63. Average Magnitude and Components of Shear (After Bedinger & Constantinides, 1969)

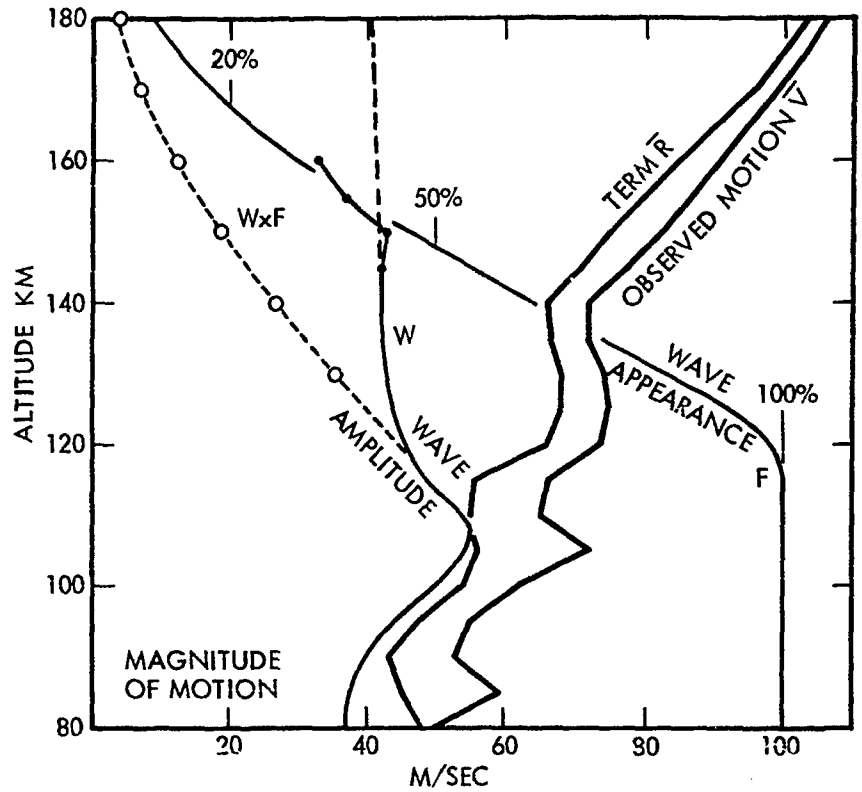

FIGURE 64. Magnitude of Drift and Internal Gravity Waves (After Kochanski, 1966)

Spreading of rocket release vapor trails of sodium, tri-methyl aluminum (TMA), and other materials show a marked change in effective diffusion coefficient at altitudes in the range 100-120 km. The effective diffusion coefficient at the lower altitudes, significantly larger than the molecular coefficient, has been called an "eddy diffusivity."

The probing of the atmospheric turbulence by chemical releases poses two questions: (1) the passage of rockets or chemical dispensers unavoidably induces disturbances which should be eliminated in the interpretation of data, and (2) the diffusion of the passive contaminant by the turbulent motion in the atmosphere does reflect the structure of the atmospheric turbulence, but the two motions are obviously not identical. Their relation should be investigated.

Radar returns from the ionization trails of meteors in the same altitude regime show the same effect as an onset of turbulence. Because of the smaller size, the inducing of turbulence by the passage of the meteor is less likely than in the case of rocket-releases.

Experimental data shown in Fig. 51 exhibit values of effective diffusivity which are larger than molecular diffusivity at altitudes below about 120 km. Since many of these data were obtained by measurements of the up-trail, which differ substantially from measurements made on the down-trail, the reality of the implied effective or "eddy" diffusion coefficients shown in Fig. 51 are controversial.

Explanation of observational data should give reasons for a well-defined turbopause at altitudes of about 100 km; below which the atmosphere is turbulent and above which it is laminar. Turbulence arises when a fluid is subjected to a strain too severe to be relieved by molecular transport in the form of a velocity, temperature, or concentration gradient. Strong destabilizing concentration gradients are uncommon in the atmosphere. The atomic oxygen gradient arising in the $O\text{-}O_2$ cycle described above is in fact stabilizing, not destabilizing, so that it will not induce turbulence. However, velocity gradients (wind shear) and temperature gradients are of common occurrence in the atmosphere.

The criteria for production of an instability leading to turbulence by velocity and temperature gradients may be described in terms of a Reynolds number Re and a Richardson number Ri. Instability due to wind shear is implied by Reynolds number, in terms of a transverse coordinate,

$$Re > Re_{crit} \sim 3000 \tag{4.8}$$

wherein Re_{crit} is a critical value of Reynolds number

Instability in the presence of a density or temperature gradient under gravity is implied by Richardson number:

$$Ri < Ri_{crit} \sim 0.04 - 1 \tag{4.9}$$

wherein Ri_{crit} is a critical value of Richardson number.

The Reynolds number is defined (Schlichting, 1960, p.13) as follows

$$Re = \frac{\text{inertial force}}{\text{frictional force}} = \frac{\rho\, u\, \partial u/\partial x}{\mu\, \partial^2 u/\partial z^2} \sim \rho\, V\, d/\mu \qquad (4.10)$$

where u = local velocity (horizontal, in x-direction)
z = vertical coordinate (perpendicular to the flow)
ρ = density of fluid
μ = viscosity of fluid
d = characteristic dimension of fluid motion
V = free stream velocity such that gradient is $\sim V/d$.

The Richardson number Ri is defined (cf. Goody, 1964, p. 367)

$$Ri = (g/T)\,(\partial T/\partial z + g/c_p) \Big/ (\partial u/\partial z)^2 \qquad (4.11)$$

Under representative conditions for typical horizontal wind speeds 100 m/sec, and wind shears of 10^{-2}-10^{-1} sec^{-1}, the effective Reynolds number is greater than the critical value Re_{crit} for altitudes below 80-110 km, implying a tendency for turbulence. At higher altitudes the Reynold's number is generally much less than Re_{crit}.

In the stratosphere and mesosphere, between altitudes 20 and about 80 km the Richardson number is always far greater than the critical value, implying strong stabilization against turbulence, as shown in Fig. 46. However, because the positive temperature gradient in the lower thermosphere is stabilizing, not destabilizing, the tendency of the lower thermosphere to turbulence is marginal below about 110 km. Relatively small disturbances in the lower atmosphere, present because of meteorological, tidal, and diurnal variation, may be amplified in propagating upwards, in the form of "internal gravity waves" (Eckart, 1960, ahd Hines et al., 1965), or even lead to the

thought of "internal gravity shocks" (Layzer, 1967). Such an amplification may be reasoned in an elementary fashion by the conservation of momentum

$$\rho u^2 = \text{constant} \tag{4.12a}$$

so that, since density decreases with altitude

$$\rho \sim e^{-z/H} \tag{4.12b}$$

the velocity will consequently increase with altitude, according to:

$$u \sim e^{+z/2H} \tag{4.12c}$$

PLASMA AND HYDROMAGNETIC EFFECTS

The significance of the ionization in the upper atmosphere is evidenced by the reflection of radio waves. The phenomenon is technologically exploited for purposes of radio communication.

The mapping of the electric and magnetic fields, together with the distributions of ions and electrons in the upper atmosphere have been recently the subject of active experimental studies of ionized metallic vapor clouds.

A parameter which described the relative importance of collisions between electrons, charged heavy particles and neutral particles is the collision frequency. Denoting the collision frequency ν_{ij} as the frequency of collisions between particles of species i and j, where i and j may be called e for electrons, i for ions, and n for neutral particles, one may write using relations of Hochstim (1969), and Ratcliffe and Weekes (1960)

$$\bar{\nu}_{ei} = 3.633 \frac{N_e}{T_e^{3/2}} \ln\left(1 + \frac{3279\, T_e^{3/2}\, T_1^{1/2}\, \nu_2}{[(N_e(T_e+T_1)]^{1/2}}\right) \approx 6.1\,(10)^{-3}\left(\frac{T}{300}\right)^{-3/2} N_e \tag{4.13}$$

$$\bar{\nu}_{en} = 2.33\ (10)^{-11}\ N_n\ [1\text{-}1.21(10)^{-4}\ T_e] \approx 4.4\ (10)^{-9}\left(\frac{T}{300}\right) N_n \qquad (4.14)$$

(for N_2 as neutral gas)

$$\bar{\nu}_{in} = 2.6\ (10)^{-9}\ \frac{N_n + N_e}{\sqrt{\bar{M}}} \text{ by Chapman according to Hochstim (1969)} \qquad (4.15)$$

where $\bar{M}$ is the mean molecular weight, N_e, N_i, and N_n are electron and ion densities (cm^{-3}), and $T = T_i = T_e$ is the temperature in degrees Kelvin.

The ratio ν_{ei}/ν_{en} is plotted in Fig. 65 as a function of altitude, using expressions of Chapman (Hines et al., 1965) and the electron density range of Fig. 64. The ratio is larger than unity for altitudes above 210 to 270 km. Below about 150 km, in the D- and E-regions, the electron to neutral collisions clearly dominate. Above altitudes from 150 to 200 km, the electron to ion collisions must also be taken into account.

Martyn (1959) estimates the value of ν_{ei}, ν_{en}, and ν_{in} to be respectively 880, 2300, and 96 sec^{-1} at the F1 ledge, and 900, 40, and 1 sec^{-1} at the F2 peak. Thus in the F1 ledge, electron collisions are mainly with neutral particles, and in the F2 layer, mainly with ions. Hochstim's (1965) computations corroborate Martyn in a general way.

In the upper F region, in which electron collisions are mainly with ions, since $\nu_{ei} \propto T^{-3/2}$, as temperature increases during the day, the collision frequency decreases. Conversely, since $\nu_{en} \propto T$, in the D- and E-regions, wherein electrons collide chiefly with neutral particles, the collision frequency will increase with increasing temperature during the day.

In the case of a large ratio of gyro frequency to collision frequency, the ions and electrons are constrained to move along rather than across the magnetic field lines. The gyro frequencies are

electron gyro frequency $\omega_{Be} = eB/mc$ (4.16a)

ion gyro frequency $\omega_{Bi} = eB/M_i c$ (4.16b)

The ratios ω_{Be}/ν_{en}, ω_{Bi}/ν_{in} are plotted in Fig. 66. Figure 67 shows a plot of theoretical values (solid line) of collision frequency and experimental determinations, quoted from Hines et al. (1965). In terms of gyro frequency criteria, the electrons follow the field for h > 75 km while the ions follow the field only for h > 125 km. In

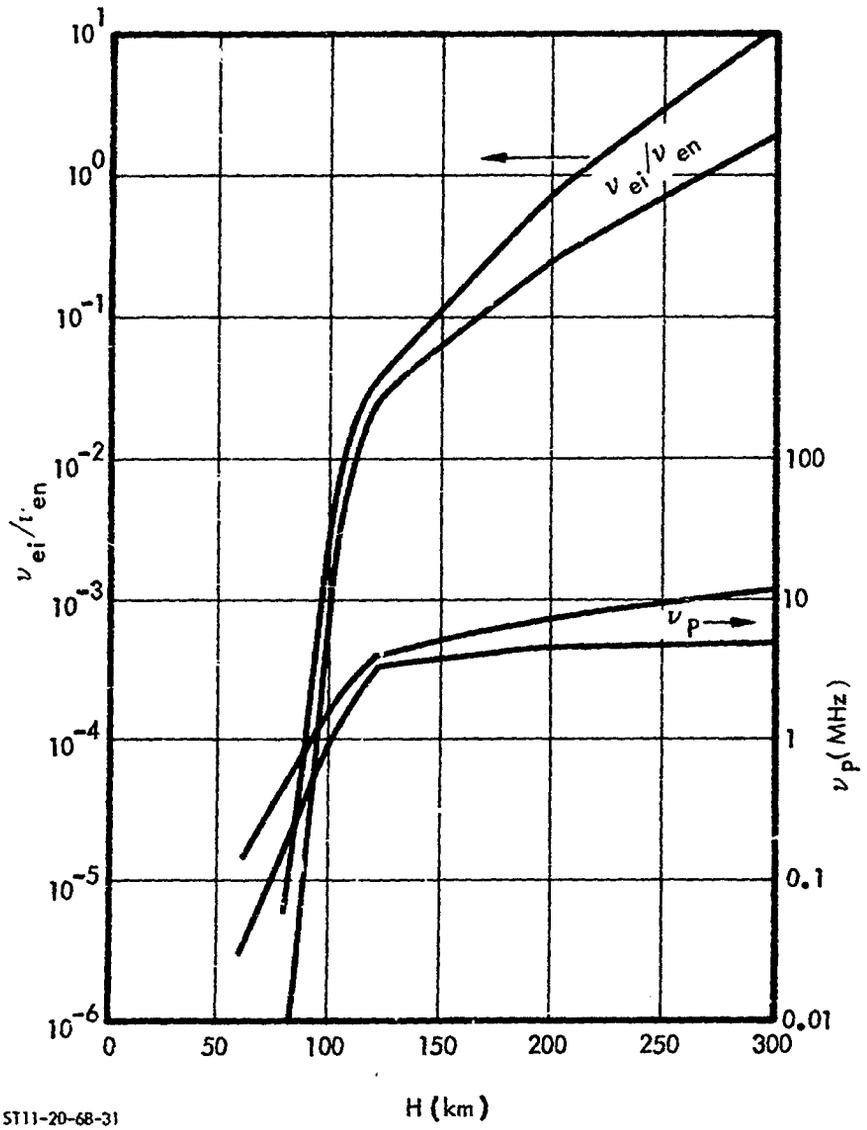

FIGURE 65. Plasma Effects (After Bauer, 1969)

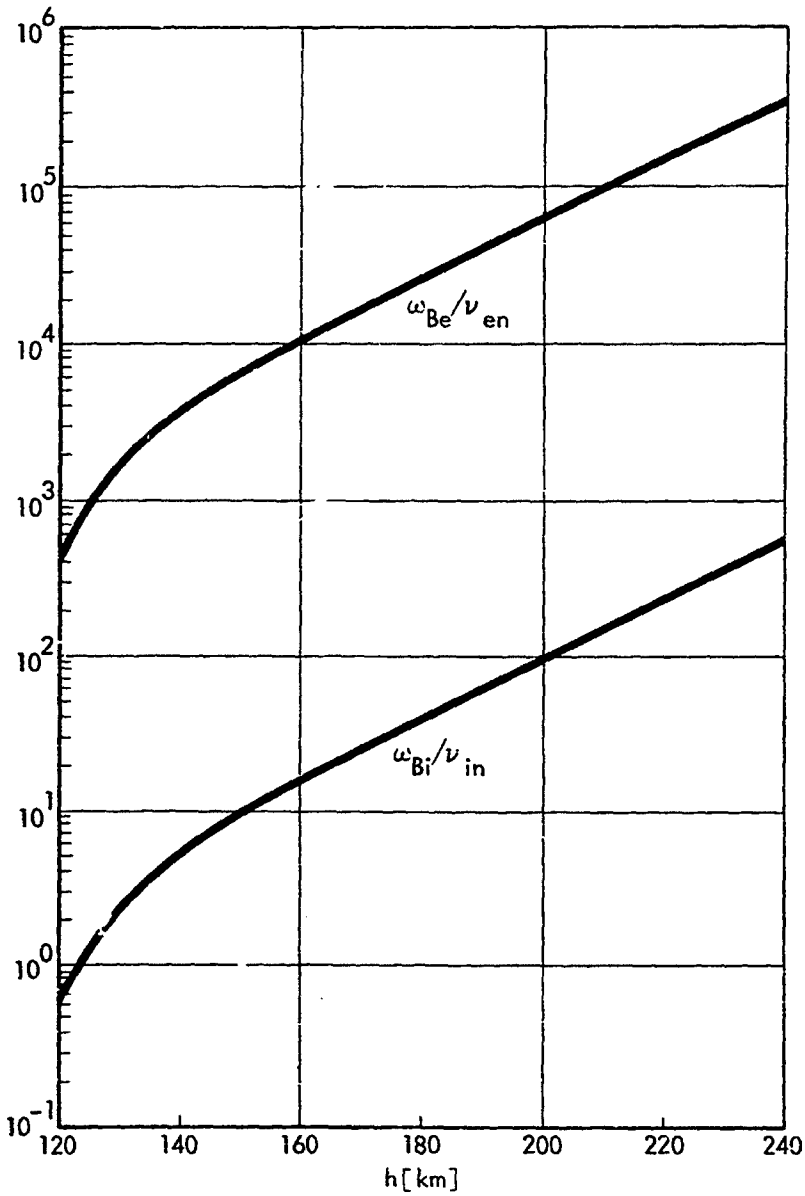

FIGURE 66: Ratio of Gyrofrequency, and Collision Frequency with Neutral Particles for Ba^+-ions and Electrons at Heights Between 120 and 240 km (After G. Haerendel, R. Lüst and E. Rieger, 1967)

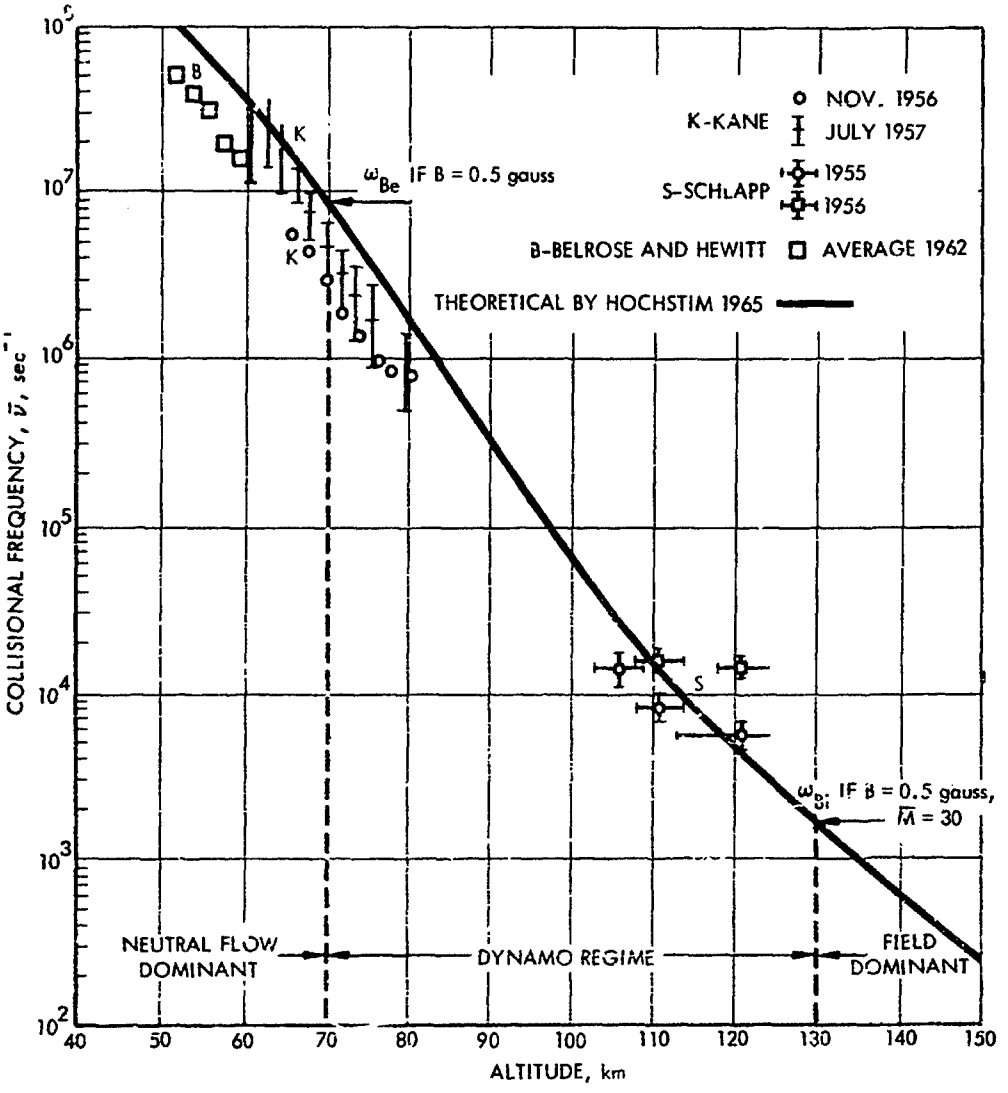

FIGURE 67. Collision Frequency $\bar{\nu}$ of Electrons

the intermediate region (75 to 125 km) the electrons and ions are constrained by different forces, suggesting the possibility of net currents, which are observed to occur. Such occurrence is the "dynamo region" discussed by Hines et al. (1965).

One energy input into the earth's atmosphere from the sun, in particular in the case of solar storms, flares and other disturbances, comes in the form of charged particles. The bulk of the energy is carried by 10 Kev protons and low-energy electrons having roughly the same velocity as the protons. The protons moving along geomagnetic field lines enter the earth's atmosphere in the auroral zones of the polar regions where they excite auroras and heating, leading to significant density variations.

A different but important effect is the reflection of radio waves from the ionosphere. Even a small electron density can cause an important effect. The plasma frequency as a function of altitude

$$\omega_p \approx (n_e\ e/mc)^{\frac{1}{2}} \tag{4.18}$$

is plotted in Fig. 65. Electromagnetic signals of frequency $\omega < \omega_p$ are reflected on normal incidence on an optically thick layer of electron density n_e, or plasma frequency ω_p.

Effects of Coulomb screening, characterized by the Debye radius, given by

$$h_D = (kT/4\pi n_e\ e^2)^{\frac{1}{2}} = 6.9\ (T/n_e)^{\frac{1}{2}}\ \text{cm}. \tag{4.17}$$

are not important in the thermosphere. Typical values of the Debye radius h_D are of the order 0.3 cm, which is less than the mean free path above 80 km and yet very much greater than the Landau radius $r_c = e^2/kT$.

Time-dependent phenomena such as magneto-hydrodynamic waves, discussed by Poeverlein (1967), may have significant effects on the

overall structure and motion of the thermosphere above 100-200 km, at an altitude dependent on the specific phenomenon under investigation as well as on the latitude and the solar activity.

A second topic under which the upper atmosphere may be described and its regions subdivided is that of chemistry. The solar insolation especially in the very energetic wavelengths causes ionization. The chemical reactions which take place in the stratosphere, mesosphere, and thermosphere are many and important in consideration of energy transformations.

In the technologically interesting regions of ionization, the chemistry of dissociation, driven by the solar radiation, and not the ionization itself, primarily determines the constitution and characteristics of the upper atmosphere.

The species that can be ionized may be arrayed in the order of ionization potential given in Table 12.

The wavelengths corresponding to the ionization potentials of all atmospheric constituents listed in Table 12, with the exception of sodium and other metals, are in the vacuum ultraviolet. The significant photoionization occurs above the sensible atmosphere, dominantly as the ionization of O_2 by the Schumann-Runge continuum radiation band. Both O_2 and NO may be ionized by Hydrogen Lyman alpha which goes through to 60-80 km.

Ionization is produced by solar ultraviolet and to a lesser extent by solar X-rays. Johnson (1961) has described the available energy to be:

Ultraviolet

1350 - 800 A 9.25 - 14.5 ev	Total flux = 5×10^{-7} w cm^{-2}

X-ray, at solar maximum

50A ± factor 2 250 ev	Total flux $\simeq 2.5 \times 10^{-8}$ w cm^{-2}

TABLE 12. IONIZATION POTENTIAL OF ATMOSPHERIC CONSTITUENTS

Species	First Ionization Potential (ev)	Wavelength, A	Comments
Na	5.12	2420	Metals have very low IP's, i.e. even small concentrations can be major sources of ionization at lower altitudes
NO	9.25	1340	NO is a minor species but with a very low IP: NO^+ is important for 70-120 km.
O_2	12.05	1030	O_2^+ is important for 100-160 km.
O	13.6	910	O^+ is important from 150-500 km.
H	13.6	910	H^+ is important above 500 km.
N_2	15.5	800	IP is so high that N_2^+ is not important
N	14.55	850	N isn't common (N_2 isn't photodissociated much by solar UV), and it has a high IP.
Ar	15.7	790	Too high IP to be important.
He	24.5	510	Too high IP to be important.

The ions produced at various altitudes, according to Bortner & Kummler (1968), Narcisi & Bailey (1965), Johnson (1965), are listed below:

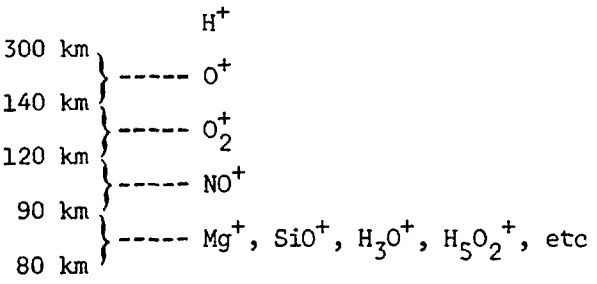

The chemical reactions involving the principal constituents of the lower thermosphere are complicated. They include the following processes:

(a) photo-ionization:

$$h\nu + O_2 \rightarrow O_2^+ + e^- \qquad (4.18)$$

$$h\nu + O \rightarrow O^+ + e^- \qquad (4.19)$$

$$h\nu + N_2 \rightarrow N_2^+ + e^- \qquad (4.20)$$

(b) charge transfer: (Exothermic charge transfer processes are rapid)

$$O^+ + NO \rightarrow NO^+ + O \qquad (4.21)$$

$$N_2^+ + O_2 \rightarrow O_2^+ + N_2 \qquad (4.22)$$

(c) recombination:

$$O + e^- \rightarrow O + h\nu \quad \text{radiative - slow} \qquad (4.23)$$

$$O^+ + e^- + M \rightarrow O + M \quad \text{3-body - slow at high altitudes and low density} \quad (4.24)$$

$$NO^+ + e^- \rightarrow N' + O'' \quad \text{dissociative - rapid} \quad (4.25)$$

Although the air constituent NO is minor, it is metastable chemically. Also because NO has the lowest ionization potential of any of the air species, NO^+ accumulates as the end-result of a chain of reactions.

At the higher altitudes of the lower thermosphere there is no NO, lots of N_2, O, and some O_2. N_2^+ charge transfers to O_2^+ and O^+. Since O^+ can not recombine as fast as O_2^+, it accumulates.

At the lower altitudes the chemistry is complicated (Bortner and Kummler, 1968).

NO is photo-ionized by Hydrogen Lyman alpha (Craig, 1965).

Mg, SiO, deposited as a result of meteor ablation around 90-100 km are easily ionized.

Hydrated water ions $H^+ (H_2O)_n$, n = 1, 2,... are present.

Because of the relatively high densities of the lower altitudes, significant numbers of negative ions, O_2^-, CO_3^-, NO_2^-, especially at night, are formed by dissociative attachment processes of type

$$e^- + AB \rightarrow A^- + B$$

Excited states due to chemi-ionization are also present.

The several subregions of the mesosphere and lower thermosphere have been categorized according to the degree of ionization by geophysicists interested in the propagation of radio waves, as the C-, D-, E- and F-regions. The C-region is in the lower mesosphere; the D-region is within the upper mesosphere; the E-region in the lower thermosphere, and the F-region is in the upper thermosphere. The ionospheric F-region has a lower limit at the top of the E-region at a height of about 140 km and no generally accepted upper height limit. Each of these regions is distinguished from the others in its chemical nature.

The bulk of the atmosphere in the F-region is neutral gas. Since mixing processes other than diffusion are of little significance, the composition of the F-region is determined by ionization production and loss processes and by diffusive separation of the chemical constituents. In the lower F-region, the principal constituents are molecular nitrogen dominating atomic oxygen. With increasing altitude, atomic hydrogen becomes the dominant constituent. The scale height at the base of the F-region is about 30 km.

The formation of the F-layer below 600 km is governed by the continuity equation

$$\frac{\partial N}{\partial t} + \text{div } (Nv) = q - L(N) \tag{4.26}$$

wherein N = electron density
v = local mean electron velocity
q = production rate of electron
L = loss rate of electrons and

$$L(N) = \alpha N^2 + \beta N \tag{4.27}$$

wherein α = recombination coefficient
β = attachment coefficient

For equal densities, the flux of ionization transport becomes (Hines et al., 1965, Eq. 4.3)

$$\text{div } (Nv) = \text{div } \left[N(v_{em} + v_T + v_D)\right] \tag{4.28}$$

by which three types of movement are recognized explicitly, i.e., movement caused by electromagnetic forces, by temperature changes of the atmosphere, and by plasma diffusion. The solution of the continuity equation is complicated if all three types of ionization movement are simultaneously taken into account.

Below about 600 km, the F-region's neutral atmosphere consists primarily of O and N_2, with O_2, N, H and He as minor constituents. The type of electron loss depends on the positive ions present. Electrons may combine directly with atomic ions or dissociatively recombine with O_2^+, N_2^+ and NO^+. The combination with atomic ions is so slow that below the F_2 peak the rate is negligible compared to that for dissociative recombination.

The most important loss reactions in the F-region are those for O (Hines et al, 1965, Eq. 4.4 and 4.5)

$$O^+ + O_2 \rightarrow O_2^+ + O \qquad (4.29a)$$

$$O_2^+ + e \rightarrow O^* + O^{**} \qquad (4.29b)$$

and those for N_2

$$O^+ + N_2 \rightarrow NO^+ + N \qquad (4.30a)$$

$$NO^+ + e \rightarrow N^* + O \qquad (4.30b)$$

The rate of the general reaction of (4.29a) and (4.30a) is (Hines et al, 1965, Eq. 4.6)

$$\frac{dn(O^+)}{dt} = - K_1 \, n(O^+) \, n(XY) \qquad (4.31)$$

The rate of the general reaction of (4.29b) and (4.30b) is

$$\frac{dN_e}{dt} = - K_2 \, N_e \, n(XY^+) \qquad (4.32)$$

In (4.31) and (4.32), K_1 and K_2 are constant rate coefficients; N_e is the electron member density; $n(XY)$ is the density of neutral diatomic molecules (O_2 or N_2); $n(XY^+)$ is the density of positive diatomic ions (O_2^+ or NO^+). The attachment coefficient (β) of (4.27) equals

describe it for the stratosphere and mesosphere. Evidently this high concentration arises from low-level photochemistry of a different nature, such as that generating smog, etc.

To summarize, at altitudes above 50 km $\xi(h) < 1$ because there is too little ozone to make the atmosphere optically thick; at altitudes below 50 km, since most of the solar radiation incident on the atmosphere has already been absorbed at higher altitudes ($\xi > 1$), there is inadequate solar radiation in the Hartley band to heat up the atmosphere.

Having explained the temperature maximum at the stratopause, the lower bound of the stratosphere and the upper bound of the mesosphere will next be described.

The lower bound of the stratosphere is given by the tropopause, which corresponds to the temperature minimum between the tropopause, or that portion of the atmosphere which is in direct "contact" with the surface of the earth, and the thermopause.

If the temperature gradient (with increasing height) within the troposphere is negative, so that the adiabatic lapse rate

$$-dT/dh < g/c_p \tag{3.10}$$

(where g = acceleration due to gravity and c_p = specific heat at constant pressure), there is possibility of a fluid mechanical static instability by which a parcel of air of slightly different temperature can move a significant vertical distance, leading to overturning of the atmosphere. Such an overturning in the troposphere is particularly visible in the case of cumulus clouds.

The vertical motion arising from static instability is of vital importance in keeping water droplets or ice crystals in suspension in the troposphere. Since the terminal velocity of a spherical water droplet of 1μ radius predicted by the Stokes' formula is about 10^{-2} cm/sec, modest mean vertical motions may keep such droplets in suspension.

$$\beta = K_1 \, n(XY) \tag{4.33}$$

and the recombination coefficient (α) of (4.27) is

$$\alpha = K_2 \tag{4.34}$$

The net loss rate for the reactions 4.29 and 4.30 is (Hines et al., 1965, Eq. 4.6c)

$$L(N)\Big|_{low} = \frac{\alpha \, \beta \, N^2}{\beta + \alpha \, N} \tag{4.35}$$

where α is constant and β is height dependent. If $\beta \gg \alpha N$, as in the lower F-region, then

$$L(N) \cong \alpha \, N^2; \; \beta \gg \alpha \, N \tag{4.36}$$

If $\beta \ll \alpha N$, as in the upper F-region, then

$$L(N)\Big|_{high} \cong \beta \, N;;\beta \ll \alpha \, N \tag{4.37}$$

and the net loss is controlled by an attachment-like process.

Although an appreciable fraction of the solar ultraviolet radiation is consumed in producing N_2^+ ions, mass spectrometry indicates N_2^+ to be relatively scarce in the entire F-region. This scarcity of N_2^+ ions implies that either the dissociative recombination of N_2^+ is so rapid that it makes no contribution to observed ionization, or that the reaction (Hines et al, 1965, Eq. 4.9)

$$N_2^+ + O \rightarrow NO^+ + N \tag{4.38}$$

preferentially prevents the rapid removal of all electrons, thereby making a substantial contribution to F-region ionization.

Measurements of the F region made at night, when q = 0, suggest that the attachment coefficient has the empirical value

$$\beta\ (\text{sec}^{-1}) = 10^{-4}\ e^{\left(\frac{300-h}{50}\right)} \qquad (4.39)$$

It is apparent that loss processes for day and night in the F-region are different, possibly due to a temperature dependence of the rate coefficients, to a progressive change in abundance of constituents, or to the different height distributions of the principal positive ions.

The temperature of the F-region is not accurately known. The electron temperature T_e and the neutral gas temperature T_n are probably equal at night, but unequal during the day.

In the ionized E-region, which ranges in height from an upper limit at about 140 km to a lower limit at about 90 km, a well defined layer of ionization is found with its peak near 100 km.

Above about 100 km, mixing processes characteristic of the lower levels appear to quench, with the consequence that diffusive separation of the chemical constituents takes place. Also at 90 to 100 km, there is an important chemical change resulting from the photo dissociation of O_2 into O, which becomes complete at about 160 km.

The ionizing radiations responsible for the E-layer must be of such nature that they penetrate the regions above without serious loss, then are absorbed within the E-region. Early attention was drawn to the possibility that the pertinent radiation may be specific to the ionization of O_2, a molecule known to be virtually absent above about 160 km. Another source would be x-rays of wave length 10-100A, shorter than the broadband 100-1200A for which N_2 has appreciable cross sections. The ionization produced N_2^+ seems to have a large recombination coefficient of 10^{-6} or 10^{-7} $cm^3 sec^{-1}$, whose effect is to remove N_2^+ ions nearly as rapidly as they are produced.

The dominant electron loss process in the E-region is one of dissociative recombination with rate coefficient α_o suggested by Bates and Massey (1947). The reaction is of the form

$$(XY)^+ + e \rightarrow (XY)^* \rightarrow X^* + Y^* \tag{4.40}$$

in which a positive diatomic species (such as N_2^+, O_2^+ or NO^+ in the D- and E-regions) combines with an electron to form one or two excited atoms.

The estimates of dissociative recombination coefficient are

$$\alpha_o\ (N_2^+) = 3(10)^{-7}\ cm^3\ sec^{-1} \tag{4.41a}$$

$$\alpha_o\ (O_2^+) = 1.7(10)^{-7}\ cm^3\ sec^{-1} \tag{4.41b}$$

$$\alpha_o\ (NO^+) = 2(10)^{-8}\ cm^3\ sec^{-1} \tag{4.41c}$$

The collision frequency for electrons in the E-region is given in Fig. 67.

The D-region extends from the lowest level of atmospheric ionization (as low as 50 km) to about 90 km. It includes the level of the mesopause, at 80 to 90 km height, where the temperature reaches a minimum variously estimated from 130^o K to 250^o K. In the D-region and below, the atmosphere is subject to convective overturning which leads to a mixing of atmospheric constituents. As a result of the mixing, the relative concentrations of most chemical species are virtually independent of height.

In addition to N_2 and O_2, in the approximate proportions of 4:1, various trace constituents play roles in important processes. For example, CO_2 and O_3 play an important part along with O_2 in maintaining radiative energy balance and so in controlling the temperature distribution. The ionization balance may be similarly influenced by the trace constituent NO.

MOTION OF PLASMAS IN THE UPPER ATMOSPHERE

The plasma in the upper atmosphere consists of electrons, ions, and neutral particles which interact among themselves and move in certain configurations of external electric and magnetic fields. In addition, induced fields are also excited by the motion of the ionized components.

In the following section an orbital theory of a single charged particle in an electric field and a magnetic field is developed, and some elementary features of the motion, together with the characteristic parameters involved, are reviewed.

Since the orbital theory does not reproduce the collective effects in the motion of an assembly of particles, it is necessary to develop a hydrodynamic theory to describe the motion and plasma phenomena in the upper atmosphere, e.g., aurora, airglow, instability, wave propagation, etc. A hydrodynamic theory describing the motion of charged particles requires the knowledge of transport coefficients: conductivity and diffusion tensors.

In a later section, a theory of transport coefficients for both the weakly ionized gas, valid at altitude up to 200 km, and the strongly ionized gas, valid at altitude above 200 km is presented. Not included in the theory, however, is the effect of fluctuations in the structure of such transport properties which exhibit anomalous transport phenomena. Discussions of the hydrodynamic equations for a plasma including such transport properties are also omitted.

ELEMENTARY FEATURES OF THE ORBITAL MOTION OF AN IONIZED GAS IN AN ELECTRIC AND MAGNETIC FIELD

The following paragraphs discuss in turn interaction processes between particles, trajectories of charged particles, and particle drift.

Interaction Processes

Consider first the short-range collisions, or binary collisions, of which the simplest type is the elastic collision. A particle of charge e and mass m placed at the origin of coordinates, exerts a

potential e/r at the point r from the origin. The distance of closest approach r_o is obtained by balancing the potential energy with the mean kinetic energy,

$$\frac{e^2}{r_o} = KT$$

yielding

$$r_o = \frac{e^2}{KT}$$

where T is the temperature, and K is the Boltzmann constant. r_o is also called the Landau impact parameter. If n is the number density, giving the mean spacing between the particles $n^{-1/3}$, the mean free path λ_f, or the distance between two consequent collisions is found from the relation

$$\pi r_o^2 \lambda_f = n^{-1}$$

giving

$$\lambda_f = (\pi r_o^2 n)^{-1} \tag{4.42}$$

and the collision time

$$\tau_{coll} = \lambda_f / V_{th} \tag{4.43}$$

where

$$V_{th} = (KT/m)^{\frac{1}{2}}$$

By rearrangement, we find

$$\tau_{coll} = \frac{\text{const}}{\ln \Lambda} \frac{1}{n} \left(\frac{KT}{e^2}\right)^2 \left(\frac{m}{KT}\right)^{\frac{1}{2}} \tag{4.44}$$

where $\ln \Lambda$ has approximately a value 10.

For a plasma, distant encounters are also important, which extend beyond the limit r_o. The theory of Debye-Hückel for electrolytes introduces a shielding distance λ_D, called Debye distance. When a single particle in a vacuum exerts a potential e/r, the same particle in a plasma does not extend its influence to such a long distance, on account of the cloud of particles surrounding it and shielding its electric field. On a dimensional argument, the balance between the kinetic energy and the potential energy is written

$$\tfrac{1}{2}\nabla\, v^2 = \frac{e}{m}\,\nabla\,\varphi \tag{4.45}$$

where v is the velocity and φ is the potential. If the thermal speed is taken as representative of the average velocity, and the potential e/λ_D is truncated at the Debye distance, and the same equation of energy balance is applied for n particles having charges n e in a Debye sphere, one finds, after omitting ∇,

$$\lambda_D^{-3}\,\frac{KT}{m} = \frac{ne}{m}\,\frac{e}{\lambda_D} \tag{4.46}$$

yielding

$$k_D = \frac{2\pi}{\lambda_D} = \overline{(4\pi ne^2/KT)^{\frac{1}{2}}} \tag{4.47}$$

The numerical coefficient $(4\pi)^{\frac{1}{2}}$ comes from an analytical theory; k_D is called the Debye wave number.

Many problems of plasmas exhibit features which do not depend on collisions of the scales r_o and λ_D, e.g., in oscillations of wavelength larger than λ_D and r_o. Under such a circumstance, the motion of an electron is characterized by a self-consistent electric field $\underset{\sim}{E}$ and is determined by the dynamical equation

$$\frac{\partial \underset{\sim}{v}}{\partial t} = -\,\frac{e}{m}\,\underset{\sim}{E} \tag{4.48}$$

and the Maxwell equation

$$\frac{\partial \underset{\sim}{E}}{\partial t} = 4\pi\ e\ n\ \underset{\sim}{v} \tag{4.49}$$

where $\underset{\sim}{v}$ is the velocity of the electron. For a constant density n, the system may be reduced to the form

$$\frac{\partial^2 \underset{\sim}{v}}{\partial t^2} = \omega_p^2 \underset{\sim}{v} = 0 \tag{4.50}$$

which has an oscillatory solution with a frequency

$$\omega_p = (4\pi\ e^2\ n/m)^{\frac{1}{2}} \tag{4.51}$$

called the plasma frequency.

Figure 68 shows plasmas of various densities and temperatures. The two limiting lines represent

$$\lambda_f \geq \lambda_D$$

and

$$\lambda_D \geq r_o$$

respectively.

Trajectories of Charged Particles

A charged particle, of mass m and charge e, moving through an electric field $\underset{\sim}{E}$ and a magnetic field $\underset{\sim}{B}$ satisfies the basic equation of motion

$$m \frac{d\underset{\sim}{v}}{dt} = e\ (\underset{\sim}{E} + \frac{\underset{\sim}{v} \times \underset{\sim}{B}}{c}) \tag{4.52}$$

The equation possesses simple solutions in several special cases as described below. When $\underset{\sim}{B}$ vanishes, and $\underset{\sim}{E}$ is constant, the particle moves with a constant acceleration $e\underset{\sim}{E}/m$. When $\underset{\sim}{E}$ vanishes, the acceleration $e\,\underset{\sim}{v} \times \underset{\sim}{B}/mc$ is perpendicular to $\underset{\sim}{v}$ and brings no change to the absolute value of $\underset{\sim}{v}$:

$$\frac{d}{dt}(m\,\underset{\sim}{v}^2) = 0 \tag{4.53}$$

entailing

$$\underset{\sim}{v}^2 \equiv v_{/\!/}^2 + v_{\perp}^2 = \text{constant}$$

Since $\underset{\sim}{B}$ does not change the parallel component of velocity, it will leave

$$v_{\perp}^2 = \text{constant}$$

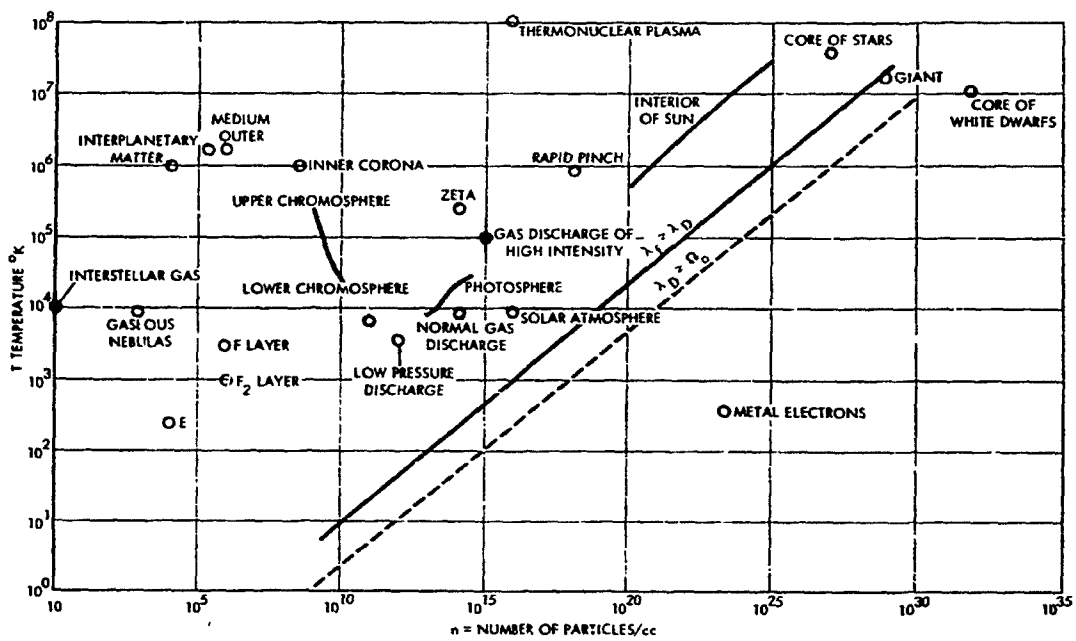

FIGURE 68. Characteristics of Plasmas (After Tchen, 1968)

If $\underset{\sim}{E}$ vanishes and $\underset{\sim}{B}$ is constant in time and space, the motion in the plane perpendicular to $\underset{\sim}{B}$ will be a gyration of angular frequency, called cyclotron frequency (or gyro frequency)

$$\omega_c = eB/mc \tag{4.54}$$

for a singly charged particle, or

$$\omega_c = Z\ e\ B/mc \tag{4.55}$$

for a multiply charged (Z times) particle. The gyration perpendicular to $\underset{\sim}{B}$ has a radius

$$r_c = \frac{v_\perp}{\omega_c} \tag{4.56}$$

The component $v_{//}$ will not be affected by $\underset{\sim}{B}$. When the two motions are combined, the resultant particle path will be a helix of constant pitch around the magnetic line of force.

Particle Drifts in An Electric Field and Gravitational Field

If $\underset{\sim}{E}$ and $\underset{\sim}{B}$ are constant in time and space, one finds a solution of 4.42, constant in time and space,

$$\underset{\sim}{v} = \frac{\underset{\sim}{E} \times \underset{\sim}{B}}{B^2} \equiv \underset{\sim}{V}_d \tag{4.57a}$$

called the drift velocity. The complete solution

$$\underset{\sim}{v} = \underset{\sim}{V}_d + \underset{\sim}{v}' \tag{4.57b}$$

satisfying 4.42 consists of a constant part $\underset{\sim}{V}_d$ and a variable part $\underset{\sim}{v}'$. The latter is determined by the following equation obtained by a substitution of 4.57a and 4.57b into 4.42:

$$m \frac{d\underset{\sim}{v}'}{dt} = e\left\{\underset{\sim}{E} + \frac{\underset{\sim}{v}' \times \underset{\sim}{B}}{c} + \frac{1}{B^2}\,(\underset{\sim}{E} \times \underset{\sim}{B}) \times \underset{\sim}{B}\right\} \qquad (4.58)$$

$$= e\left\{E_{/\!/} + \frac{\underset{\sim}{v}' \times \underset{\sim}{B}}{c}\right\}$$

Any motion defined by 4.58 consists of a gyration around the magnetic line of force independent of $\underset{\sim}{E}$, at the cyclotron frequency, and a uniform acceleration along the line of force due to $E_{/\!/}$. The effect of $\underset{\sim}{E}$ in 4.57a and 4.58 will also be present in 4.57b and, therefore, will change the radius of gyration 4.43. In view of such a change, a drift of the center of gyration (or "guiding center") of the particle will occur. This feature is shown diagrammatically in Fig. 69.

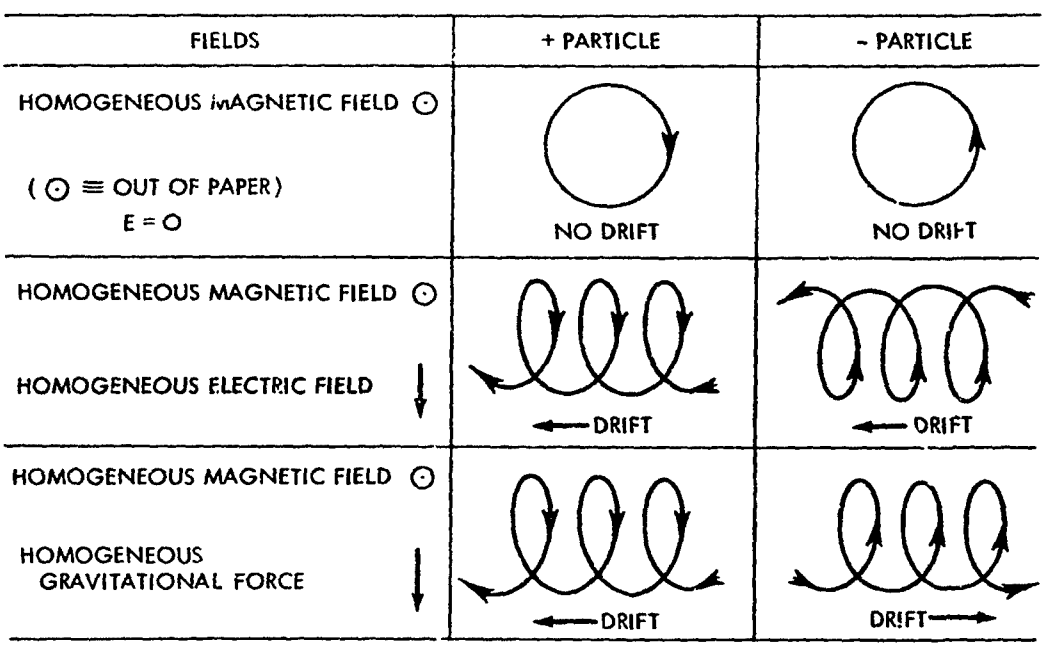

FIGURE 69. Drifts Produced by an Electric Field and a Gravitational Field

It is to be remarked that the role of an electric force eE can be replaced by any other force (e.g., a gravity - mg) to produce a similar feature as described above. In view of the change of charge e into m the gravitational drift

$$V_d = g_\perp / \omega_c \tag{4.59}$$

will depend on the sign of the charge of the particle.

Particle Drifts in An Inhomogeneous Magnetic Field

Consider a particle moving in an inhomogeneous magnetic field parallel to the z-axis, with a strength varying along the x-axis. The particle which gyrates in the xy plane will change its radius of gyration over the orbit, so that a drift will result, as shown in Fig. 70. By using the first order approximation in $V_d/v_\perp$, Alfvén (1950) developed the formula

$$\frac{V_d}{v_\perp} = \tfrac{1}{2} r_c \frac{\nabla_\perp B}{B} \tag{4.60}$$

where $\nabla_\perp B$ is the gradient of B in the plane perpendicular to $\underset{\sim}{B}$ and $\nabla \underset{\sim}{B}$.

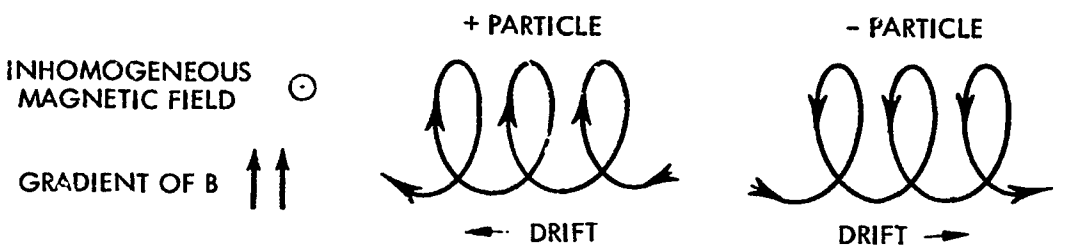

FIGURE 70. Drift by an Inhomogeneous Magnetic Field

If a particle moves with a velocity $v_{//}$ along a curved magnetic field with a radius of curvature R, we expect a similar drift

$$V_d = \frac{mv_{//}^2}{R} \frac{1}{m\omega_c} \tag{4.61}$$

$$= v_{//}^2/R\omega_c$$

according to 4.59 with the gravity force $mg_\perp$ replaced by the centrifugal force $mv_{//}^2/R$. By neglecting the current for a strong $\underset{\sim}{B}$, we have

$$\frac{1}{R} = \frac{v_\perp B}{B}$$

The two drifts 4.60 and 4.61 from the inhomogeneous magnetic field amount to

$$V_d = \frac{1}{\omega_c R} (v_{//}^2 + \tfrac{1}{2} v_\perp^2) \tag{4.62}$$

They are in the same direction of $\underset{\sim}{B} \times \nabla \underset{\sim}{B}$.

The orbital motion of a single particle in an external electric and magnetic field described in this section is not a valid description of the motion of an assembly of particles. Such an assembly involves new effects, such as the normal and shear stresses due to the interaction between the particles of like kinds or unlike kinds, and the effect of the self-consistent electric field induced by the motion of the particles. A hydrodynamic theory to include these effects is elaborated in the following section.

TRANSPORT PROPERTIES OF PLASMAS IN THE UPPER ATMOSPHERE

In the following description of aggregates of charged particles, the topics discussed in turn are: weakly ionized plasmas such as the ionosphere below 200 km, arbitrary degrees of ionization such as the higher ionosphere, and the expression of some features in geomagnetic polar coordinates.

Weakly Ionized Plasma

The important role played by the development of electric and magnetic field on the motion of a plasma is a fundamental feature of plasma dynamics, as distinguished from the hydrodynamics of a neutral gas. The diffusion and conductivity properties of plasmas are important in studying the origin and structure of plasma inhomogeneities in the ionosphere, and their scattering of radio waves. For atmospheric conditions of dimension inhomogeneities longer than the mean free path, it is necessary to consider the hydrodynamic equations of motions of all constituents: electrons, ions, and neutral molecules, together with the Maxwell equations of the fields.

The equations of motion of the three components, denoted by indices a and b are:

$$m_a n_a \frac{d\underset{\sim}{v}_a}{dt} = -\nabla p_a + m_a n_a \underset{\sim}{g} + n_a e_a \left[\underset{\sim}{E} + \frac{\underset{\sim}{v}_a \times \underset{\sim}{B}}{c}\right] - m_a n_a \sum_{b \neq a} \nu_{ab} (\underset{\sim}{v}_a - \underset{\sim}{v}_b) \tag{4.63a}$$

$$\frac{d}{dt} = \frac{\partial}{\partial t} + \underset{\sim}{v}_a \cdot \nabla \tag{4.63b}$$

where the number density n_a and the velocity $\underset{\sim}{v}_a$ satisfy the equation of continuity

$$\frac{\partial n_a}{\partial t} + \nabla \cdot (n_a \underset{\sim}{v}_a) = P - L \tag{4.64}$$

The right-hand side represents the production and loss processes which will be subsequently neglected. Other notations are: m_a is the mass, p_a the pressure, $\underset{\sim}{g}$ the gravitational acceleration, e_a the charge, $\underset{\sim}{E}$ the electric field, $\underset{\sim}{B}$ the magnetic field, and ν_{ab} the collision frequency between the particles of kinds a and b.

In the low altitude of the atmosphere (i.e., up to heights of about 250 km), the magnetic field can be considered as constant in time and position, as the electron pressure is small compared to $B^2/8\pi$. Consequently, the Maxwell equation

$$\text{curl } \underset{\sim}{E} = 0 \tag{4.65}$$

is valid. In view of the small Debye length, the condition of quasi-neutrality holds

$$n_i = n_e = n \tag{4.66}$$

entailing

$$\text{div } \underset{\sim}{j} = 0 \tag{4.67a}$$

where

$$\underset{\sim}{j} = en\,(\underset{\sim}{v}_i - \underset{\sim}{v}_e) \tag{4.67b}$$

is the electric current. The divergence-free condition of the current is a consequence of the equation of continuity for the electrons and ions.

Further the pressures satisfy the equation of state

$$p_a = nKT_a\,, \quad K = \text{Bolzmann constant} \tag{4.68}$$

For constant T_a and $\underset{\sim}{v}_n$ (n = neutral molecules), one may complete the system of equations for the determination of the variables: n_a, $\underset{\sim}{v}_a$, p_a, $\underset{\sim}{E}$, $\underset{\sim}{j}$. It will be convenient to express the gravity

$$\underset{\sim}{g} = 0, 0, -g$$

in terms of the scale height

$$H_a = \frac{KT_a}{gm_a} \tag{4.69}$$

and add the following notations

$$\underset{\sim}{e}_g = 0, 0, 1 \tag{4.70a}$$

$$\underset{\sim}{e}_B = \underset{\sim}{B}/B \tag{4.70b}$$

$$E_a^* = \frac{e_a}{m_a} \underset{\sim}{E} + \Omega_a \underset{\sim}{v}_a \times \underset{\sim}{e}_B \tag{4.70c}$$

$$\Omega_a = e_a B/m_a \quad \text{(gyrofrequency, negative for electrons)} \tag{4.70d}$$

$$v_{th_a} = (KT_a/m_a)^{\frac{1}{2}} \tag{4.70e}$$

Consider now the ionosphere up to 200 km, where the collisions between a charge particle and a neutral molecule predominate. In calculating the transport properties, neglecting the inertial terms of the momentum equation, one considers the asymptotic behavior, reduced to

$$0 = \Omega_a \underset{\sim}{v}_a \times \underset{\sim}{e}_B - \nu_{an} (\underset{\sim}{v}_a - \underset{\sim}{v}_n) + \frac{e_a}{m_a} \underset{\sim}{E} - \underset{\sim}{F}_a \tag{4.71}$$

where

$$F_a = v^2_{tha} \left(\frac{\nabla T_a}{T_a} + \frac{\nabla n}{n} + \frac{\underset{\sim}{e}_g}{H_a} \right) \tag{4.72}$$

By further introducing the notations

$$\underset{\sim}{v}_a^* = \underset{\sim}{v}_a - \underset{\sim}{v}_n, \quad a = e, i \tag{4.73a}$$

$$\kappa_a = \frac{\Omega_a}{\nu_{an}} = \frac{e_a B}{m_a c \nu_{an}} \tag{4.73b}$$

$$\underset{\sim}{u}_a = \left(\frac{e_a}{m_a} \underset{\sim}{E}_n - \underset{\sim}{F}_a\right)/\Omega_a \tag{4.73c}$$

$$\underset{\sim}{E}_n = \underset{\sim}{E} + \underset{\sim}{v}_n \times \underset{\sim}{B}/c \tag{4.73d}$$

the asymptotic momentum equation 4.71 is reduced to

$$\underset{\sim}{v}_a^* \times \underset{\sim}{e}_B - \frac{1}{\kappa_a} \underset{\sim}{v}_a^* + \underset{\sim}{u}_a = 0 \tag{4.74a}$$

giving the components of $\underset{\sim}{v}_a^*$ parallel and perpendicular to $\underset{\sim}{B}$:

$$v_{a\parallel}^* = \kappa_a u_{a\parallel} \tag{4.74b}$$

$$v_{a\perp}^* = \frac{1}{1 + \kappa_a^2} \left(\kappa_a^2 \underset{\sim}{u}_a \times \underset{\sim}{e}_B + \kappa_a \underset{\sim}{u}_a\right)_\perp \tag{4.74c}$$

or in terms of $\underset{\sim}{E}_n$ and $\underset{\sim}{F}_a$:

$$n_a e_a v_{a\parallel}^* = \sigma_{a\parallel} E_{n\parallel} - \delta_{a\parallel} \frac{m_a}{e_a} \underset{\sim}{F}_{a\parallel}$$

$$n_a e_a v_{a\perp}^* = \sigma_{aP} E_{n\perp} - \delta_{aP} \frac{m_a}{e_a} \underset{\sim}{F}_{a\perp} \tag{4.75a}$$

$$+ \sigma_{aH} \left(\underset{\sim}{E}_n \times \underset{\sim}{e}_B\right)_\perp - \delta_{aH} \frac{m_a}{e_a} \left(\underset{\sim}{F}_a \times \underset{\sim}{e}_B\right)_\perp$$

where

$$\delta_{a//} = \sigma_{a//} = \frac{n_a e_a^2}{m_a \Omega_a} K_{a//}; \quad K_{a//} = \kappa_a$$

$$\delta_{aP} = \sigma_{aP} = \frac{n_a e_a^2}{m_a \Omega_a} K_{aP}; \quad K_{aP} = \frac{\kappa_a}{1 + \kappa_a^2} \tag{4.75b}$$

$$\delta_{aH} = \sigma_{aH} = \frac{n_a e_a^2}{m_a \Omega_a} K_{aH}; \quad K_{aH} = \frac{\kappa_a^2}{1 + \kappa_a^2}$$

The generalized Ohms law (4.75a) for the particles a can be rewritten as

$$n_a \underset{\sim}{v}_a^* = \frac{1}{e_a} \hat{\underset{\approx}{\sigma}}_a \cdot \underset{\sim}{E}_n - \hat{\underset{\approx}{D}}_a \cdot \nabla N_a \tag{4.76}$$

where

$$\nabla N = n \left[\frac{\nabla n}{n} + \frac{\nabla T_a}{T_a} + \frac{e \underset{\sim}{a}}{H_a} \right]$$

and the diffusion tensor $\hat{\underset{\approx}{D}}_a$ is shown related to the conductivity tensor $\hat{\underset{\approx}{\sigma}}_a$ by the relation

$$\hat{\underset{\approx}{D}}_a = \hat{\underset{\approx}{\sigma}}_a \frac{KT_a}{e^2 n_a} \tag{4.77}$$

called the Einstein relation.

In a cartesian coordinate system where the z-axis (//) is parallel to $\underset{\sim}{B}$ (as in Fig. 71), $\hat{\underset{\approx}{\sigma}}_a$ and $\hat{\underset{\approx}{D}}_a$ have the form

$$(\hat{\sigma}_a)_{ij} = \begin{vmatrix} \sigma_{aP} & -\sigma_{aH} & 0 \\ \sigma_{aH} & \sigma_{aP} & 0 \\ 0 & 0 & \sigma_{//} \end{vmatrix}$$

$$(\hat{D}_a)_{ij} = \begin{vmatrix} D_{aP} & -D_{aH} & 0 \\ D_{aH} & D_{aP} & 0 \\ 0 & 0 & D_{a//} \end{vmatrix}$$

The columns and the rows are numerated by the indices i and j respectively. σ_{aP} is called the Pedersen, σ_{aH} the Hall, and $\sigma_{a//}$ the direct conductivity.

$\sigma_{//}$ is the conductivity parallel to the magnetic field and is that which would exist for all directions in absence of the magnetic field.

σ_P is the conductivity parallel to that component of electric field that is normal to the magnetic field. σ_P is often called the "Pedersen conductivity."

σ_H is the conductivity for a direction perpendicular to both electric and magnetic fields. σ_H is often called the "Hall conductivity."

From the above transport relations for each constituent, and from their difference for ions and electrons, the relation for the current density $\underset{\sim}{j}$ may be derived.

$$\underset{\sim}{j} = \hat{\underset{\approx}{\sigma}} \cdot \underset{\sim}{E}_n - e \hat{\underset{\approx}{D}} \cdot \nabla N \qquad (4.80a)$$

where

$$\hat{\underset{\approx}{\sigma}} = \hat{\sigma}_i - \hat{\sigma}_e \; ; \; \hat{\underset{\approx}{D}} = \hat{\underset{\approx}{D}}_i + \hat{\underset{\approx}{D}}_e \qquad (4.80b)$$

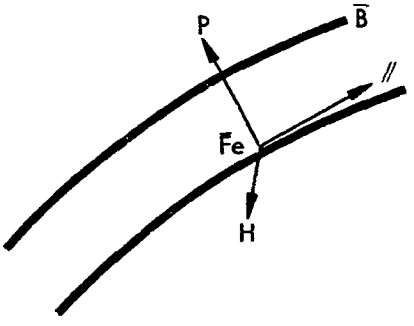

$\bar{F}e$, AND $\bar{B}$ ARE LOCALLY IN THE PLANE OF THE PAPER
// IS PARALLEL TO $\bar{B}$
P IS NORMAL TO // IN THE PLANE OF $\bar{F}e$ AND $\bar{B}$
H IS NORMAL TO //, P AND TO $\bar{F}e$, $\bar{B}$

FIGURE 71. The //, P, H Coordinate System

As indicated by 4.75b, the conductivity tensor for each species

$$\hat{\underset{\approx}{\sigma}}_a = \frac{n_a e_a^2}{m_a \Omega_a} \hat{\underset{\approx}{K}}_a$$

depends on the tensor $\hat{\underset{\approx}{K}}_a$, and the global conductivity $\hat{\underset{\approx}{\sigma}}$ and diffusivity $\hat{\delta}$ for the mixture of ions and electrons are explicitly $\hat{\sigma}$ and $\hat{\delta}$:

$$\sigma_{//} = \frac{nec}{B} (K_i - K_e)_{//} , \quad \delta_{//} = \frac{nec}{B} (K_i + K_e)_{//} \tag{4.81a}$$

$$\sigma_P = \frac{nec}{B} (K_i - K_e)_P , \quad \delta_P = \frac{nec}{B} (K_i + K_e)_P \tag{4.81b}$$

$$\sigma_H = - \frac{nec}{B} (K_i - K_e)_H , \quad \delta_H = \frac{nec}{B} (K_i + K_e)_H \tag{4.81c}$$

Figure 72 shows the tensors $\hat{\underset{\sim}{\kappa}}_a$ versus altitude. According to 4.76 and neglecting ∇N_a and $\underset{\sim}{v}_n$

$$v_{a_{/\!/}} = \frac{1}{n_a e_a} \sigma_{a_{/\!/}} E_{/\!/}$$

$$= \frac{e_a}{m_a \Omega_a} K_{a_{/\!/}} E_{/\!/}$$

or

$$\frac{v_{a_{/\!/}} B}{cE_{/\!/}} = K_{a_{/\!/}} \tag{4.82}$$

and similarly for other components. Thus, Fig. 72a shows the formula 4.82. Furthermore, according to 4.81, the quantities

$$A_{/\!/} \equiv \frac{B}{nec} \sigma_{/\!/} = (K_i - K_e)_{/\!/} \text{ , etc}$$

are shown in Fig. 72b.

Arbitrary Degree of Ionization

The above transport properties have been derived for the case of a weakly ionized plasma, where the collision between the charged particles themselves is negligible compared to the collision between a charged particle and a neutral particle. This is the case a ltitudes lower than 200 km. At higher altitudes, the collision between the ion and electron is not negligible and has to be included in the study of transport properties and plasma motions. The plasma has then a high degree of ionization. Thus for an arbitrary degree of ionization, the transport properties are found to be Gurevich and Tsedilina, 67):

$$\sigma_{e/\!/} = \frac{e^2 n}{m_e(\nu_{en} + \nu_{ei})} \tag{4.83a}$$

$$\sigma_{e\underline{p}} = \frac{e^2 n}{m_e A}\left[\nu_{ei} + \nu_{en}\,(1 + \Omega_i^2/\nu_{in}^2)\right] \tag{4.83b}$$

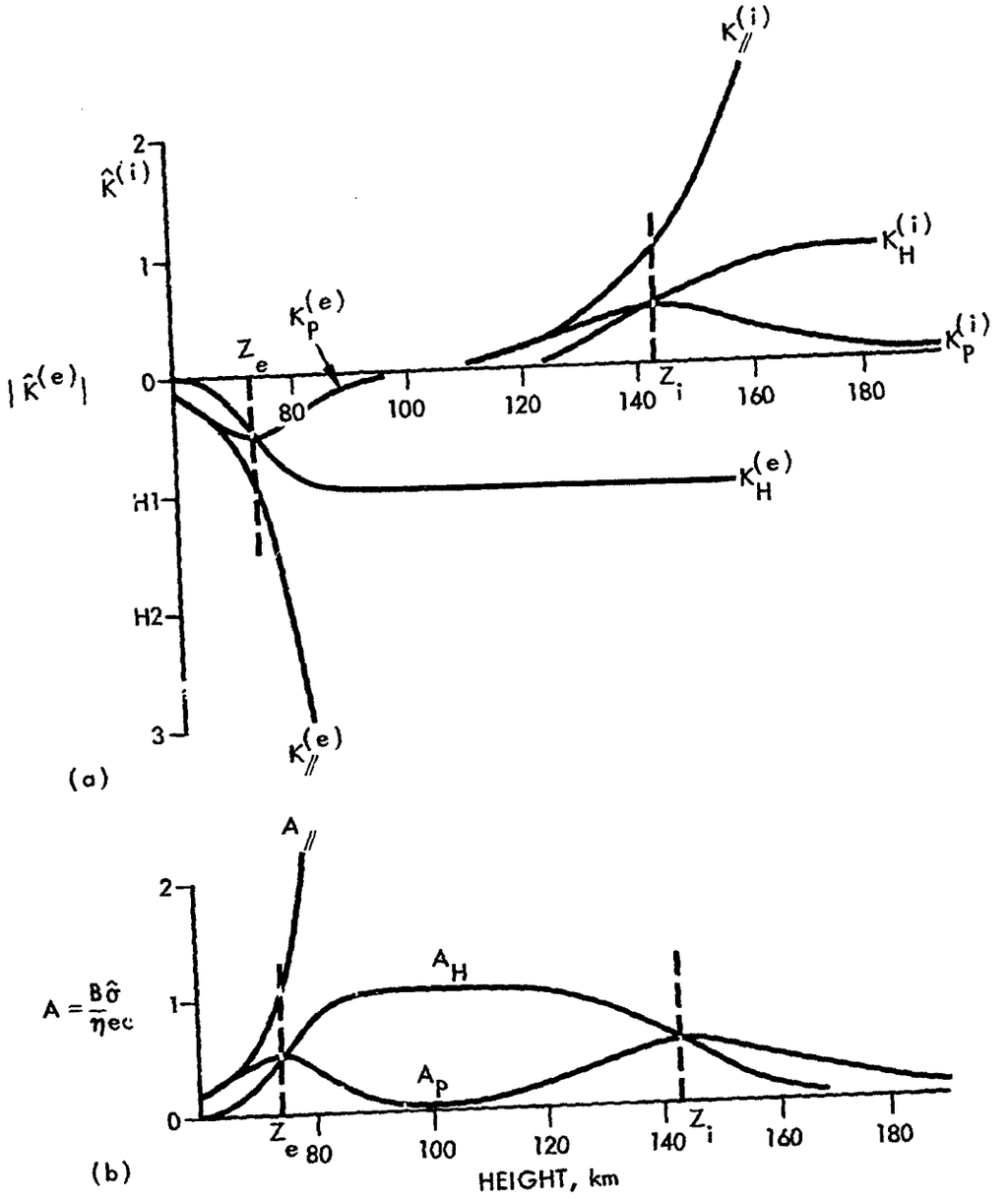

FIGURE 72. Ionospheric Drift Velocity and Conductivity of Ionosphere (Adapted from Hines et al., 1965)

$$\sigma_{eH} = -\frac{e^2 n}{m_e A}\,\Omega_e\left[1 + m_e\,\nu_{ei}/m_i\nu_{in} + \Omega_i^2/\nu_{in}^2\right] \tag{4.83c}$$

$$\sigma_{i//} = \frac{e^2 n}{m_i\,\nu_{in}}\,\frac{\nu_{en}}{\nu_{ei} + \nu_{en}} \tag{4.83d}$$

$$\sigma_{i\perp} = \frac{e^2 n}{m_i \nu_{in} A}\,(\nu_{en}^2 + \nu_{en}\nu_{ei} + \Omega_e^2) \tag{4.83e}$$

$$\sigma_{iH} = \frac{e^2 n\,\Omega_i}{m_i \nu_{in}^2 A}\,(\nu_{en}^2 + m_i\nu_{ei}\nu_{in}/m_e + \Omega_e^2) \tag{4.83f}$$

$$D_{e//} = \frac{KT}{m_e}\,\frac{1}{\nu_{en} + \nu_{in}}\,(1 + 2\,\frac{m_e\nu_{ei}}{m_i\nu_{in}}),\quad T_e = T_i \equiv T \tag{4.84a}$$

$$D_{e\perp} = \frac{KT}{m_e A}\left[(\nu_{en} + \nu_{ei})(1 + 2\,\frac{m_e\nu_{ei}}{m_i\nu_{in}}) + \frac{\Omega_i^2}{\nu_{in}^2}\,(\nu_{en} + 2\nu_{ei})\right] \tag{4.84b}$$

$$D_{eH} = \frac{-KT\Omega_e}{m_e A}\left[1 + 3\,\frac{m_e\nu_{ei}}{m_i\nu_{in}} + \frac{\Omega_i^2}{\nu_{in}^2}\right] \tag{4.84c}$$

$$D_{i//} = \frac{KT}{M_i}\,\frac{1}{\nu_{in}}\,\frac{\nu_{en} + 2\nu_{ei}}{\nu_{en} + \nu_{ei}} \tag{4.84d}$$

$$D_{i\perp} = \frac{KT}{m_i A}\,\frac{1}{\nu_{in}}\left[(\nu_{en} + \nu_{ei})(\nu_{en} + 2\nu_{ei}) + \Omega_i^2(1 + 2\,\frac{m_e\nu_{ei}}{m_i\nu_{in}})\right] \tag{4.84e}$$

$$D_{iH} = \frac{KT}{m_i A}\,\frac{1}{\nu_{in}^2}\left[\nu_{en}^2 + \Omega_e^2 - \frac{m_i}{m_e}\,\nu_{ei}\nu_{in}\right] \tag{4.84f}$$

$$A = (\nu_{en} + \nu_{ei})^2 + \Omega_e^2(1 + 2\,\frac{m_e\nu_{ei}}{m_i\nu_{in}} + \frac{\Omega_i^2}{\nu_{in}^2}) \tag{4.84g}$$

The Einstein relation (Eq. 4.77) is invalid for a plasma with an arbitrary degree of ionization.

The following conclusions and observations can be drawn:

1. With the exception of D_H, all transport properties transverse to the magnetic field decrease with decreasing collision frequency, while all parallel components increase. The large parallel conductivity in the upper atmosphere suggests that disturbances produced in the sporadic E-layer may influence a plasma inhomogeneity in the higher altitude by the joining lines of force.

2. The current density $ne\underset{\sim}{v}^*$ formulated above in Eq. 4.44 is useful in transforming the equation of continuity into an equation of diffusion, by a substitution for $n\underset{\sim}{v}_a$. Such an equation is an equation of diffusion of the second order, if the self-consistent electrostatic field $\underset{\sim}{E}$ is neglected. The inclusion of the effect of such a field will transform into a diffusion equation of fourth order, which is responsible for a spreading of a plasma inhomogeneity in the atmosphere along with the diffusion process.

3. In the presence of an external electric field $\underset{\sim}{E}_o$, the drift velocities of the electrons and ions are

$$\underset{\sim}{V}_{eo} = \underset{\sim}{v}_n - \frac{\hat{\sigma}_e}{en} \underset{\sim}{E}_{eff,e} \tag{4.85a}$$

$$\underset{\sim}{V}_{io} = \underset{\sim}{v}_n + \frac{\hat{\sigma}_i}{en} \underset{\sim}{E}_{eff,i} \tag{4.85b}$$

depending on the effective electric fields for electrons and ions:

$$\underset{\sim}{E}_{eff,e} = \underset{\sim}{E}_o + \frac{1}{c}\underset{\sim}{v}_n \times \underset{\sim}{B} - \frac{m_e g}{e} \tag{4.86a}$$

$$\underset{\sim}{E}_{eff,i} = \underset{\sim}{E}_o + \frac{1}{c}\underset{\sim}{v}_n \times \underset{\sim}{B} + \frac{m_i g}{e} \tag{4.86b}$$

4. The motion of plasmas in the atmosphere will depend on the regime of the plasmas, i.e., whether they contain fluctuations or not. The presence of the micro-fluctuations will change the transport properties, and hence the motion and the structure of plasma inhomogeneities in the atmosphere. A preliminary attempt of the investigation of such nonlinear effects has been made by Tchen (1969).

5. Experiments with visible artificial ion clouds as plasma inhomogeneities have been performed as a means of studying the interaction processes between the interplanetary plasma and the artificial plasma inhomogeneities (Haerendel, Lüst, and Rieger, 1967). The experiments help in the understanding of the interplanetary plasma and its properties.

Geomagnetic Polar Coordinates

For many purposes it is advantageous to use a system of magnetic polar coordinates described in the following paragraphs:

In the F-region and above, $\underset{\approx}{\sigma}_{//}$ is very much larger than $\underset{\approx}{\sigma}_P$ and $\underset{\approx}{\sigma}_H$ which become vanishingly small.

In the D- and E-regions, a horizontal current system may be imagined to be flowing in a relatively thin spherical shell with possible conjugate sources and sinks in the Northern and Southern Hemispheres. In this special case, except at highest latitudes, vertical current density may be ignored. Consider a coordinate system (x, y, z) whose axes point to the south, east, and zenith, respectively. In this new coordinate system, the tensor $\hat{\sigma}$ of (4.78) becomes, when I is the magnetic dip angle, positive in the Northern Hemisphere. (Hines et al., 1965).

$$\overset{\wedge}{\underset{\approx}{\sigma}} \equiv \begin{vmatrix} \sigma_{\underline{p}} \sin^2 I + \sigma_{/\!/} \cos^2 I & \sigma_{/\!/} \sin I & (\sigma_{/\!/} - \sigma_{\underline{p}}) \sin I \cos I \\ -\sigma_H \sin I & \sigma_{/\!/} & \sigma \cos I \\ (\sigma_{/\!/} - \sigma_{\underline{p}}) \sin I \cos I & -\sigma_H \cos I & \sigma \cos^2 I + \sigma_{/\!/} \sin^2 I \end{vmatrix} \tag{4.87}$$

Since vertical current density J_z vanishes, one may eliminate E_{+z}, for example, from the three component equation (4.80a), written in the x,y,z coordinate system, leading to a two dimensional relationship between horizontal components of the total electric field and J_x, J_y of the current density in the form

$$J_x = \sigma_{xx} E_x + \sigma_{xy} E_y \tag{4.88a}$$

$$J_y = \sigma_{xy} E_x + \sigma_{yy} E_y \tag{4.88b}$$

wherein

$$\sigma_{xx} = \Gamma^{-1} \sigma_p \sigma_{/\!/} \tag{4.88c}$$

$$\sigma_{xy} = \Gamma^{-1} \sigma_2 \sigma_{/\!/} \sin I \tag{4.88d}$$

$$\sigma_{yy} = \Gamma^{-1} \sigma_p (\sigma_{/\!/} \sin^2 I + \sigma_3 \cos^2 I) \tag{4.88e}$$

$$\Gamma = \sigma_p \cos^2 I + \sigma_{/\!/} \sin^2 I) \tag{4.88f}$$

$$\sigma_3 = \sigma_p + \frac{\sigma_{/\!/}^2}{\sigma_p} \tag{4.88g}$$

σ_{xx}, σ_{xy}, σ_{yy} may be regarded as components of a two-dimensional conductivity tensor relating horizontal current density to horizontal components of the total electric field.

In the special case where $\underset{\sim}{E}$ is independent of height, the height integrated conductivity tensor, with components $\int \sigma_{xx}\, dz$, $\int \sigma_{xy}\, dz$, $\int \sigma_{yy}\, dz$ relates the height integrated horizontal component of the

current density $\int \underset{\sim}{J}\, dz$ to the horizontal component of the total electric field. These components which play an important part in theories of the dynamo current system are shown, for typical mid-day condition, in Fig. 73.

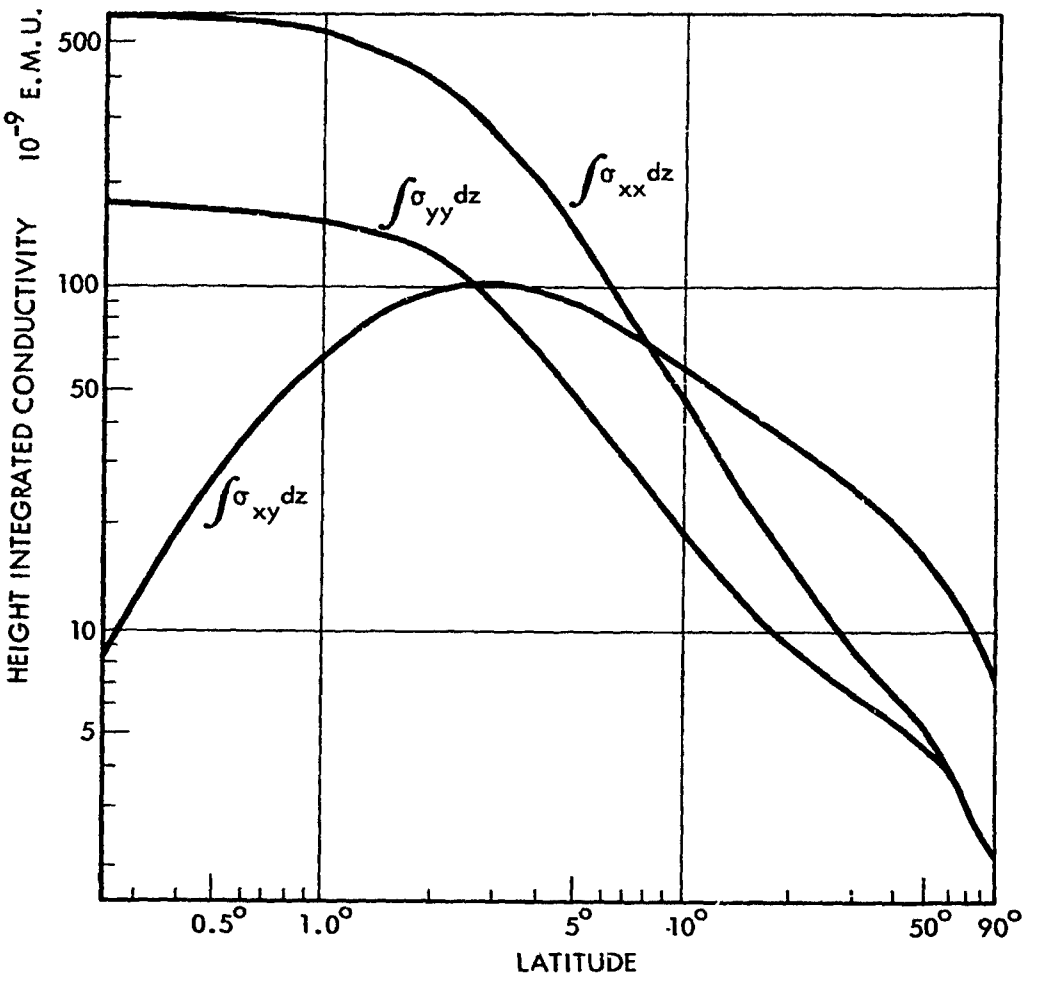

FIGURE 73. Height Integrated Conductivity Versus Latitude (After J. A. Fejer, 1953)

Over much of the earth (i.e., in latitudes higher than 10 deg), the height integrated conductivity $\int \sigma_{xy}\, dz$ by which meridional currents result from east-west variations of potential, is seen to predominate. At the magnetic dip equator, however, $\int \sigma_{xy}\, dz$ vanishes, and large values are assumed by the height integrated conductivities $\int \sigma_{xx}\, dz$, by which meridional fields produce meridional currents, and $\int \sigma_{yy}\, dz$, by which east-west fields produce east-west currents.

Although in the foregoing treatment the gravitational and pressure terms of 4.63a are neglected, it may be that these terms can assume importance in the F-region and above. Symmetry about the magnetic equator and the zero value of the current density parallel to $\underset{\sim}{B}$ in the F-region and above are assumed.

The pressure and gravitational terms in the H component of 4.80a reduce to

$$v_{en} \cong v_{in} \cong \frac{-E_P}{B} \tag{4.89}$$

In vector notation the common transverse drift velocity of 4.89 is $\frac{\underset{\sim}{E} \times \underset{\sim}{B}}{B^2}$ when measured with respect to the neutral gas, and $\frac{\underset{\sim}{E} \times \underset{\sim}{B}}{B^2}$ when measured with respect to the coordinate system in which $\underset{\sim}{E}$ is measured.

In the // component (parallel to $\underset{\sim}{B}$) of 4.89, and the corresponding equation for ions, the pressure and gravitational terms cannot be neglected. The condition which follows from $\underset{\sim}{J} = 0$ is

$$v_{e_{//}} = v_{i_{//}} = v_{//} \tag{4.90}$$

leading to (Hines et al., 1965)

$$m_e \omega_e v_{//} = F_{e_{//}} = -e E_{//} + m_e g \sin I - \frac{1}{N} \nabla_{//} P_e \tag{4.91a}$$

$$m_i \omega_i v_{//} = F_{i_{//}} = e E_{//} + m_i g \sin I - \frac{1}{N} \nabla_{//} P_i \tag{4.91b}$$

Addition of 4.91a and 4.91b and substitution of

$$p_e = p_i = KTN \tag{4.92}$$

when K is Boltzmann's constant and T is the temperature, assumed equal for ions and electrons, results in the velocity of "ambipolar diffusion" along the lines of force, to be

$$v_{//} = \frac{\sin I}{(m_e \omega_e + m_i \omega_i)} \left[(m_e + m_i)g + 2 \frac{K}{N} \frac{\partial (TN)}{dz} \right] \tag{4.93}$$

where z is the height and (TN) is assumed independent of latitude.

The upward component v_z of velocity $v_{//}$ is given by

$$v_z = - v_{//} \sin I \tag{4.94}$$

Moreover, isothermal conditions are assumed and we use the dimensionless height

$$h = \frac{z}{H} \tag{4.95a}$$

where the ion scale height is

$$H = \frac{KT}{m_i g} \tag{4.95b}$$

and if m_e and $m_e \omega_e$ are neglected in comparison with m_i and $m_i \omega_i$, then 4.93 and 4.94 become

$$v_z = \frac{-g}{\omega_i} \left[1 + \frac{2}{N} \frac{\partial N}{\partial h} \right] \sin^2 I \tag{4.96}$$

Equation 4.96 indicates the vertical component of the velocity of ambipolar diffusion due to gravity and pressure along the magnetic lines of force.

Equations 4.89 and 4.94 indicated drift velocity with respect to the neutral medium which itself may move with neutral particle velocity $\underset{\sim}{v}_n$ with respect to the earth. If the assumption is made for the F-region that neutral particle velocity $\underset{\sim}{v}_n = 0$, then 4.89, 4.94, and 4.96 indicate velocities with respect to earth.

BIBLIOGRAPHY

Alfvén, H., Cosmical Electrodynamics, Clarendon Press, London, 1950.

Allen, C. W., Astrophysical Quantities (2nd ed.), University of London Athlone Press, 1963.

Aller, L. H., Astrophysics, The Atmospheres of the Sun and Stars, New York: The Ronald Press Company, pp. 181-189, 507, 1963.

Babcock, H. W., Ap. J. Vol. 133, University of Chicago Press, p. 435, 1961.

Banks, P. M., "The Thermal Structure of the Ionosphere," Proc. I.E.E.E., Vol. 57, p. 258, 1969.

Bates, D. R. and H. S. W. Massey, Proc. Roy. Soc., Vol. 192, p. 1, 1947.

Bauer, Ernest, "Physics of the Upper Atmosphere: Lecture Notes," IDA Note N-621(R), 1969.

Bedinger, J. F., private communication, June 1968.

Bedinger et al., "Upper Atmosphere Winds and Their Interpretation - I," Planetary and Space Science, Vol. 16, p. 159, 1968.

Bedinger, J. F. and D. Layzer, "Vapor Trails and Turbulence in the Lower Thermosphere," COSPAR, Prague, 1969.

Bedinger, J. F. and R. Constantinides, "Investigation of Temporal Variations of Winds," Geophysics Corp. of America, Report GCA-TR-69-3-N, August 1969.

Belrose, J. S. and L. W. Hewitt, "Variation of Collision Frequency in the Lowest Ionosphere with Solar Activity," Nature, Vol. 202, p. 267, 1964.

Bjerknes, V. and H. Solberg, Avh. Norske Vidensk. Akad., Oslo (I), Vol. 7, 1929.

Blamont, J. E. and C. de Jager, "Upper Atmospheric Turbulence Near the 100 Km Level," Ann. de Geophys., Vol. 17, p. 134, 1961.

Blamont, J. E. and J. M. Baguette, "Mesures Deduites Des Deformations De Six Nuages De Métaux Alcalins Formes Par Fusées Dans La Haute Atmosphere," Annales De Géophysique, Vol. 17, pp. 319-337, 1961.

Blamont, J. E. et al., "Atmospheric Motions Studied by Sodium Vapor Trails Released by Rockets," COSPAR Information Bulletin 13, p. 10, January 1963.

Blamont, J. E. and Y. Boublil, "Étude de la Propagation d'une onde de choc et des phènoménes optiques obtenus a partir d'explosions daus l'ionosphère," Ann. Geophysique, Vol. 21, p. 1-12, 1965.

Bortner, M. and R. Kummler, "The Chemical Kinetics and the Composition of the Earth's Atmosphere," General Electric Reentry Systems Report GE-9500-ECS-SR-1, 1968.

Buch, H., "Hemispheric Wind Conditions During the Year 1950," MIT Planetary Circulations Project, AF19(122)-153, 1954.

Butler, S. T. and K. A. Small, "The Excitation of Atmospheric Oscillations," Proc. Roy. Soc., Vol. 274, pp. 91-120, 1963.

Champion, K. S. W., "Variations With Season and Latitude of Density, Temperature and Composition in the Lower Thermosphere," Space Research VII, North-Holland Publishing Company, Amsterdam, 1967.

Champion, K. S. W., "Physical Properties of the Lower Thermosphere," Space Research VIII, North-Holland Publishing Company, Amsterdam, 1968.

Champion, K. S. W., "Review of the Properties of the Lower Thermosphere," Space Research IX, North-Holland Publishing Company, Amsterdam, 1969.

Chapman, S., "The Electrical Conductivity of the Ionosphere," Nuovo Cimento, Vol. 4, Serial 10, Supp. 4, p. 1385, 1956.

Chapman, S. and D. G. Cowling, "Mathematical Theory of Non-Uniform Gases," Cambridge University Press, 1964.

Charney, J. G., Journal of Metecrology, Vol. 4, No. 5, p. 135, October 1947.

Charney, J. G., "On the Scale of Atmospheric Motions," Geofysiske Publikasjoner, Vol. 17, No. 2, pp. 3-17, 1948.

Charney, J. G. and P. Drazin, "Propagation of Planetary Scale Disturbances from the Lower into the Upper Atmosphere," JGR, Vol. 66, pp. 83-109, 1961.

CIRA, COSPAR International Reference Atmosphere, North Holland Publishing Company, Amsterdam, 1965.

Colegrove, F. D., F. S. Johnson and W. B. Hanson, JGR, Vol. 70, p. 4931, 1965.

Cooley, J. W. and J. W. Tukey, "An Algorithm for the Machine Calculation of Complex Fourier Series," Math. of Computation, Vol. 19, No. 90, pp. 297-301, 1965.

Craig, R. A., "The Upper Atmosphere - Meteorology and Physics," International Geophysics Series, Vol. 8, Academic Press, New York, 1965.

Delcroix, J. L., Plasma Physics, Wiley and Sons, New York, 1965.

Dickinson, R. E., private communication, 1968.

Dodson, H. W., "In Radio Astronomy," I.A.U. Symposium, No. 4, p. 327, 1957.

Eady, E. T., Tellus, Vol. 1, No. 3, 1949.

Eckart, C., Hydrodynamics of Oceans and Atmospheres, Pergamon Press, New York, 1960.

Ehmert, A. and G. Pfotzer, Mitt. Max Planck Inst. Phys. Stratosphare, Vol. 6, 1956.

Eliassen, A. and E. Kleinschmidt, Jr., "Dynamic Meteorology," Encyclopedia of Physics (S. Flugge, ed.), Vol. 48, Springer Verlag, Berlin, 1957.

Evans, W. F. J. et al., "Altitude Profile of the IR Atmospheric System of Oxygen in the Dayglow," JGR, Vol. 73, p. 2885, 1968.

Fejer, J. A., "Semi-Diurnal Currents and Electron Densities in the Ionosphere," J. Atmos. Terr. Phys., Vol. 4, p. 215, 1953.

Fjørtoft, R., Geofysiske Publikasjoner, Vol. 16, No. 5, 1946.

Fjørtoft, R., Geofysiske Publikasjoner, Vol. 17, No. 6, 1950.

Fjørtoft, R., "Stability Properties of Large-Scale Atmospheric Disturbances," Compendium of Meteorology, American Meteorological Society, Boston, Massachusetts, p. 454, 1961.

Fleagle, R. G. and J. A. Businger, "An Introduction to Atmospheric Physics," International Geophysics Series, Vol. 5, Academic Press, New York, 1963.

Friedman, H., National Geographic, pp. 718-724, 1965.

Gilmore, F. R., "Equilibrium Composition and Thermodynamic Properties of Air to 24,000°K," RAND RM-1543, 1955.

Golomb, B. and M. A. MacLeod, "Diffusion Coefficients in the Upper Atmosphere from Chemi-Luminescent Trails," JGR, Vol. 71, pp. 2299-2370, 1966.

Goody, R. M., Atmospheric Radiation - I: Theoretical Basis, Oxford University Press, 1964.

Gurevich, A. V. and E. E. Tsedilina, "Motion and Spreading of Inhomogeneities in a Plasma," Usp. Fiz. Nauk, Vol. 91, pp. 609-643, April 1967 (translation into English: Soviet Phys. Uspekhi, Vol. 10, pp. 214-236, September-October 1967).

Haerendel, G., R. Lüst, and E. Rieger, "Motion of Artificial Ion Clouds in the Upper Atmosphere," Planet. Space Sci., Vol. 15, pp. 1-18, 1967.

Herzberg, G., Molecular Spectra and Molecular Structure, D. Van Nostrand Company, Inc., New York, 1966.

Herzfeld, K. F. and T. A. Litovitz, Absorption and Dispersion of Ultrasonic Waves, Academic Press, New York, 1959.

Hines, C. O. et al., Physics of the Earth's Upper Atmosphere, Prentice-Hall, New Jersey, 1965.

Hinteregger, H. E., L. A. Hall and G. Schmidtke, COSPAR Working Group IV, Florence, Italy, May 15, 1964.

Hirschfelder, J. O., C. F. Curtiss and R. B. Bird, Moleculary Theory of Gases and Liquids, Wiley and Sons, 1954.

Hochstim, A. R., "Effective Collision Frequencies and Electric Conductivities of Weakly Ionized N_2, O_2, N, O, NO, and Dry Air," IDA Research Paper, P-124, 1965.

Hochstim, A. R. and G. A. Massel, "Calculations of Transport Coefficients in Ionized Gases," Kinetic Processes in Gases and Plasmas, p. 141, Academic Press, 1969.

Hodges, R. R., "Generations of Turbulence in the Upper Atmosphere by Internal Gravity Waves," JGR, Vol. 72, No. 13, p. 3455, 1967.

Hoiland, E., Arch Math. Naturvidensk., Vol. 46, No. 2, 1942.

Hunt, B. G., JGR, Vol. 71, p. 1385, 1966.

Johnson, E. R. and K. H. Lloyd, "Determination of Diffusion Coefficients from Observations on Grenade Glow Clouds," Australian J. Physics, Vol. 16, pp. 490-494, 1963.

Johnson, F. S., "Temperatures in the High Atmosphere," Ann. Geoph., Vol. 14, p. 94-108, 1958.

Johnson, F. S., Satellite Environment Handbook, 1st Ed., p. 84, 1961.

Johnson, F. S., "Solar Radiation," Satellite Environment Handbook, Stanford UP, 2nd Ed., Chapter 4, 1965.

Justus, C. G., "Energy Balance of Turbulence in the Upper Atmosphere," JGR, Vol. 71, pp. 3773-3777, 1966.

Kane, J. A., "Re-evaluation of Ionospheric Electron Densities and Collision Frequencies Derived from Rocket Measurements of Refractive Index and Attenuation," J. Atmos. Terr. Phys., Vol. 23, p. 338, 1961.

Kasprzak, W. T., D. Krankowsky and A. O. Nier, "A Study of Day-Night Variations in the Neutral Composition of the Lower Thermosphere," JGR, Vol. 73, p. 6765, 1968.

Klostermeyer, J., "Gravity Waves in the F-Region," J. Atmos. Terr. Phys., Vol. 31, p. 25, 1969.

Kochanski, A., "Atmospheric Motions from Sodium Cloud Drifts," JGR, Vol. 69, p. 3651, 1964.

Kochanski, A., "Atmospheric Motions from Sodium Cloud Drifts at Four Locations," Monthly Weather Review, Vol. 94, p. 199, 1966.

Kochanski, A., private communication, September 1968.

Kolmogoroff, A. N., "Local Structure on Turbulence in Incompressible Fluid," C. R. Acad. Sci., URSS, Vol. 30, p. 299, 1941a.

Kolmogoroff, A. N., "On Logarithmically Normal Law of Distribution," C. R. Acad. Sci., URSS, Vol. 31, p. 99, 1941b.

Kondrat' ev, K. Ya., Radiative Heat Exchange in the Atmosphere, Pergamon Press (revised edition), 1965.

Kreplin, R. W. and B. N. Gregory, "Solar X-Ray Monitoring During the IQSY," NRL Memo, 19 July 1965.

Landau, L. D. and E. M. Lifschitz, Fluid Mechanics, Pergamon Press (Addison Wesley), Chapters 1 and 2, 1959.

Landsberg, H. E., F. E. Berry et al., Handbook of Meteorology, 1945.

Layzer, D., "Gravity Shock Waves and Stratification in the Upper Atmosphere," Nature, Vol. 213, p. 576, 1967. (See also Bedinger et al., 1968.)

Leavy, C. B., "Atmospheric Ozone - An Analytic Model for Photochemistry in the Presence of Water Vapor," JGR, Vol. 74, pp. 417-426, 1969.

Lorenz, E. N., "The Nature and Theory of the General Circulation of the Atmosphere," World Meteorological Organization, 1967.

MacDonald, G. J. F., "Motions in the High Atmosphere," Geophysics, "The Earth's Environment," Gordon and Breach, 1962.

Mahoney, J. R., private communication, 1968.

Manring, E., J. Bedinger and H. Knaflich, "Some Measurements of Winds and of the Coefficient of Diffusion in the Upper Atmosphere," Space Research II, North-Holland Publishing Company, Amsterdam, 1961.

Margules, M., "Poltzmann Festshrift," 585, Leipzig, 1904.

Martyn, D. F., "Normal F-Region of the Ionosphere," Proc. I.R.E., Vol. 47, p. 147, 1959.

Meadows, E. B. and J. W. Townsend, Jr., "Diffusive Sporation in the Winter Night Time Arctic Upper Atmosphere, 112 to 105 km," Annales De Géophysique, Vol. 14, pp. 80-93, 1958.

Mintz, Y., "The General Circulation of Planetary Atmosphere," Appendix 8 of The Atmospheres of Mars and Venus (W. W. Kellogg and C. Sagan, ed.), NAS-NRC Publication 944, 1961.

Murgatroyd, R. J., "Winds and Temperatures Between 20 km and 100 km - A Review," Quarterly J. of Roy. Meteor. Soc., Vol. 83, No. 358, p. 448, October 1957.

Nagata, T., T. Tohabatsu and H. Tsuruta, "Observations of Mesospheric Ozone Density in Japan," Space Research VIII, p. 639, North Holland Publishing Company, 1968.

Narcisi, R. S. and A. D. Bailey, "Mass Spectrometric Measurements of Positive Ions at Altitudes from 64 to 112 Km," JGR, Vol. 70, p. 3687, 1965.

Newell, R. E., "The General Circulation of the Atmosphere Above 60 Km," Meteorological Monographs, Vol. 8, No. 98, p. 31, 1968.

Obasi, G. O. P., "Poleward Flux of Angular Momentum in the Southern Hemisphere," J. Atmos. Sci., Vol. 20, pp. 516-528, 1963.

Obasi, G. O. P., "On the Maintenance of the Kinetic Energy of Mean Zonal Flow in the Southern Hemisphere, Tellus, Vol. 17, pp. 95-105, 1965.

Obayashi, T. and Y. Hakura, JGR, Vol. 65, p. 313, 1960.

Oort, A. H., "On Estimates of the Atmospheric Energy Cycle," Monthly Weather Review, Vol. 92, pp. 483-493, 1964.

Oort, A. H. and A. Taylor, "On the Kinetic Energy Spectrum Near the Ground," Monthly Weather Review, Vol. 97, pp. 623-636, 1969.

Öpik, U., "Physics of Meteor Flight in the Atmosphere," Interscience, New York, 1958.

Parker, E. N., Astro Physics Journal, Vol. 128, p. 664, 1958.

Peixoto, J. P. and A. R. Crisi, "Hemispheric Humidity Conditions During the IGY," MIT Planetary Circulations Project, AF19(628)-2408, 1965.

Phillips, N. A., "Numerical Weather Prediction," Advances in Computers, Vol. 1, (F. Alt, ed.), Academic Press, New York, 1960.

Pitteway, M. L. V. and C. O. Hines, "The Viscous Damping of Atmospheric Gravity Waves," Can. J. Phys., Vol. 41, p. 1935, 1963.

Plass, G. N., "The Influence of the 9.6 Micron Ozone Band on the Atmospheric Infra-red Cooling Rate," Quarterly J. of Roy. Meteor. Soc., Vol. 82, pp. 30-44, 1956a.

Plass, G. N., "The Influence of the 15μ Carbon-Dioxide Band on the Atmospheric Infra-red Cooling Rate," Quarterly J. of Roy. Meteor. Soc., Vol. 82, p. 310-324, 1956b.

Poeverlein, H., "Characteristic Heights for Hydromagnetic Processes in the Atmosphere," JGR, Vol. 72, p. 251, 1967.

Pokhunkov, A. A., "A Study of the Neutral Composition of the Upper Atmosphere at Altitudes Above 100 km," Izv. Akad. Nauk SSSR, Geophysical Series, No. 11, pp. 1649-1657 (AGU translation by R. Mudge, pp. 1099-1105), November 1960.

Ratcliffe, J.A., and K. Weekes, "The Ionosphere," Physics of the Upper Atmosphere, J.A. Ratcliffe (ed.), Chap. 9, Academic Press, 1960.

Rayleigh, Lord, Scientific Papers, Vol. 6, p. 447, 1916.

Reiter, E. R. and A. Burns, "The Structure of Clear Air Turbulence Derived from 'TOPCAT' Aircraft Measurement," J. Atmospheric Science, Vol. 23, pp. 206-212, 1966.

Richardson, L. F., "Weather Prediction by Numerical Process," Chicago University Press, 1922.

Richardson, L. F., "Atmospheric Diffusion Shown On a Distance-Neighbor Graph," Proc. Roy. Soc., Vol. 110, p. 709, 1926.

Robinson, G. D., "Some Current Projects for Global Meteorological Observation and Experiment," Quarterly J. of Roy. Meteor. Soc., Vol. 93, p. 409, 1967.

Rosenberg, A. N., "Ionospheric Winds, A Statistical Analysis," Space Research, 8, North Holland Publishing Company, Amsterdam, pp. 673-678, 1967.

Rosenberg, N. W., "Chemical Releases in the Upper Atmosphere (Project Firefly), A Summary Report," JGR, Vol. 68, pp. 3057-3064, 1963.

Rosenberg, N. W., "Chemical Releases at High Altitudes," Science, Vol. 152, p. 1017, 1966.

Rossby, C. G. and colleagues, J. Mar. Research, Vol. 2, No. 1, 1939.

Saltzman, B. and S. Teweles, "Further Statistics on the Exchange of Kinetic Energy Between Harmonic Components of the Atmospheric Flow," Tellus, Vol. 16, pp. 432-435, 1964.

Schlapp, D. M., "Some Measurements of Collision Frequency in the E-Region of the Ionosphere," J. Atmos. Terr. Phys., Vol. 16, p. 340, 1959.

Schlichting, H., Boundary Layer Theory, McGraw-Hill, Inc., New York, Fourth Edition, 1960.

Schulz, G. J., "Vibrational Excitation of N_2, CO, and H_2 by Electron Impact," Physics Review, Vol. 135, p. A988, 1962.

Sechrist, C. F., Jr., E. A. Mechtly, T. S. Shirke, and T. S. Theon, J. Atmos. Terres. Physics, Vol. 31, p. 145, 1969.

Shimazaki, T., "Dynamic Effects on Atomic and Molecular Oxygen Density Distributions in the Upper Atmosphere: A Numerical Solution to Equations of Motion and Continuity," J. Atmos. Terr. Phys., Vol. 29, p. 725, 1967.

Siebert, M., "Atmospheric Tides," Advances in Geophysics, Vol. 7, pp. 105-187, Academic Press, New York (H. E. Landsberg, J. van Miegham, ed.), 1961.

Solberg, H., Geofysiske Publikasjoner, Vol. 5, No. 9, 1928.

Starr, V. P., Physics of Negative Viscosity Phenomena, McGraw-Hill, Inc., New York, 1968.

Starr, V. P., J. P. Peixoto, N. E. Gaut, data submitted for publication, personal communication, 1969.

Tchen, C. M., "On the Spectrum of Energy in Turbulent Shear Flow," J. Research NBS, Vol. 50, pp. 51-62, 1953.

Tchen, C. M., "Transport Processes as Foundations of the Heisenberg and Obukhoff Theories of Turbulence," Physical Review, Vol. 93, pp. 4-14, 1954.

Tchen, C. M., "Lecture Notes on Plasma Dynamics," 1968.

Tchen, C. M., "Gravity Waves and Turbulence in the Upper Atmosphere," IDA Report (in preparation).

Tchen, C. M., "Cascade Model of Shear Turbulence," CCNY Report, 1969a.

Tchen, C. M., "Fluctuation Theory of Ambipolar Diffusion in a Magnetoplasma," CCNY Report, 1969b.

Thompson, P. D., Numerical Weather Analysis and Prediction, MacMillan Company, New York, 1961.

U.S. Standard Atmosphere 1962, ESSA-NASA-USAF, U.S. Government Printing Office, Washington, D.C., 1962.

U.S. Standard Atmosphere Supplements 1966, ESSA-NASA-USAF, U.S. Government Printing Office, Washington, D.C., 1966.

Valley, S. L. (Editor), "Handbook of Geophysics and Space Environment," AFCRL and Office of Aerospace Research, USAF, pp. 9-2 to 9-14, 1965.

Van der Hoven, J., "Power Spectrum of Horizontal Wave Speed in the Frequency Range from 0.0007 to 900 Cycles per Hour," Journal of Meteorology, p. 160, 1957.

Van Zahn, U., "Mass Spectrometric Measurements of Atomic Oxygen in the Upper Atmosphere: A Critical Review," JGR, Vol. 72, p. 5933, 1967.

Walker, J. C. G., "Electron and Nitrogen Vibrational Temperature in the E-Region of the Ionosphere," Planetary and Space Science, Vol. 16, p. 321, 1968.

Wallace, L. and M. B. McElroy, "The Visual Dayglow," Planetary and Space Science, Vol. 14, p. 677, 1966.

Watanabe, K., "Ultraviolet Absorption Processes in the Upper Atmosphere," Advances in Geophysics, Vol. 5, (H. E. Landsberg and J. van Miegham, ed.), Academic Press, New York, 1958.

Whitten, R. C. and I. G. Poppoff, Physics of the Lower Ionosphere, Prentice-Hall, New Jersey, 1965.

Zimmerman, S. P. and K. S. W. Champion, "Transport Processes in the Upper Atmosphere," JGR, Vol. 68, p. 3047, 1963.

Zimmerman, S. P., "Parameters of Turbulent Atmosphere," JGR, Vol. 71, pp. 2439-2444, 1966.

Zimmerman, S. P. and R. S. Narcisi, "The Winter Anomaly and Related Transport Phenomena," personal communication; preprint submitted to Journal of Atmospheric and Terrestrial Physics, 1969.

Zimmerman, S. P., "Experimental Evidence of Turbulence in the Upper Atmosphere," University of Illinois, Aeronomy Report No. 32, Meteorological and Chemical Factors in D-Region, Aeronomy Record of the Third Aeronomy Conference, Ed. by C. F. Sechrist, J., pp. 134-141, April 1, 1969.

Zipf, E., "Deactivation of Excited States," IAGA Symposium on Laboratory Measurements of Aeronomic Interest, 1968.

UNCLASSIFIED
Security Classification

DOCUMENT CONTROL DATA - R & D
(Security classification of title, body of abstract and indexing annotation must be entered when the overall report is classified)

1 ORIGINATING ACTIVITY (Corporate author)
INSTITUTE FOR DEFENSE ANALYSES
400 Army-Navy Drive
Arlington, Va.

2a. REPORT SECURITY CLASSIFICATION
FOR OFFICIAL USE ONLY

2b GROUP
---

3 REPORT TITLE
Determination of Winds and Other Atmospheric Parameters by Satellite Techniques, Volume IV: Physics of the Atmosphere

4 DESCRIPTIVE NOTES (Type of report and inclusive dates)
Study S-341, December 1969

5 AUTHOR(S) (First name, middle initial, last name)
Alan J. Grobecker, Henry Hidalgo, Reinald G. Finke, John A. Laurmann

6 REPORT DATE
December 1969

7a. TOTAL NO OF PAGES
222

7b. NO OF REFS
147

8a CONTRACT OR GRANT NO
IDA Independent Research Program

b. PROJECT NO

c

d

9a. ORIGINATOR'S REPORT NUMBER(S)
S-341

9b. OTHER REPORT NO(S) (Any other numbers that may be assigned this report)
None

10 DISTRIBUTION STATEMENT
None

11 SUPPLEMENTARY NOTES
N/A

12 SPONSORING MILITARY ACTIVITY
Advanced Research Projects Agency
Washington, D. C.

13 ABSTRACT

The physical characteristics of the terrestrial atmosphere are reviewed for the purpose of providing a physical background for a study of requirements and techniques for the determination from satellites of winds and other atmospheric parameters. The nature of the atmosphere, its physical processes, and the variability of its parameters are described. Topics treated, in turn, are solar radiation as it affects the atmosphere, the troposphere, stratosphere and mesosphere, the thermosphere and the ionosphere.

DD FORM 1 NOV 65 1473

UNCLASSIFIED
Security Classification